2019-05-06

The non-classical MHC-II molecule DO regulates diversity of the immunopeptidome and selection of the CD4 regulatory T cell lineage

Mollie M. Jurewicz
University of Massachusetts Medical School

THE NON-CLASSICAL MHC-II MOLECULE DO REGULATES DIVERSITY OF THE IMMUNOPEPTIDOME AND SELECTION OF THE CD4 REGULATORY T CELL LINEAGE

A Dissertation Presented By

MOLLIE M. JUREWICZ

Submitted to the Faculty of the

University of Massachusetts Graduate School of Biomedical Sciences

in partial fulfillment of the requirements for the degree of

DOCTOR OF PHILOSOPHY

May 6th, 2019

IMMUNOLOGY AND MICROBIOLOGY

THE NON-CLASSICAL MHC-II MOLECULE DO REGULATES DIVERSITY OF THE IMMUNOPEPTIDOME AND SELECTION OF THE CD4 REGULATORY T CELL LINEAGE

A Dissertation Presented By

MOLLIE M. JUREWICZ

This work was undertaken in the Graduate School of Biomedical Sciences

(Immunology and Microbiology)

Under the mentorship of

Lawrence J. Stern, Ph.D., Thesis Advisor

Eric S. Huseby, Ph.D., Member of Committee

Andrea Reboldi, Ph.D., Member of Committee

Michael Brehm, Ph.D., Member of Committee

Lisa K. Denzin, Ph.D., External Member of Committee

Kenneth Rock, M.D., Chair of Committee

Mary Ellen Lane, Ph.D.,

Dean of the Graduate School of Biomedical Sciences

May 6th, 2019

Dedication

I dedicate this work to my mother, who instilled in me scientific curiosity, and to my husband, who nurtured and cultivated it.

Acknowledgments

Thank you to my mentor Larry Stern, for his support, his guidance, and his kindness. His endless enthusiasm for science inspires those around him to look further and learn more, while his fund of knowledge seems to have no bounds. He has taught me to think better, to focus more on the details of experimental results, and to challenge myself in learning new techniques. I am very grateful to have had the opportunity to be trained by him for the past six years.

Thank you to the members of my thesis committee, Leslie Berg, Ken Rock, and Eric Huseby, for providing many helpful suggestions throughout my graduate career. Many thanks to the members of my dissertation committee, Ken, Eric, Andrea Reboldi, Mike Brehm, and my outside examiner Lisa Denzin.

Thank you so very much to current and former members of the Stern Lab, in particular Pia Negroni and James Birtley, whose friendship have meant more to me than words can describe. I would like to acknowledge Padma Nanaware for performing all the MS experiments and analysis described herein, the results of which were central to our understanding of the biology of DO. Thank you to Liying Lu and Guoqi Li, who made MHC-I and MHC-II complexes for binding and tetramer studies in this work, and for always being so kind and helpful to everyone in the lab. Many thanks to Mauricio Calvo-Calle and John Cruz, who are willing to provide help whenever needed and who assisted with HHV-6 epitope studies.

Thank you to Peter Trenh and Zach Maben for friendship, support, and expertise in structural biology, and to Liusong Yin for early discussions about DM and DO function. Thank you to the rest of the family that is the Stern Lab, for making daily life in the lab memorable and enjoyable: Richa Arya, Aniuska Becerra, Sydney Blevins, Loretta Lee, Karthik Ramesh, Tessa Santoro, Zu Ting Shen, Inyoung Song, Grant Weaver, and Kerstin Zimmermann.

Many, many thanks to Sharlene Hubbard for invaluable assistance with mouse breeding, weaning, and tail DNA isolation. Any and all mouse work described in this thesis was possible due to her efforts.

Thank you to the staff, faculty, post-docs, and students in the Pathology Department, who have provided support and guidance throughout my time at UMMS. In particular, thank you so very much to Jeff Colbert, to whom I am grateful for both friendship and scientific mentorship. He is an extraordinary teacher and scientist, and he has been incomparably patient and generous with his time. Thank you to members of the Swain Lab for technical assistance, reagents, and helpful scientific discussion, and especially to Priya Devarajan and Allen Vong, who provided insightful suggestions for studies of the effect of DO expression in flu infection.

Thank you to my fellow students Barry Kriegsman, Jim Conley, and Beth Olesin for friendship and commiseration. Many thanks to the administrative staff in the

Pathology Department, and thank you to Joan Veinot, for being willing to answer and help with any administrative issues, and always to do so with humor.

Thank you to my wonderful family. To my amazing parents, who are somehow endlessly supportive and generous, and who taught me social responsibility, compassion, and the values of diligence and hard work. To my five sisters and brothers, each of whom has shaped me in innumerable ways. To my father, whose moral compass has guided my own. Thank you to my grandparents, for their limitless support and love.

Most of all, I would like to thank my husband Jonathan and the light of our lives, our pitador Aiko. Our little family carried me through this process, and lifted me up with snuggles and encouragement. I am forever in awe of my husband, who is not only a phenomenal scientist, but whose fortitude, integrity, and capacity for change are an inspiration.

Abstract

Presentation of antigenic peptides on MHC-II molecules is essential for induction of tolerance to self and for effective immunity against foreign pathogens. The non-classical MHC-II molecule DO (HLA-DO in humans, H2-O in mice) functions in selection of MHC-II epitopes by competitively inhibiting the peptide exchange factor DM. Previous studies have suggested a role for DO in development of autoimmunity and in the immune response to retroviral infection, presumably via modulation of the MHC-II peptidome, but the precise effect of DO has been difficult to discern. Through characterization of the full spectrum of peptides from DO-sufficient and DO-deficient cells, we demonstrate that DO functions to broaden the diversity of peptide species presented on MHC-II. DO is regulated differently from other components of the MHC-II processing machinery, with expression limited to B cell and dendritic cell subsets, as well as thymic epithelial cells, suggesting a role for DO in mediating central tolerance. In a mouse model lacking DO, we show that selection of T regulatory cells (Tregs) is increased and that DO-deficient Tregs are more activated and exert greater suppressive capacity. Despite augmented Treg function, mice lacking DO display enhanced susceptibility to autoimmunity, with altered germinal center (GC) Tregs and B cells indicative of an aberrant GC reaction. These data suggest that DO expression serves to fine-tune the immunopeptidome in order to promote self-tolerance to a wide spectrum of epitopes and to select a Treg population with appropriate specificity for self-antigens.

TABLE OF CONTENTS

List of Tables

List of Figures

List of Copyrighted Materials Produced by the Author

Jurewicz MM and Stern LJ. Class II MHC antigen processing in immune tolerance and inflammation. *Immunogenetics*. 71(3), 171-187 (2019).

Nanaware PP, Jurewicz MM, Leszyk JD, Shaffer SA, and Stern LJ. HLA-DO modulates the diversity of the MHC-II self-peptidome. *Mol Cell Proteomics*. 18(3): 490-503 (2019).

List of Third Party Copyrighted Material

The following figures were reproduced from a journal (permission not required):

Figure Number	Publisher
Figure 1.2	Elsevier Publishing

List of Symbols, Abbreviations, or Nomenclature

ADH	Yeast alcohol dehydrogenase
AIRE	Autoimmune regulator
ANAs	Anti-nuclear antibodies
APC	Antigen-presenting cell
β2m	β2-microglobulin
BM	Bone marrow
BrdU	5-Bromo-2'-deoxyuridine
CLIP	Class II-associated invariant chain peptide
CIITA	Class II major histocompatibility complex transactivator
cTEC	Cortical thymic epithelial cell
CRISPR	Clustered regularly interspaced short palindromic repeats
DC	Dendritic cell
DFR	Distribution-free resampling
dLN	Draining lymph node
DO-KO	DO knockout
dsDNA	Double-stranded DNA
DT	Diphtheria toxin
DTR	Diphtheria toxin receptor
DTT	Dithiothreitol
EBV	Epstein-Barr virus
ELBM	Epitope-linked β2m
FACS	Fluorescence-activated cell sorting
FBS	Fetal bovine serum
FDR	False discovery rate
FP	Fluorescence polarization
FSC	Forward scatter
GC	Germinal center
G-CSF	Granulocyte-colony stimulating factor
GFP	Green fluorescent protein
GO	Gene ontology
HA	Hemagglutinin
HBV	Hepatitis B virus
HCV	Hepatitis C virus
HHV	Human herpesvirus
HLA	Human leukocyte antigen
HPLC	High-performance liquid chromatography
IAA	Iodoacetic acid
IC_{50}	Half maximal inhibitory concentration
IFN-γ	Type II interferon
IL	Interleukin
K_d	Dissociation constant
K_i	Inhibitor constant
KLH	Keyhole limpet hemocyanin
LC-MS/MS	Liquid chromatography with tandem mass spectrometry

LD50	Lethal dose, 50%
LN	Lymph node
mAb	Monoclonal antibody
MALDI	Matrix-assisted laser desorption/ionization
MBP	Myelin basic protein
MHC	Major histocompatibility complex
MIG	Molecular identifier group
MS	Mass spectrometry
mTEC	Medullary thymic epithelial cell
NA	Neuraminidase
NK	Natural killer
NP	Nucleoprotein
NS1	Nonstructural protein 1
nt	Nucleotide
OVA	Ovalbumin
PA	Polymerase
PBS	Phosphate-buffered saline
PCR	Polymerase chain reaction
PMA	Phorbol 12-myristate 13-acetate
PR8	Influenza A/PR8/1934 (H1N1)
Rag	Recombination-activating gene
SD	Standard deviation
SEM	Standard error of mean
sgRNA	Single-guide RNA
SP	Single-positive
SSC	Side scatter
TCR	T cell receptor
TEC	Thymic epithelial cell
TFA	Trifluoroacetic acid
Tfh	T follicular helper cell
Tfr	T follicular regulatory cell
Tg	Transgenic
ThCTL	T helper cytotoxic cells
TLR	Toll-like receptor
TNF-α	Tumor necrosis factor α
Treg	T regulatory cell
TSSP	Thymus-specific serine protease
UMI	Unique molecular identifier
WT	Wild-type

Preface

The work presented in this thesis has been already published, has been submitted for publication, or is in the process of being prepared for submission. Chapter I contains portions published in a review for *Immunogenetics* as part of a topical collection entitled *Biology and Evolution of Antigen Presentation*: Jurewicz MM and Stern LJ. Class II MHC antigen processing in immune tolerance and inflammation. *Immunogenetics*. 71(3), 171-187 (2019). In Chapter II, which was published in Molecular and Cellular Proteomics (Nanaware PP, Jurewicz MM, Leszyk JD, Shaffer SA, and Stern LJ. HLA-DO modulates the diversity of the MHC-II self-peptidome. *Mol Cell Proteomics*. 18(3): 490-503 (2019)), I present work performed in collaboration with a post-doctoral fellow in the Stern laboratory, Padma Nanaware, for which we are co-first authors. I generated and characterized the WT and DO-KO cell lines used for this work, performed RNAseq analysis, isolated mouse B cells for MS experiments, performed mouse immunization experiments, and together with my mentor Lawrence Stern conceived of the study design. Dr. Nanaware performed all mass spectrometric experiments and analysis described, as well as DM sensitivity assays. In Chapters III and IV, I performed all experimental work. Liying Lu generated MHC-II influenza epitope tetramers used in Chapter IV. Appendix I is under revision at Analytical Biochemistry; I performed all experiments described in this work, using recombinant protein provided by the NIH tetramer facility, and with MHC-I complexes prepared by Guoqi Li for differential scanning fluorimetry experiments. Appendix II includes study of HHV-

6B-restricted MHC-I epitopes; this work was performed with the help of Dr. Mauricio Calvo-Calle, who assisted with restimulation assays and performed data analysis, John Cruz, who isolated PBMCs from all donors and assisted with restimulation assays, and Guoqi Li, who generated MHC-I tetramers. A brief description of author contributions is included at the beginning of each chapter or appendix.

I have contributed to other works (either published or being prepared for publication) during my time in the laboratory of Lawrence Stern, which will not be described in my thesis. These include Birtley *et al.* (*Nature Communications*, 2019) and unpublished observations of the WT vs. $DO^{-/-}$ thymic immunopeptidome.

CHAPTER I

Overview of MHC-II presentation

Presentation of peptide antigens by class II Major Histocompatibility Complex (MHC-II) molecules is critical for maintenance of self-tolerance and for initiation of effective immune responses. Immunological tolerance to antigens presented on MHC-II molecules begins at the selection stage of T cell development in the thymus and continues in the periphery. CD4 T cells necessarily interact with self-ligands presented by MHC-II molecules for positive selection in the thymus as well as require tonic stimulation by peripheral MHC-II-peptide complexes for survival. During the process of negative selection in the thymus, development of T cells with T cell receptor specificities overtly reactive to self is prevented, and cells with borderline reactivity are directed into the CD4 T regulatory lineage. A peripheral immune response is initiated when antigen-presenting cells (APCs) present peptides that alert the adaptive immune system to mount a targeted response against invading pathogens. Entry of self and foreign antigens into the endo/lysosomal pathway, proteolytic processing, and selection of peptides for presentation are influenced by APC type, maturation state, and external environment. Thus, the set of peptides presented by MHC-II molecules, known as the MHC-II immunopeptidome, is determined by these factors. The nonclassical MHC-II molecule DO has been shown to modulate presentation of MHC-II epitopes and thereby may affect processes that govern self-tolerance and immunity in which MHC-II presentation plays a central role.

MHC-II synthesis and peptide loading pathways

MHC-II molecules are constitutively expressed on professional APCs such as dendritic cells, macrophages, and B cells, as well as thymic epithelia, and are upregulated on many other cell types by IFN-γ. Expression of MHC-II genes is primarily regulated by the class II transactivator (CIITA), which necessarily interacts with multiple DNA-binding proteins to initiate transcription of MHC-II genes and MHC-II antigen processing pathway components[6,7]. Following synthesis of MHC-II α and β subunits in the ER (Figure 1.1), nascent MHC-II molecules bind the invariant chain (Ii) protein, allowing for stabilization of the MHC heterodimer, spatial restriction of peptide loading, and transport to the endocytic compartment for peptide loading[8,9]. The MHC-II-Ii complex then translocates through the Golgi complex into the endocytic pathway by way of a dileucine targeting motif present in the cytoplasmic domain of Ii[10-12]. As endocytic vesicles acidify, endolysosomal proteases termed cathepsins acquire increased proteolytic activity and cleave the MHC-II-bound invariant chain until only a residual peptide (CLIP, or class II-associated invariant chain peptide) remains bound in the MHC-II peptide-binding site[13-15]. Proteins transported into the lumen of the endosome unfold and are digested by endosomal proteases to allow for MHC-II binding[16-19]. The nonclassical MHC-II peptide exchange factor HLA-DM (H2-M in mice, hereafter referred to as DM) also resides in endosomal/lysosomal compartments and catalyzes the removal of CLIP from the peptide-binding groove of MHC-II molecules, with resultant exchange of CLIP for endosomal peptides[20-22]. DM can act on other peptides in addition to CLIP,

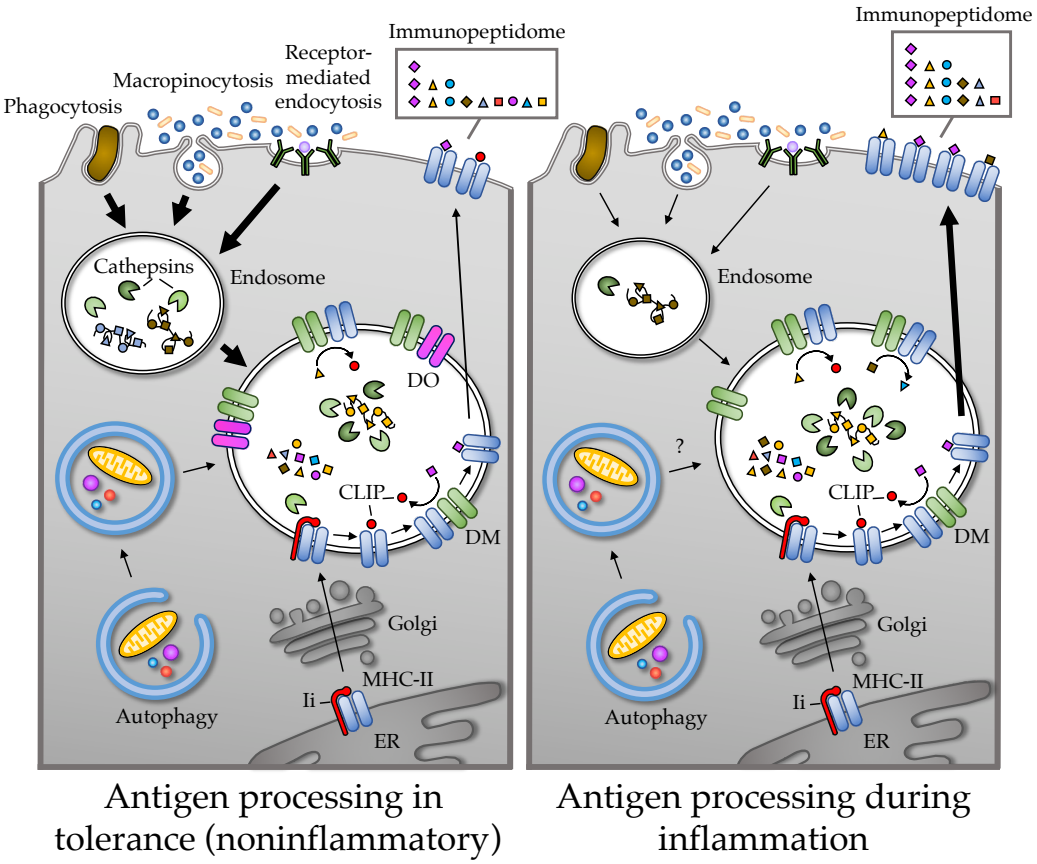

Figure 1.1. Antigen processing in tolerance and inflammation. MHC Class II dimers are synthesized in the ER and loaded with invariant chain, after which they traffic to the endosome. Cathepsins cleave the invariant chain (Ii) to the residual peptide CLIP, which is then removed by the peptide exchange factor DM and exchanged for peptides derived from proteolyzed self- and foreign antigens. The MHC-II-peptide complex traffics to the cell surface for presentation to CD4 T cells. To maintain tolerance in noninflammatory conditions (left panel), the immunopeptidome in APCs is comprised of diverse self-peptide antigens acquired through extracellular uptake pathways as well as autophagy. Components of the antigen processing machinery including the DM inhibitor DO further enhance the diversity of the peptides presented. Upon activation and initiation of an inflammatory response (right panel), antigen sampling is reduced, endosomal proteases are redistributed to late endosomes, DO expression is downregulated, and MHC-II expression is substantially increased. (The effects of inflammation on the process of autophagy in APCs are incompletely understood.) During inflammation, these changes result in greater efficiency of MHC-II antigen presentation as well as reduced diversity in the MHC-II peptidome in an immune response.

such that multiple cycles of peptide exchange can occur[23,24]. The DM-MHC-II interaction has been shown to be transient[25-27], increasing the rates of peptide binding to and peptide release from MHC-II without altering the equilibrium affinity, consistent with an enzyme-like catalytic activity[21,28]. Because the

efficiency of DM-mediated catalysis varies for different MHC-II-peptide complexes, the net effect of DM activity is to exchange peptides that interact more weakly with MHC-II for those that interact with greater affinity. The precise features of the MHC-II-peptide interaction that are targeted by DM are controversial, with recent work focusing on conformational flexibility as an important determinant[4,20,29-31]. Overall, DM thus serves an editing function, selecting for peptides with optimal interaction with MHC-II. DM activity is competitively inhibited by another nonclassical MHC-II molecule, HLA-DO (H2-O in mice, hereafter referred to as DO), which tightly binds to DM in the endoplasmic reticulum and traffics together with DM into the endocytic pathway, preventing a fraction of the DM from interacting with MHC-II[25,28,32-37]. Following removal of CLIP and loading of antigenic peptide, the MHC-II-peptide complex then traffics to the plasma membrane for presentation at the cell surface to CD4 T cells. While the basic mechanism of peptide loading appears to be shared by all cells that constitutively express MHC-II, the acquisition and processing of MHC-II antigens can occur via diverse pathways (Figure 1.1) to promote presentation of epitopes from a broad range of antigens.

Acquisition of antigens for processing in MHC-II pathways

MHC-II-expressing cells acquire antigen by distinct cellular processes that allow professional APCs to sample their external environment. Classically, extracellular proteins were thought to predominate as antigenic sources in MHC-II presentation, but many studies have demonstrated that the MHC-II peptidome largely consists of

peptides derived from endogenous – rather than exogenous – source proteins[38-40]. These endogenous peptides can derive from proteins expressed at the plasma membrane and in endo/lysosomal compartments, as expected from the location of the MHC-II loading machinery in the endocytic pathway, but peptides from other intracellular compartments such as the nucleus, mitochondria, ER/Golgi, and cytosol also are found in abundance. The predominance of endogenous peptides has been shown to persist in inflammatory conditions[41-43] and thus may have implications for maintenance of tolerance during an immune response. The fact that very low fractional occupancy of MHC-II by pathogen-derived peptides in virally-infected cells[41], which is also observed for MHC-I peptides[44], is sufficient to elicit effective immunity demonstrates that minimal shifts in the immunopeptidome can have important immunological consequences.

Acquisition and processing of MHC-II antigens

Capture of extracellular antigen occurs via multiple processes with varying degrees of efficiency in different types of antigen-presenting cells. Canonically, acquisition of antigen for MHC-II presentation occurs by different modes of endocytosis, followed by processing of antigens in progressively more acidic intracellular compartments. Macropinocytosis, a nonspecific and actin-dependent that allows for fluid-phase uptake of extracellular material via invagination of the cell membrane, serves as a primary means of exogenous antigen internalization in immature DCs and macrophages[45-47]. Phagocytosis, an additional fundamental uptake mechanism that occurs principally in DCs and macrophages, is characterized by internalization

of relatively large (>0.3 μm) particulate antigens[48] and primarily occurs following recognition of surface receptors such as the C-type lectin pattern-recognition receptor DEC-205 or the opsonic Fcγ receptors[49-52]. Signal transduction following ligation of different phagocytic surface receptors varies but has been shown in all cases to culminate in actin polymerization and phagosome formation[53]. The phagosome, derived primarily from the plasma membrane, then fuses with lysosomes to form phagolysosomes[54]. Proteolysis of internalized proteins within the phagolysosome is accomplished in DCs by cathepsins and other endosomal proteases, while NOX2 is recruited to the phagosomal membrane to regulate antigen proteolysis[55]. B cells, by contrast, principally depend upon receptor-mediated endocytosis to capture extracellular antigen[56-58]. Antigen is internalized during this process after binding to the B cell receptor (BCR), or to surface Fc or complement receptors, after which endocytosis – most often mediated by entry via clathrin-coated vesicles – occurs[59,60].

Evidence for acquisition of MHC-II antigenic source proteins via alternate or nonconventional pathways has accumulated over the past two decades. Perhaps chief among these is the process of autophagy, whereby cytoplasmic components are digested by the cell for degradation and processing[61]. Incorporation of the cytosol into autophagosomes was initially described in yeast as the cellular response to starvation, and as such, an essential energy source for cell survival[62]. Since its discovery, however, autophagy has been determined to be critical for myriad cellular and organismal processes, including aging and development, as well as for antigen presentation[63-65]. All forms of autophagy (macro-, micro-, or

chaperone-mediated) intersect with the endocytic pathway and thus deliver nuclear, microsomal, and cytoplasmic proteins for presentation on MHC-II[66-68]. Processing of antigens via macroautophagy has been demonstrated to be important in DCs, in which constitutive formation of autophagosomes has been shown, as well as in B cells, for presentation of both self- and foreign antigens[66,69-71]. Although antigen processing pathways in thymic epithelial cells (TECs) are considerably less well-examined than in professional APCs, TECs are thought to rely primarily upon constitutive macroautophagy to present MHC-II antigens[72-74]. In medullary TECs (mTECs), incorporation of antigens into autophagosomes has been shown to allow for presentation of the many tissue-specific antigens under the transcriptional control of AIRE[75]. Antigen transfer via trogocytosis, in which an immune synapse forms between cells to mediate intercellular transfer of proteins, has also been shown to allow for capture and presentation of MHC-peptide complexes by both APCs and non-APCs[76-78]. In the thymus, peptides presented as a result of trogocytosis between DCs and mTECs is posited to aid in increasing presentation of rare thymic antigens by MHC-II[79-81]. While the mechanism of transfer from DCs to many cell types remains unclear, MHC-II-peptide uptake by T cells has been demonstrated to be mediated via the TCR and the costimulatory molecule CD28[82]. Recycling of MHC-II molecules also serves as an alternative means of presentation of MHC-II epitopes; peptide loading on recycled MHC-II following endocytosis has been shown to occur in early endosome compartments[83-86]. Of note, the antigen acquisition processes of trogocytosis and recycling in early endosomes in most cases seem to be independent of DM and cathepsin activity, such that peptide

species loaded or exchanged on recycled or trogocytosed MHC-II may be comprised of epitopes absent from the MHC-II peptidome generated by canonical pathways[83,87,88], although in some cases DM-mediated editing has been observed[89]. Still another mechanism capable of generating antigens presented on MHC-II molecules relies on components of MHC-I machinery, including the proteasome, TAP, and ERAP[90,91]; however, the mode of intersection of the MHC-I and MHC-II processing pathways has not been determined. It has thus become clear that the MHC-II immunopeptidome can be influenced by multiple processing pathways that serve to present antigens from endogenous and exogenous sources, and that canonical MHC-II acquisition and processing is not the sole determinant of the MHC-II-bound peptide repertoire.

Source proteins in the MHC-II peptidome

Recent advances in mass spectrometry technology have significantly improved both accuracy and sensitivity of detection of peptides eluted from purified MHC proteins, allowing for qualitative and quantitative characterization of MHC peptidomes. Mass spectrometry can thus be leveraged as a powerful tool to identify source proteins from which MHC-II peptides derive in order to assess effects of perturbations in MHC processing such as cellular maturation or infection, and the relative contributions of different processing pathways. Increases in the sensitivity of mass spectrometry has allowed studies of APCs characterized ex vivo[2,43,92], likely reflective of in vivo peptidomes, as compared to classical immunopeptidome studies of cultured cells. Recent work has demonstrated that the MHC-II peptidome

is substantially comprised of peptides derived from nuclear or cytosolic proteins (25-55% of total peptides eluted from HLA-DR)[2,38], presumably largely due to the self-degradative autophagic process. Several studies have quantified peptides derived from extracellular source proteins as constituting only ~10-20% of the MHC-II peptidome, with the remaining peptides derived from endogenous source proteins located in various cellular compartments, including the plasma membrane, mitochondria, endosomes or lysosomes, and ER/Golgi[2,38-40]. A caveat of these analyses is that classification of peptides as sourced from endogenous proteins does not preclude acquisition of (at least a portion of) these proteins via uptake of necrotic or apoptotic cells. Recent work examining source proteins in the peptidome of mouse lymphatic fluid compared to the HLA-DR1-bound peptidome of splenic dendritic cells posited that lymph-derived epitopes were loaded at the surface or in early endosomal compartments based on their sensitivity to DM-mediated exchange and endosomal digestion, suggesting a DM-independent mechanism for presentation of low affinity autoantigens derived from extracellular sources[2]. In the context of infection or inflammation, the MHC-II peptidome has been shown to include only a very small fraction of foreign peptide sequences present within a much larger set of host-derived sequences, as characterized in the settings of experimentally-induced colitis in mice (~0.2% of 2188 total sequences), a mouse model of malaria infection (42 malaria-derived out of 372 sequences), or vaccinia infection of cultured B cells (1% of the peptidome, as estimated by comparing intensities of several hundred peaks)[41-43]. Further quantitative analysis is required to determine the proportion of foreign peptides presented on MHC-II

molecules with respect to total peptide component (as compared to the fraction of different sequences), but these studies suggest that even during inflammation or infection, the MHC-II peptidome largely consists of peptides derived from self.

Implications of MHC-II processing for immune tolerance

Positive and negative selection of T cells in the thymus depends on interactions of developing T cells with local antigen-presenting cells, and so antigen presentation events in the thymus play a key role in guiding selection of CD4 T cells as well as in development of regulatory CD4 T cells. Differential processing and presentation pathways in various cell populations can result in distinct peptidomes in different tissues, and antigens produced in this manner present a challenge for central and peripheral tolerance mechanisms in the restraint of autoimmunity.

MHC-II presentation in central tolerance

Somatic gene arrangement of the T cell receptor (TCR) occurs in the thymus and generates T cells with diverse specificities for different MHC-II-peptide complexes. Presentation of self-ligands on MHC-II in the thymus positively selects only those T cells that express TCRs capable of recognizing the peptide-MHC complex[93]. Positive selection is mediated by cortical thymic epithelial cells (cTECs), which have been posited to present a unique MHC-II ligandome due to proteolytic activities of cathepsin L and thymus-specific serine protease (TSSP)[79,94,95] (Table 1.1). Evidence for a requirement for distinct peptide species in

Table 1.1. Expression of antigen processing components in mouse and human APCs.

Cell type	MHC-II expression	Endosomal proteases[b]	DM	DO	Ratio of DM:DO	Refs (human)	Refs (mouse)
Immature DCs	+++	**Cat S**, Cat D, Cat E, Cat H, SPPL2A (mu) **Cat D, Cat G, Cat S, AEP** (hu)	✓	✓	Low	96-101	Immgen[e]; 94,102-112
Mature DCs	+++++	Cat D, Cat H, Cat L, AEP (ms), **Cat S** (hu and ms), Cat B (hu)	✓	-	High	96 98,101,113	Immgen; 102,103,109,112,114
Macrophages	++	**Cat B, Cat E, Cat F, Cat L, Cat S, AEP**	✓	-	High	115-119	Immgen; 104,120-126
Monocytes	+	Cat B[c], Cat G, Cat K[c], Cat L[c], Cat S[c] (hu)	✓	-	High	97,127-130	Immgen
Mature B cells	++	**Cat B, Cat D**, **Cat L, Cat S,** SPPL2A (ms), **Cat E**, **Cat G**, AEP (hu)	✓	✓	Low	13,131-136	Immgen; 104,105,137-140
GC B cells	+++	Cat S	✓	-	High	131,135,141	Immgen; 137,142
cTECs[a]	++	**Cat L**, TSSP (ms) Cat G, **Cat V** (hu)	✓	-	High	99,143-145	Immgen; 94,95,146,147
mTECs[a]	++	Cat L[c], Cat S[c]	✓	✓	Low	143,145,148	Immgen; 146,147,149,150
Thymic DCs[a]	+++	**Cat S** (hu and ms), **AEP** (ms)	?	?	?	151,152	94,124,146
Endothelium/epithelium[d]	++	Cat B, Cat D, Cat L (hu), **Cat S** (hu and ms)	✓	?	?	153-160	161-163

Abbreviations: DCs: dendritic cells; GC: germinal center; cTECs: cortical thymic epithelial cells; mTECs: medullary thymic epithelial cells; Cat: cathepsin; SPPL2A: signal peptide peptidase-like 2a; AEP: asparagine endopeptidase; TSSP: thymus-specific serine protease; hu: human; ms: mouse.

[a]Relative MHC-II expression is estimated based on data in references included. For thymic DCs, no published data is available regarding DM and DO expression.

[b]Proteases in which enzymatic activity is reported are in bold, as are the references that report enzymatic activity (demonstrated via active site labeling or through effects on antigen presentation of specific epitopes). Of note, endosomal proteases have been shown in many instances to exhibit redundancy in their activity and specificity.

[c]mRNA expression demonstrated only.

[d]Human endothelium and epithelium basally express MHC-II, while mouse MHC-II has been reported both to be expressed basally on epithelium and endothelium as well as only in response to inflammation (e.g. exposure to IFN- γ). MHC-II levels shown are in the context of inflammation. No published data are currently available on DO expression in human or mouse endothelium/epithelium in the periphery.

[e]Immunological Genome Project (www.immgen.org)

the positively-selecting MHC-II peptidome was demonstrated by rescue of the defect in CD4 T cell selection observed in cathepsin L-deficient mice[94] via reconstitution with MHC-II-deficient bone marrow[164]. These results suggested that in mice deficient in cathepsin L, the efficiency of negative selection of T cells is increased due to overlapping immunopeptidomes of MHC-II-expressing hematopoietic APCs and cTECs. A substantially reduced MHC-II peptide repertoire in H2-M-deficient mice demonstrated a similar effect on the CD4 T cell compartment[165,166], highlighting the importance of (at least somewhat) distinct peptides presented by positively- and negatively-selecting APCs in effective thymic selection of CD4 T cells.

If positive selection is required to ensure that developing CD4 T cells can recognize MHC-II-peptides, the process of negative selection is necessary to remove CD4 T cells that are overtly reactive with self-ligands[167]. By deleting T cells with exceedingly high affinity for MHC-II bound to peptide autoantigens in the thymus, peripheral immune responses to self-antigens can be subverted. MHC-II presentation by mTECs of peptides derived from self-peptides is mediated by promiscuous expression of tissue-restricted antigens by AIRE, which allows for deletion of CD4 T cells with high affinity for autoantigens expressed in peripheral tissues[168]. MHC-II processing and presentation of tissue-restricted antigens has been shown to involve nonconventional pathways such as macroautophagy and

trogocytosis (discussed above). Recent analysis of thymus MHC-II peptidomes has confirmed the diverse spectrum of source proteins presented by thymic APCs[169,170], but whether the thymus-associated MHC-II immunopeptidome is comparatively unique relative to other tissues remains a subject for future work.

Presentation of ligands by MHC-II in the thymic medulla also controls development of thymocytes into an alternative CD4 T cell fate. Selection of the suppressive Foxp3-expressing T regulatory (Treg) population occurs in the thymic medulla through recognition of MHC-II-peptide complexes, at a threshold of affinity/avidity thought to lie above the threshold for conventional T cell selection but below the threshold for clonal deletion[171-174]. Examination of T cell activation by the Hogquist group using reporter mice expressing Nur77, which is rapidly upregulated following TCR signaling, demonstrated the importance of TCR specificity in selection of Tregs[175]. The consequence of Treg selection within a high affinity or avidity window is suggested to result in activation of Tregs in the periphery at low agonist doses, so that they may outcompete conventional T cells for MHC-II ligand binding[176,177]. Seminal work from the Hsieh group demonstrated through TCR retrogenic technology that Treg self-reactivity is observed over a broad range of affinity, indicating Tregs are likely to participate in suppression of immunity to both self and non-self[178]. MHC-II peptide ligands responsible for Treg selection have not been determined, and identification of these peptides may provide greater understanding of the determinants of Treg selection, particularly with regard to ligand avidity and affinity.

Peripheral tolerance and the MHC-II immunopeptidome

Following thymic egress, mature CD4 T cells migrate to the periphery and populate the secondary lymphoid organs. A portion of clonotypes that exit the thymus are reactive to self, owing to the fact that negative selection is an imperfect process[179]. Peripheral tolerance mechanisms serve to dampen or eliminate autoreactive T cells by inducing anergy or mediating clonal deletion. T cells that bind their cognate ligands in the absence of positive costimulatory molecules become hyporesponsive (or anergic), thereby circumventing autoimmune attack of healthy tissue[180]. Other costimulatory molecules such as PD-1 provide negative signals that inhibit T cell activation, effectively suppressing self-reactivity[181]; in mouse models deficient in PD-1, autoimmune disease develops with features of lupus, including arthritis and glomerulonephritis[182]. CD4 T cells also require tonic stimulation by MHC-II ligands to survive, and the absence of tonic signals results in clonal deletion by apoptotic cell death[183,184]. A third mechanism of peripheral tolerance occurs via Treg-mediated suppression of effector T cells. Thymic Tregs enter the periphery endowed with suppressive function, and peripheral induction of Tregs, particularly in sites such as the gut where naïve CD4 T cells encounter commensal and food-derived antigens, can help to restrain overactive or self-reactive T cell responses[185,186]. The precise mechanism(s) by which Treg-mediated suppression occurs is a matter of some debate[187,188], but models of Treg deficiency conclusively demonstrate the vital function of these cells in regulating the development of autoimmunity and in preventing excessive immunopathology during infection[189-192].

Alterations in the MHC-II peptidome that can occur in specific tissues or in certain disease states have the potential to compromise the efficacy of peripheral tolerance mechanisms. Tissue- or cell-specific differences in antigenic sources, processing, or peptide loading may generate distinct peptide repertoires presented by particular APCs in particular locations (Table 1.1). Local sources of captured exogenous antigen are likely to vary considerably in different organs, and disparate metabolic or gene expression profiles of tissue-specific APCs may further diversify the immunopeptidome in various locations throughout the body[43,193-195]. Such differences may have implications in maintenance of tolerance based on the weak expression of tissue-restricted antigens mediated by AIRE in mTECs[196,197], in cases where TCR agonist density increases sufficiently enough in the periphery to activate a T cell selected in the thymus with only weak affinity for its cognate antigen. In addition, post-translational modifications of self-peptides in the periphery can lead to generation of novel epitopes capable of binding and activating T cells that then initiate an autoimmune response. In such cases, if epitopes fail to be generated in the thymus, developing T cells with specificity for these antigens may escape negative selection. For example, citrullination of peptides or proteins has been observed in rheumatoid arthritis, multiple sclerosis, and type 1 diabetes (T1D) and have been implicated in the etiology of disease[198,199]. Trans-splicing of peptides derived from proteins present in the insulin secretory granule has been suggested to generate new epitopes that can be loaded onto MHC-II and presented by pancreatic beta cells and recognized by diabetogenic CD4 T cells[200-202]. Differential proteolytic activity in different cells or different cellular locations

could alter proteolysis of antigens and result in a qualitatively different immunopeptidome, as suggested by altered processing of myelin basic protein (MBP) and insulin proteins in thymic APCs due to cathepsin S activity[152]. Differential expression of DM, or differential trafficking of antigens through DM-containing compartments, in the periphery as compared to thymus could further influence the content of the MHC-II peptidome and impact autoimmunity[203,204]. Lastly, regulation of the MHC-II peptidome may also be conferred by resistance of certain MHC alleles to editing by DM, and this has been suggested to contribute to the genetic association of certain HLA-DR and HLA-DQ allotypes with autoimmunity in diabetes and celiac disease[30,31,205].

MHC-II processing in inflammation

Professional APCs undergo a maturation process in the context of inflammation that results in alterations in MHC-II processing and presentation pathways. Changes in multiple components of the MHC-II presentation pathway in addition to upregulation of MHC-II expression may serve to focus the peptide repertoire by amplifying presentation of stable MHC-II-peptide complexes, which has been shown to be a feature of immunodominant epitopes derived from foreign antigens[206-208]. Induction of CIITA by IFN-γ in non-professional APCs such as endothelial cells – which do not constitutively express MHC-II molecules – results in substantial surface expression of MHC-II[156,209]. Such changes allow for efficient and widespread presentation of inflammation-associated epitopes derived from invading pathogens or autoantigens. Due to the preponderance of self-ligands in the

MHC-II peptidome, however, these changes may also have implications for breakdown of tolerance under inflammatory conditions.

Inflammation-associated alterations in antigen acquisition, MHC-II processing and presentation

During an immune response, targeted and precise activation of T cells is necessary to eliminate pathogenic insults. Some processes of antigen acquisition are downmodulated when APCs are activated, representing a shift in priority from antigen sampling to more efficient antigen presentation (Figure 1.1). Macropinocytotic activity in activated DCs has been shown to be reduced in some contexts and unaffected in others[210,211], while activation of macrophages has been demonstrated to reprogram antigen uptake to favor macropinocytosis over receptor-mediated phagocytosis[212]. In contrast, DC activation appears not to affect the efficiency of antigen capture via receptor-mediated phagocytosis[213], although MHC-II trafficking pathways are altered to prevent MHC-II ubiquitination and targeted degradation in lysosomes, preserving captured MHC-II-peptide complexes for recycling[214]. With regard to nonconventional antigen acquisition by autophagy in the context of inflammation, presentation of many bacterial and viral antigens has been shown to be dependent on macroautophagy[215-217], supporting a continued role for this process during an immune response.

Changes in the antigen processing and presentation machinery during inflammation serve to poise APCs to most efficiently orchestrate an effective immune response (Figure 1.1). Concurrent with alterations in antigen sampling,

synthesis of MHC molecules is also regulated in APCs to maximize presentation of MHC-II epitopes during inflammation. Surface MHC-II levels are 10-fold higher in mature DCs compared to immature DCs, owing to a transient burst in MHC-II biosynthesis upon DC activation[98,102]. IFN-inducible CIITA-mediated upregulation of MHC-II and associated processing and loading machinery also confers antigen-presenting ability to endothelium and epithelium[98,218-220]. Redistribution of MHC-II molecules from endosomes and lysosomes to the plasma membrane in DCs and macrophages further maximizes antigen-presenting efficiency, as does the enhanced stability of surface peptide-MHC complexes upon DC maturation[98,102,221]. In addition to overall enhanced MHC-II presentation and upregulation of costimulatory molecules, inflammatory signals result in changes in antigen processing and peptide loading machinery that likely affect the spectrum of peptides presented on MHC-II (Figure 1.1 and Table 1.1). Cathepsins are redistributed to MHC-containing compartments, and antigen processing efficiency is enhanced in DC exposed to TLR ligands[222,223]. Acquisition of cathepsin E activity has been shown in primary B cells activated with PMA or *Staphylococcus aureus* in vitro[133,224]. DO expression is downmodulated following DC maturation and B cell entry into germinal centers[101,111,112,131,141], effectively increasing DM activity. Removing inhibition of DM has the potential to allow for editing of a subset of the MHC-II peptidome, although the determinants that dictate sensitivity vs. resistance of peptides to DM-mediated editing remains a topic of active investigation[4,29,225-230]. These alterations, together with overall reduction in antigen acquisition during

inflammation, result in augmentation of antigen-presenting capacity and presentation of stable MHC-peptide complexes to T cells.

Potential effects of inflammation on peripheral tolerance

MHC-II peptide elution studies suggest that epitopes derived from pathogens comprise only a small fraction of the overall peptide repertoire. Due to the predominance of self-ligands in the MHC-II peptidome, increased surface expression of MHC-II on APCs during inflammation will likely result in increased peptide density of certain self-peptides. In addition, proteins upregulated by the inflammatory process, for example by induction of IFN-stimulated genes, can enter the endo/lysosomal pathway and represent an additional source of antigens potentially upregulated in inflammatory immunopeptidomes. Thus, during an inflammatory response, the increased expression of MHC-II molecules carrying particular self-peptides together with increased expression of costimulatory molecules, as well as enhanced secretion of cytokines and chemokines, may result in unwanted activation of T cells that under homeostatic conditions are only mildly reactive to self. Consistent with this idea, the etiology of autoimmune disorders has been linked to exposure to pathogens; initial onset of autoimmunity is shown in many instances to coincide with recent viral infection[231,232]. The mechanism whereby inappropriate activation of autoreactive T cells occurs in these contexts is often attributed to molecular mimicry[233,234]. Degenerate TCR specificity has indeed been shown in studies of MBP-reactive T cell clones, which were found to bind pathogen-derived peptides[235-237], and TCRs crossreactive for self- and foreign

antigens have been observed in other contexts as well[238,239]. Yet, given the considerable levels of self-pMHC on the surface of APCs during inflammation[41,43], activation of autoreactive T cell clones may also occur in an antigen-specific manner, such that increased ligand density in combination with costimulatory molecule expression initiates an inappropriate response to self. This idea shares features with the concept of bystander activation[233] associated with breakdown of tolerance, but is distinct in that additional uptake of self-antigen appears not to be required, given the predominance of self-pMHC in the immunopeptidome in both homeostatic and inflammatory conditions. Moreover, Tregs selected with higher affinity or avidity for self-antigen may be similarly activated by upregulated presentation of self-peptides, particularly if selection of Tregs is mediated by ubiquitous proteins or by antigens commonly overexpressed during inflammation. Thus, in addition to suppressing autoreactive T cell proliferation under homeostatic conditions, thymically-derived Tregs may in an inflammatory context have an important role in suppressing unwanted self-reactivity. Identification of thymic Treg peptide ligands could lend support for this proposed function, as well as reinforce the basis for selection of Tregs within an avidity/affinity window above that of conventional T cells.

Overview of the non-classical MHC-II molecules DO and DM

The non-classical MHC-II molecules DO and DM are central components of the MHC-II processing and antigen presentation pathway. These nonpolymorphic MHC-II molecules are homologous to classical MHC-II proteins but are unable to

bind peptide. Both DO and DM have been shown to affect selection of the epitopes presented on MHC-II in biochemical studies, antigen presentation assays, and mouse models. DM is necessary for efficient removal of CLIP from MHC-II heterodimers and also serves a peptide-editing function by catalyzing exchange of MHC-II peptides, although the determinants of DM action are incompletely understood. DO clearly functions as a competitive inhibitor of DM, but because its role is implicitly linked to the function of DM, the biological effects of DO expression have been difficult to discern.

Discovery of DO and DM

DO was first discovered over 30 years ago in studies mapping the human MHC locus[240,241]. Using cross-hybridization, α and β chains displaying similarity to classical MHC-II molecules were identified and initially called DZA and DOB, later DNA and DOB, and finally DOA and DOB[240-243]. Corresponding mouse genes were identified shortly thereafter[244,245]. In contrast, DM was only identified several years later in a comprehensive search for MHC-II genes, perhaps due to its lesser identity with classical MHC-II molecules (30%), compared to the homology between DO, DP, DQ, and DR (60%)[246]. While classical MHC-II molecules are encoded by the most polymorphic genes in the mammalian genome, DO and DM have been shown to display limited polymorphism[243,247-249]. Recent work has demonstrated that the few residues that do vary in different DM haplotypes affect presentation of autoimmune epitopes[250], and DM polymorphisms have additionally been correlated with onset and pathogenesis of rheumatoid arthritis and type 1

diabetes[251-256]. Single-nucleotide polymorphisms in DO have been associated with poorer outcome in cancer patients[257,258] as well as with altered clearance of hepatitis C infection[259,260].

While DM is expressed wherever MHC-II is expressed, DO displays much more limited expression and is restricted to immature DCs, mature B cells, and mTECs[137,149,261,262]. DM is coordinately regulated with other MHC-II genes by CIITA and is IFN-γ-inducible[6,7,218], whereas expression of DO appears only partly induced by CIITA transcriptional activity and so is subject to as-of-yet unidentified additional transcriptional regulation[263]. Levels of DM are reported to always be in excess of DO levels[37], and instability of the DO molecule prevents its egress from the ER on its own, such that it must first bind DM in order to traffic to endosomes[264]; both of these observations support the idea that DO serves to modulate DM activity while preserving DM's function in removing CLIP from MHC-II heterodimers. Further regulation of the DM/DO interaction is accomplished by its sensitivity to low pH and by downregulation of both molecules during certain cell developmental transitions. As endosomes mature and acidify, the net DM activity has been shown to increase[265-267], and recent data suggest that low pH-induced structural changes in DO are responsible for increased DM activity due to release of DM from inhibition by DO[267]. While both DO and DM are downregulated as DCs mature and as B cells enter the germinal center, DO is downregulated to a much greater degree, resulting in enhanced DM activity in these cells[101,111,112,131,141,262]. Thus, DM activity is modulated by multiple mechanisms

that are posited to alter the content of the MHC-II peptidome in DO-expressing cells.

Molecular mechanisms of DO and DM action

Since the discovery of DO and DM, significant effort has been made to understand their function at the molecular level. Recent resolution of crystal structures of DM in complex with MHC-II as well as DM in complex with DO lent insight into the

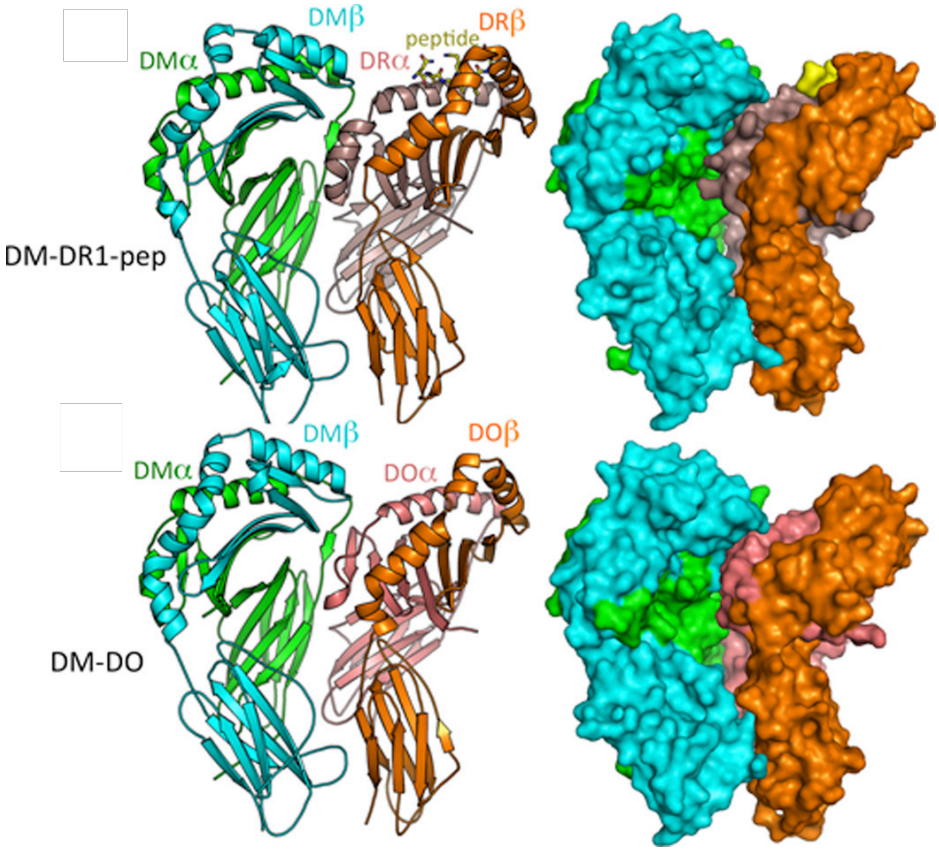

Figure 1.2. Similar binding modes of DM/DR and DM/DO (reviewed in Mellins and Stern[5]).

mechanisms of action of DO and DM in selection of MHC-II peptides. Pos *et al.* demonstrated that when in complex with DM, HLA-DR undergoes a

conformational change in which residues of the α subunit shift, occluding the N-terminal region of the peptide-binding site[20]. The Pheα51 MHC-II residue was shown to occupy the P1 pocket, interfering with hydrogen bonding between the α chain and the atoms of the peptide, and providing a mechanism whereby MHC-II-peptide interactions are destabilized to allow for peptide exchange[20]. Guce *et al.* demonstrated similar binding of DO to DM as was shown for DR to DM (Figure 1.2), except that Pheα54 in DO was shown to occupy the region that corresponds to the MHC-II P1 pocket[32]. Mutagenesis of residues in DM important for its interaction with MHC-II further demonstrated the corresponding binding modes of DO/DM and DR/DM, with such mutations affecting both affinity of DM/DO binding and catalysis of MHC-II peptide exchange by DM[32]. Given these data, and based on the substantial homology between DO and MHC-II, it was determined that DO acts as a substrate mimic and competitive inhibitor of DM, thus preventing its interaction with MHC-II[32].

An additional feature that has long been described for the DM/MHC-II interaction is differential sensitivity of MHC-II-peptide complexes to DM action. The factors that influence this interaction and thereby potentially govern DM sensitivity have been posited in past years to include destabilization of hydrogen bonds in the N-terminal region of the bound peptide[268], interaction of DM with the MHC-II P1 pocket[26,226,269], and distortion of the peptide-binding groove[270], among others. For each of these parameters, the underlying affinity of the MHC-II-peptide interaction is predicted to determine the degree of sensitivity to DM action. Indeed, stability of the interaction between MHC-II and peptide has been shown to correlate

with DM sensitivity, with less stable peptide species displaying greater sensitivity to dissociation from the MHC-II peptide-binding groove in the presence of DM[207,270]. Based on resolution of the DM/DR complex, Pos *et al.* proposed a model whereby the strength of interactions between the peptide and the P1 pocket is the primary determinant of DM action[230]. Additional evidence from our group and others, however, suggest that the conformation of the MHC-II-peptide complex more accurately determines its DM sensitivity[4,25,227,271], and this idea is supported by analysis of the effect of residues with different binding properties at various positions in the MHC-II peptide-binding groove on DM sensitivity. Yin *et al.*, for example, demonstrated that P1 pocket occupancy affects peptide kinetic stability, binding affinity, and DM sensitivity, but that these effects can be reversed by substitution of the P9 pocket residue[4]. The differential impact of P1 pocket occupancy vs. conformational properties of the MHC-II-peptide complex on DM sensitivity, particularly for alleles in which DM sensitivity is much less well-described, require further study to definitively determine their contributions as determinants of DM action.

Effects of DO and DM on epitope selection

DM has been shown to be important both in removal of CLIP from the MHC-II binding groove and in editing of antigenic peptides presented at the cell surface, with greater DM activity postulated to result in more stringent editing of the peptide repertoire. The net DM activity resulting from the ratio of DM to DO protein levels (Table 1.1) is therefore posited to influence the content of the immunopeptidome

presented on MHC-II-expressing cells, such that presentation of particular epitopes is reduced by the presence and/or levels of DM[24,207,208,272]. In human transfected cell systems, reduced expression of DM leads to presentation of a set of peptides with lower MHC-II-peptide affinity[29,30]. Examination of presentation of particular epitopes, including those shown to be immunodominant in autoimmune disease, has shown that certain peptides are dependent on DM for presentation (i.e. DM-sensitive), while presentation of other peptides has been shown to be unaffected by DM levels (DM-resistant)[251,272-275]. Similarly, DO expression has been observed to exert differential effects, with presentation increased, decreased, or unchanged, depending on the epitope(s) studied[276-280]. These observations have led to development of a model of epitope immunodominance governed by overall DM activity, whereby epitopes resistant to DM-mediated exchange become more prevalent in the MHC-II peptidome as DM activity increases[207,281-283]. As a competitive inhibitor of DM, DO would therefore function to modulate DM activity and the MHC-II peptidome, as would regulation of DO expression at certain cell developmental transitions. An alternative model for DO action suggests that rather than modifying the immunopeptidome through inhibition of DM editing, the primary function of DO is to focus antigen presentation on late endosomal compartments, based on the fact that the interaction of DM and DO is pH-sensitive[33,36,264,267,279,280]. By tightly binding DM until the endosome becomes very acidic, DO has been suggested to prevent efficient peptide exchange from occurring in early endosomes, resulting in preferential loading of foreign antigens trafficking to late endosomes or lysosomes[253,267,280,284]. A focus on late endo-lysosomes has

been postulated to allow B cells to prioritize presentation of antigens internalized through the BCR, which presumably would not release bound cargo until relatively low pH[262,285]. These proposed functions of DO are not necessarily mutually exclusive, and further experimentation may prove that the mechanism of DO action in fact integrates the two models, such that inhibition of epitope selection by DO and pH susceptibility of the DM/DO interaction together shape the immunopeptidome.

Summary of published studies of DO and DM function in vivo

Limited work has been performed in the context of DO or DM deficiency in vivo, perhaps due to the phenotypes initially described for mouse models targeting DO or DM. In mice lacking DM, CLIP removal and peptide exchange are impaired, resulting in both a restricted MHC-II peptidome as well as defective negative selection of CD4 T cells[165,166,286,287]. Due to almost complete CLIP occupancy of surface MHC-II molecules, the peripheral T cell repertoire is reduced in number by 50-80%[165,286]. DO deficiency, by contrast, has been shown to have a significantly less dramatic effect on the peptide and T cell repertoires. Early studies of the DO-knockout mouse demonstrated effects on antigen presentation, depending on the epitope studied ([276-280] and discussed above). Mass spectrometric analysis of DO-sufficient and -deficient mouse cells has suggested that DO affects the MHC-II peptidome, with a proportion of peptides identified as uniquely presented by both DO-knockout and WT cells[276,280]. DO deficiency has also been reported to result in a mild autoimmune phenotype characterized by increased titers of anti-nuclear

antibodies[288], and ectopic expression of HLA-DO in DCs prevented diabetes onset in the NOD mouse model, reportedly due to altered presentation of self-peptides[253]. Early characterization of the DO$^{-/-}$ mouse also reported increased numbers of CD4 single-positive (SP) thymocytes[276]. These observations, together with DO expression in mTECs[145,147-150], suggest a role for DO in regulating selection of T cells. Differences in the particular peptides selected for presentation as well as the relative amounts of peptides that are selected are expected to be important in APC interactions with T cells. In particular, DO may play a role in negative selection in the thymus, based on its expression in medullary thymic epithelial cells (mTECs), where a diverse set of self-peptides would be most advantageous for efficient clonal deletion of autoreactive T cells. DM and DO may also modulate the density of particular epitopes, potentially further influencing clonal deletion or affecting

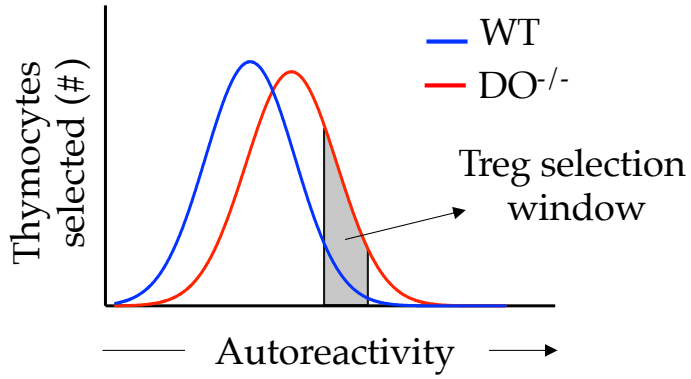

Figure 1.3. Possible effect of DO ablation on T cell selection in the thymus.

diversion of CD4 T cells into the T regulatory (Treg) population (Figure 1.3).

In the context of responses to immunogens or pathogens, few data are available as to the effect of DO and DM (when this project was initiated, no studies had yet examined responses to infection in a DO$^{-/-}$ mouse model.) The role of DM

in mediating selection of viral epitopes was shown in biochemical work demonstrating a link between MHC-peptide stability and immunogenicity of vaccinia virus epitopes[207]. DM function has also been studied in vivo in *Leishmania major* infection, which demonstrated that DM was required for initiation of the CD4 T cell response to an immunodominant *L. major* MHC-II epitope[289]. Humoral immune responses have been shown to be diminished in the absence of DM, both in response to immunization with model antigens as well as following infection with vesicular stomatitis virus[290,291]. DO deficiency has been similarly shown to exert effects on the antibody-mediated response to immunization or infection. An increase in neutralizing antibody titers in $DO^{-/-}$ mice inoculated with retrovirus was recently reported[259], in line with an earlier study from the same group in which DO-deficient B cells were shown to gain preferential access to the GC[292]. Conversely, immunization of $DO^{-/-}$ mice with the model antigens KLH and OVA showed a reduction in IgG antibody responses compared to WT mice, as well as diminished IL-2 and IFN-γ production by CD4 T cells in the absence of DO[288]. Taken together, these data indicate a role for DM and DO in the immune response to pathogens, likely due to effects on presentation of pathogen-derived epitopes.

Scope of thesis

In this work, we sought to understand the effects of the nonclassical MHC-II molecule DO in antigen presentation at the cellular level, as well as to understand the biological consequences of DO in negative selection of T cells and during a response to infection. While the biochemical function of DO as a competitive

inhibitor of DM is clear[32], the biological effects of DO expression have remained much less well understood. DO has been shown previously to have different, often contradictory effects on antigen presentation, depending on the epitope studied[276-280]. To resolve these inconsistencies, we used mass spectrometric (MS) analysis to perform global profiling of the MHC-II self-peptidome in both the presence and absence of DO. Results of these studies demonstrate that DO serves to broaden the MHC-II peptidome, with many more peptides comprising the peptide repertoire. We show that when DO is absent, peptides no longer present in the peptidome are sensitive to DM editing. Due to the fact that MHC-II expression remains unchanged, more abundant peptides are also presented at greater density in the absence of DO. These data demonstrate that DO alters the composition of the immunopeptidome by both increasing its diversity and modifying the distribution of more abundant peptides.

Given that DO expression has been demonstrated in the thymus, we sought to examine its function in selection of the CD4 T cell repertoire. We show via sequencing of TCRα chains in a TCRVβ transgenic mouse model that the predominant effect of DO is on the Treg population, with clonotypic diversity substantially diminished when DO is absent due to increased frequencies of highly abundant clonotypes. Using a mouse model of DO deficiency, we demonstrate that the frequency of Tregs is augmented, and that these Tregs are more activated and exhibit greater suppressive capacity compared to Tregs selected in the presence of DO. Despite enhanced frequency and function of Tregs, $DO^{-/-}$ mice displayed elevated levels of anti-nuclear antibodies, in agreement with an earlier report[288].

Based on our observation that DO$^{-/-}$ Tregs have a reduced capacity to differentiate into GC-resident Tregs, we postulate that an aberrant GC reaction results in development of hallmarks of autoimmunity in DO$^{-/-}$ mice. Using a model of experimental Sjogren's syndrome, we show that mice deficient in DO are more predisposed to development of autoimmunity, with a similar reduction in GC-resident Tregs. We thus describe a previously unexplored function for DO in selection of the Treg lineage, as well as demonstrate consequences of perturbation of DO expression in autoimmunity.

DO has been shown previously to exert effects in models of immunization and infection, primarily with regard to antibody-mediated effects[259,288]. We reasoned that due to the multitude of epitopes presented on MHC-II molecules during influenza infection, for which T cell responses have also been reported[293], influenza would serve as an opportune model antigen to study the effect of DO on modulation of epitope hierarchy. We expected in the absence of DO that DM activity would be augmented, that immunodominant epitopes would be presented to a greater degree, and that such an effect would therefore enhance the immune response to influenza A. Instead, we observed a marked delay in recovery from influenza A infection in DO$^{-/-}$ mice as well as increased morbidity. We observed altered antigen presentation by DO-deficient APCs, reduced CD4 and CD8 epitope-specific responses, and decreased cytokine responses. Based on our observation that Tregs are increased when DO is absent, we hypothesized that the suppressed immune response in DO$^{-/-}$ mice was due to overactive Tregs. Treg depletion studies

proved difficult to interpret, however, and so the basis for the phenotype we observed is currently unclear.

In summary, we have delineated the effect of the non-classical MHC-II molecule DO at the cellular level, as well as identified novel functions of DO in T cell selection and influenza A epitope presentation. These data impact the understanding of biological processes critical for tolerance and immunity and have the potential to aid in development of therapeutics to treat autoimmune disease and infectious disease.

CHAPTER II

HLA-DO modulates the diversity of the MHC-II self-peptidome

This chapter corresponds to a manuscript published in Molecular and Cellular Proteomics:

Nanaware P.P, **Jurewicz M.M.**, Leszyk J.D., Shaffer S.A., and Stern L.J. (2019). HLA-DO modulates the diversity of the MHC-II self-peptidome.

Author contributions

The work I performed in this chapter included generation and characterization of the HLA-DO-deficient B cell lines, RNAseq analysis, isolation of B cells for MS experiments, and mouse immunization experiments.

Abstract

Presentation of antigenic peptides on MHC-II molecules is essential for tolerance to self and for initiation of immune responses against foreign antigens. DO (HLA-DO in humans, H2-O in mice) is a non-classical MHC-II protein that has been implicated in control of autoimmunity and regulation of neutralizing antibody responses to viruses. These effects likely are related to a role of DO in selecting MHC-II epitopes, but previous studies examining the effect of DO on presentation of selected CD4 T cell epitopes have been contradictory. To understand how DO modulates MHC-II antigen presentation, we characterized the full spectrum of peptides presented by MHC-II molecules expressed by DO-sufficient and DO-deficient antigen-presenting cells in vivo and in vitro using quantitative mass spectrometry approaches. We found that DO controlled the diversity of the presented peptide repertoire, with a subset of peptides presented only when DO was expressed. Antigen-presenting cells express another non-classical MHC-II protein, DM, which acts as a peptide editor by preferentially catalyzing the exchange of less stable MHC-II peptide complexes, and which is inhibited when bound to DO. Peptides presented uniquely in the presence of DO were sensitive to DM-mediated exchange, suggesting that decreased DM editing was responsible for the increased diversity. DO-deficient mice mounted CD4 T cell responses against wild-type antigen-presenting cells, but not vice versa, indicating that DO-dependent alterations in the MHC-II peptidome could be recognized by circulating T cells. These data suggest that cell-specific and regulated expression of HLA-DO serves to fine-tune MHC-II peptidomes, to enhance self-tolerance to a wide spectrum of

epitopes while allowing focused presentation of immunodominant epitopes during an immune response.

Introduction

Antigen presentation by MHC-II molecules is required for development of CD4 T cells and regulation of CD4-mediated cellular and humoral immune responses. The non-classical MHC-II molecule DO has been implicated in modulating immune responses to both self and foreign antigens. Mouse strains with inactive H2-Ob genes have increased neutralizing antibody responses to some persistent viruses[259], possibly related to increased ability of DO-deficient B cells to enter the germinal center[292], and HLA-DO variants in humans have been associated with resistance to HBV and HCV[259]. DO knockout (DO-KO) mice also exhibit increased titers of autoantibodies, together somewhat paradoxically with decreased antibody responses to immunized protein antigens[288]. DO expression is regulated differently from the coordinate regulation of other proteins involved in MHC-II antigen processing[263], with expression restricted to medullary thymic epithelial cells, immature dendritic cells (DCs), and mature B cells[137,149,261,262]. DO expression is also downregulated following entry of B cells into the germinal center and following maturation of DCs[101,111,112,131,141,262], coinciding with the onset of inflammation. This pattern of expression suggests a potential role for DO in maintenance of T cell tolerance. Ectopic overexpression of DO in dendritic cells has been shown to prevent diabetes in NOD mice, consistent with this idea[253], and CD4 T cells from DO-KO mice show differential TCRBV usage, also indicating a potential role for DO in regulating T cell selection in the thymus[276,288].

Presumably, these effects of DO result from modulation of MHC-II antigen processing. DO is posited to regulate peptide loading onto classical MHC-II

proteins through interaction with the MHC-II peptide-exchange factor DM[5], which is required for efficient MHC-II peptide exchange[20,22] and which has been shown to control CD4 epitope selection[207,230,272,281]. DO has been shown to act as a tight-binding competitor of DM[32,36,37]. The inhibition of DM by DO is pH-dependent, potentially restricting efficient antigen presentation to low pH late endosomal compartments[33,267,279,285]. Several studies have shown that DO-KO murine and human cells have alterations in MHC-II antigen presentation[111,262,276-279,294]. However, in these studies, the effect of DO seems to vary with the epitope studied, with presentation of particular peptides increased, decreased, or unchanged by expression of DO[276-280]. This variation is difficult to reconcile with the biochemical effect of DO as a competitive inhibitor of DM, and the fundamental question of how DO affects the overall spectrum of MHC-II bound peptides has remained unanswered.

To definitively determine the role of DO in modulating the MHC-II peptidome, we used CRISPR/Cas9 gene editing to target DO in a human lymphoblastoid cell line and characterized MHC-II bound peptides from DO-deficient and DO–sufficient cells by quantitative mass spectrometry. We found that DO regulates the diversity of MHC-II antigen expression, by increasing the number of different peptides presented without changing the overall MHC-II expression level. Many low abundance peptides were presented only in the presence of DO. We confirmed these observations using a mouse model of DO deletion and determined through immunization experiments that the immune system is sensitive to these DO-dependent alterations in the peptide repertoire. This work defines a

role for DO in mediating qualitative and quantitative changes in the MHC-II peptidome and provides a mechanistic basis for the biological consequences of DO expression.

Results

Generation and validation of DO-KO and WT clones

In order to study the effect of DO on the self-peptide repertoire, we used CRISPR/Cas9 gene editing to delete HLA-DO from the HLA-DR-expressing lymphoblastoid cell line LG-2. Following transfection of sgRNAs, cellular clones were isolated, expanded, and sequenced to evaluate DNA modifications at target sites in HLA-DOβ exon 1 (Figure 2.1A). A clone (DO-KO-1) targeted by sgRNA-1 was shown to harbor 1-nt and 7-nt deletions, while a clone targeted by sgRNA-2 (DO-KO-2) showed 1-nt and 4-nt deletions. An additional clone (WT) – subjected to the identical transfection process with sgRNA-2 but without any modifications in the HLA-DOβ locus on either chromosome – was selected as a control. Deletion of DOβ was confirmed by western blot in DO-KO cells (Figure 2.1B). HLA-DM and HLA–DR expression was determined by FACS analysis to be consistent among all clones (Figure 2.1C-E). To examine presentation of specific epitopes previously demonstrated to be DM-sensitive (CLIP) or DM-resistant ($A2_{[104-117]}$), we used antibodies specific for their DR-bound forms (CerCLIP and UL-5A1, respectively). Expression of CerCLIP was decreased ~2-fold in DO-KO clones compared to WT,

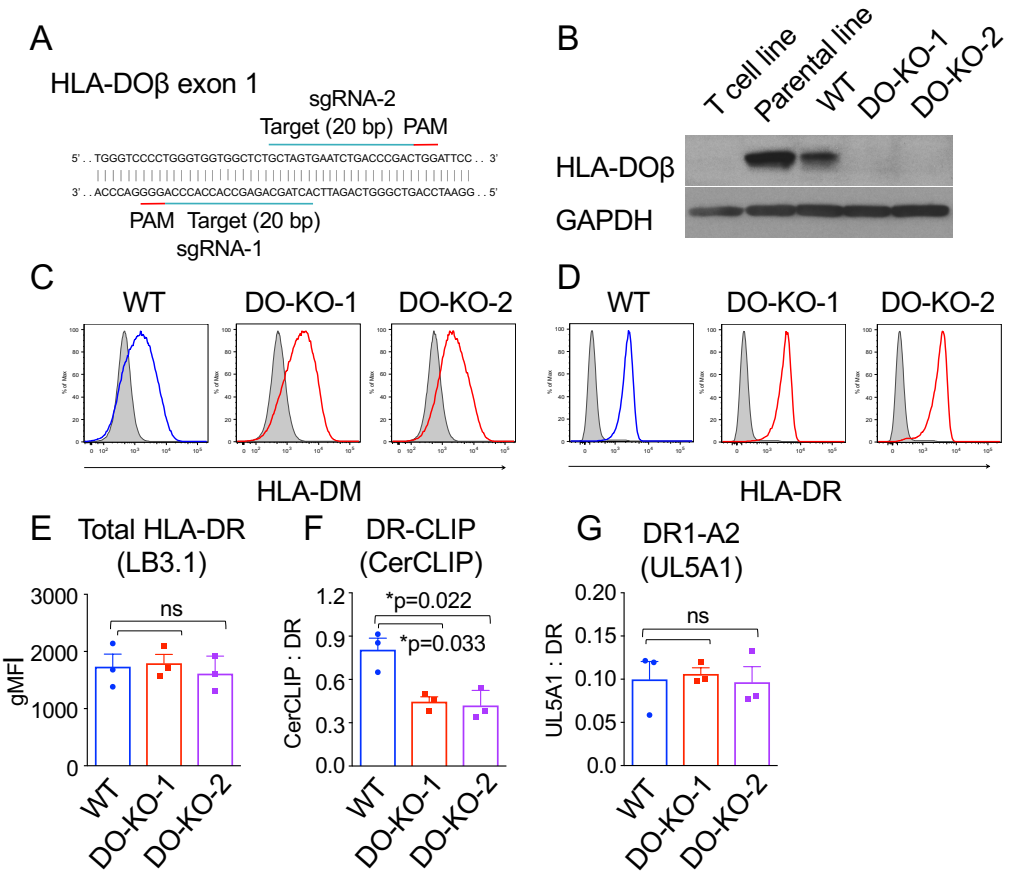

Figure 2.1. Generation of DO-KO and WT clones. (A) sgRNAs and target sequences for HLA-DO knockout. (B) Western blot for HLA-DOβ performed with lysates from indicated cell lines. (C,D) Intracellular HLA-DM (C) and surface HLA-DR (D) expression are similar among WT and DO-KO clones by FACS analysis. Isotype controls, gray. (E,F,G) Surface expression of peptide-MHC complexes, using mAbs LB3.1 (total HLA-DR), CerCLIP (DR-CLIP[3]), and UL5A1 (DR1-A2$_{104-117}$). Mean ± SD (n=3) shown. Paired parametric t-test used to calculate p-values. gMFI, geometric mean intensity.

while expression of UL-5A1 was unchanged (Figure 2.1F-G), consistent with the expected DO inhibition of DM editing activity.

Reduced HLA-DR immunopeptidome presented by DO-KO compared to WT cells

To evaluate the influence of HLA-DO on the full spectrum of peptides presented by MHC-II, we characterized the immunopeptidomes presented by HLA-DR1 from DO-KO and WT cells. We purified HLA-DR1 from DO-KO-1 and WT clones by immunoaffinity, released peptides by acid treatment, and characterized the resultant peptide pools by HPLC/MS/MS using a high-sensitivity mass spectrometer with search parameters set to provide a conservative false discovery rate. Similarly to

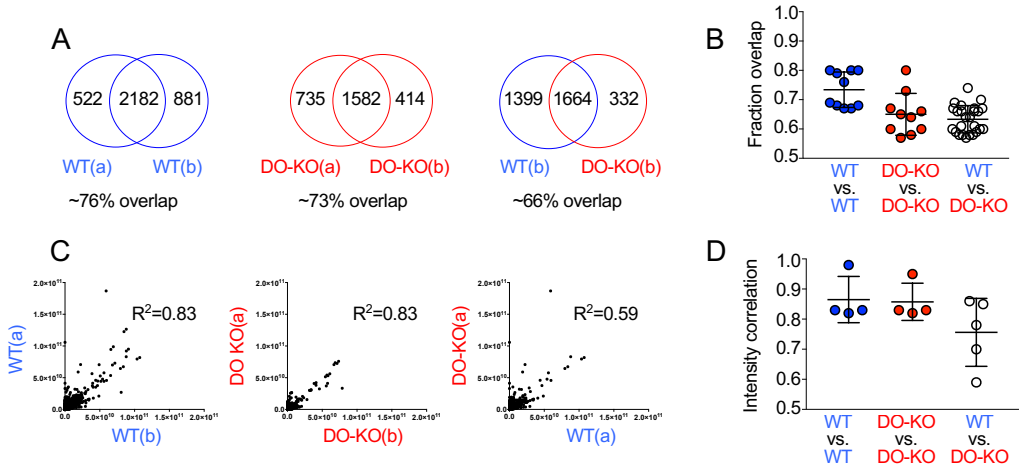

Figure 2.2. Qualitative and quantitative mass spectrometry analysis. (A,B) Data-dependent acquisition analysis, comparing peptide sequences identified in fragmentation spectra (MS/MS) of WT and DO-KO samples. (A) Overlap between replicate WT samples (WT[a]) and WT[b]), replicate DO-KO-1 samples (DO-KO[a] and DO-KO[b]), or between WT and DO-KO-1 samples. Each sample was analyzed in triplicate with peptide lists combined. (B) Peptide identification overlap for all pairwise combinations of 5 WT samples and 5 DO-KO-1 samples. (C,D) Data-independent acquisition analysis, comparing intensities in parent ion (MS1) spectra of ion signatures (frames) identified in both WT and DO-KO-1 samples. (C) Correlation of intensities in various samples analyzed in panel B. (D) MS1 intensity correlation for all pairwise combinations of 5 WT and 5 DO-KO-1 samples.

previous comparative immunopeptidome reports[43,295,296], we observed ~70% overlap between peptides identified in replicate WT or DO-KO samples (Figure 2.2A-B). Integrated parent ion peak areas were highly reproducible sample-to-sample (Figure 2.2C-D), while overlap of WT and DO-KO samples was

comparatively lower (Figure 2.2A-D). A total of 6116 distinct peptide sequences were identified in 5 samples of WT cells (Figure 2.3A), similar to the numbers of

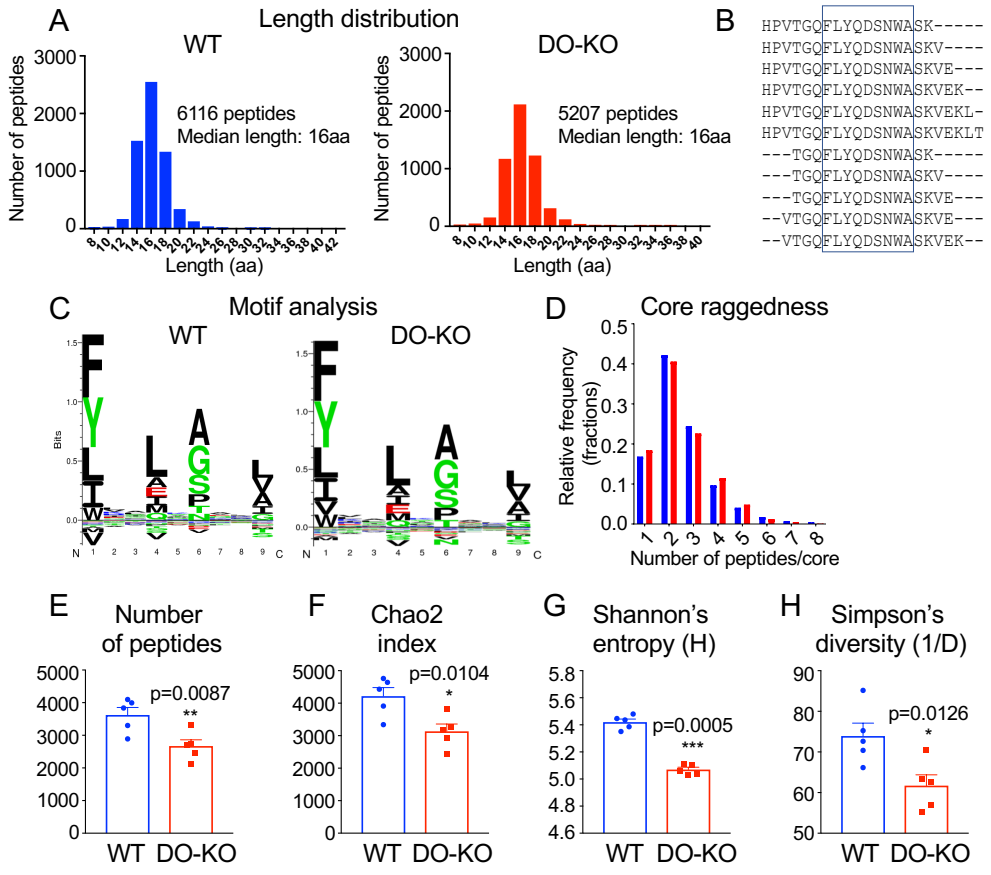

Figure 2.3. DO expression results in presentation of a greater number of peptides. (A) Similar length distribution of eluted peptides. B) Core epitope illustrated for nested set of peptides from human transferrin receptor. (C) Similar sequence motifs within aligned core sequences for WT and DO-KO-1 cells. (D) Similar trimming of peptides for WT vs. DO-KO-1. (E) Species richness. The number of unique peptides eluted from WT was significantly greater than for DO-KO-1 in each of 5 independent experiments. (F,G,H) Diversity indices. Chao2 index (F), Shannon's entropy (G) and Simpson's reciprocal diversity index (H) are greater for WT than for DO-KO-1, calculated for peptides observed in each of five biological replicates of both WT and DO-KO-1. Paired parametric t-test used to calculate p-values.

peptides identified in recent high-density immunopeptidome studies for other human and mouse MHC proteins[296]. A smaller number of peptides, 5207, was identified in samples from DO-KO-1 cells processed in parallel (Figure 2.3A).

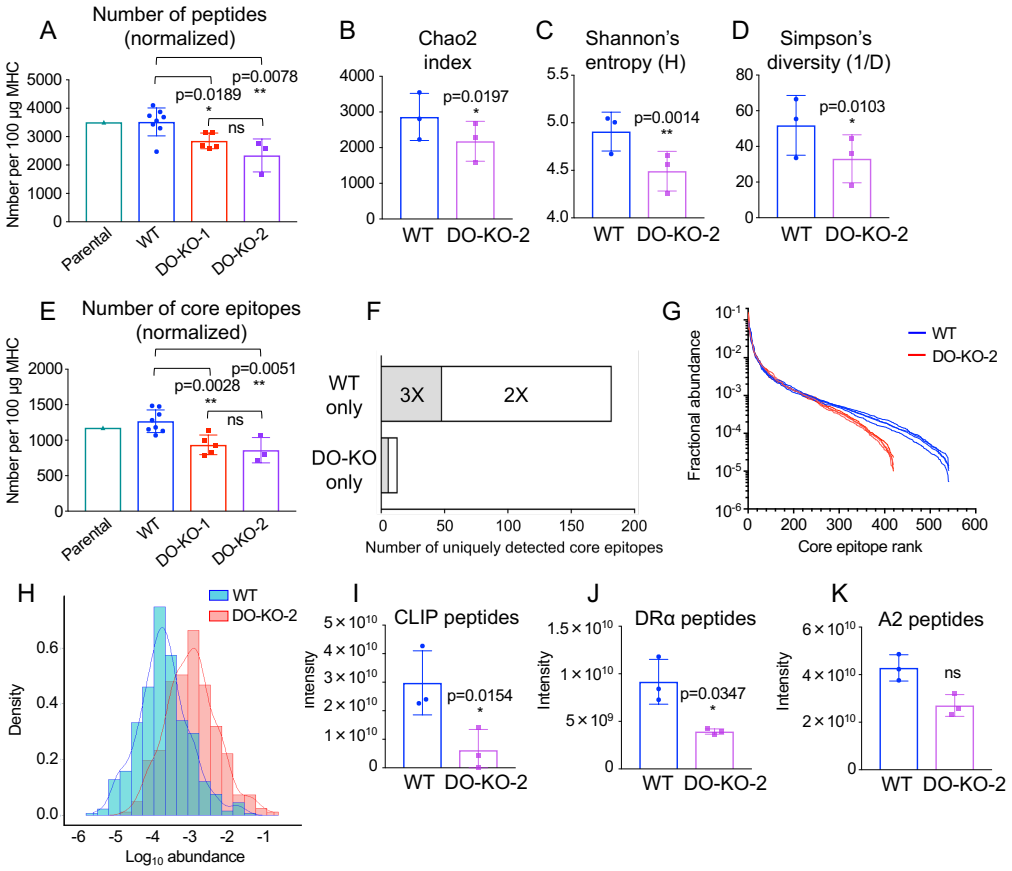

Figure 2.4. Identification and characterization of peptides from DO-KO-2. (A) Peptides were eluted from WT and DO-KO Clone 2 (DO-KO-2) independently in 3 different experiments, peptides from WT and DO-KO Clone 1 (DO-KO-1) were eluted i in 5 different experiments, and peptides were eluted once from the parental LG2 line as a control. The number of peptides eluted in each biological sample is represented as the normalized number of peptides/100µg HLA-DR1. The number of peptides eluted from all WT replicates is significantly greater than for DO-KO-1 and DO-KO-2. Mean ± SD for all biological replicates is shown, and an unpaired nonparametric Mann-Whitney test was used to calculate p-values. (B,C,D) Chao2 (B), Shannon's entropy (C) and Simpson's diversity (D) indices indicate the WT peptidome is more diverse than the DO-KO-2 peptidome. Mean ± SD is shown, and a paired parametric t-test was used to calculate p-values. (E) The normalized number of core epitopes/100µg of HLA-DR1 was analyzed as described in the main text. The WT peptidome is comprised of a greater number of epitopes as compared to the peptidomes of DO-KO-1 and DO-KO-2. Mean ± SD for all biological replicates is shown, and an unpaired nonparametric Mann-Whitney test was used to calculate p- values. (F) Greater numbers of unique core epitopes are identified in WT as compared to DO-KO-2 samples. Bar shading indicates number of replicate samples for which the core epitope was identified. For example, the gray bar labeled "3X" indicates epitopes identified in each of 3 WT samples and none of the 3 DO-KO-2 samples, the light bar labeled "2X" indicates samples identified in 2/3 WT samples and no DO-KO-2 samples, etc. (G) Rank abundance plot. Fractional intensity of core epitopes from WT (blue) or DO-KO-2 (red) in each biological sample is represented as an individual line. (H) Histogram of fractional intensities of core epitopes, overlaid with a kernel density plot. (I,J,K) A set of peptides with known DM sensitivity was analyzed as described in the main text. Amounts of the DM-sensitive peptides CLIP (I) and DRα (J) were greater in WT cells as compared to DO-KO-2 cells. Amounts of the DM-resistant A2 peptides (K) were unaffected. Mean ± SD is shown, and a paired parametric t-test was used to calculate the p-values.

A broad distribution of peptide lengths centered around 15-16 residues was observed similarly for both WT and DO-KO-1 (Figure 2.3A). As is typical for MHC-II peptidomes, many peptides were present as nested sets surrounding a common core epitope. This is illustrated in Figure 2.3B for 11 peptides from the human transferrin receptor protein, found in both WT and DO-KO, which share the FLYQDSNWA core that binds to HLA-DR1 (Figure 2.3B). We used the MHC-II binding prediction resource NetMHCIIpan3.1[297] to predict 9-residue HLA-DR1-binding cores for each of the eluted peptides. Sequence preferences within these cores were essentially identical for WT and DO-KO-1 (Figure 2.3C), as was the average number of nested peptides per core and their distribution (Figure 2.3D). Thus, many features of the HLA-DR1 peptidome were not significantly altered as a result of DO.

The most apparent difference between WT and DO-KO peptidomes was that in the absence of DO, fewer different peptide sequences were presented. For each of 5 replicate sets of WT and DO-KO-1 cultures processed in parallel, or 3 replicate sets for WT and DO-KO-2, fewer peptides were isolated from DO-KO than from WT (Figure 2.3E, 2.4A). In biodiversity analysis, the number of different species ("richness") is considered to be a primary criterion of diversity, but other diversity measures are available that differentially weight the contribution of rare versus abundant species[298]. The Chao2 index provides an extrapolated estimate of the total richness including rare species missed by undersampling[299]. The Shannon diversity index considers the relative abundance of different species, with even distributions assigned higher diversity values than skewed distributions. Simpson's

entropy also considers relative abundance, preferentially weighting more abundant species[298]. By all of these measures, diversity was significantly larger for the set of peptides eluted from WT as compared to DO-KO-1 (Figure 2.3F-H) or DO-KO-2 (Figure 2.4B-D).

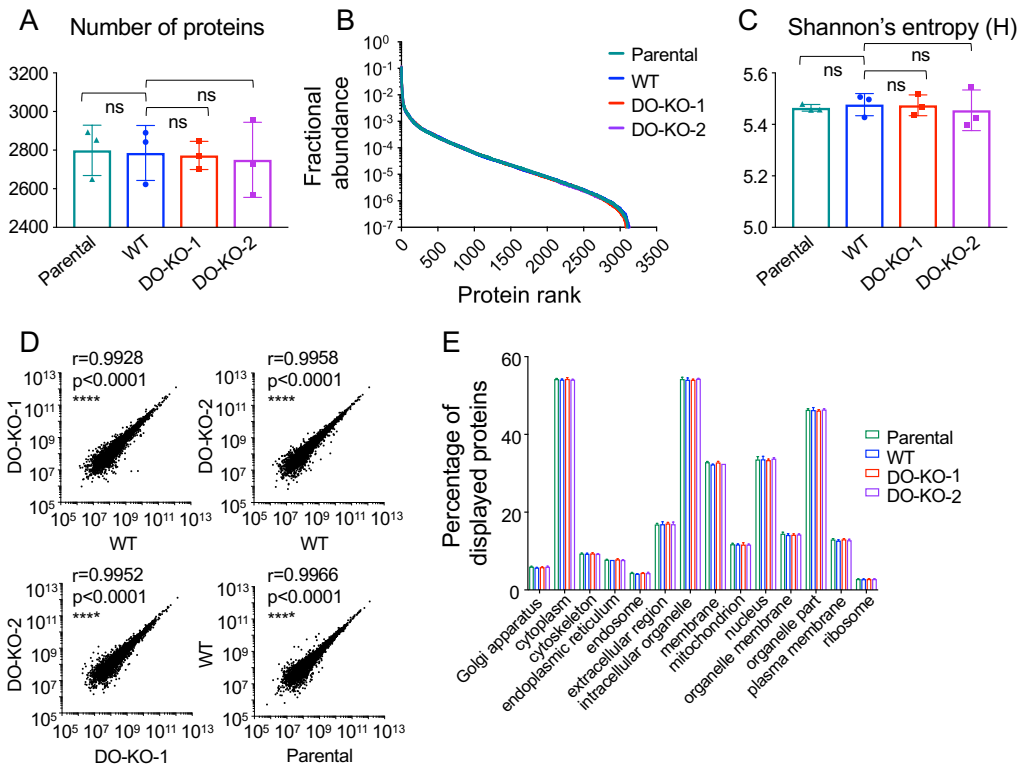

Figure 2.5. Whole-cell proteomic analysis of WT and DO-KO clones. (A) Whole proteomes from parental, WT, DO-KO-1 and DO-KO-2 were analyzed in 3 independent experiments. Numbers of proteins identified were not significantly different between parental, WT and DO-KO clones. (B) Rank abundance plot. Average fractional intensity of proteins from parental (green), WT (blue), DO-KO-1 (red) and DO-KO-2 (purple) are represented as an individual line. (C) Shannon's entropy did not show any significant differences between different sample types. Mean ± SD is shown, and a paired parametric t-test was used to calculate p-values. (D) Protein intensity correlation plot between different sample types showed a strong Pearson's correlation coefficient as indicated. (E) Source protein cellular component analysis using GO terms shows similar overall subcellular localization distribution of proteins in parental, WT, DO-KO-1 and DO- KO-2 cells. No significant differences were observed between WT and DO-KO samples using elution data from 3 independent experiments (a multiple t-test correction using the Benjamini, Krieger and Yekutieli method was performed to adjust the p-value.)

Validation of immunopeptidome differences

We investigated several potential explanations for the reduced number of peptides observed for DO-KO cells. We used whole-cell quantitative proteomics to determine whether deletion of DO had any effect on overall protein levels; no significant skewing was observed (Figure 2.5). We used RNASeq to evaluate potential alterations due to CRISPR/Cas9 off-targeting effects. Both the DO-KO clones and the WT clone exhibited some changes in gene expression compared to

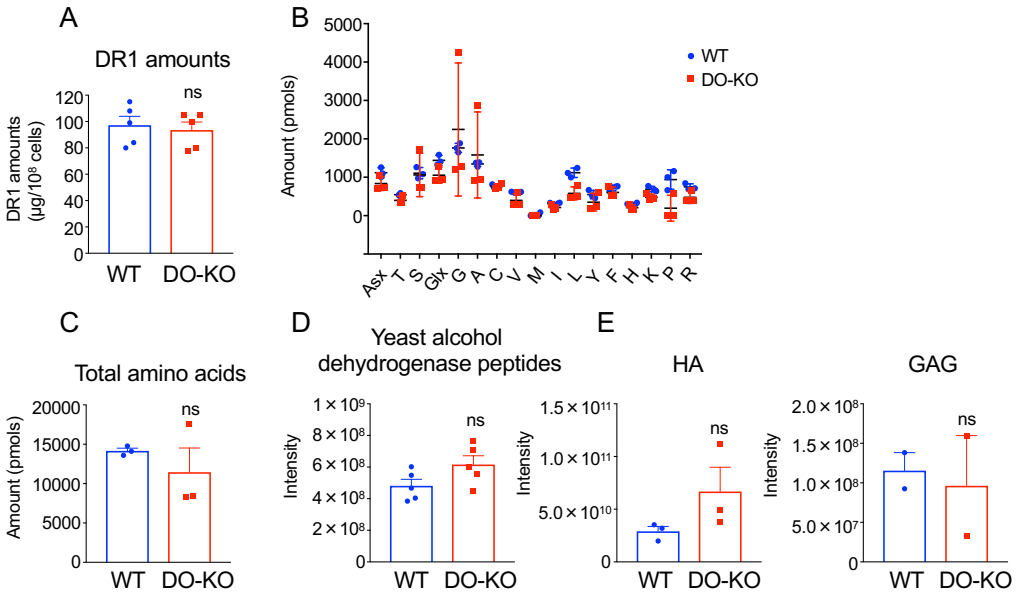

Figure 2.6. Equal amounts of DR1, eluted amino acids and mass spectrometry controls were detected in WT and DO-KO-1 samples. (A) To ensure that equal amounts of DR1- peptide complexes were used for peptide elution from WT and DO-KO cells, amounts of DR1 from the extracted membrane fraction was determined by ELISA, for all independent experiments. In every experiment, equal amounts of DR1 were present in the WT and DO-KO membrane fractions. **(**B,C) Amino acid analysis of peptides from WT and DO-KO was performed to ensure that equal amounts of peptides were eluted. Similar amounts of individual amino acids (B) were found in WT (blue) and DO-KO (red) in 3 independent experiments. Analysis of the total number of amino acids (C) in WT and DO-KO indicates similar total amounts of amino acids were eluted from both sets of cells. Mean ± SD is shown, and a paired parametric t-test was used to calculate p-values. (D) Yeast alcohol dehydrogenase peptides were spiked into the pools of eluted WT and DO-KO peptides as controls and were detected at equal levels in WT and DO-KO. (E) DR1-GAG (3 experimental replicates) or DR1-HA (2 experimental replicates) peptide complexes were spiked into the membrane fractions of WT and DO-KO clones as controls to ensure equal recovery of total peptides in WT and DO-KO. GAG and HA peptides were detected without any significant differences between WT and DO-KO.

the parental LG-2 line, but there was no correlation of these differences with peptides differentially present in WT or DO-KO, and clustering of functional annotations for differentially-expressed genes did not indicate any systematic effect on antigen presentation pathways. The reduced number of peptides in DO-KO potentially could be explained by elution of peptides from fewer MHC molecules, but the amounts of HLA-DR1 purified from WT and DO-KO cells were not different (Figure 2.6A), consistent with cell surface expression levels (Figure 2.1). Peptides from recombinant peptide-MHC complexes spiked into cell lysates before immunoaffinity isolation as internal controls were recovered similarly for WT and DO-KO samples (Figure 2.6E), indicating that differential purification did not contribute significantly to the observed differences. For 3 pairs of samples, we removed a fraction of the eluted peptide mixture and measured the total amount of peptide by quantitative amino acid analysis. No significant differences in the total amount of peptidic material were observed between the samples (Figure 2.6B), indicating that the elution efficiency did not differ between WT and DO-KO. In addition, no significant differences in the distribution of amino acid residues was observed (Figure 2.6C), suggesting that the observed differences between WT and DO-KO were not due to factors such as overall hydrophobicity, which can limit the ability to volatilize and enter the spectrometer for analysis. Sample-dependent factors that could suppress ionization did not contribute to differential detection of peptides in WT and DO-KO samples, as control peptides from yeast alcohol dehydrogenase spiked into each sample were detected with similar efficiency (Figure 2.6D). Thus, the reduced number of peptides identified for DO-KO as

compared to WT samples represents an actual difference in the cellular peptide abundances and is not a consequence of experimental factors.

Fewer epitopes presented in the absence of DO

As each peptide in a nested set represents a different version of the same epitope, we asked whether DO deletion reduced the number of distinct epitopes presented

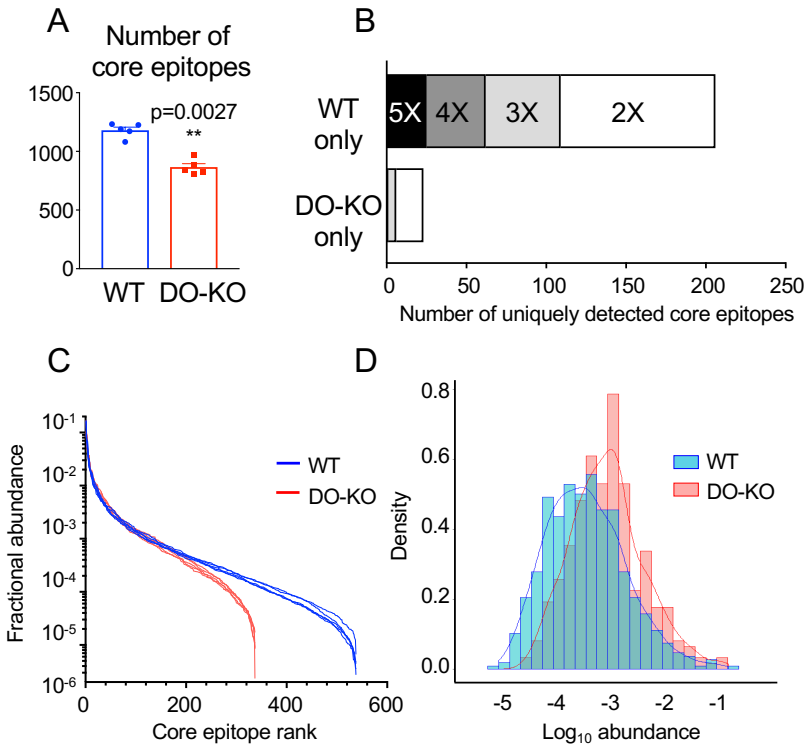

Figure 2.7. DO expression results in presentation of greater numbers of and a broader distribution of core epitopes. (A) The number of unique core epitopes observed in WT was significantly greater than for DO-KO-1 cells in each of 5 independent experiments. Mean ± SD (n=5) shown. Paired parametric t-test used to calculate p-values. (B) More core epitopes are identified uniquely in WT as compared to DO-KO-1 samples. Bar shading indicates number of replicate samples for which the core epitope was identified. For example, the black bar labeled "5X" indicates epitopes identified in each of 5 WT samples and none of the 5 DO-KO-1 samples, the dark gray bar labeled "4X" indicates samples identified in 4/5 WT samples and no DO-KO-1 samples, etc. (C) Rank abundance plot. Fractional intensity of core epitopes from WT (blue) or DO-KO-1 (red) in each biological sample is represented as an individual line. (D) Histogram of fractional intensities of core epitopes, overlaid with a kernel density plot.

as it did the number of individual peptides. We combined records for each peptide sharing the same core epitope, thus counting each set of related epitopes only once. DO-KO-1 and DO-KO-2 cells presented fewer core epitopes then did WT cells, with each DO-KO replicate having fewer cores than WT samples processed in parallel (Figure 2.7A, Figure 2.4E).

To help understand the greater diversity of epitopes presented by WT as compared to DO-KO cells, we looked for core sequences present in both peptidomes, or unique to only WT or DO-KO. Of 704 distinct core epitopes detected in each of the 5 WT replicates tested, 25 core sequences were not detected in any of the DO-KO-1 samples. By contrast, only one core epitope was present in each of the DO-KO-1 samples but was not detected in any of WT samples (Figure 2.7B). This same pattern held if we relaxed the identification criteria and considered peptides present in fewer replicates. For example, 37 additional core epitopes were present in 4 of the 5 WT replicate samples but were absent from any DO-KO-1 sample, whereas no additional core epitopes were detected in 4 of 5 DO-KO-1 samples and were absent from any WT sample. A similar pattern was observed for the second DO-deficient clone DO-KO-2, although in this case the test is less stringent due to the fact that only three replicates samples were analyzed (Figure 2.4). Overall, the WT peptidome appears to contain many peptides that are absent from or present at much lower frequency in the DO-KO peptidome.

One method to visualize diversity is by a rank abundance plot, in which the relative abundance of each species is plotted on a logarithmic scale against the species rank (i.e. 1 for the most abundant species, 2 for the next most abundant,

etc.). This analysis shows a steeper profile for DO-KO-1 as compared to WT, with the WT curve showing a more even distribution and a long tail, indicating that many more low-abundance peptides are present in WT as compared to DO-KO-1 (Figure 2.7C). Since the total molar amount of MHC (and peptide) present in WT and DO-KO samples was identical (Figure 2.6A), this would imply that the average fractional abundance of peptides in the DO-KO-1 samples was higher than for WT, as the same total amount of peptide was represented by fewer different sequences. This can be seen in the density plot (histogram) of abundances of identified core epitopes, which shows a slight shift to higher abundances for the DO-KO peptides (Figure 2.7D). Similar shifts in rank abundance and density plots were observed for DO-KO-2 relative to WT samples processed in parallel (Figure 2.4G-H). Thus, one component of the increased diversity of WT as compared to DO-KO peptidomes is an increased representation of lower-abundance species.

Validation of intensity differences

Although individual peptides are detected in the mass spectrometer with different efficiencies depending on their charge, hydrophobicity and other factors, parent ion intensities as used above in diversity and rank abundance analysis provide reliable quantitation when averaged over many ions[300]. To validate the quantitation of individual peptides, we used a stable isotope-labeling approach, in which synthetic peptides carrying ^{13}C and/or ^{15}N labels were introduced into eluted peptide samples before analysis and used as internal standards. Using volcano plot analysis (Figure 2.9D), we selected 9 peptides: 1 with parent ion intensities greater in WT than in

DO-KO samples, 2 with intensities greater in DO-KO than in WT samples, and 6 with intensities approximately equal between the samples. We used the most abundant peptide containing each core epitope for analysis. The peptides sampled a range of masses, charges, hydrophobicities, and observed intensities. For most of the peptides, both +3 and +4 ions were observed; these were summed for the quantitation. A good correlation was observed between the observed intensities and the calculated amounts of peptides present (Figure 2.8A), validating the peak

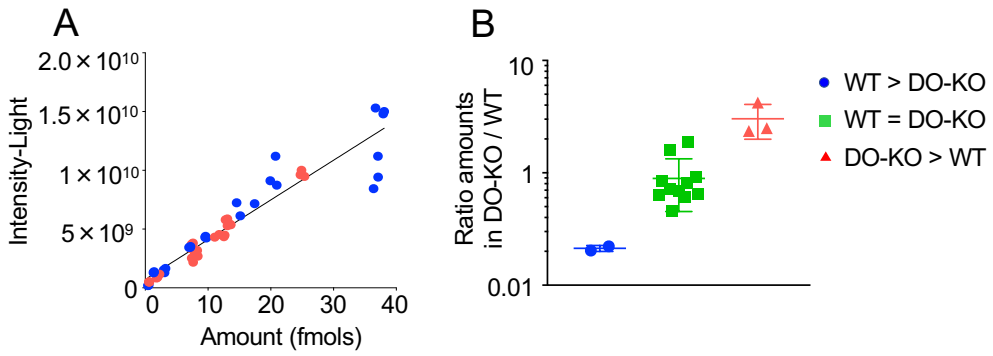

Figure 2.8. Stable isotope-labeled peptide analysis validates MS1 intensity analysis. (A) Observed intensity versus amount measured using ^{13}C- and ^{15}N-labeled internal standards, for 9 selected peptides, each assayed in 3 replicate injections of a WT (blue) or DO-KO-1 (red) sample. Pearson correlation coefficient indicated. (B) Observed DO-KO-1/WT abundance ratio for peptides selected from groups with intensity greater in WT than DO-KO (blue), approximately equal intensity in WT and DO-KO (green), or greater in DO-KO than WT (red). Mean ± SD shown (n=3-10).

integration and sample normalization procedures. Three replicates of one peptide fell off the line defined by the other peptides, presumably due to sequence-specific factors. The calculated amount of each peptide present in the WT and DO-KO eluates was used to determine an abundance ratio, which varied 20-fold between peptides, and which clearly distinguished peptides in the WT>DO-KO, WT≈DO-KO, and DO-KO>WT sets (Figure 2.8B).

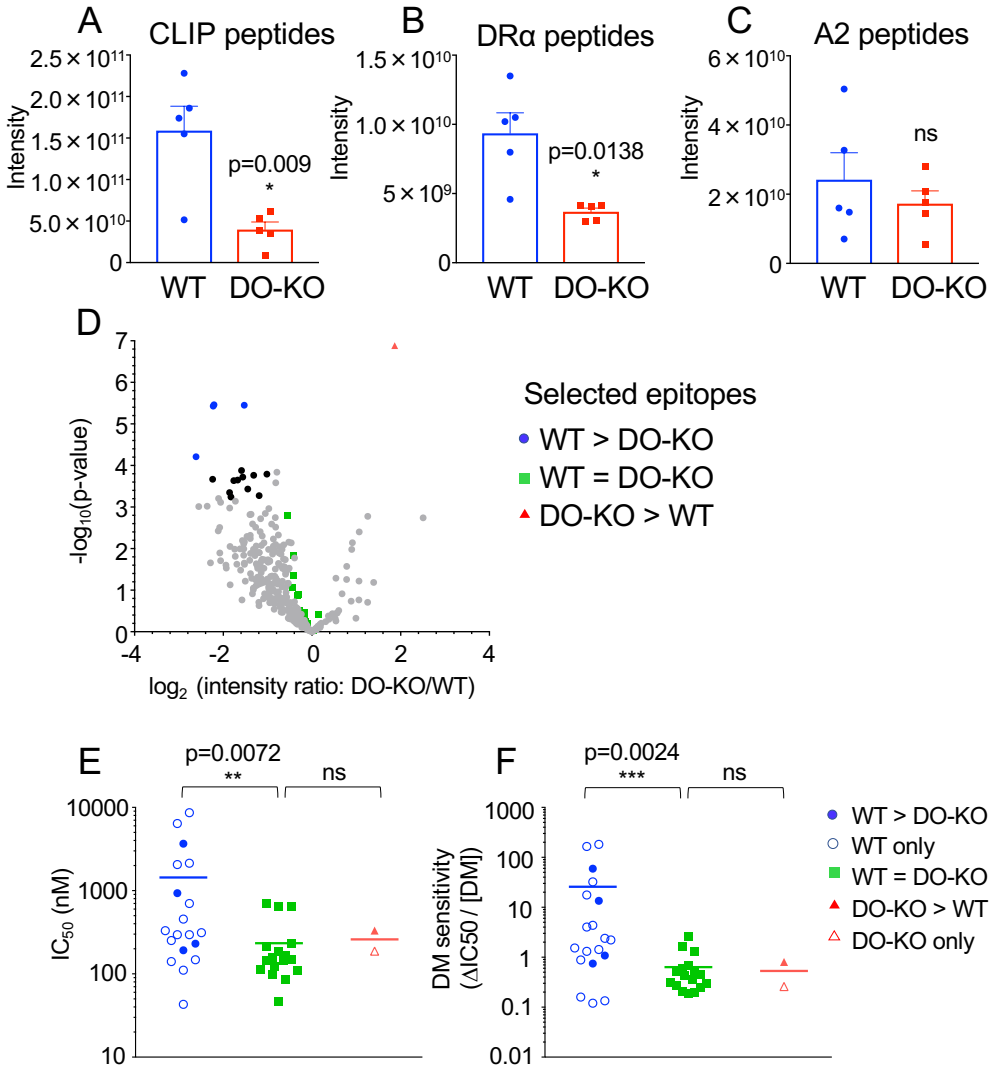

Figure 2.9. DO expression increases presentation of low affinity and DM-sensitive peptides. (A-C) Relative abundance levels for peptides with known DM sensitivity were analyzed in 5 WT and DO-KO-1 samples: DM-sensitive CLIP peptides [1] with core epitope MRMATPLLM (A), DM-sensitive DRα peptides [2] with core epitope FASFEAQGA (B), and DM-resistant A2 peptides [4] with the core epitope WRFLRGYHQ (C). Mean ± SD (n=5) shown. Paired parametric t-test used to calculate p-values. **(**D) Volcano plot for cores identified in each of all 5 biological samples for WT and DO-KO-1 samples. Cores with intensity ratio differences >2-fold and p-values <5.75E-04 (Benjamini-Hochberg-adjusted) are shown as black dots. Cores showing significant differences and selected for binding affinity studies, DM sensitivity studies and absolute quantification studies are shown in blue for WT>DO-KO, red for DO-KO>WT, and green for WT≈DO-KO. (E) Binding affinity was characterized for sets of peptides observed in DO-KO only (1 peptide), WT only (15 peptides), or for peptides with intensities of WT>DO-KO (4 peptides), WT<DO-KO (1 peptide), or WT=DO-KO (17 peptides). (F) The DM sensitivities for the same sets of peptides were assessed. Mean ± SD from 3 independent experiments shown for all peptides in each group; unpaired nonparametric Mann-Whitney test used to calculate p-values.

Analysis of epitope source protein intracellular localization

Because DO has been suggested to control the intracellular location of antigen loading through its effects on DM[34,267,285,301], we evaluated the GO-annotated

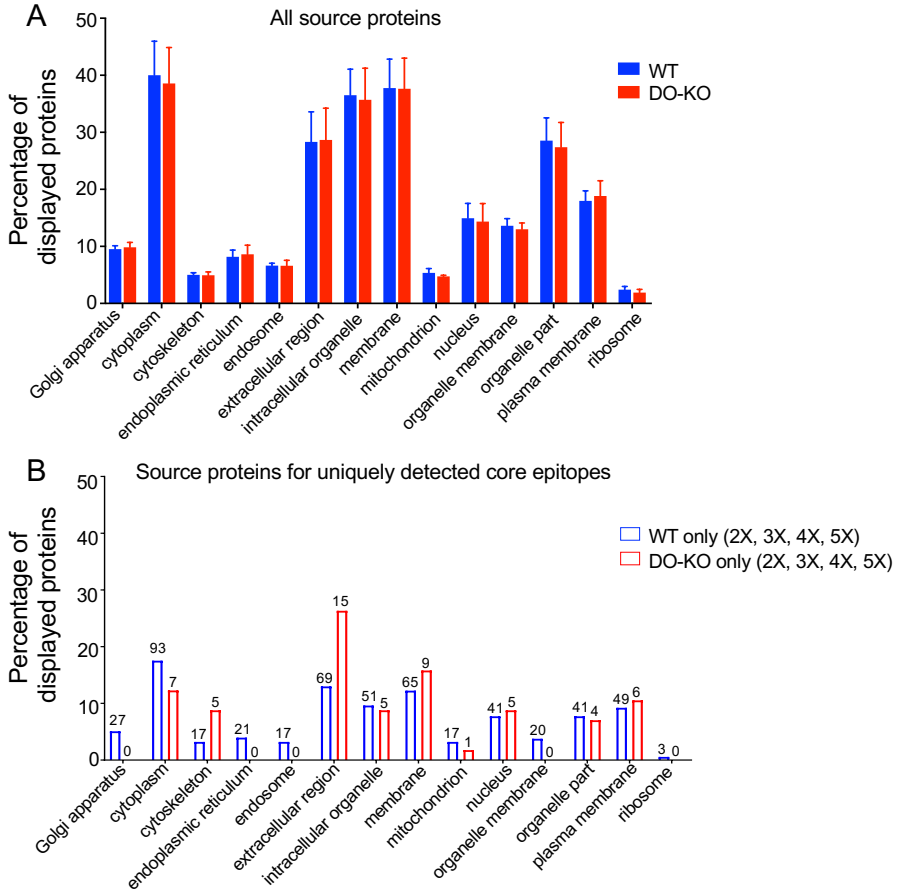

Figure 2.10. Source protein analysis for peptides eluted from WT and DO-KO-1 cells. (A) Source protein cellular component analysis using GO terms shows similar overall subcellular localization distribution of peptides in WT and DO-KO cells. No significant differences were observed between WT and DO-KO samples using elution data from 5 independent experiments (a multiple t-test correction using the Benjamini, Krieger and Yekutieli method was performed to adjust the p-value.) (B) Source protein cellular component analysis for uniquely detected core epitopes in at least 2, 3, 4 or 5 WT or DO-KO samples as defined in Fig 3B. Due to the small number of core epitopes detected uniquely in DO-KO samples, no statistical analysis was performed. Numbers above bars correspond to numbers of unique core epitopes in each compartment.

cellular compartments[302,303] for source proteins from which the eluted peptides were derived. These were not appreciably different between WT and DO-KO,

suggesting that the location of antigen loading was not substantially altered by the presence of DO (Figure 2.10). We repeated this analysis for core epitopes identified uniquely in WT or DO-KO samples (identified as in Figure 2.7B.) For core epitopes unique to WT, the distribution of source proteins was similar to that for all peptides (Figure 2.10B). Comparison with DO-KO is hampered by the paucity of peptides found uniquely in these samples, but an increased representation of peptides derived from extracellular sources (secreted proteins and medium components) is apparent (Figure 2.10B), providing one possible explanation for some of the peptidome differences observed in the presence of DO. DO-KO mice previously have been observed to have increased capacity as compared to WT to present peptides derived from exogenous soluble protein antigens[279]. However, extracellular proteins comprised only a small part of the overall peptidome, and we observed DO-dependent differences in peptide presentation for epitopes derived from many intracellular sources, both intracellular and extracellular. Moreover, many epitopes were presented preferentially in WT as compared to DO-KO. Thus, we sought other explanations for the effect of DO on MHC-II peptidome diversity.

DO expression allows for presentation of a population of DM-sensitive peptide antigens

Given the role of DM in epitope selection[207,282,304] and the function of DO as an inhibitor of DM[32,36,37], we sought to determine whether DO-dependent differences in the MHC-II peptidome were related to sensitivity to DM-mediated exchange. We first examined the relative abundance of three epitopes for which DM

sensitivity has been previously characterized, summing the intensities of individual peptides that contain the respective core epitopes. CLIP and DRα peptides were observed at lower abundance in the absence of DO (Figure 2.9A-B, Figure 2.4I-J), whereas A2 peptides were not significantly different (Figure 2.9C, Figure 2.4K), as expected from their known DM sensitivities, and consistent with surface expression data by FACS (Figure 2.1F-G). To extend this analysis to additional peptides, we characterized the binding affinity and DM sensitivity of 38 additional peptides, grouped into sets according to their representation in WT and DO-KO-1 peptidomes (Figure 2.9D-F). The DO-KO>WT and DO-KO-only peptides fell within the range of the WT≈DO-KO peptide set, whereas the WT>DO-KO and WT-only peptides included several species with lower binding affinity and higher DM sensitivity. These results support the idea that the increased complexity of the WT as compared to the DO-KO peptidome is due at least in part to increased representation of DM-sensitive epitopes that are lost when DO modulation of DM editing activity is absent.

DO control of peptide diversity evaluated in a mouse model

Given the DO-dependent peptide differences observed in human B cells, we sought to evaluate whether such differences would be similarly observed in a mouse model of DO deficiency. We made use of H2-O$^{-/-}$ mice, which previously have been shown to exhibit autoimmune and immunodeficient phenotypes[279,288]. As was observed for human B cells, H2-O deletion did not affect surface expression of MHC-II on mouse B cells (Figure 2.11A), consistent with previous reports[279,288].

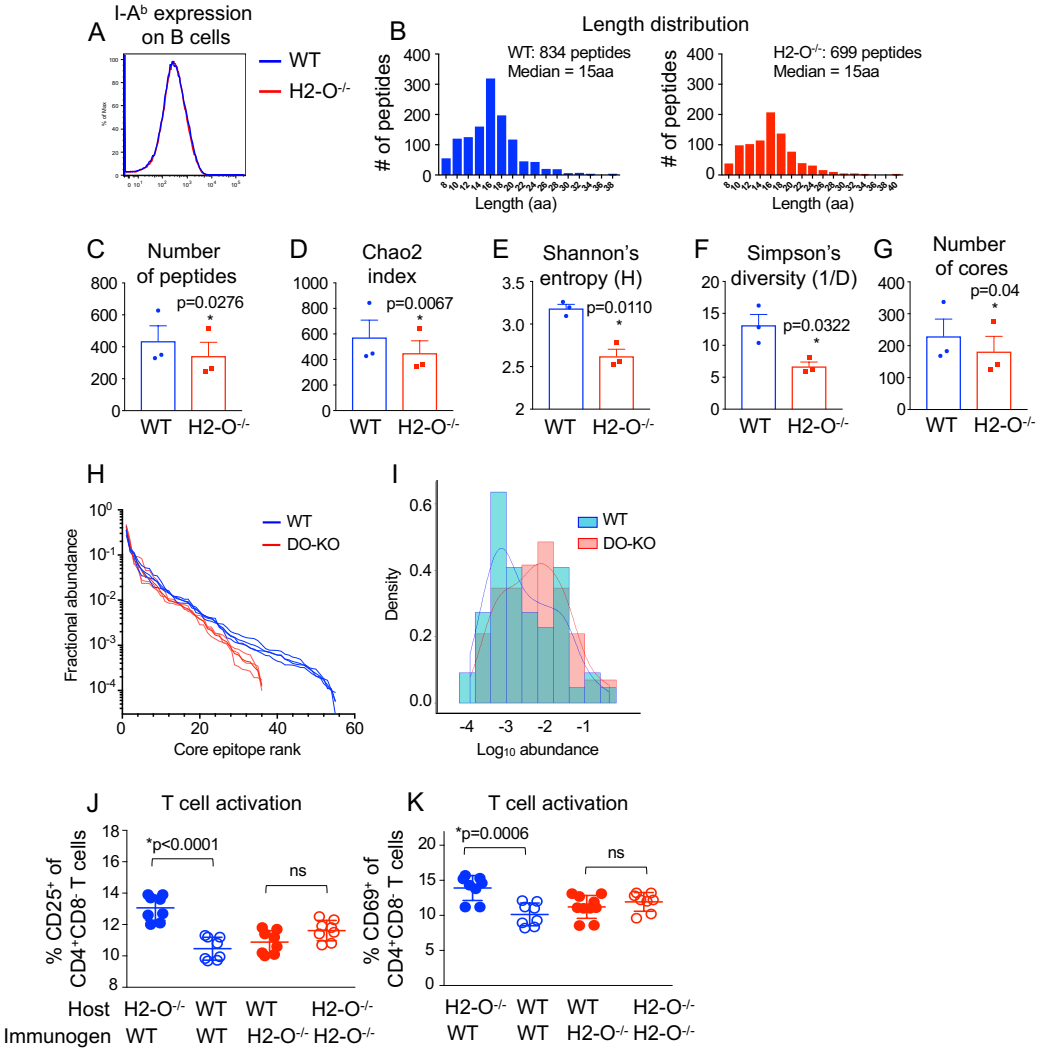

Figure 2.11. DO control of peptide diversity in a mouse model. (A) Equivalent I-A^b expression on splenic WT and H2-O$^{-/-}$ B cells. (B) Similar length distribution for peptides eluted from WT and H2-O$^{-/-}$ B cells. (C) Species richness. More unique peptides were eluted from WT than H2-O$^{-/-}$ B cells in each of 3 independent experiments. Mean ± SD is shown. (D,E,F) Diversity indices. Chao2 index (D), Shannon's entropy (E) and Simpson's reciprocal diversity index (F) are greater for WT than for H2-O$^{-/-}$, calculated for peptides observed in each of 3 biological replicates of both WT and H2-O$^{-/-}$. (G) The number of unique core epitopes observed from WT was significantly greater than for H2-O$^{-/-}$ in each of 3 independent experiments. Paired parametric t-test used to calculate p-values. (H) Rank abundance plot. Fractional intensity of core epitopes from WT (blue) or H2-O$^{-/-}$ (red) in each biological sample is represented as individual lines. (I) Histogram of fractional intensities of core epitopes, overlaid with a kernel density plot. (J,K) CD4 T cell activation measured by expression of CD25 (J) or CD69 (K) was observed when H2-O$^{-/-}$ mice (host) were immunized with WT splenocytes, but not when WT recipients were immunized with H2-O$^{-/-}$ splenocytes, or with splenocytes from syngeneic controls. CD25 and CD69 expression was assessed following gating on CD4$^+$CD8$^-$Foxp3$^-$ cells. Mean ± SD shown (n=8 mice/group, performed in 3 separate experiments with 2-3 mice/group). Unpaired nonparametric t-test used to calculate p-values.

We immunoaffinity-purified I-A^b from WT and H2-$O^{-/-}$ splenic B cells, eluted bound peptides, and characterized peptidomes by mass spectrometry. As was observed for human B cells, a broad length distribution was observed for peptides eluted from both WT and H2-$O^{-/-}$ mouse B cells (Figure 2.11B). As observed for human B cells, DO deletion in mice caused reductions in the number of unique peptides and the number of core epitopes presented by MHC-II, with reduced peptide diversity as measured by several indices, and skewed rank abundance and density plots (Figure 2.11C-I). To test whether the immune system is sensitive to DO-dependent peptide differences, we performed a cross-immunization experiment. H2-O-deficient and WT mice were immunized with irradiated splenocytes from WT and H2-O-deficient mice, with syngeneic splenocyte immunizations serving as controls. CD4 T cells of H2-$O^{-/-}$ recipient mice were activated when immunized with WT splenocytes, but CD4 T cells of WT recipients immunized with H2-$O^{-/-}$ splenocytes were not significantly activated, nor were CD4 T cells of syngeneic control recipient mice (Figure 2.11J-K). This unidirectional pattern, in which T cells were selectively activated only after having developed in the H2-$O^{-/-}$ mouse and when presented with WT peptides, suggest that peptides displayed on WT antigen-presenting cells (APCs) are recognized by H2-$O^{-/-}$ T cells due to the absence of these epitopes in the H2-$O^{-/-}$ mouse.

Discussion

The role of DO in MHC-II antigen presentation has been the subject of numerous biochemical and immunological studies, but understanding of the biological function of DO has been complicated by conflicting reports, in which differing effects have been described depending on the epitope(s) examined[36,37,111,131,141,277-280,294,305,306]. In addition, previous mass spectrometric studies of DO function were limited by the technology available at the time and only allowed for analysis of qualitative differences in eluted peptides[36,276,280]. We sought to definitively determine the overall peptidome-wide effect of DO on MHC-II antigen presentation as well as its in vivo effects. We thus performed a comprehensive analysis of the effect of DO on the self-peptide repertoire. We generated DO-KO and WT control cells using CRISPR/Cas9-mediated targeted gene deletion, and we eluted MHC-II-bound peptides from WT and DO-KO cells. We found that while many features of the DO-KO and WT peptidomes were similar, a striking difference was that fewer different peptide sequences were presented in the absence of DO. We ruled out several explanations that could account for these differences in peptide numbers, including different antigen source proteins and lower MHC input. We analyzed DO-KO versus WT peptidomes using unfragmented MS1 parent ion intensities, to avoid sampling issues intrinsic to conventional data-dependent acquisition proteomics, and validated the intensity-based analysis using isotope-labeled peptides. We calculated several measures of peptidome diversity and found that repertoire diversity was significantly reduced in the absence of DO. The picture that emerges from this quantitative analysis is of a steeper abundance

profile in the absence of DO, with abundant epitopes presented in even more copies and many of the low abundance epitopes lost. Epitopes presented preferentially in WT exhibited lower binding affinity and increased DM sensitivity, demonstrating that increased DM activity is at least in part responsible for peptide differences in WT vs. DO-KO. We analyzed the peptidome presented by a single human MHC-II protein HLA-DR1. Other MHC-II proteins with similar DM sensitivities would be expected to behave similarly, but some autoimmune-linked MHC-II proteins have reduced DM sensitivity[30,205,271] and may show different behavior. To extend our observations to a mouse model and test their immunological relevance in vivo, we performed elutions from I-A^b isolated from mouse B cells and similarly observed reduced peptide numbers in the absence of DO. Immunization experiments showed that H2-$O^{-/-}$ cells were selectively activated by WT APCs and not vice versa, suggesting that epitopes presented on WT cells were not recognized as self-antigens by T cells that were selected or developed in the absence of DO. These data indicate that expression of DO results in an altered MHC-II B cell peptidome and have broad implications with regard to the role of DO in immunological processes including thymic selection, peripheral tolerance, and entry and selection of B cells in the germinal center.

This study considerably extends previously reported analyses of the effect of DO on the MHC-II peptidome, in which the authors observed as many peptides presented uniquely in the presence of DO as peptides presented uniquely in the absence of DO[276,280]. Another study concluded that DO expression increases the stringency of DM editing[36], at odds with reports demonstrating that DO is an

inhibitor of DM[32,33,36,37]. These analyses were limited by the available technology to comparing qualitative differences in MALDI spectra, with identification of very few if any individual peptide sequences. With advances in mass spectrometry sensitivity and mass accuracy[295,307], we were able to characterize essentially the entire peptidomes of intact and of DO-deleted LG-2 cells (we estimate that lowest abundance peptides characterized in our study are present at only a few copies per cell or less). Using quantitative methods, we were able to obtain reliable peptidome comparisons and to characterize the full abundance profile, rather than simply the number of different peptides presented. These results suggest an apparent excess of peptides over MHC-II in loading compartments, as the restricted number of different peptide species in the absence of DO, presumably through increased DM editing, did not result in a lower number of peptide-MHC molecules but did result in decreased peptide diversity. This indicates substantially different constraints on MHC-II as compared to MHC-I processing, where peptide abundance is posited to limit presentation[308]. While DO has been thought to focus antigen presentation by way of restricting presentation to very low pH compartments[33,267,279,285], we did not find evidence of differential sampling of intracellular compartments in the absence or presence of DO. Instead, and in contrast to conclusions made in previous MS analyses of DO function[36,276,280], we find that DO expression *broadens* antigen presentation, by promoting presentation of low affinity and/or DM-sensitive antigens. Our results suggest that when DO is downregulated relative to DM, for example upon B cell entry into the germinal center[131,141] or during DC maturation[101,112], the diversity of the MHC-II peptidome will be reduced, with

increased DM editing leading to presentation of a more focused and limited peptide repertoire.

We attribute much of the effect of DO expression on broadening the MHC-II peptide repertoire to inhibition of DM, with peptides more susceptible to DM-mediated peptide exchange preferentially presented when DM activity is reduced in the presence of DO. DO inhibition of DM activity has been demonstrated in vitro and in vivo[32,33,36,37]. Two recent studies have reported data on the effect of DM modulation/deletion on MHC-II peptidomes. In a study of DR3-expressing T2 cells transfected with different levels of DM, Alvaro-Benito *et al.* found that higher DM expression was associated with presentation of MHC-II-bound peptides with lower predicted MHC-II binding affinity[29]. In a study comparing the peptide repertoires of 293T cells transfected with HLA-DQ molecules differentially associated with type 1 diabetes, Zhou *et al.* found that in the absence of DM, peptides with lower binding affinity and faster dissociation were presented[30]. These studies are in agreement with our data with respect to DM-sensitive epitopes, in which peptides eluted only in the presence of DO were determined to be more sensitive to DM-mediated exchange.

At the cellular level, the results of this study indicate that DO exerts a selective effect on the MHC-II peptide repertoire, such that certain epitopes are presented only when DO is expressed, while other abundant peptide species are presented at lower density. While this work has delineated the overall effect of DO with respect to the MHC-II peptidome, these data also provide a mechanistic basis for epitope studies in which differing effects of DO have been

demonstrated[36,37,111,131,141,277-280,294,305,306]. Results of our analysis suggest that depending on the specific features of the epitope examined, including whether it is DM-sensitive or –resistant as well as its abundance, DO expression can result in greater presentation, little change, or lesser presentation of a particular peptide species. In the context of the larger scope of the function of DO in antigen presentation, these data may also explain previous observations observed in settings in which DO expression has been modulated. Mice lacking DO have been shown to bear an autoimmune phenotype[288], and ectopic expression of DO in DCs was shown to result in prevention of diabetes in NOD mice[253]. Based on our analysis, we posit that DO expression serves to prevent autoimmunity by allowing for deletion of autoreactive clonotypes in the thymus as well as by mediating presentation of a broad spectrum of self-antigens to promote peripheral tolerance. DO expression is downregulated relative to DM following exposure to inflammatory stimuli[101,112,137,141,262], and the consequent focusing of the MHC-II peptidome on immunodominant (i.e. DM-resistant[207,272,281]) epitopes may allow for a more efficient immune response. Such a role for DO regulation has been borne out in studies in which lack of DO has been shown to confer resistance to retrovirus as a result of neutralizing antibody production[259], as well as to enable preferential entry into germinal centers[292]. Cell-specific expression of DO, which is then downregulated with the onset of inflammation, could allow for shifts in the MHC peptidome that serve the purpose of promoting tolerance (when DO is expressed) and generating an efficient immune response (when DO is downregulated).

In summary, this work defines a role for DO in regulating the MHC-II peptidome by effectively increasing the breadth of peptides presented to CD4 T cells and by modulating epitope density. Restricted and regulated expression of DO suggest the immune system has evolved to allow for presentation of an optimal MHC-II peptide repertoire to both promote tolerance and initiate an efficient immune response.

Materials and Methods

Generation of DO-knockout (DO-KO) and WT clones

Single-guide RNAs (sgRNAs) designed to target exon 1 of HLA-DOβ (sgRNA-1: 5' gACTAGCAGAGCCACCACCCA 3' and sgRNA-2: 5' GCTAGTGAATCTGACCCGAC 3') using the CRISPR Design Tool (http://tools.genome-engineering.org)[309] were cloned into the pX330-U6-Chimeric_BB-CBh-hSpCas9 plasmid, which was a gift from Feng Zhang[310] (Plasmid #42230, Addgene, Cambridge, MA), and which was modified by insertion of a GFP sequence. The px330-GFP vector was then transfected into the human lymphoblastoid HLA-DR1 homozygous LG-2 cell line[311,312] using the Amaxa Nucleofector Kit V (Lonza, Walkersville, MD) according to the manufacturer's instructions, with protocol Y-001 and the Nucleofector II system (Lonza). Transfected cells were sorted for GFP expression on a FACSAria (Becton Dickinson, Franklin Lakes, NJ) and then grown at 37°C, 5% CO_2 in RPMI supplemented with 10% fetal bovine serum, 100 IU/ml/100 ug/ml penicillin/streptomycin (Corning, Corning, NY), and 2 mM Glutamax (Thermo Fisher, Waltham, MA) for 1 week, followed by limiting dilution to isolate single-cell clones. PCR with primers specific for HLA-DOβ was performed using DNA isolated from expanded clonal populations, and amplicons were then gel-purified and cloned into the pCR2.1 vector using the TOPO-TA cloning kit (Thermo Fisher Scientific, Waltham, MA). DNA isolated from mini-preps of bacterial clones was sequenced to determine whether indels were present in exon 1 of HLA-DOβ. Clones were cultured in the medium described above.

Western blot

Total protein was isolated from a negative control T cell line (SUP-T1, [ATCC, Manassas, VA]), from the parental LG-2 line, and from the WT, DO-KO-1, and DO-KO-2 clones by cell lysis in cold RIPA buffer (50 mM Tris-HCl, 150 mM NaCl, 1% [v/v] Triton X-100, 1% [w/v] sodium deoxycholate, 0.1% [w/v] SDS, pH 7.4) containing protease inhibitor (Roche, Indianapolis, IN). Protein was quantified using a bicinchoninic acid protein assay (Thermo Fisher Scientific), and 40 μg of each lysate was loaded onto a Novex 12% Tris-Glycine gel (Thermo Fisher Scientific) and then transferred to a PVDF membrane. Membranes were blocked overnight with 10% nonfat dry milk, probed for HLA-DOβ (DOB.L1, Santa Cruz Biotechnology, Santa Cruz, CA), and then re-probed with anti-GAPDH (Millipore, Burlington, MA) to confirm equal protein loading.

Flow cytometric analysis

DO-KO and WT clones were blocked with 10 μg/ml human IgG (Sigma Aldrich, St. Louis, MO), and then stained for surface expression of HLA-DR (Thermo Fisher Scientific). Co-staining of viable cells was performed using the Live/Dead Fixable Dead Cell Stain Kit (Thermo Fisher Scientific) for all antibodies. For HLA-DM staining, cells were permeabilized using the BD Cytofix/Cytoperm kit according to the manufacturer's instructions (BD Biosciences, San Jose, CA) and then similarly blocked using human IgG. Permeabilized cells were incubated with PE-conjugated MaPDM.1 (Santa Cruz Biotechnology) to evaluate DM expression. Isotype

controls were used for all antibodies. To assess presentation of the CLIP and HLA-$A2_{(104-117)}$ (A2) epitopes, LG-2 clones were incubated with the CerCLIP (FITC-conjugated, BD Biosciences) or UL-5A1[4,313] (followed by incubation with FITC-conjugated anti-mouse IgG F(ab')2 [Thermo Fisher Scientific]) antibodies together with HLA-DR to calculate ratios of expression for mean fluorescence intensity (MFI) of epitopes to HLA-DR in order to account for any small differences in DR expression. Antibodies used in additional experiments (details below) were anti-mouse CD4 (RM4-5), CD8α (53-6.7), CD25 (PC61), CD69 (H1.2F3), and $I\text{-}A^b$ (AF6-120.1) (BD Biosciences), as well as anti-mouse CD11b (M1/70) and CD43 (S11) (BioLegend, Dedham, MA) and CD45R/B220 (RA3-6B2) (Thermo Fisher Scientific). Prior to staining, mouse cells were blocked with 50 μg/ml anti-mouse CD16/CD32 (2.4G2, BioXCell, West Lebanon, NH). Cells were acquired on an LSR II flow cytometer (Becton Dickinson) and analyzed using FlowJo version 9.8.5 software (Tree Star, Ashland, OR).

RNAseq

RNA isolation, library preparation, and sequencing were performed at the Broad Institute (Cambridge, MA). Briefly, RNA was isolated using a Trizol-based method followed by purification using silica spin columns. Quantification of RNA was then performed using the Quant-iT RiboGreen RNA Assay Kit (Thermo Fisher Scientific), and RNA quality was measured as RNA Quality Score via Caliper GX (PerkinElmer, Waltham, MA). 200 ng of total RNA was used for library preparation, which was performed with an automated variation of the Illumina

TruSeq Stranded mRNA Sample Preparation Kit (Illumina, San Diego, CA) according to the manufacturer's instructions, with indexed adapters designed by the Broad Institute. Pooled libraries were normalized to 2 nM and then denatured with 0.1 N NaOH. Flowcell cluster amplification and sequencing were performed according to the manufacturer's instructions (Illumina) using either the HiSeq 2000 or HiSeq 2500 sequencing platform, with a 101bp paired-end read. The Broad Picard Pipeline was used for data de-multiplexing and data aggregation.

For analysis of sequencing data, filtering of rRNA and low-quality reads was first performed. Transcripts were then quantified by RSEM v1.2.7[314] with Bowtie 2[315] using the hg19(GRCh37) assembly. RefSeq annotations were downloaded on 2/5/17 from the UCSC genome browser[316,317]. Functional annotation clustering was performed using DAVID 6.8[318,319]. A correlation analysis was also performed using RNAseq and mass spectrometric data (below) to evaluate whether clonal or CRISPR off-target effects could account for presentation of fewer peptides in DO-KO. The Pearson correlation coefficients, when comparing intensities of peptides found with greater intensity in WT or found only in WT vs. the fold-change expression of corresponding genes downregulated in DO-KO, were -0.012 and -0.102 for DO-KO-1 and DO-KO-2 compared to WT, indicating that reduced peptide numbers in the absence of DO were not due to changes in gene expression.

Experimental design and statistical rationale

WT, DO-KO-1 and DO-KO-2 human LG-2 clones were used to determine the qualitative and quantitative differences in peptide diversity modulated by HLA-

DO. LG-2 cells express the MHC-II proteins HLA-DR1 (DRA1*01:01,DRB1*01:01), HLA-DQ5 (DQA1*01:01,DQB1*05:01), and HLA-DP4 (DQA1*01:03,DQB1*04:01) at an approximate 100:17:2 ratio[312]; only HLA-DR1 was analyzed in the present study. HLA-DR1-bound peptides were isolated from ~10^8 cells using immunoaffinity purification and were further identified using LC-MS/MS. For DO-KO-1, five biological replicates from independent cell cultures with paired WT replicates were analyzed. For DO-KO-2, three biological replicates from independent cell cultures with paired WT replicates were analyzed. To evaluate the role of the murine HLA-DO ortholog H2-O, we used splenic B cells from littermate H2-$O^{-/-}$ and WT C57BL/6 mice. These mice express I-A^b as their only MHC-II protein. Three biological replicates of paired WT and DO-KO samples from ~10 mice/replicate were used, totaling 3x10^8 cells/replicate. For both human and mouse samples, pairs of WT and DO-KO samples were processed in parallel, with each biological replicate tested in three technical replicates. Only peptides identified with 1% FDR were considered. For systematic comparison across the peptides between different samples using their MS1 intensities for volcano plot analysis, we applied a multiple comparison correction using the original Benjamini-Hochberg method to calculate p-values. The Benjamini, Krieger and Yekutieli method was used for comparison of differential source protein localization analysis in WT and DO-KO samples using GO terms. We used a paired parametric t-test to calculate p-values for differences in number of peptides, cores and diversity measures between WT and DO-KO. Also, paired nonparametric t-tests, unpaired nonparametric Mann-Whitney t-tests, and specific

t-tests were used for different analyses, which are indicated in the figure legends of each plot. Prism (version 7.03, GraphPad, San Diego, CA) was used for statistical analysis and graphing data. R version 3.3.2 was used for histogram and kernel density plots.

Isolation of HLA-DR1-bound peptides

Membrane solubilized fractions isolated from ~10^8 cells of each WT and DO-KO LG-2 clone were used for elution experiments. Five independent samples each for WT and DO-KO from separate cell cultures were analyzed, with five sets of WT and DO-KO pairs processed in parallel. Cells were suspended in ice-cold hypotonic buffer (10 mM Tris-HCl, pH 8.0, containing protease inhibitors). Repeated (4-5) freeze-thaw cycles were used for cell disruption. Cellular debris was removed by centrifuging the lysate at 4,000 x g for 5 min at 4°C. The supernatant was collected and further centrifuged at 100,000 x g for 1 h at 4°C to pellet the membrane fraction. The membrane pellet was solubilized in ice-cold 50 mM Tris-HCl, 150 mM NaCl, pH 8.0, containing protease inhibitors and 5% β-octylglucoside, and then mixed slowly overnight at 4°C. Supernatant containing the solubilized membrane was recovered by centrifuging the lysate at 100,000 x g for 1 h at 4°C. 2.5 µg of DR1-GAG or DR1-HA complex was added to the membrane fraction as controls. An immunoaffinity column of protein A agarose-LB3.1 antibody, prepared as previously described[312], was used for isolation of DR1-bound peptide complexes. The column was equilibrated with buffer (50 mM Tris-HCl, 150 mM NaCl, pH 8.0, containing protease inhibitors) for 2 h. The membrane fraction was first

equilibrated with protein A agarose beads for 1 h at 4°C and then allowed to mix slowly to prevent nonspecific binding of proteins to beads. The precleared supernatant was incubated with LB3.1 antibody conjugated to the protein A agarose affinity column for 1 h at 4°C and allowed to mix slowly. The column was washed with several buffers in succession as follows: 1) 50 mM Tris-HCl, 150 mM NaCl, pH 8.0, containing protease inhibitors and 5% β-octylglucoside (5 times the bead volume); 2) 50 mM Tris-HCl, 150 mM NaCl, pH 8.0, containing protease inhibitors and 1% β-octylglucoside (10 times the bead volume); 3) 50 mM Tris-HCl, 150 mM NaCl, pH 8.0, containing protease inhibitors (30 times the bead volume); 4) 50 mM Tris-HCl, 300 mM NaCl, pH 8.0, containing protease inhibitors (10 times the bead volume); 5) 1X PBS (30 times the bead volume); and 6) HPLC water (100 times the bead volume). Bound complexes were acid-eluted, and MHC-peptide concentration from the membrane fraction was measured by ELISA. Peptides were further separated using a Vydac C4 macrospin column (Hichrom, Berkshire, UK). Firstly, the mixture of DR1 and peptides were bound to the column, and after subsequent washes with 0.1% TFA, the peptides were eluted using 30% acetonitrile in 0.1% TFA. Eluted peptides were lyophilized using a SpeedVac and were resuspended in 25 µl of 5% acetonitrile and 0.1% TFA. This fraction was further divided into 3 different portions that were considered as technical replicates of the same sample. 2 pmols of ADH digest was added, and a total of 3/25 µl was injected, so that the amount of ADH per injection was 240 fmols. Each fraction was analyzed using a Q Exactive™ Hybrid Quadrupole-Orbitrap™ Mass Spectrometer (Thermo

Fisher Scientific). 3 samples from clone DO-KO-2, 3 additional WT clone samples, and a single sample of the parental LG-2 line were analyzed similarly.

Liquid chromatography – mass spectrometry (MS)

For LC/MS/MS analysis, peptide extracts were reconstituted in 25 µL 5% acetonitrile containing 0.1% (v/v) trifluoroacetic acid and separated on a nanoACQUITY (Waters Corporation, Milford, MA) UPLC with technical triplicate injections. In brief, a 3.0 µL injection was loaded in 5% acetonitrile containing 0.1% formic acid at 4.0 µL/min for 4.0 min onto a 100 µm I.D. fused-silica pre-column packed with 2 cm of 5 µm (200Å) Magic C18AQ (Bruker-Michrom, Auburn, CA) and eluted using a gradient at 300 nL/min onto a 75 µm I.D. analytical column packed with 25 cm of 3 µm (100Å) Magic C18AQ particles to a gravity-pulled tip. The solvents were A) water (0.1% formic acid); and B) acetonitrile (0.1% formic acid). A linear gradient was developed from 5% solvent A to 35% solvent B in 90 minutes. Ions were introduced by positive electrospray ionization via liquid junction into a Q Exactive hybrid mass spectrometer (Thermo Fisher Scientific). Mass spectra were acquired over m/z 300-1750 at 70,000 resolution (m/z-200), and data-dependent acquisition selected the top 10 most abundant precursor ions in each scan for tandem mass spectrometry by HCD fragmentation using an isolation width of 1.6 Da, collision energy of 27, and a resolution of 17,500.

Peptide identification

Raw data files were peak processed with Proteome Discoverer (version 2.1, Thermo Fisher Scientific) prior to database searching with Mascot Server (version 2.5, Matrix Science, Boston, MA) against the combined database of UniProt_Human, UniProt_Bovine and UniProt_EBV databases, with 115,105 entries downloaded on 8/5/16. (The LG-2 cell line carries the Epstein-Barr virus genome and was cultured in medium containing fetal bovine serum.) Search parameters included "no enzyme" specificity to detect peptides generated by cleavage after any residue. The variable modifications of oxidized methionine and pyroglutamic acid for N-terminal glutamine were considered. The mass tolerances were 10 ppm for the precursor and 0.05Da for the fragments. Search results were then loaded into the Scaffold Viewer (Proteome Software, Inc., Portland, OR) for peptide/protein validation and label-free quantitation. Scaffold assigns probabilities using PeptideProphet or the LDFR algorithm for peptide identification and the ProteinProphet algorithm for protein identification, allowing the peptide and protein identification to be scored on the level of probability. An FDR of 1% was adjusted for reliable identification of peptides. Peptide lists were filtered to remove contaminants such as keratins and IgG-derived peptides. Core epitopes were identified for the HLA-DRB1*0101 allele using the NetMHCIIpan3.0 server; the top scoring 9-residue sequence within each sequenced peptide was used as the core epitope[320]. Peptides with a length of less than 9 amino acids were excluded from the core epitope analysis. A similar analysis using a different prediction algorithm, P9[321], identified essentially the same cores (~92% identical).

Label-free quantitation

Label-free relative quantitation of all peptides eluted from WT and DO-KO LG-2 cells was performed using precursor intensity analysis in Scaffold, Scaffold Q+/Q+S[322-324]. Scaffold uses the precursor intensity information from the Thermo Proteome Discoverer. The software normalizes total precursor intensity values across the samples and calculates fold change or $\log_2$ normalized intensity across the samples while considering different statistical parameters like t-test, ANOVA and coefficient of variance. The log2 normalized intensity values were converted to intensities for subsequent analyses. Triplicate technical replicates were run for each sample. Only peptides that were observed in at least two of three technical replicates in a particular sample were used for intensity analysis, with missing values imputed as the minimum intensity observed in that sample, and a single average value used to represent the three technical replicates. For analysis of core epitope intensities, the intensity values for all peptides sharing the same core epitope were summed within each technical replicate, using an approach similar to PLAtEAU[29], except that NetMHCIIpan rather than overlap analysis was used to identify core epitopes. Missing values were imputed and technical replicates were averaged for core epitopes as described above for peptides. For calculation of diversity statistics, rank abundance plots, density histograms, and volcano plots, only core epitopes present in all of the biological replicates were considered. To determine fractional intensities in the rank abundance plot, the intensity for each core was divided by the total intensity for all core epitopes present in that sample. To determine average fractional intensities in the density plot, an average of all biological replicates was calculated. For correlation analysis, SIEVE software[322,325]

was used, with frame parameters adjusted to m/z range of 300-1700, frame time width of 1.5 min, m/z width of 10ppm, and retention time from 10-80 min. The intensity analysis shown for pairs of biological replicates in Figure 2.2 included 10,000 frames.

Diversity calculations

Shannon's diversity index (H) and Simpson's diversity index (D) were calculated to analyze the diversity of WT and DO-KO peptidomes. These indices consider not only the number of species (peptides) but also how evenly peptide abundances are distributed in the entire sample. Diversity calculations were performed only for peptides identified in all biological samples as described above. Shannon's entropy (H) was calculated as:

$$H = -\sum_{i=1}^{R} p_i \, ln(p_i)$$

where R is the number of peptides and p_i is the proportion of the total ion intensity represented by peptide i. The higher the entropy value, the more diverse the sample. Simpson's diversity index was calculated as:

$$\mathrm{D} = \sum_{i=1}^{R} {p_i}^2$$

Simpson's reciprocal diversity index was calculated as 1/D, with higher values representing more diverse samples. Chao2 (for replicated incidence data) for peptides was calculated as:

$S_{Chao2} = S_{obs}+(Q_1^2/2Q_2)$

where S_{obs} is the number of observed species, Q_1 is the number of singletons (species occurring once), and Q_2 is the number of doubletons (species occurring twice).

Absolute quantification using stable isotope-labeled peptides

Nine peptides were selected for intensity validation by referencing a volcano plot analysis of differences in intensities of the WT and DO-KO-1 vs. their significance values adjusted using Benjamini-Hochberg's correction: one peptide that was observed with higher core epitope intensity in WT vs. DO-KO-1 samples (WT>DO-KO), two peptides that were observed at higher core epitope intensity in DO-KO-1 vs. WT samples, (WT<DO-KO), and six peptides that were observed with relatively equal core epitope intensities in the two samples (WT≈DO-KO) (Figure 2.9D). We selected core epitopes that were observed in each of the five biological replicates, and for differentially expressed core epitopes, that showed a statistically significant difference of 2-fold or greater after adjustment for multiple comparisons. For each core epitope, we selected the most abundant peptide containing that epitope for synthesis and absolute quantification studies. Peptides with ^{13}C and ^{15}N labels incorporated at specific residues were synthesized by 21st Century Biochemicals (Marlborough, MA) and spiked into new samples of WT and DO-KO-1 as internal controls to quantify the chemically-identical unlabeled (light) peptides present in these samples. The purity and quantification of these peptides were confirmed using amino acid analysis. DR1-bound peptides were eluted from WT or DO-KO-1 LG-2 cells as described in the previous section, and a mixture of

isotope-labeled peptides at 60 fmols/injection was spiked into the sample. The data were analyzed as 3 technical replicates. Quantitation of the selected peptides was performed using Skyline software (V3.7, University of Washington, Seattle, WA) by generating extracted ion chromatograms of the MS1 signals for the M, M+1, and M+2 isotopes of each precursor. For most peptides, both +3 and +4 charge state ions were observed; intensities of these were summed for each peptide. Summed areas were then compared to the corresponding heavy peptide areas to determine absolute amount of peptide.

Soluble recombinant HLA-DR1 and HLA-DM

Soluble extracellular domains of recombinant HLA-DR1 (DR1) (DRA*0101/DRB1*010101) and DM (DMA*0101/DMB*0101) for binding affinity and DM sensitivity measurements were expressed in Drosophila S2 cells and purified by immunoaffinity chromatography followed by Superdex200 (GE Healthcare, Chicago, IL) size exclusion chromatography as previously described[22,326].

Binding affinity and DM sensitivity measurements

For three abundant self-peptides, DM sensitivity has been previously characterized: CLIP, the invariant chain chaperone fragment efficiently removed by DM[22,327], DR$\alpha_{52\text{-}68}$, the human ortholog of the YAe epitope[328] known to be highly sensitive to DM exchange[2], and the transplantation alloepitope A2$_{104\text{-}117}$[313] previously demonstrated to be highly resistant to DM-mediated exchange[4]. For these peptides,

we summed the intensities of all peptides sharing the respective core epitopes and compared summed intensities between replicate samples of WT and DO-KO-1 cells. For a broader analysis, we selected 38 peptides comprising the 9 peptides used for stable isotope quantitation, 2 additional peptides with greater core epitope intensity in WT peptidomes than in DO-KO-1 as indicated by volcano plot analysis (WT>DO-KO), 11 with average core epitope intensity similar in WT and DO-KO-1 samples as indicated by volcano plot analysis (WT≈DO-KO), 15 core epitopes identified exclusively in WT, and one core epitope identified exclusively in DO-KO-1 (Figure 2.9D). For each core epitope, we selected the most abundant peptide containing that epitope for synthesis and binding analysis. A fluorescence polarization (FP) assay was used to measure the IC_{50} of each selected peptide, using N-terminally-acetylated influenza hemagglutinin $HA_{306–318}$ (Ac-PRFVKQNTLRLAT) labeled with Alexa Fluor 488 tetrafluorophenyl ester (Invitrogen, Carlsbad, CA) via the primary amine at K_5 as probe peptide as previously described[329]. The DR1 concentration used was selected by titrating DR1 against fixed labeled peptide concentration (25 nM) and choosing the concentration of DR1 that showed ~50% maximum binding. For calculating IC_{50} values, 100 nM DR1 was incubated with 25 nM Alexa488-labeled $HA_{306–318}$ probe peptide, in combination with a serial dilution of test peptides, beginning at 10 μM followed by 2-fold dilutions. The reaction mixture was incubated at 37°C. The capacity of each test peptide to compete for binding of probe peptide was measured by FP after 72 h at 37°C. FP values were converted to fraction bound by calculating [(FP_sample − FP_free) / (FP_no_comp − FP_free)], where FP_sample represents the FP value

in the presence of test peptide; FP_free represents the value for free Alexa488-conjugated $HA_{306–318}$; and FP_no_comp represents values in the absence of competitor peptide. We plotted fraction bound versus concentration of test peptide and fit the curve to the equation $y = 1 / (1 + [pep] / IC_{50})$, where [pep] is the concentration of test peptide, y is the fraction of probe peptide bound at that concentration of test peptide, and IC_{50} is the 50% inhibitory concentration of the test peptide. To measure DM sensitivity, an $IC_{50,DM}$ was obtained by including 500 nM DM in the binding competition assay, and ΔIC_{50} was calculated as ($IC_{50,DM} - IC_{50}$) as described[1]. DM sensitivity was calculated as ΔIC_{50} / [DM], where [DM] is the concentration of DM.

Whole cell proteomics

For in-gel digestion and LC-MS/MS analysis, total protein was isolated as above for western blot. 50 µg of whole cell lysate was run on an SDS-PAGE system to separate proteins from lower molecular weight contaminants, and the entire protein region of the gel was then excised and subjected to in-gel trypsin digestion after reduction with DTT and alkylation with IAA. Peptides eluted from the gel were lyophilized and re-suspended in 100 µL of 5% acetonitrile (0.1% [v/v] TFA) with 1 pmol ADH digest. An injection of 1.5 µL was loaded by a Waters nanoACQUITY UPLC in 5% acetonitrile (0.1% formic acid) at 4.0 µL/min for 4.0 min onto a 100 µm I.D. fused-silica pre-column packed with 2 cm of 5 µm (200Å) Magic C18AQ (Bruker-Michrom). Peptides were eluted at 300 nL/min from a 75 µm I.D. gravity-pulled analytical column packed with 25 cm of 3 µm (100Å) Magic C18AQ

particles using a linear gradient from 5-35% of mobile phase B (acetonitrile + 0.1% formic acid) in mobile phase A (water + 0.1% formic acid) for 120 minutes. Ions were introduced by positive electrospray ionization via liquid junction at 1.5kV into a Thermo Scientific Q Exactive hybrid mass spectrometer. Mass spectra were acquired over *m/z* 300-1750 at 70,000 resolution (*m/z* 200) with an AGC target of 1e6, and data-dependent acquisition selected the top 10 most abundant precursor ions for tandem mass spectrometry by HCD fragmentation using an isolation width of 1.6 Da, max fill time of 110ms, and AGC target of 1e5. Peptides were fragmented by a normalized collisional energy of 27, and fragment spectra acquired at a resolution of 17,500 (*m/z* 200). Raw data files were peak-processed with Proteome Discoverer (version 1.4, Thermo Scientific) followed by identification using Mascot Server (version 2.5, Matrix Science) against an *Epstein-Barr virus* (Swiss-Prot), *Human* (Swiss-Prot), *Bovine* (UniProt) FASTA file (downloaded 8/2016). Search parameters included Trypsin/P specificity, up to 2 missed cleavages, a fixed modification of carbamidomethyl cysteine, and variable modifications of oxidized methionine, pyroglutamic acid for Q, and N-terminal acetylation. Assignments were made using a 10 ppm mass tolerance for the precursor and 0.05 Da mass tolerance for the fragments. All non-filtered search results were processed by Scaffold (version 4.4.4, Proteome Software, Inc.) utilizing the Trans-Proteomic Pipeline (Institute for Systems Biology) with a 0.96% false-discovery rate.

Mice

H2-O-deficient mice were provided by Dr. Xinjian Chen at the University of Utah School of Medicine, following backcrossing to C57BL/6 mice for 10 generations. H2-O$^{-/-}$ mice were bred at the University of Massachusetts Medical School with C57BL/6 mice obtained from Jackson Laboratory (Bar Harbor, ME), and mice heterozygous for H2-O$^{-/-}$ were bred to obtain H2-O$^{-/-}$ and WT littermate controls for B cell isolation and immunization experiments. Mice were cared for and used in accordance with institutional guidelines.

Isolation of B cells from H2-O-deficient and WT mice

Spleens were isolated from H2-O-deficient and WT littermate mice, dissociated into single-cell suspensions, and splenic B cells were evaluated for I-A^{b} expression by first gating on the B220^{+}CD43^{-}CD11b^{-} population and performing flow cytometric analysis as above. To isolate mature B cells from the splenocyte population, CD43- and CD11b-expressing cells were depleted using biotinylated anti-mouse CD43 and CD11b (BioLegend) in conjunction with the EasySep Mouse Streptavidin RapidSpheres Isolation Kit (Stem Cell Technologies, Cambridge, MA) according to the manufacturer's instructions. Purity post-isolation was determined by FACS to be >90% for each sample, with an average purity of 94±2.6%.

Isolation and characterization of I-A^b-bound peptides

Mouse B cells (~$3x10^8$) were solubilized in 50 mM Tris-HCl, 150 mM NaCl, pH 8.0, containing protease inhibitors and 5% β-octylglucoside and were processed as for LG-2 membrane fractions described above, except that whole cell lysates instead of solubilized membrane fractions were used, before loading on an affinity column of I-A^b-specific mAb M5114 coupled to CNBr-activated Sepharose, with elution and analysis as described above for isolation of HLA-DR1-bound peptides. Peptide sequences were identified as described above except that the UniProt Mouse database which was downloaded on 10/7/16 with 57,984 entries.

Mouse immunization

6-8-week-old H2-O-deficient and WT littermate mice were immunized i.p. with $4x10^7$ irradiated (3000 rads) age- and sex-matched splenocytes from WT or H2-O-deficient mice. Spleens from recipient mice were harvested 15h later, and single-cell suspensions were prepared. Following red blood cell lysis, splenocytes were subjected to flow cytometric analysis as above, using anti-mouse CD4, CD8, CD25, and CD69 antibodies, by first gating on the $CD4^+CD8^-$ population and then assessing expression of CD25 and CD69. Similar CD4 T cell activation results were observed at 3 days after immunization.

Data availability

All raw files have been deposited at MassIVE data repository (http://massive.ucsd.edu) developed by Center for Computational Mass

Spectrometry (University of California, San Diego) with the project accession MSV000082570 (PXD010301).

CHAPTER III

Expression of the non-classical MHC-II molecule H2-O regulates Treg selection and function

Author contributions:

I performed all work presented in this chapter.

Abstract

MHC-II antigen presentation is critical for induction and maintenance of self-tolerance, and for prevention of autoimmunity. The nonclassical MHC molecule DO has been shown to affect presentation of antigens to T cells by modulating the spectrum of peptides presented on MHC-II. By competitively inhibiting the peptide exchange factor DM and reducing the efficiency of peptide exchange, DO broadens and diversifies the MHC-II immunopeptidome. Here, we report a previously undescribed role for DO expression in mediating selection and function of the T regulatory (Treg) subset. In the absence of DO, the clonotypic diversity of the Treg population is decreased, with highly abundant clonotypes selected with greater frequency. We show that Tregs are increased in the $DO^{-/-}$ mouse due to lack of thymic-specific expression of DO, and that this results in greater activation of the Treg population. While $DO^{-/-}$ Tregs display enhanced ability to suppress lymphoproliferation, Tfr differentiation is impaired and autoantibody levels increased, both in naïve mice and in a model of autoimmune disease. These data provide insight into the role of DO in selecting a self-tolerant T cell repertoire as well as into the factors that govern T regulatory selection.

Introduction

Presentation of antigens on MHC-II is central to induction and maintenance of immunological tolerance to self, and therefore critical for prevention of deleterious autoimmune responses. Thymic selection of CD4 T cells necessitates interaction of thymocytes with self-ligands presented by MHC-II molecules, while tonic stimulation by MHC-II-peptide complexes in the periphery is requisite for T cell survival. The orthologous nonclassical MHC-II molecules HLA-DO (human) and H2-O (mouse) (referred to hereafter as DO) function in selection of epitopes presented on MHC-II molecules by competitively inhibiting the peptide exchange factor HLA-DM/H2-M (DM), which removes CLIP from the MHC-II peptide-binding groove to allow for binding of antigenic peptides and edits the spectrum of MHC-II-bound peptides to remove weakly-bound species[20,32,37]. DO expression has been demonstrated in many studies to affect presentation of certain epitopes[111,262,276-279], and we have recently shown that DO serves to increase the breadth and diversity of the B cell immunopeptidome[330]. In addition to its expression in B cells[261,262], DO has been shown to display distinct patterns of expression and regulation compared to other components of the MHC-II pathway. Expression of DO is restricted to immature dendritic cells (DCs), mature B cells, and medullary thymic epithelial cells (mTECs), and DO is downregulated as DCs mature and as B cells enter the germinal center (GC)[101,111,112,131,137,141,149,261,262]. Based on this unique expression pattern and given its role in broadening the MHC-

II peptidome, DO may serve to fine-tune the peptide repertoire in order to maintain central and peripheral tolerance to an array of autoantigens.

Positive selection of developing thymocytes is necessary to ensure that CD4 T cells appropriately recognize MHC-II peptide complexes, while negative selection in the thymus eliminates T cells overtly reactive to self. The processes that govern central tolerance have been shown to be exquisitely specific with respect to both allelic and peptide requirements for recognition[167,179,331]. Modulation of the MHC-II peptidome by DO is therefore likely to affect the repertoire of the CD4 T cell clonotypes selected, resulting in different antigen specificities. Early characterization of the $DO^{-/-}$ mouse reported increased selection of CD4 single-positive (SP) thymocytes[276], and ectopic expression of DO in DCs was shown to prevent diabetes development in the NOD mouse[111]; both of these results support a role for DO in modulating T cell selection. Similarly to the effect of DO on B cells[330], DO expression in mTECs and other thymic antigen-presenting cells (APCs) may qualitatively and quantitatively alter the immunopeptidome presented to developing CD4 T cells. Indeed, analysis of peptides eluted from MHC-II isolated from mouse thymic cell lysates demonstrated a similar broadening effect of DO on the peptide repertoire (unpublished observations) as was observed for human and mouse B cells[330], such that in the absence of DO, highly abundant peptide species are presented at greater density, while many lesser abundant peptides are no longer presented. This dual effect observed in peptide elution studies can be attributed to lifting inhibition of DM when DO is absent, with highly DM-sensitive peptides removed from the presented peptidome[330]. Conventional

CD4 T cells specific for peptide species normally present in the repertoire may escape deletion in mice lacking DO, whereas deletion of clonotypes specific for more abundant peptides may be more efficient. In addition, selection of CD4 T cells into the T regulatory (Treg) lineage is posited to occur at an affinity or avidity threshold above that of negative selection[171,173,179,332], such that alterations in the immunopeptidome due to DO expression in the thymic medulla may exert effects on the efficiency of Treg selection.

Based on the manner in which DO has been shown to modulate the MHC-II peptidome, in this work we sought to examine the effect of DO on the TCR repertoire and on the functional capacity of conventional and regulatory T cell subsets. Our results indicate that DO functions in the thymus primarily to allow for optimal selection of CD4 T cells into the Treg lineage. While Tregs selected in the absence of DO ($DO^{-/-}$ Tregs) exhibit greater suppressive capacity, this effect appears to come at the expense of efficient Treg function in the GC, with $DO^{-/-}$ mice exhibiting elevated levels of autoantibodies concomitant with reduced GC Tregs. When challenged with autoantigens, $DO^{-/-}$ mice similarly display increased autoantibody levels with fewer Tregs again observed in the GC. These data identify a previously unknown consequence of DO expression and highlight the importance of this molecule in restraint of autoimmunity.

Results

DO increases Treg diversity and alters CDR3 amino acid usage

Based on our observation that the diversity and density of self-peptide species presented on MHC-II is modulated by DO expression[330], we reasoned that DO may function in the thymus to efficiently delete T cells reactive to self as well as to mediate optimal selection of T cells into the Treg lineage. In order to examine the effect of DO on the T cell repertoire at the clonotype level, we crossed DO$^{-/-}$ mice with TCRVβ transgenic mice previously used in studies of self-reactivity, YAe62β[333,334]. These mice were further crossed with TCRα$^{+/-}$ Foxp3^{GFP} mice, and TCRα sequencing was performed for CD4 naïve T cells, CD8 naïve T cells, and

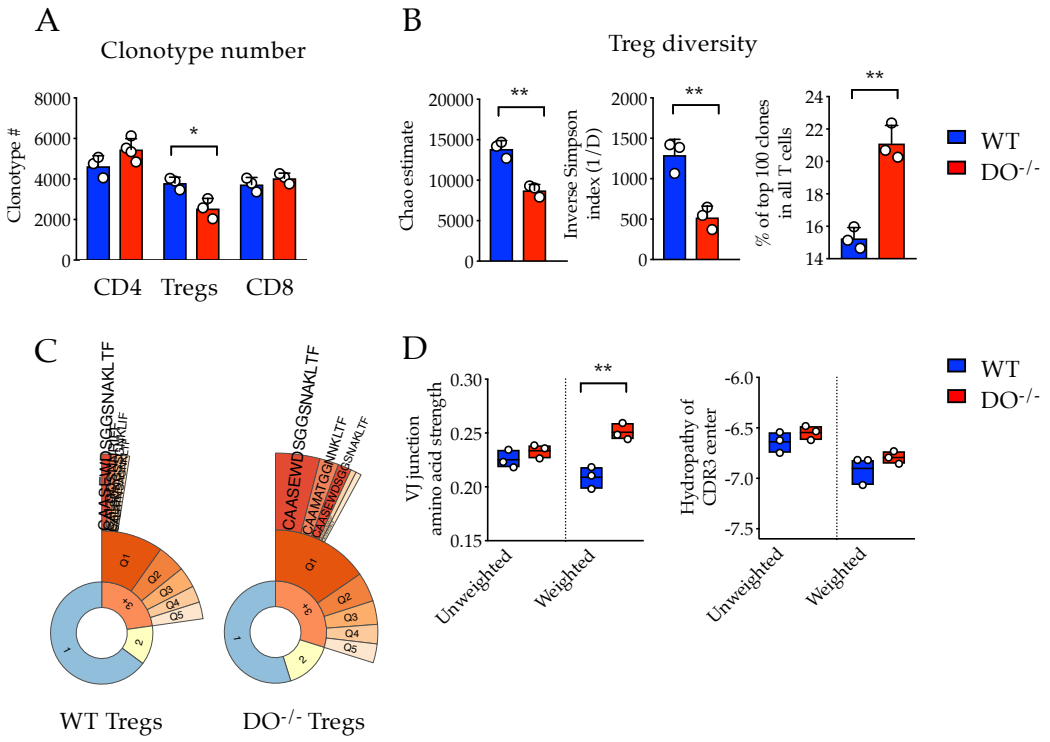

Figure 3.1. DO increases Treg clonotypic diversity and modulates CDR3 properties of Treg clonotypes. (A) Clonotype numbers of CD4 naïve T cells, Tregs, and CD8 naïve T cells were determined following processing of TRAV sequencing data using the MIGEC→MiXCR→VDJTools pipeline. (B) Diversity of the Treg population is shown, as determined by calculation of the Chao1 and Simpson diversity indices, as well as by analysis of the proportion of the top 100 clonotypes in the total Treg population. (C) Analysis of Treg clonotypic frequency distribution using quantile plots, which depicts the fraction of clonotypes identified once (blue), twice (yellow), or three or more (orange) times, with higher-order clonotypes then further divided into quantiles (designated "Q"). The CDR3 sequences for the top 5 clonotypes, as well as their proportions, are shown for Q1. Representative $DO^{-/-}$ and WT samples are shown. (D) Analysis of amino acid strength at the VJ junction (left, weighted and unweighted) and hydropathy of the central 5 amino acids of the CDR3 (right, weighted and unweighted) are shown. For each data point (n=3), cells were isolated from 3 $DO^{-/-}$ or WT YAe62β $TCR\alpha^{+/-}$ $Foxp3^{GFP}$ mice. Mean ± SD shown. Unpaired parametric t-tests were performed to assess significant differences; *p<0.05, **p<0.01.

Tregs sorted from $DO^{-/-}$ or wild-type (WT) YAe62β $TCR\alpha^{+/-}$ $Foxp3^{GFP}$ mice. Data processing was performed using an established pipeline[335,336], which allowed for barcoding of RNA transcripts by UMIs and efficient error correction, and therefore for systematic quantitation of TCR clonotypes. We observed that when DO was absent, clonotype numbers were significantly reduced in the Treg population, numbers of CD4 conventional T cell clonotypes were only slightly increased, and as expected no effect was observed on CD8 T cells (Figure 3.1A). Analysis of diversity indices demonstrated a substantial decrease in clonotype diversity in the $DO^{-/-}$ Treg population by several measures, including the Chao1 index[330], which provides an estimate of species richness and accounts for issues with undersampling, and the Simpson index[330], which calculates species diversity weighted by abundance (Figure 3.1B). These results suggested that differences in the diversity of $DO^{-/-}$ Treg clonotypes were largely due to increased frequencies of particular clonotypes. When the proportion of the top 100 clonotypes within the total Treg population was assessed, the effect of DO on the most abundant clonotypes was apparent (Figure 3.1B). Depiction of repertoire clonality using

quantile plots similarly demonstrated the effect of DO on highly-abundant Treg clonotypes, with clonotypes observed at higher frequencies constituting a much greater proportion of the total Treg population (Figure 3.1C). To ascertain the effect of DO on self-reactivity of Tregs, we examined the mean amino acid strength at the VJ junction and the mean hydropathy of the central 5 amino acids of the CDR3, both of which represent the primary region that interacts with the MHC-II peptide complex and which may influence the degree of self-reactivity of a given TCR[337]. Analysis of all $DO^{-/-}$ and WT Treg clonotypes showed no significant differences in these parameters between $DO^{-/-}$ or WT Treg CDR3 regions, although a slight increase in both variables is appreciable for $DO^{-/-}$ Tregs (Figure 3.1D). When weighting of these variables was performed to account for the effect of DO on highly abundant clonotypes, the amino acid strength of VJ junction residues displayed a significant increase in $DO^{-/-}$ Tregs compared to WT (Figure 3.1D). A slight shift in CDR3 hydropathy was observed for $DO^{-/-}$ Tregs compared to WT upon weighting, which may represent a meaningful increase that alters the self-reactivity of clonotypes selected in the absence of DO (Figure 3.1D). In sum, we show that the predominant effect of DO expression on the T cell repertoire is to skew selection of highly abundant Treg clonotypes, and in doing so to affect amino acid properties of the overall Treg population that potentially influence self-reactivity.

DO regulates Treg number and phenotype

Given the effect of DO on Treg clonotypes in the YAe62β mouse, we next examined Treg populations in C57BL/6 mice deficient in DO compared to WT. Although numbers of total CD4 T cells have been demonstrated previously to be unaltered in these mice[279,288], the effect of DO on Tregs has not thus far been reported. We observed an increase in Tregs in both number and frequency in the absence of DO (Figure 3.2A-B). Tregs in the thymus, spleen, peripheral LNs, and mesenteric LNs were all shown to be significantly increased in $DO^{-/-}$ mice (Figure 3.2A-B). DO is expressed not only in mTECs but also in mature B cells and DC subsets[137,149], and so we examined the possibility that greater differences between $DO^{-/-}$ and WT mice in peripheral Tregs compared to thymic Tregs arose from peripheral expansion. Examination of Treg frequencies at 2 weeks of age, soon after Treg selection begins[338,339], demonstrated a similar increase in Tregs early in development as was observed in the adult $DO^{-/-}$ mouse (Figure 3.2C), suggesting that Treg expansion in the periphery is unlikely to account for the observed increase in Tregs. We further examined peripheral expansion of $DO^{-/-}$ Tregs by evaluating their proliferative capacity; BrdU was injected for 3 days into $DO^{-/-}$ and WT $Foxp3^{GFP}$ mice, and $Foxp3^{GFP+}$ T cells were stained for anti-BrdU. No apparent difference in Treg proliferation was observed between $DO^{-/-}$ and WT (Figure 3.2D). To assess the capacity of $DO^{-/-}$ and WT Tregs to undergo homeostatic proliferation in response to WT compared to $DO^{-/-}$ APCs, which would present an altered repertoire of peptides, we co-transferred congenically-marked $DO^{-/-}$ and WT Tregs into $DO^{-/-}$ or WT $TCR\beta^{-/-}TCR\delta^{-/-}$ (TCR-deficient) mice together with CD4 T cells

and determined the proportion of DO$^{-/-}$ and WT Tregs 9 days after transfer. In each experiment, DO$^{-/-}$ and WT Tregs accounted for ~50% of Foxp3^{+} cells (Figure 3.2E),

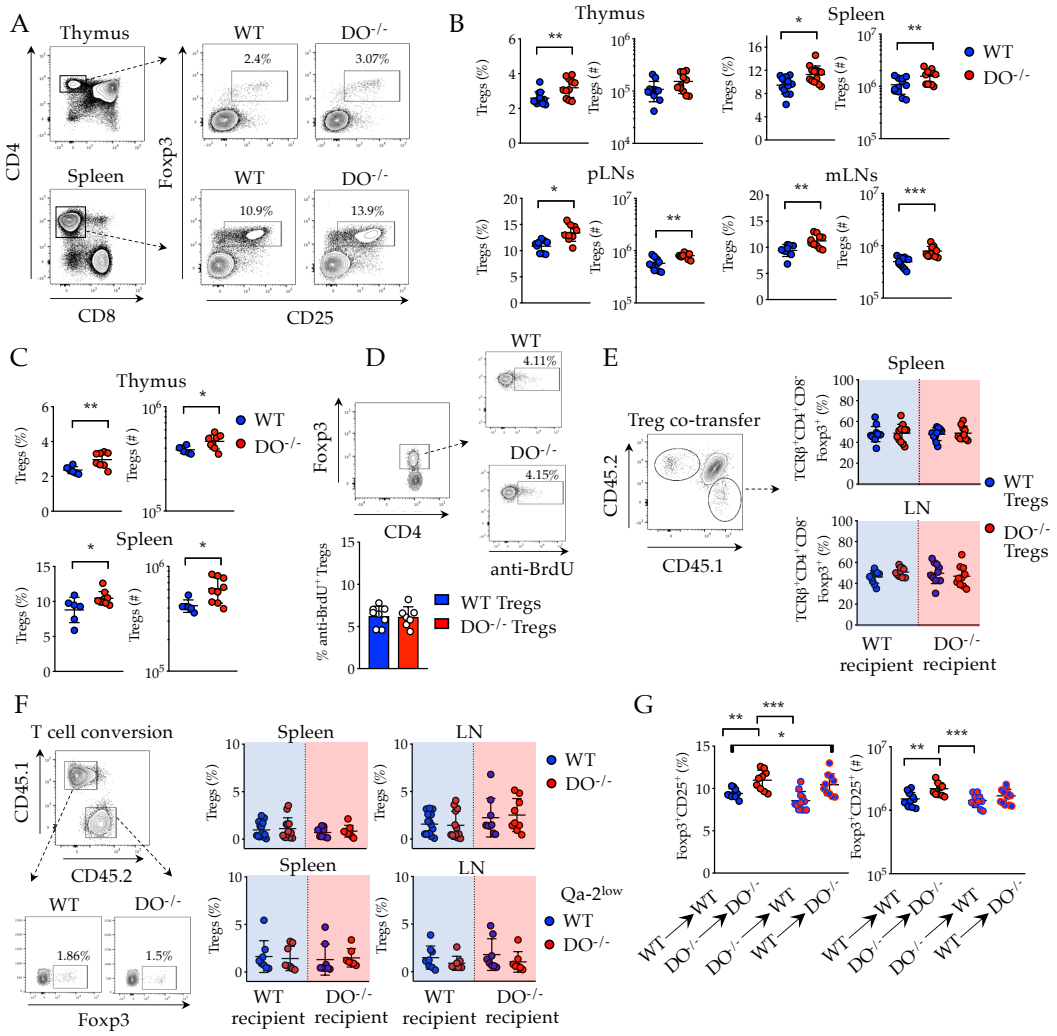

Figure 3.2. Thymic expression of DO augments selection of Tregs. (A) Tregs were identified by first gating on $CD4^+CD8^-$ T cells in thymus and peripheral lymphoid organs, followed by examination of Treg frequency ($CD25^+Foxp3^+$) within the $CD4^+CD8^-$ gate. (B) Treg frequency and number are shown for thymus, spleen, peripheral LNs (inguinal, axillary, and brachial, shown as pLNs) and mesenteric LNs (mLNs) in $DO^{-/-}$ and WT mice. (C) Thymic and splenic Treg frequency and number in mice aged 14-18 days were examined in $DO^{-/-}$ and WT mice. (D) Analysis of Treg proliferation was performed in $DO^{-/-}$ and WT mice by injection of 1 mg/day of BrdU for 3 consecutive days. (E) Following co-transfer of equal numbers of congenically-marked $DO^{-/-}$ and WT Tregs (identified as $TCR\beta^+CD4^+CD8^-Foxp3^{GFP+}$) into $DO^{-/-}$ or WT (recipient) TCR-deficient mice, together with $DO^{-/-}$ or WT CD45.1/CD45.2 CD4 T cells, homeostatic proliferation was evaluated 9 days later. (F) Equal numbers of congenically-marked sorted naïve $DO^{-/-}$ and WT Foxp3-negative CD4 T cells to $DO^{-/-}$ or WT TCR-deficient mice (top panel) were transferred to assess the capacity of $DO^{-/-}$ or WT T cells to convert to Tregs (identified as $TCR\beta^+CD4^+CD8^-Foxp3^{GFP+}$) in lymphoid tissue. The Qa-2^{low} fraction of naïve CD4 T cells was similarly transferred (bottom panel). (G) Bone marrow chimeric mice were generated, in which $DO^{-/-}$ or WT mice were lethally irradiated and reconstituted with $DO^{-/-}$ or WT bone marrow, to determine the sufficiency of thymic DO expression in selecting altered frequencies of Tregs ($Ly5.2^+TCR\beta^+CD4^+CD8^-CD25^+Foxp3^{GFP+}$). Mean ± SD shown, with results from 3-4 independent experiments and 2-4 mice/experiment. Unpaired parametric t-tests were performed to determine significant differences; *$p<0.05$, **$p<0.01$, ***$p<0.001$.

indicating lack of DO does not affect the proliferative capacity of Tregs. An additional mechanism that potentially could account for increased peripheral Treg frequencies is peripheral conversion of naïve T cells into Tregs, a phenomenon that most often occurs at mucosal sites but has in some cases been reported to occur in lymphoid tissues in response to self-antigen stimulation[340-343]. Congenically-marked naïve Foxp3-negative $DO^{-/-}$ and WT CD4 T cells were sorted from $DO^{-/-}$ and WT $Foxp3^{GFP}$ mice and co-transferred into $DO^{-/-}$ and WT TCR-deficient mice. 3 weeks later, spleen and LNs were harvested, and $Foxp3^{GFP}$-expressing cells were quantified. No differences were observed between $DO^{-/-}$ and WT CD4 naïve T cells in their ability to convert to Tregs in either $DO^{-/-}$ or WT recipients (Figure 3.2F). Recent thymic emigrants (Qa-2^{low}-expressing naïve CD4 T cells) have been described as preferentially converting to Tregs in the periphery[344], but similarly to when all CD4 naïve T cells were co-transferred, no differential effects between $DO^{-/-}$ and WT Qa-2^{low} naïve T cells were observed with regard to their rate of

conversion to Tregs (Figure 3.2F). Lastly, to determine whether expression of DO in the hematopoietic compartment or in radioresistant thymic epithelial cells is sufficient to select greater numbers of Tregs, we generated bone marrow chimeras, in which $DO^{-/-}$ and WT mice were lethally irradiated and reconstituted with either $DO^{-/-}$ or WT bone marrow. 8 weeks later, $DO^{-/-}$ mice were shown to have increased frequencies and numbers of Tregs relative to WT mice, irrespective of whether they were reconstituted with $DO^{-/-}$ or WT bone marrow (Figure 3.2G), suggesting that thymic-specific expression of DO mediates the observed alterations in Treg selection. We next examined phenotypic changes in $DO^{-/-}$ Tregs compared to WT in the thymus and periphery. Similar to previous reports that describe activated or effector Tregs[339,345,346], we observed increased PD-1 and ICOS expression in $DO^{-/-}$

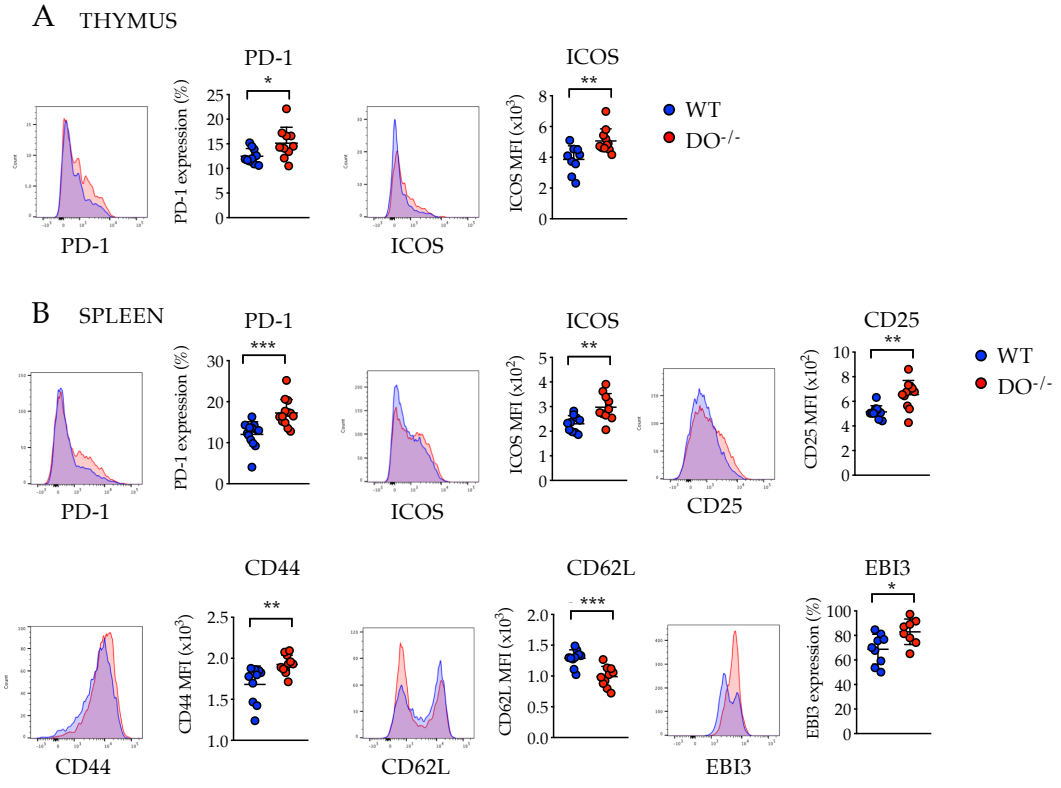

Figure 3.3. DO modulates Treg phenotype in the thymus and periphery. (A) Thymic DO$^{-/-}$ and WT Tregs (gated on CD4^{+}CD8^{-}CD25^{+}Foxp3^{+}) were evaluated for expression of PD-1 and ICOS. (B) Splenic DO$^{-/-}$ and WT Tregs were evaluated for levels of PD-1, ICOS, CD25, CD44, CD62L, and EBI3 (gating was performed as in A). Mean ± SD shown, with results from 3-4 independent experiments and 2-4 mice/experiment. Unpaired parametric t-tests were performed to determine significant differences; *p<0.05, **p<0.01, ***p<0.001.

Tregs in the thymus (Figure 3.3A), while in splenic DO$^{-/-}$ Tregs, expression of PD-1, ICOS, CD44, CD25, and EBI3 were increased, and CD62L was decreased (Figure 3.3B). The effect of lack of thymic expression of DO thus increases selection of Tregs and results in enhanced activation of the Tregs selected.

DO alters Treg suppressive function

Due to the fact that activated Tregs have been shown to exert greater suppressive function compared to their more naïve counterparts[346,347], we next assessed whether

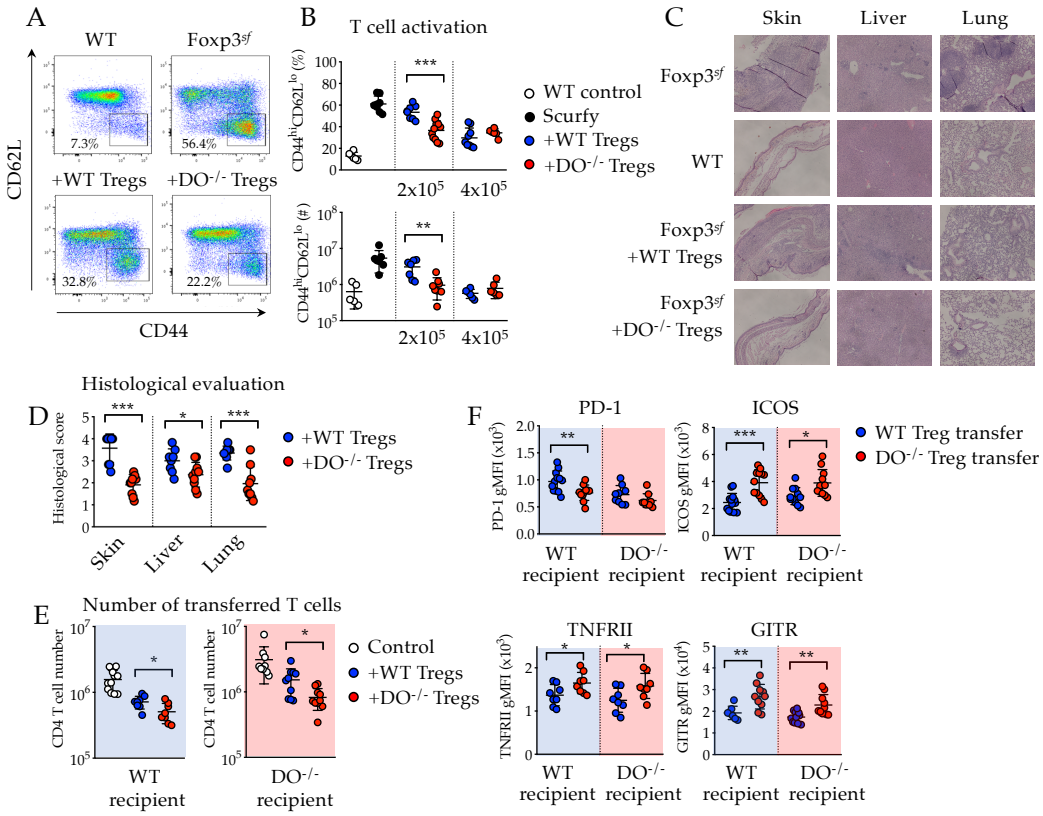

Figure 3.4. DO regulates Treg suppressive capacity. (A) Transfer of $DO^{-/-}$ or WT Tregs was performed in the Foxp3-deficient scurfy mouse model. Following transfer of Tregs at day 1 or 2 of life, CD4 T cell activation (shown as frequency of $CD44^{hi}CD62L^{lo}$ cells, gated on $CD4^{+}CD8^{-}$) was assessed at 21 days of age. Result from a WT littermate mouse is shown for reference. (B) Quantification of T cell activation ($CD44^{hi}CD62L^{lo}$ within the $CD4^{+}CD8^{-}$ population) by frequency (top panel) and number (bottom panel) at day 21 was performed in $Foxp3^{sf}$ mice, in which transfer of $DO^{-/-}$ or WT Tregs was performed at day 1 to 2 of life. (C) H&E staining of skin, liver, and lung samples isolated at day 21 from $Foxp3^{sf}$, WT, $Foxp3^{sf}$ treated with $2x10^5$ WT Tregs, and $Foxp3^{sf}$ treated with $2x10^5$ $DO^{-/-}$ Tregs are shown, using 10x magnification. (D) Histological evaluation of H&E staining of skin, liver, and lung samples shown in (C) by scoring of infiltration and tissue morphology. (E) The effect of differential antigen presentation by $DO^{-/-}$ or WT APCs on $DO^{-/-}$ or WT Treg suppressive capacity was assessed, as measured by suppression of proliferation of congenically-marked $DO^{-/-}$ or WT CD4 Foxp3-negative naïve T cells in TCR-deficient mice by $DO^{-/-}$ or WT Tregs. Quantification of proliferation was performed by enumerating CD4 conventional T cells ($TCR\beta^{+}CD4^{+}CD8^{-}$) based on congenic marker expression. (F) Examination of Treg phenotype during acute inflammation was performed, in which congenically-marked $DO^{-/-}$ and WT Tregs (identified as $TCR\beta^{+}CD4^{+}CD8^{-}Foxp3^{GFP+}$) were co-transferred to $DO^{-/-}$ or WT TCR-deficient mice 5 days after transfer of scurfy T cells. Mean ± SD shown, with results from 3-4 independent experiments and 2-4 mice/experiment, except for scurfy experiments, which are dependent on number of scurfy mice/litter and for which 1-3 mice/experiment were used. Unpaired parametric t-tests were performed to determine significant differences; *$p<0.05$, **$p<0.01$, ***$p<0.001$.

DO impacts the capacity of Tregs to suppress autoreactive T cell effector function. Using the $Foxp3^{sf}$ (scurfy) mouse model, which due to a frameshift mutation in the Foxp3 gene is Treg-deficient and therefore succumbs to lymphoproliferative disease at 3-4 weeks of age[348], we demonstrated that transfer of $DO^{-/-}$ Tregs more efficiently reverts autoimmunity in the scurfy mouse, with fewer numbers of $DO^{-/-}$ Tregs exerting greater suppression compared to WT Tregs (Figure 3.4A-B). Numbers and frequencies of CD4 effectors in both spleen and LN were shown to be reduced when $2x10^5$ $DO^{-/-}$ Tregs were transferred compared to WT Tregs (Figure 3.3B). Histological analysis of skin, lung, and liver further demonstrated the greater suppressive effect of $2x10^5$ $DO^{-/-}$ Tregs, with greater preservation of tissue integrity and less lymphocyte infiltration (Figure 3.4C-D). To exclude the possibility that antigen presentation to $DO^{-/-}$ Tregs by WT APCs in the scurfy mouse model resulted in greater activation and therefore enhanced suppression by $DO^{-/-}$ Tregs, we performed an in vivo Treg suppression assay in $DO^{-/-}$ and WT TCR-deficient

mice, in which sorted naïve Foxp3-negative CD4 T cells were transferred alone or together with DO$^{-/-}$ or WT Tregs. Suppression of proliferation was not affected by the presence or absence of DO in APC populations (Figure 3.4E), suggesting increased suppression was an intrinsic property of Tregs selected in the absence of DO. We next co-transferred congenically-marked DO$^{-/-}$ and WT Tregs 5 days after scurfy T cell transfer into DO$^{-/-}$ or WT TCR-deficient mice, in order to discern the effect of differential peripheral antigen presentation by DO$^{-/-}$ or WT APCs on Treg activation as well as to examine any phenotypic changes in Tregs during inflammation that may account for the greater suppressive capacity of DO$^{-/-}$ Tregs. Expression of ICOS remained increased in DO$^{-/-}$ Tregs compared to WT, irrespective of transfer to DO$^{-/-}$ or WT TCR-deficient mice (Figure 3.4F), indicating differential antigen presentation does not impact its expression on DO$^{-/-}$ Tregs. PD-1 expression appeared to be affected by both the inflammatory setting and antigen presentation; relative to PD-1 expression by WT Tregs transferred to WT recipients, lesser PD-1 expression was observed in all other contexts (Figure 3.4F), suggesting PD-1 is regulated both in response to presentation of a greater density of self-antigens on MHC-II molecules (in WT Tregs when transferred to DO$^{-/-}$ TCR-deficient mice) as well as downregulated in DO$^{-/-}$ Tregs during acute inflammation when antigen density is likely augmented. We also observed greater expression of GITR and TNFRII in DO$^{-/-}$ Tregs compared to WT, independent of differential antigen presentation by DO$^{-/-}$ or WT APCs (Figure 3.4F); Treg suppressive function has been reported to be maximally effective when these molecules are expressed[345,349,350]. Taken together, these data suggest that the DO$^{-/-}$

Treg phenotype is predominantly cell-intrinsic, and that during inflammation $DO^{-/-}$ Tregs upregulate molecules that augment Treg suppressive capacity to a greater degree than their WT counterparts.

DO impacts Tfr differentiation and autoimmunity

Previous examination of immunological alterations in the $DO^{-/-}$ mouse model demonstrated a mild autoimmune phenotype in these mice, characterized by elevated titers of anti-nuclear antibodies (ANAs) beginning at 5 months of age[288], although in another study this effect was not observed[259]. We assessed ANAs in serum isolated from 6-month-old $DO^{-/-}$ and WT littermate mate, and similarly to Gu *et al*.[288], $DO^{-/-}$ mice were shown to display higher levels of antibodies specific for dsDNA (Figure 3.5A). Elevated Treg numbers intuitively would seem to counter development of autoimmune disease; however, the recently described germinal center (GC)-resident T follicular regulatory (Tfr) cell subset, which differentiates from Tregs, has been implicated in mediating the humoral response in several contexts of autoimmunity[351-353]. Recent work delineating the effect of Treg-specific deletion of Helios on Treg function reported increased autoantibody levels based on the reduced ability of Helios-deficient Tregs (generated by Cre-mediated deletion of floxed Helios in Foxp3-expressing cells) to differentiate into Tfr[354]. In another study, PD-1 expression by Tregs was shown to negatively regulate differentiation of Tregs into Tfr and to reduce Tfr suppressive capacity[355]. Based on the similar autoimmune phenotype of the $DO^{-/-}$ mouse to the $Helios^{fl/fl}$ x $Foxp3^{Cre}$ mouse as well as the augmented expression of PD-1 on $DO^{-/-}$ Tregs, we

evaluated GC cell subsets in 12-week-old DO$^{-/-}$ and WT mice to determine whether an aberrant GC reaction could account for the elevated ANAs observed in the DO$^{-/-}$ mouse. GC B cells and T follicular helper (Tfh) cells were found to be increased in DO$^{-/-}$ mice, while the frequency of Tfr cells was decreased (Figure 3.5B), suggesting insufficient regulation of interactions between autoreactive B cells and T cells in the GC and therefore lack of restraint of autoantibody production in the DO$^{-/-}$ mouse. Using the Treg co-transfer model employed above, in which scurfy T cells were transferred followed by transfer of congenically-marked DO$^{-/-}$ and WT

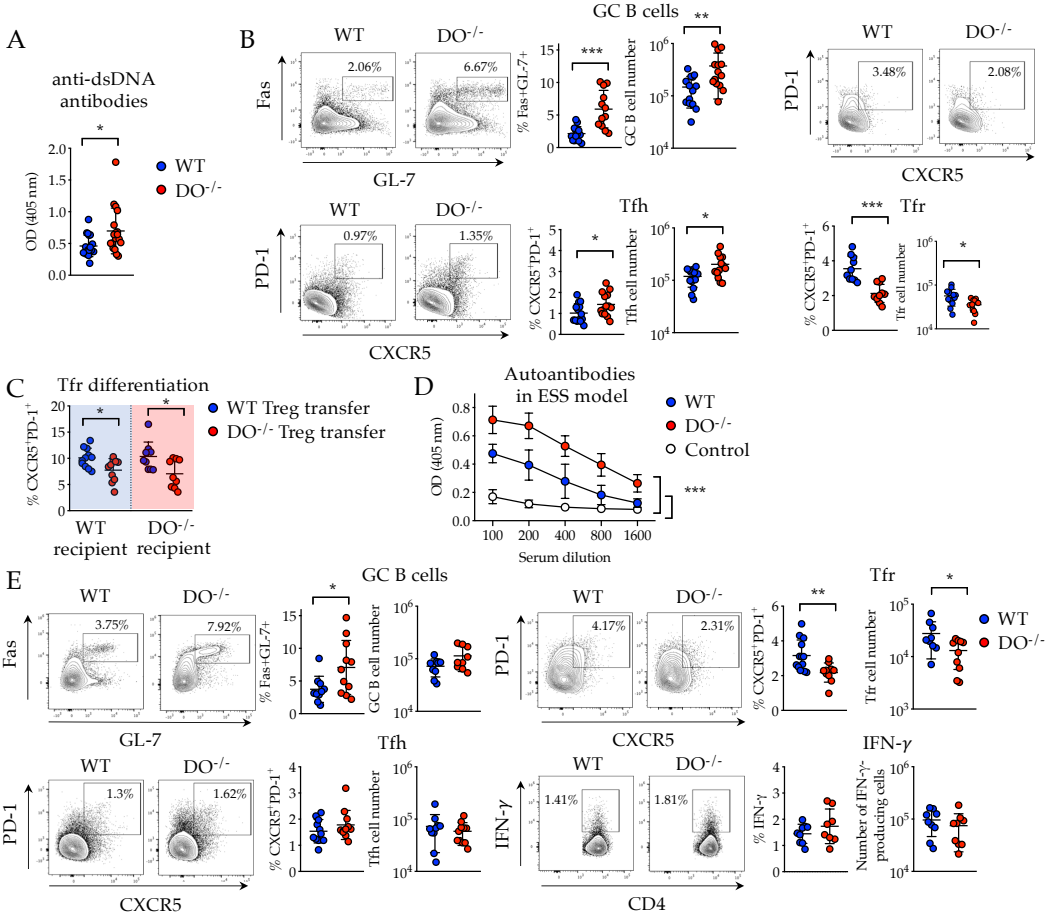

Figure 3.5. DO impacts differentiation of Tfr and development of autoimmunity. (A) Anti-dsDNA antibodies were measured in sera (diluted 1:50) isolated from 6-month-old $DO^{-/-}$ and WT mice. (B) Cell subsets important in the GC reaction were assessed in 12-week-old $DO^{-/-}$ and WT mice. GC B cells ($Fas^+GL\text{-}7^+$, gated on $B220^+IgD^-$), Tfh cells ($CXCR5^+PD\text{-}1^+$, gated on $CD4^+CD8^-B220^-Foxp3^-$), and Tfr ($CXCR5^+PD\text{-}1^+$, gated on $CD4^+CD8^-B220^-CD25^+Foxp3^+$) were quantified in spleens. (C) The capacity of $DO^{-/-}$ and WT Tregs to differentiate into Tfr was examined; 5 days following transfer of scurfy T cells, congenically-marked $DO^{-/-}$ and WT Tregs were transferred, and Tfr (identified as $TCR\beta^+CD4^+CD8^-B220^-Foxp3^{GFP+}CXCR5^+PD\text{-}1^+$) differentiation was assessed 7 days later. (D) Anti-dsDNA antibody levels were assessed by serial dilution in an induced model of experimental Sjogren's syndrome (ESS) for $DO^{-/-}$ and WT mice. Control mice were immunized with adjuvant alone, and sera were collected at 5 weeks post-immunization and diluted twofold. (E) Cervical LNs were isolated at 5 weeks post-immunization in the ESS model and examined for GC cell subsets, identified as in (B), as well as for IFN-γ expression by CD4 T cells. Mean ± SD shown, with results from 3-4 independent experiments and 2-4 mice/experiment. Unpaired parametric t-tests were performed to assess significant differences, and multiple t-tests were used to determine statistical differences in (D); *$p<0.05$, **$p<0.01$, ***$p<0.001$.

Tregs 5 days later, we examined whether Treg differentiation to Tfr is affected by differential antigen presentation by $DO^{-/-}$ or WT APCs. Fewer Tfr were observed in the $DO^{-/-}$ Treg population when transferred to either $DO^{-/-}$ or WT TCR-deficient mice, indicating Tfr differentiation is unaffected by antigen presentation by $DO^{-/-}$ vs. WT APCs (Figure 3.5C). To further probe the role of Tfr in the development of autoimmunity in the $DO^{-/-}$ mouse, we immunized female $DO^{-/-}$ and WT littermate mice with salivary gland-derived autoantigens to induce experimental Sjogren's syndrome (ESS), a chronic disease model that in humans is characterized by autoimmune attack of moisture-producing glands and can coincide with systemic organ dysfunction including pneumonitis and nephritis[356,357]. Ablation of Tfr in mice via Treg-specific targeting of Bcl6 has also recently been demonstrated to exacerbate disease in the ESS model, as evidenced by elevated levels of anti-dsDNA antibodies, reduced saliva secretion, and lymphocytic infiltration of the salivary glands in the absence of Tfr[353]. Upon induction of ESS in $DO^{-/-}$ and WT littermate mice, anti-dsDNA antibody levels were significantly increased in $DO^{-/-}$

mice at 5 weeks post-immunization compared to WT mice (Figure 3.5D). Examination of cell subsets within the cervical LNs isolated at this time point demonstrated increased frequencies of GC B cells and decreased frequencies and numbers of Tfr (Figure 3.5E), again implicating lack of regulation of the GC response in the increase in anti-dsDNA antibodies observed in $DO^{-/-}$ mice. These data indicate that $DO^{-/-}$ Tregs, while increased in number and endowed with greater suppressive capacity, are functionally deficient in their ability to suppress the autoimmune GC reaction, resulting in aberrant autoantibody production and increased susceptibility to autoimmunity.

Discussion

The results reported in this work provide insight into a previously undescribed role for thymic expression of the nonclassical MHC-II molecule DO in mediating selection of T cells into the T regulatory lineage. DO has been shown to alter the global MHC-II self-peptidome by increasing the breadth of peptides presented, such that when DO is absent, abundant self-peptides are presented at greater density, while many low abundance peptides are no longer presented[330]. Given that Tregs are positively selected on self-peptide ligands during the process of negative selection, DO-dependent differences in Treg selection are likely due to increased presentation of abundant peptides, rather than to lack of presentation of low abundance peptides, consistent with the avidity model of Treg selection[171,332]. We further show that when DO is absent, altered selection of Tregs results in greater

Treg activation and suppressive capacity. Despite the enhanced effector phenotype and function of $DO^{-/-}$ Tregs, these cells appear to be deficient in their ability to differentiate into Tfr, resulting in increased levels of autoantibodies at 6 months of age as well as in the induced experimental model of Sjogren's syndrome. These data indicate that DO is required to select Tregs at the appropriate frequency and with the appropriate phenotypic and functional properties, and that perturbation of DO expression predisposes mice to autoimmunity due to Treg dysfunction.

The phenotype observed for $DO^{-/-}$ Tregs shares features with several recently described Treg subsets and suggests DO plays a role in selection of Tregs with distinct properties. Similar to $DO^{-/-}$ Tregs, Tregs that express high levels of PD-1, GITR, and CD25 have been demonstrated to be highly self-reactive, to exhibit lesser diversity, and to more efficiently suppress lymphoproliferation compared to Tregs expressing lower levels of these molecules[345]. Aire-dependent selection of Tregs early in life has been shown to generate a Treg compartment uniquely capable of reversing autoimmune pathology associated with Aire deficiency, compared to Tregs generated in the adult mouse[339]. Tregs selected during this perinatal window of development expressed higher levels of PD-1, EBI3, and ICOS, similar to the phenotype displayed by $DO^{-/-}$ Tregs[339]. Analysis of perinatal mTECs also identified a previously undescribed aspect of regulation of DO expression; compared to mTECs in the adult mouse, perinatal mTECs were shown to exhibit lower expression of DO and higher DM expression, indicative of presentation of a different peptide repertoire early in life[339]. Yang *et al*. conclude that a distinct repertoire of Tregs, selected on an altered MHC-II

immunopeptidome, are required early in life to guard against autoimmune attack of particular tissues[339]. In the case where DO expression is lacking throughout life, as we have examined here, the effect on T cell selection may be to generate a Treg repertoire that fails to protect against development of autoimmunity in adult organisms due to inappropriate specificity of the Treg population for the self-antigens that predominate during adulthood.

Based on results of peptide elution studies[330], we posit that peptides presented at greater abundance due to lack of DO are responsible for the observed Treg alterations in frequency, phenotype and function described here. Identification of the peptide ligands that bind these differentially selected Tregs would not only lend support to this hypothesis but could also provide greater understanding of the mechanism whereby Tregs are selected with regard to peptide affinity and/or avidity. Our data also do not necessarily rule out that selection of CD4 conventional T cells is unaffected by DO expression, as the number of CD4 naïve T cell clonotypes appeared to be increased to a minor degree in TCR sequencing experiments. This result would seem to be consistent with less efficient deletion of CD4 T cell clonotypes specific for peptides no longer present in the $DO^{-/-}$ immunopeptidome, but effects on CD4 conventional T cell number and phenotype were not apparent in our studies. We therefore postulate that the predominant function of DO in the thymus is to regulate Treg selection. This idea is supported by the fact that DO is expressed both in the thymic medulla and in the periphery[137,149]; while the thymic vs. peripheral MHC-II immunopeptidome may differ to some degree, it has nevertheless been difficult to reconcile the idea that

DO expression is necessary for clonal deletion given that its expression persists in peripheral APCs, where presentation of DO-dependent peptides would appear to serve little function in maintaining peripheral tolerance. If DO is expressed primarily to mediate Treg selection, however, it would seem more likely that the immune system has evolved to express DO so that Treg clonotypes are both positively selected and provided with appropriate tonic stimulation in the periphery. In addition to the effects of DO on Treg selection, we show that $DO^{-/-}$ mice are predisposed to displaying hallmarks of autoimmunity, in agreement with an earlier report[288]. We attribute increased autoantibody levels to a deficiency in the differentiation of $DO^{-/-}$ Tregs to Tfr, a GC-resident subset which has been shown to functionally suppress the GC reaction in models of autoimmunity and infection[351-353,355,358]. It should be noted that significant increases in GC B cells were also observed in $DO^{-/-}$ mice compared to WT, in both unchallenged and autoantigen-challenged mice. Whether this GC B cell increase is due to defective Tfr function or arises *de novo* in $DO^{-/-}$ mice is unclear. DO-deficient B cells have been shown previously to gain preferential entry to the GC[292], suggesting a mechanism whereby $DO^{-/-}$ B cells receive more help from Tfh cells and thus populate the GC to a greater degree. Moreover, previous examination of the cellular source responsible for ANA production in $DO^{-/-}$ mice indicated that lack of DO in the hematopoietic compartment was sufficient to induce autoimmunity[288]. It is therefore possible that several GC subsets (B cells, Tfh, Tfr) contribute to the observed autoimmune phenotype and that the sum of the aberrant interactions of these cells results in greater autoimmunity in $DO^{-/-}$ mice.

In summary, we have demonstrated that DO functions in optimal selection of the Treg compartment, and that ablation of DO expression results in greater autoimmune phenotypes, which appears linked to to Treg dysfunction. These data not only define a novel function of thymic DO expression but may lead to greater understanding of the mechanism of Treg selection.

Table 3.1. Primer sequences and amplification parameters used for TCR sequencing

Step	Forward primer sequence 5'-3'	Reverse primer sequence(s) 5'-3'	Reaction conditions
cDNA synthesis	CTACACGACGCTCTTC CGATCTNNNNUNNNN UNNNNUCTTrGrGrGrGr G	1) CTCAGCGTCATGAGCAGGTTAAAT 2) CAGGAGGATTCGGAGTCCCATAA 3) TTTTACAACATTCTCCAAGA 4) TTCTGAATCACCTTTAATGA 5) ATGAGATAATTTCTACACCT 6) TTTGGCTTGAAGAAGGAGCG 7)TTCAAAGCTTTTCTCAGTCA 8) TGGTCTCTTTGAAGATATCT	Anneal primers at 72° C 3 min; 42° C 90 min; 50° C 2 min, 42° C 2 min, 10 cycles; 70° C 15 min Hybrid oligo removed by addition of uracil DNA glycosylase (37° C, 40 min)
PCR-1	TCTTTCCCTACACGAC GCTCTTCCGATCT	TTTTGTCAGTGATGAACGTT	95° C 2 min; 95° C 20 sec, 70° C 10 sec with -1° C/cycle, 70° C 30 sec, 10 cycles; 95° C 20 sec, 60° C 10 sec, 70° C 30 sec, 15 cycles; 70° C 3.5 min
PCR-2	TCTTTCCCTACACGAC GCTCTTCCGATCT	AGTTCAGACGTGTGCTCTTCCGATCT NNNNGGTACACAGCAGGTTCTGGGT TCTGGA	95° C 2 min; 95° C 20 sec, 60° C 10 sec, 70° C 30 sec, 8 cycles; 70° C 3.5 min
PCR-3	AATGATACGGCGACC ACCGAGATCTACACTC TTTCCCTACACGACGC TCTTCCGATCT	CAAGCAGAAGACGGCATACGAGATx xxxxxGTGACTGGAGTTCAGACGTGTG CTCTTC*	95° C 2 min; 95° C 20 sec, 60° C 10 sec, 70° C 30 sec, 8 cycles; 70° C 3.5 min
PCR-4	AATGATACGGCGACC ACCGAG	CAAGCAGAAGACGGCATACGA	95° C 2 min; 95° C 20 sec, 57° C 10 sec, 70° C 30 sec, 7 cycles; 70° C 3.5 min

*xxxxxx designates TruSeq i7 sequence (ACAGTG, GCCAAT, CTTGTA, GTGAAA, CGATGT, TGACCA, CAGATC, AGTCAA, ATGTCA, CCGTCC)

Materials and Methods

Mice

H2-O-deficient mice were kindly provided by Dr. Xinjian Chen at the University of Utah School of Medicine, following backcrossing to C57BL/6 mice for 10 generations. H2-O$^{-/-}$ (DO) mice were further backcrossed at the University of Massachusetts Medical School to C57BL/6 mice obtained from Jackson Laboratory (Bar Harbor, ME). Heterozygous matings were performed to obtain DO$^{-/-}$ and WT littermate controls for experiments. The DO$^{-/-}$ mouse was also bred with B6.Cg-*Foxp3*^{tm1Mal}/J (Foxp3^{GFP}) mice, B6.SJL-*Ptprc*^{a}*Pepc*^{b}/BoyJ (Ly5.1) mice, and B6.129P2-*Tcrb*^{tm1Mom}*Tcrd*^{tm1Mom}/J (TCRβ$^{-/-}$TCRδ$^{-/-}$) mice purchased from Jackson Laboratory, and with YAe62β^{333,334} and TCRα$^{+/-}$ mice provided by Dr. Eric Huseby (University of Massachusetts Medical School). Experiments were performed with 6-10-week-old mice, unless otherwise indicated, using littermate controls. In transfer experiments, congenically-marked nonlittermate mice were age- and sex-matched. Females hemizygous for the Foxp3^{sf} gene (B6.Cg-*Foxp3*^{sf}/J) were purchased from Jackson Laboratory and bred with C57BL/6 males to obtain hemizygous Foxp3^{sf} males, and cell transfer was performed at 1-2 days of age. All mice were cared for and used in accordance with institutional guidelines.

Flow cytometric analysis

Single-cell suspensions of thymi, lymph nodes (LNs), or spleens were blocked with 50 μg/ml anti-CD16/CD32 (BioXCell, West Lebanon, NH) prior to antibody

staining. Staining was performed with the following antibodies purchased from BioLegend (San Diego, CA): TCRβ (H57-597), CD8α (53-6.7), CD44 (IM7), CD62L (MEL-14), CD45.1 (A20), CD45.2 (104), B220 (RA3-6B2), PD-1 (29F.1A12), CD357 (GITR; DTA-1), CD120b (TNF R Type II/p75; TR75-89). Antibodies purchased from BD Biosciences (Franklin Lakes, NJ) were TCR Vβ8.1, 8.2 (MR5-2), CD4 (RM4-5), CD25 (PC61), I-A^b (AF6-120.1), Qa-2 (1-1-2), GL7 (GL7), Fas (Jo2), and CXCR5 (2G8). Antibodies purchased from Thermo Fisher Scientific (Waltham, MA) were Foxp3 (FJK-16s), IgD (11-26c), ICOS (C398.4A), Live/Dead fixable stain, and streptavidin. The Foxp3/Transcription Factor Staining Buffer Set (Thermo Fisher Scientific) was used for fixation and permeabilization prior to staining for Foxp3 and EBI3 (R&D Systems, Minneapolis, MN). For intracellular cytokine staining, cells were stimulated for 4 hours with 50 ng/ml PMA and 1 μg/ml ionomycin (both from Sigma-Aldrich, St. Louis, MO) in the presence of GolgiPlug (BD Biosciences), followed by surface staining, fixation and permeabilization using the Cytofix/Cytoperm Fixation/Permeabilization Solution Kit (BD Biosciences), and staining with IFN-γ (BD Biosciences). Mice were injected for 3 consecutive days with 1 mg/day of 5-bromo-2'-deoxyuridine (BrdU, BD Biosciences), and proliferating cells were detected using the BrdU Flow Kit according to the manufacturer's instructions (BD Biosciences). Analysis of flow cytometric data was performed using FlowJo (version 10.3.5, Treestar, Ashland, OR).

T cell sorting

For T cell receptor (TCR) sequencing experiments, $CD19^-$ cells were isolated by negative selection from spleens of $DO^{-/-}$ or WT YAe62β $TCR\alpha^{+/-}$ $Foxp3^{GFP}$ mice using the EasySep Mouse CD19 Positive Selection Kit II according to the manufacturer's instructions (Stem Cell Technologies, Cambridge, MA). Sorting was performed on a FACSAria (Becton Dickinson, Franklin Lakes, NJ) to isolate CD4 naïve T cells ($TCR\beta^+$, $CD4^+$, $CD8^-$, $I\text{-}A^{b-}$, $B220^-$, $Foxp3^{GFP-}$, $CD44^{low}$, $CD62L^{high}$), CD8 naïve T cells ($TCR\beta^+$, $CD8^+$, $CD4^-$, $I\text{-}A^{b-}$, $B220^-$, $CD44^{low}$, $CD62L^{high}$) and Tregs ($TCR\beta^+$, $CD4^+$, $CD8^-$, $I\text{-}A^{b-}$, $B220^-$, $CD25^+Foxp3^{GFP+}$). Prior to sorting naïve CD4 T cells ($TCR\beta^+$, $Live/Dead^-$, $CD4^+$, $CD8^-$, $Foxp3^{GFP-}$, $CD44^{low}$, $CD62L^{high}$), Qa-2^{low} naïve T cells ($TCR\beta^+$, $Live/Dead^-$, $CD4^+$, $CD8^-$, $Foxp3^{GFP-}$, $CD44^{low}$, $CD62L^{high}$, Qa-2^{low}), or Tregs ($TCR\beta^+$, $Live/Dead^-$, $CD4^+$, $CD8^-$, $CD25^+$, $Foxp3^{GFP+}$) from $DO^{-/-}$ or WT $Foxp3^{GFP}$ mice for T cell transfers, $CD4^+$ cells were isolated using the mouse $CD4^+$ T cell Isolation Kit according to the manufacturer's instructions (Miltenyi Biotec, Auburn, CA). Tregs were further enriched prior to sorting using CD25 microbeads (Miltenyi Biotec).

TCR sequencing

CD4 naïve T cells ($4x10^6$), CD8 naïve T cells ($3x10^6$), and Tregs ($1x10^6$) were sorted as described above from spleens of 3 $DO^{-/-}$ or WT YAe62β $TCR\alpha^{+/-}$ $Foxp3^{GFP}$ mice per sample, sorted cells were resuspended in TRIzol reagent (Thermo Fisher Scientific), and total RNA was extracted according to the manufacturer's instructions. RNA was reprecipitated using sodium acetate and

ethanol[359] and subjected to analysis on a fragment analyzer (Agilent Technologies, Lexington, MA) to assess RNA quality. cDNA was reverse transcribed, from 1.5 μg RNA for CD4 and CD8 naïve T cells and from 300 ng RNA for Tregs, and sequence libraries prepared as previously described[336] with minor modifications, including use of TruSeq sequencing and index primers (Illumina, San Diego, CA) and variations in PCR conditions. Primers and amplification details are described in Table 1. Library sequencing of TCRα (TRAV) chains was performed on a MiSeq instrument (Illumina) using 250 bp paired-end reads. Raw data were downsampled to the lowest number of sequencing reads per cell type prior to processing using FASTX-Toolkit (http://hannonlab.cshl.edu/fastx_toolkit/). Sequencing reads were demultiplexed and UMI-based error correction was performed using MIGEC[360] with a molecular identifier group (MIG) of 3, followed by alignment and clonotype assembly using MiXCR[361]. VDJTools[362] was used for all post-processing analysis of TCR clonotypes.

Bone marrow chimeras

Recipient $DO^{-/-}$ and WT Ly5.1 mice were lethally irradiated with 1100 rads in split doses, and ~$5x10^6$ bone marrow cells isolated from Ly5.2 $DO^{-/-}$ and WT $Foxp3^{GFP}$ mice were then injected i.v. for reconstitution. Recipient mice were analyzed for Treg frequency and number by flow cytometric analysis 8 weeks later.

In vivo suppression assays and T cell transfers

Transfer of Tregs to Foxp3^{sf} (scurfy) mice was performed as previously described[348]; briefly, Foxp3^{sf} male mice were injected i.p. with 2x10^5 or 4x10^5 DO$^{-/-}$ or WT Tregs on day 1 or 2 of life, and spleen and LNs were isolated from Treg-injected and control mice at 3 weeks of age. Treg suppression assays were also performed in DO$^{-/-}$ and WT TCRβ$^{-/-}$TCRδ$^{-/-}$ mice, in which 2x10^6 DO$^{-/-}$ or WT Foxp3^{GFP-} CD4 naïve T cells were transferred i.v., alone or together with 4x10^5 congenically-marked DO$^{-/-}$ or WT Tregs; spleen and LNs were harvested 7 days later. To assess Treg homeostatic proliferation, 4x10^6 Ly5.1/2 DO$^{-/-}$ or WT CD4 T cells isolated by magnetic bead separation were co-transferred i.v. with 4x10^5 each of congenically-marked DO$^{-/-}$ and WT Tregs into DO$^{-/-}$ or WT TCRβ$^{-/-}$TCRδ$^{-/-}$ mice, and spleen and LNs were isolated 9 days post-transfer. To evaluate the capacity of naïve T cells to convert to Tregs, 1x10^6 each of congenically-marked DO$^{-/-}$ and WT Foxp3^{GFP-} CD4 naïve T cells or 5x10^5 each of congenically-marked Qa-2^{low}Foxp3^{GFP-} CD4 naïve T cells were co-transferred i.v. into DO$^{-/-}$ or WT TCRβ$^{-/-}$TCRδ$^{-/-}$ mice, and spleen and LNs were harvested at day 21. Treg phenotype was examined in the context of an inflammatory response via i.v. transfer of 3x10^6 Foxp3^{sf} CD4 and CD8 T cells (isolated using the Pan T cell Isolation Kit according to the manufacturer's instructions [Miltenyi Biotec]), followed by i.v. transfer of 3x10^5 each of congenically-marked DO$^{-/-}$ and WT Tregs 5 days later. Spleen and LNs were then harvested 7 days after Treg co-transfer. Mice were age- and sex-matched in all assays.

Anti-double-stranded (ds) DNA antibody ELISA

To assess dsDNA-specific antibodies, high-binding microtiter plates were coated overnight at 4°C with 25 μg/ml calf thymus DNA (Sigma-Aldrich, St. Louis, MO). Plates were washed with PBS containing 0.05% Tween 20 (PBS-T), and washing was performed at each subsequent step. Plates were incubated for 1 h at RT with blocking buffer (PBS containing 3% fetal calf serum). Sera diluted at the indicated concentrations in blocking buffer were added to plates for 2 h at RT, followed by overnight incubation at 4°C with goat anti-mouse IgG(H+L) alkaline phosphatase (AP) antibody (Southern Biotech, Birmingham, AL) diluted 1:500 in blocking buffer. AP substrate (p-nitrophenyl phosphate, Sigma) was added for 10' at RT in the dark, and the reaction was terminated by addition of 25 μl 5 N NaOH. Absorbance was read at 405 nM using a Victor X5 Plate Reader (Perkin Elmer, Waltham, MA).

Experimental Sjogren's syndrome (ESS) model

Induction of ESS was performed as previously described[353], with minor modifications. Submandibular salivary glands were isolated from $DO^{-/-}$ and WT female mice, homogenized in ice-cold PBS using a Polytron homogenizer (Kinematica AG, Lucerne, Switzerland), and centrifuged. Supernatant was collected and total protein quantified using a bicinchoninic acid protein assay (Thermo Fisher Scientific), and salivary gland protein was emulsified in complete Freund's adjuvant (Thermo Fisher Scientific). $DO^{-/-}$ and WT female littermate mice were immunized subcutaneously with a final concentration of 2 mg/ml salivary

gland protein, and 2 weeks later mice were rechallenged with 1.25 mg/ml salivary gland protein emulsified in incomplete Freund's adjuvant (Thermo Fisher Scientific). Control mice were immunized with adjuvant alone. At 5 weeks following the first immunization, serum was collected by cardiac puncture to assess anti-dsDNA antibody levels, and cervical lymph nodes were isolated for flow cytometric analysis and intracellular cytokine staining.

Histopathology

Skin, liver, and lung tissues isolated from 21-day-old Foxp3^{sf} and WT mice were fixed in 10% formalin, followed by embedding in paraffin and sectioning. Tissue sections were stained with hematoxylin and eosin, and images were acquired on a Zeiss Axio Observer Z1 (Carl Zeiss, Jena, Germany). Blinded histological evaluation was performed as previously described[363].

Statistical analysis

Unpaired nonparametric Mann-Whitney student t-tests and multiple t-tests were used to calculate statistical significance. Prism (version 8.01, GraphPad, San Diego, CA) was used for statistical analysis and to generate graphical plots.

CHAPTER IV

The nonclassical MHC molecule H2-O is required for efficient recovery from influenza A infection

Author contributions:

I performed all experimental work in this chapter. Liying Lu generated tetramers used to identify flu-specific T cells, and the NP311 TCR Tg mouse was generated by the Huseby Lab at UMMS.

Abstract

Presentation of peptides derived from foreign antigens on MHC-II molecules is necessary for protective immunity against invading pathogens. The nonclassical MHC-II molecule DO (HLA-DO in humans, H2-O in mice) modulates the repertoire of peptides presented to CD4 T cells through inhibition of the peptide exchange factor DM. DO has been shown previously to exert effects on humoral immunity in models of immunization and infection, indicative of a role for DO in mediating B cell function. Here, we demonstrate that DO plays a role early in the response to influenza A, and that DO-deficient mice are unable to recover efficiently from A/PR8 infection. Reduced antigen presentation of multiple epitopes and dampened epitope-specific T cell responses were observed in influenza-infected $DO^{-/-}$ mice compared to WT, with the exception of the NP311-325 MHC-II epitope, which was presented more efficiently by $DO^{-/-}$ APCs, suggesting the hierarchical pattern of influenza epitope presentation is altered in the absence of DO. In addition, innate immune cell numbers were reduced, CD8 T cell epitope responses were decreased, and cytokine levels were blunted in A/PR8-infected $DO^{-/-}$ mice compared to WT. Based on this overall pattern of suppressed immunity, we reasoned increased Treg numbers were responsible for the observed response to influenza A in $DO^{-/-}$ mice, but exploring this potential mechanism proved difficult given the models available for Treg depletion. In sum, we show that mice lacking DO fail to mount sufficient immunity to influenza A infection and demonstrate that DO impacts multiple arms of the immune response.

Introduction

Recognition of antigens presented on MHC-II molecules is a central component of the adaptive immune response against invading pathogens. Initiation of this response is mediated by acquisition and processing of foreign antigens by antigen-presenting cells, which then present proteolytically cleaved antigenic peptides on MHC-II via cognate interactions with CD4 T lymphocytes[364]. The helper function of activated antigen-specific CD4 T cells is critical for mounting an effective immune response through induction and maintenance of CD8 T cell cytotoxic activity as well as for selection of plasma and memory B cells in the germinal center (GC) reaction[365,366]. The nonclassical MHC molecule H2-O (hereafter referred to as DO) has been shown to play a role in modulating epitope selection in MHC-II antigen processing and presentation[5,367] and to have effects in the efficiency of the immune response to retroviruses[259]. DO function is exerted through binding and inhibition of H2-M (DM), an endosomal/lysosomal-resident molecule which mediates CLIP removal from MHC-II, catalyzes peptide exchange, and is postulated to edit the peptide repertoire and facilitate greater presentation of immunodominant epitopes[230,368]. We have recently demonstrated that DO increases the breadth of the MHC-II self-peptidome by inhibiting DM and allowing for low-abundance epitopes to be presented, while at the same time reducing presentation of other more abundant epitopes[369]. These observations, together with results of in vitro biochemical and crystallographic studies of DO and DM[32,207,272,278], support a role for DO in shaping the peptide repertoire upon initiation of an immune response[288,367]. Following a pathogenic insult, DO thus may be important in

selecting the epitopes that mediate the CD4 T cell response and in doing so, may help determine the efficiency of pathogen clearance.

DO and DM have been implicated in presentation of MHC-II viral epitopes as well as in immune responses to infection or immunization. The effect of DM-mediated selection of viral epitopes is supported by biochemical work demonstrating an association between MHC-peptide stability and immunogenicity of vaccinia virus peptides[207]. In addition, study of DM function in presentation of *Leishmania major* epitopes and in the humoral response to protein antigens in vivo, which demonstrated the requirement of DM for the CD4 T cell response to an immunodominant MHC-II epitope and for induction of efficient humoral immunity, further implicate a role for peptide editing in shaping the adaptive immune response[289,290]. The function of DO in the context of inflammation or infection has been primarily shown with regard to antibody-mediated effects. Immunization of mice deficient in DO with the model antigens KLH and OVA demonstrated reduced IgG antibody responses compared to WT mice[288], while recent work by Denzin *et al.* reported increased neutralizing antibodies following retroviral infection in mice lacking DO[259]. In vivo modulation of DO in the B cell response to haptenated antigens also suggests that lack of DO expression in B cells confers a competitive advantage for entry into germinal centers[292]. With regard to the effect of DO on T cell responses following immunization, diminished IL-2 and IFN-γ production by CD4 T cells was observed when DO was absent, attributed to a deficiency in antigen presentation[288]. These data indicate that expression of DO

influences cellular responses in adaptive immunity, presumably due to modulation of epitopes presented on MHC-II.

Here, we sought to examine the effect of DO on the immune response to influenza A. Clearance of and protection from influenza virus has been definitively shown to be dependent upon CD8 T cells and the antibody response[370-373], whereas the helper function of CD4 T cells appears most critical for effective recovery from influenza infection[372-374]. Recent work has also highlighted the contributions of cytolytic CD4 T cells (ThCTL) and T follicular helper (Tfh) cells, as well as innate immune subsets including natural killer (NK), NKT, and mast cells during infection with influenza[375-381]. Based on the function of DO in MHC-II epitope selection, we reasoned that lack of DO would skew presentation of influenza-derived epitopes and alter the efficiency of the immune response following infection. We inoculated both $DO^{-/-}$ and WT mice with influenza A and observed a marked delay in recovery from influenza infection in $DO^{-/-}$ mice compared to WT. Lymphocytes failed to proliferate in the absence of DO to the same degree as in WT mice, resulting in substantially fewer cell numbers and reduced epitope-specific responses in both CD4 and CD8 T cells. Antigen presentation early in infection was shown to be altered in the absence of DO, with reduced numbers of dendritic cells (DCs) and NK cells in the lung. Cytokine responses were similarly blunted early in infection and at the peak of the T cell response. Based on this overall pattern of suppression as well as on increased Treg numbers in the $DO^{-/-}$ mouse, we examined whether augmented Treg function was responsible for the defect in the immune response to influenza A in the $DO^{-/-}$ mouse. While we found numbers of lung-resident Tregs to

be increased in the DO$^{-/-}$ mouse, attributing the defect observed to altered Treg function proved difficult due to nonspecific effects of Treg depletion methods. Thus, while we cannot conclusively determine whether Tregs are responsible for the overall suppression of the immune response to influenza A in the DO$^{-/-}$ mouse, we demonstrate the requirement of DO for efficient recovery from infection and show that DO is necessary to establish sufficient innate and adaptive immunity to influenza A.

Results

DO is required for efficient recovery from influenza A infection

In order to determine whether DO plays a role in the immune response to influenza, DO$^{-/-}$ and WT littermate mice were inoculated with a sublethal dose of influenza A

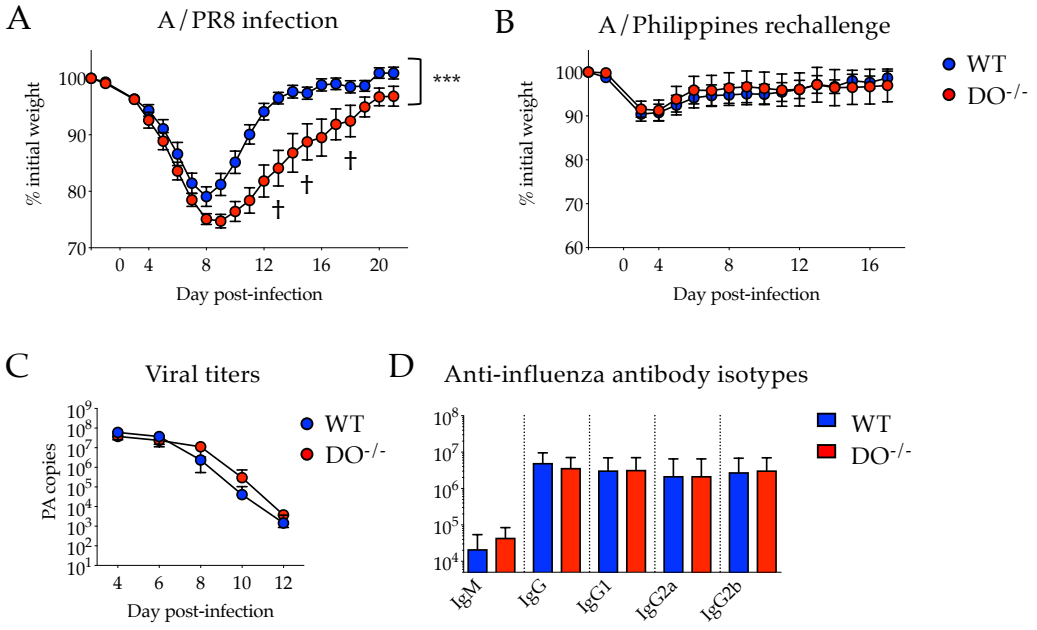

Figure 4.1. DO is required for efficient recovery from influenza A infection. (A) $DO^{-/-}$ and WT mice were inoculated via intranasal instillation with 0.5 LD50 A/PR8 (H1N1) and weighed daily for 21 days. In each cohort of 5 mice inoculated, 1 out of 5 $DO^{-/-}$ mice was sacrificed (denoted by †) due to significant moribundity associated with infection. Results shown (mean ± standard error of mean [SEM]) are compiled from 3 independent experiments, with 5 mice/group/experiment. Statistical analysis of survival using the Gehan-Breslow-Wilcoxon test showed a p-value of 0.038, while two-way ANOVA (using a mixed-effects model with the Geisser-Greenhouse correction) yielded a p-value<0.0001 (***). (B) At day 45 post-infection with A/PR8 and after complete recovery, $DO^{-/-}$ and WT mice were rechallenged with 300 LD50 A/Philippines (H3N2). Results are compiled from 2 independent experiments, with 4-5 mice/group/experiment. Mean ± SEM shown. (C) Viral titers were determined by quantification of the A/PR8 polymerase gene in lung homogenates over time following infection with 0.5 LD50 A/PR8. Data are shown from 2 independent experiments, with 2-4 mice/group, with mean ± SD. (D) Isotype antibody titers were determined by serial dilution of sera isolated at day 21 from $DO^{-/-}$ and WT mice post-infection with A/PR8. Data are compiled from 2 independent experiments, with 4-5 mice/group/experiment, and mean ± SD shown. Unpaired parametric t-tests were performed, unless otherwise indicated.

(PR8, 0.5 LD50) via intranasal instillation and then monitored for 21 days following infection. Recovery from weight loss associated with influenza infection occurred at approximately 14 days post-inoculation in WT mice, as has been previously demonstrated[382,383], whereas in $DO^{-/-}$ mice this recovery was shown to be markedly delayed (Figure 4.1A). $DO^{-/-}$ mice displayed greater weight loss overall, with an approximate 7-day delay in complete recovery (Figure 4.1A). In addition, in each experiment in which mice were inoculated and weight loss monitored, 1 out of 5 $DO^{-/-}$ mice lost >30% of its initial body weight and exhibited significant moribundity, requiring that it be sacrificed prior to completion of the experiment due to the physical symptoms associated with lethality of infection (Figure 4.1A). These data suggest that expression of DO plays a substantial role in the immune response to influenza infection. Isolation of lung tissue and quantitation of viral titers post-infection demonstrated slight increases in viral titers (Figure 4.1C) at later time points in infection in $DO^{-/-}$ mice compared to WT, indicative of a deficiency in the immune response. Mice were also rechallenged with a lethal dose of heterosubtypic influenza virus (A/Philippines, 300 LD50) at day 45

following infection with PR8. No differences were observed between $DO^{-/-}$ and WT mice in their capacity to recover from heterosubtypic viral challenge (Figure 4.1B), for which clearance is mediated primarily by the memory T cell response. Influenza-specific antibody isotype titers at day 21 post-infection with PR8 appeared unimpaired in $DO^{-/-}$ mice (Figure 4.1D). These data, together with the role of DO in antigen presentation, point to alterations in the primary T cell response as the likely basis for the deficiency of mice lacking DO in recovery from influenza infection.

Lymphoid tissue cellularity and T cell responses are diminished in influenza-infected $DO^{-/-}$ mice

To understand the basis for increased susceptibility of $DO^{-/-}$ mice to primary influenza infection, $DO^{-/-}$ and WT mice were examined at several time points post-infection with 0.5 LD50 PR8. At day 4 following infection, the mediastinal lymph nodes (draining LNs [dLNs]) and lungs of $DO^{-/-}$ mice displayed fewer total cells compared to LNs and lungs from WT mice (Figure 4.2A). By day 8 post-infection, spleens and dLNs isolated from $DO^{-/-}$ mice showed substantially diminished cellularity compared to WT mice, with total cell numbers decreased by approximately half (Figure 4.2A-B). While frequencies of the cell subsets that predominate in the spleen and dLN were not shown to be different between $DO^{-/-}$ and WT mice (Figure 4.2C-E), injection of BrdU prior to isolation of lungs, spleen, and dLNs at day 8 demonstrated reduced proliferation of CD4 T and CD8 T cells, as well as B cells, although to a lesser extent (Figure 4.3A-B). Reduced lung and

lymphoid tissue cellularity in DO$^{-/-}$ mice thus appeared not to be attributed to a deficient response in any one cell type, but rather to a reduced capacity of lymphocytes to respond and proliferate in DO$^{-/-}$ mice following influenza infection.

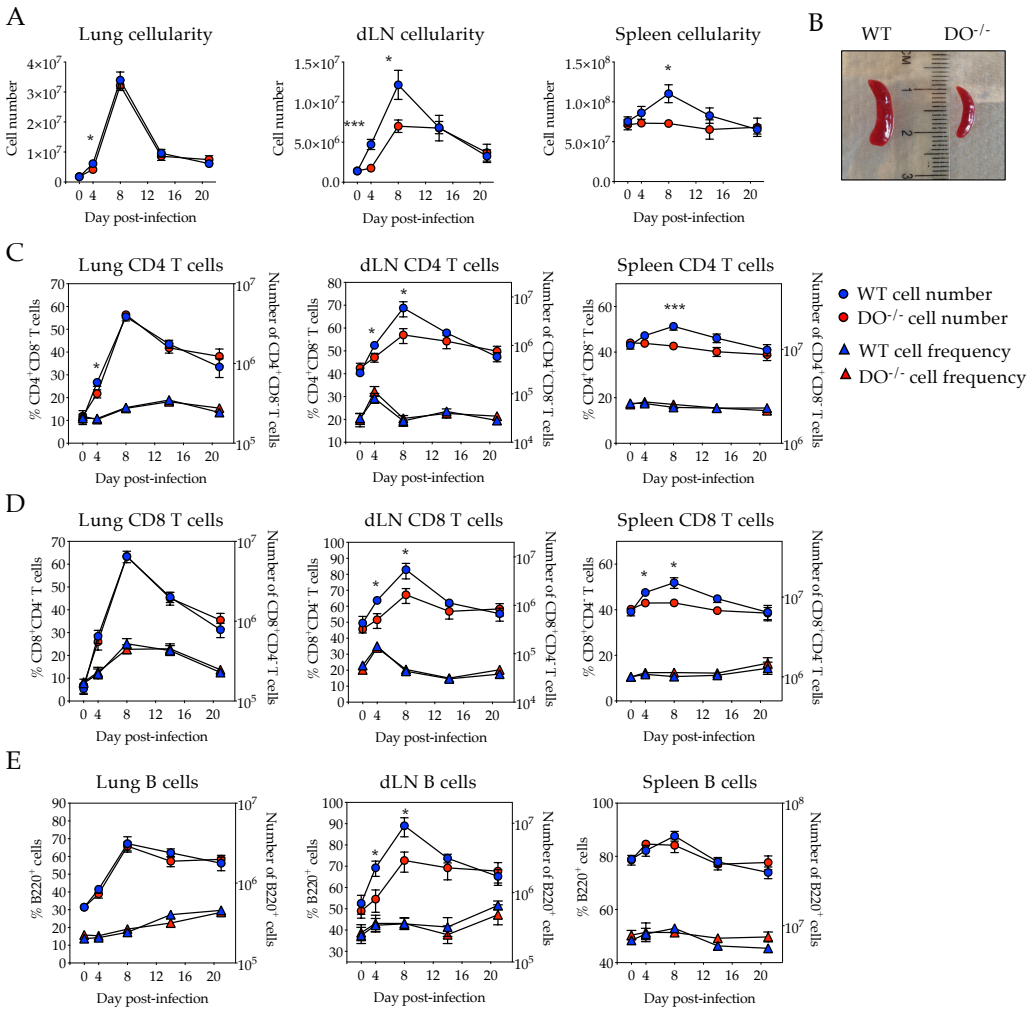

Figure 4.2. DO deficiency results in diminished lymphoid and lung tissue cellularity following influenza A infection. (A) Total cellularity of lungs, dLNs, and spleens in uninfected DO$^{-/-}$ and WT mice and over time following A/PR8 infection (0.5 LD50) is shown. (B) Spleens isolated from DO$^{-/-}$ and WT littermate mice at day 8 post-infection are depicted. (C) Frequency and number of CD4 T cells (CD4^{+}CD8^{-}) in lungs, dLNs, and spleens of DO$^{-/-}$ and WT mice are shown before infection and over time following infection with A/PR8. (D) Frequency and number of CD8 T cells (CD8^{+}CD4^{-}) in lungs, dLNs, and spleens of DO$^{-/-}$ and WT mice are shown before infection and over time following infection with A/PR8. (E) Frequency and number of B cells (B220^{+}) in lungs, dLNs, and spleens of DO$^{-/-}$ and WT mice are shown before infection and over time following infection with A/PR8. Data are compiled from 2-3 independent experiments, with 3-5 mice/group. Unpaired parametric t-tests were performed, mean ± SEM shown, *p<0.05, ***p<0.001.

DO alters presentation of influenza-derived CD4 T cell epitopes

Several MHC-II-restricted influenza A epitopes have been recently demonstrated to be presented in a DM-dependent manner[293], highlighting the impact of peptide editing on influenza-specific T cell responses. To determine the effect of DO on presentation of individual epitopes during influenza A infection, we used lung and dLN cells isolated from DO$^{-/-}$ and WT mice at day 4 post-infection as APCs to

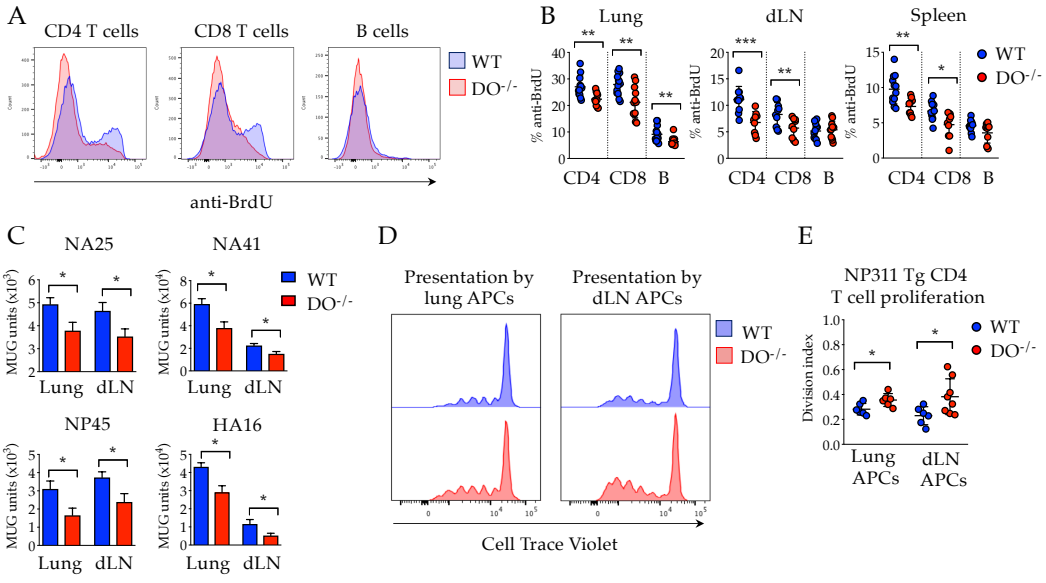

Figure 4.3. DO alters presentation of influenza-derived epitopes. (A) Injection of BrdU 24h prior to analysis at day 8 post-infection was performed to examine proliferation of CD4 (gated on CD4$^+$CD8$^-$) and CD8 (gated of CD8$^+$CD4$^-$) T cells, as well as B cells (gated on B220$^+$) in DO$^{-/-}$ and WT mice. Representative overlaid histograms are shown for anti-BrdU staining in lungs of infected mice. (B) Quantification of proliferation by anti-BrdU is shown for CD4 T cells, CD8 T cells, and B cells in DO$^{-/-}$ and WT mice, compiled from 3 experiments, with 3-5 mice/group/experiment. (C) Antigen presentation of the influenza epitopes NA25, NA41, NP45, and HA16 by DO$^{-/-}$ lung and dLN APCs was shown to be reduced compared to presentation by WT APCs following co-culture with T cell hybridomas specific for each epitope. (D) NP311-specific CD4 T cells were co-cultured with lung and dLN APCs isolated at day 4 post-infection from DO$^{-/-}$ and WT mice, and T cell proliferation was measured by dilution of Cell Trace Violet. Representative histograms shown. (E) The division index, or the average number of divisions cells underwent in the original population, was determined for NP311-specific CD4 T cells stimulated with DO$^{-/-}$ lung or dLN APCs compared to WT APCs. Data are shown for 2 independent experiments, with APCs isolated from 4-6 mice/group/experiment. Unpaired parametric t-tests

stimulate T cell hybrids specific for the NA25, NA41, NP45, and HA16 epitopes (Table 4.1). For every epitope tested, T cell stimulation was shown to be reduced in response to presentation by DO$^{-/-}$ APCs (Figure 4.3C). We similarly assessed

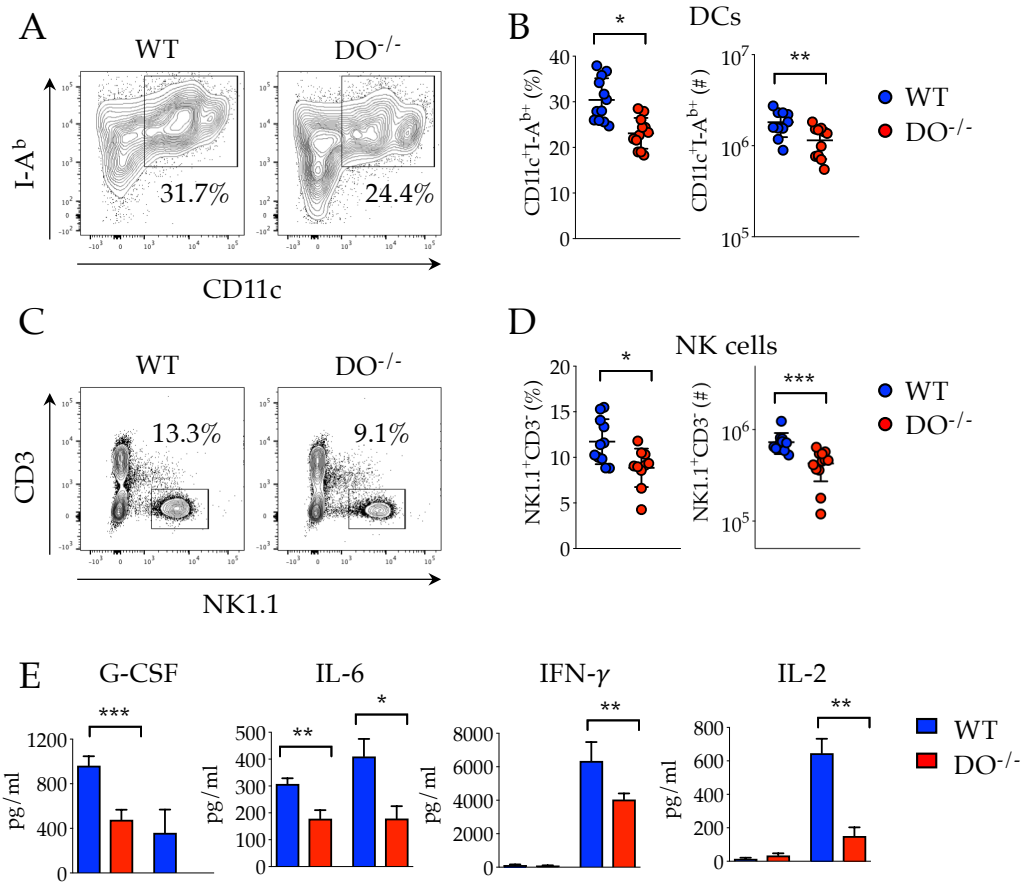

Figure 4.4. Innate cellular and cytokine responses are diminished during influenza A infection when DO is absent. (A) DCs were identified by expression of CD11c and MHC-II (I-A^b), following elimination of the lymphocyte population by visualization of cells by FSC and SSC. Representative plot shown for DO$^{-/-}$ and WT lung samples at day 4 post-infection. (B) Quantification of DCs in DO$^{-/-}$ and WT lungs at day 4 post-infection by frequency (left) and number (right). Data are shown for 3 independent experiments, with 3-5 mice/group/experiment. (C) NK cells were identified by expression of NK1.1 and lack of co-expression of CD3. Representative plot shown for DO$^{-/-}$ and WT lung samples at day 4 post-infection. (D) Quantification of NK cells in DO$^{-/-}$ and WT lungs at day 4 post-infection by frequency (left) and number (right). Data are shown for 3 independent experiments, with 3-5 mice/group/experiment. (E) Analysis of G-CSF, IL-6, IFN-γ, and IL-2 in sera isolated from A/PR8-infected DO$^{-/-}$ and WT mice at days 4 and 8 post-infection. Data are compiled from 2-3 independent experiments, with 3-4 mice/group/experiment. Unpaired parametric t-tests were performed, mean ± SD shown, *p<0.05, **p<0.01, ***p<0.001.

presentation by lung and dLN APCs to T cells specific for the NP311 epitope (Table 4.1), for which a TCR transgenic mouse model was recently generated. In contrast to T cell activation by other epitopes (Figure 4.3C), NP311-specific CD4 T cells were shown to proliferate to a greater degree when stimulated with infected $DO^{-/-}$ APCs compared to WT (Figure 4.3D-E). These data suggest that in the absence of DO, presentation of influenza-derived epitopes is skewed, with much of the response reduced compared to WT. We next assessed DC frequency and number in lungs at day 4 post-infection to determine whether antigen presentation is in large part reduced due to fewer professional APCs. Frequencies and numbers of DCs were reduced in the lungs of $DO^{-/-}$ mice at day 4 post-infection compared to WT (Figure 4.4A-B). In addition, NK cells were shown to be reduced in frequency and number (Figure 4.4C-D), suggesting innate immunity is also compromised in the absence of DO. Levels of IL-6 and G-CSF, both of which participate in the innate immune response early in influenza infection, were reduced in mice lacking DO at day 4 post-infection (Figure 4.4E), suggesting defective immunity is induced early in infection when DO is absent.

Lack of DO diminishes epitope-specific T cell responses

Altered antigen presentation in the $DO^{-/-}$ mouse early in infection is likely to affect the magnitude of T cell responses elicited later in infection, which would presumably impact the efficiency of the overall immune response to influenza A. At day 8 post-infection, we observed reduced IFN-γ and IL-2 levels in $DO^{-/-}$ compared to WT mice (Figure 4.4E). We next examined influenza epitope-specific

T cell responses in lung, dLN, and spleen using MHC-I (D^b) and MHC-II ($I\text{-}A^b$) tetramers (Figure 4.5A). Frequencies of some epitopes were found to be significantly decreased in $DO^{-/-}$ mice, while others showed a downward trend

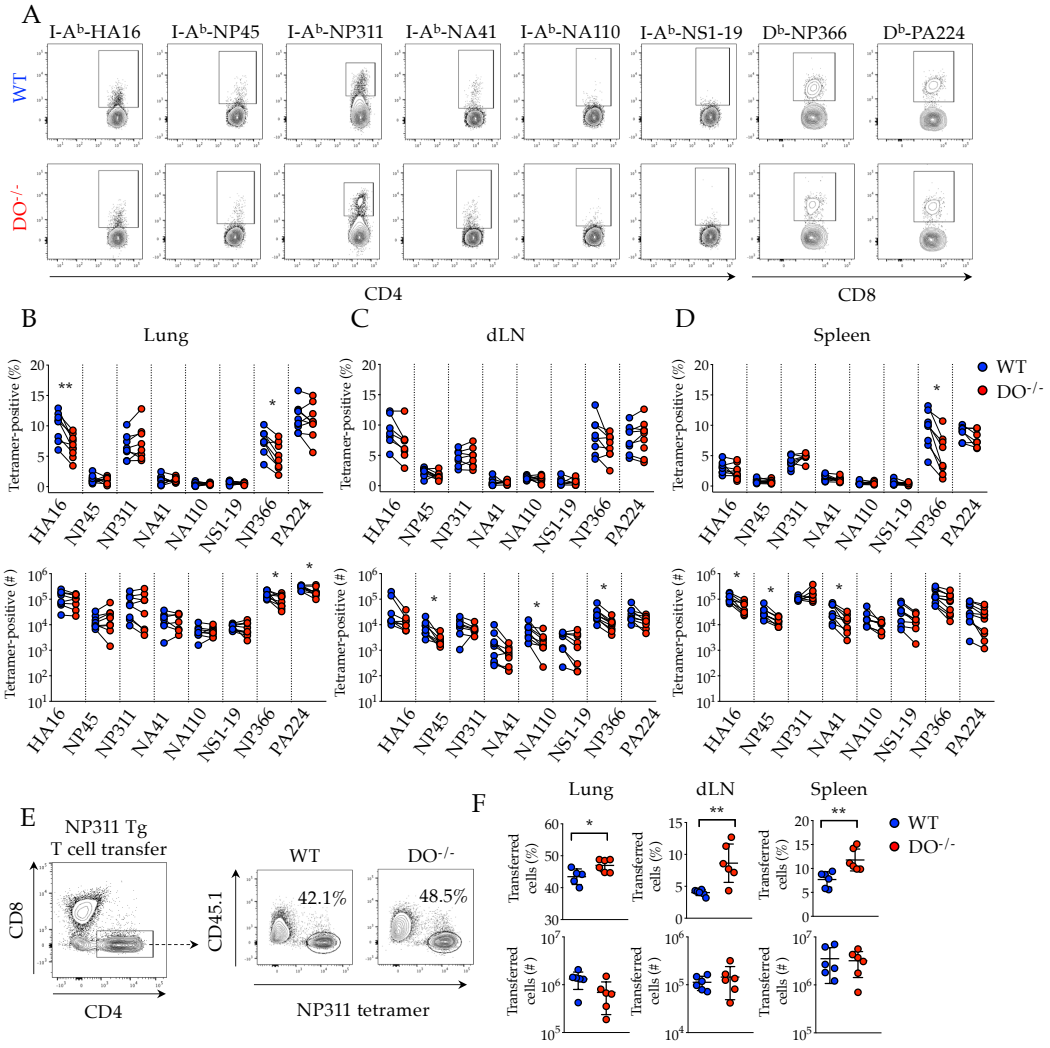

Figure 4.5. Lack of DO reduces epitope-specific CD4 and CD8 T cell responses in influenza A infection. (A) Epitope-specific responses were assessed using $I\text{-}A^b$ tetramers specific for the CD4 T cell epitopes HA16, NP45, NP311, NA41, NA110, and NS1-19 (gated on $CD4^+CD8^-CD44^{high}$), as well as D^b tetramers specific for the CD8 T cell epitopes NP366 and PA224 (gated on $CD8^+CD4^-CD44^{high}$). Representative dotplots are shown for each tetramer for $DO^{-/-}$ and WT lung samples at day 8 post-infection. (B-D) Epitope-specific T cell responses were quantified in lung (B), dLN (C), and spleen (D) in $DO^{-/-}$ and WT mice at day 8 post-infection with regard to frequency and number. (E) Transferred NP311 Tg CD4 T cells were identified by staining for the NP311 $I\text{-}A^b$ tetramer and lack of staining for a congenic marker, gated on $TCR\beta^+CD4^+CD8^-$ T cells. Representative dotplots of $DO^{-/-}$ and WT lung samples shown. (F) Transferred NP311-specific T cells were identified as in (E) and quantified in lungs, dLNs, and spleens of $DO^{-/-}$ and WT recipient mice by frequency and number. Data are compiled from 2 independent experiments, with 3-4 mice/group/experiment. Unpaired parametric t-tests were performed, mean ± SD shown, *$p<0.05$, **$p<0.01$, ***$p<0.001$.

(Figure 4.5B-D). Responses to the NP311 epitope again were shown to be distinct, with increased, albeit minor, frequencies of NP311-specific T cells observed in all tissues (Figure 4.5B-D). When total cell numbers of tetramer-positive CD4 and CD8 T cells were determined, the downward trend in $DO^{-/-}$ mice became more apparent, particularly in lymphoid tissue (Figure 4.5B-D). Given that a TCR Tg mouse model that expresses a TCR specific for the NP311 epitope is available, we examined the ability of NP311 Tg CD4 T cells to proliferate and expand in $DO^{-/-}$ vs. WT mice, with the idea that comparison of T cell proliferation using an identical cellular source (i.e. one that is unaffected by possible differences in T cell selection due to DO) may provide insight into the mechanism of reduced T cell responses in the $DO^{-/-}$ mouse. Similar to results observed in NP311-specific responses at day 8, NP311 Tg CD4 T cells were found to be greater in frequency in the $DO^{-/-}$ mouse, while total cell numbers were unchanged or reduced (Figure 4.5E-F). Taken together, these data suggest that T cell responses in the absence of DO are insufficiently generated, and even that responses specific for an epitope that is likely DM-resistant and presented at greater density are suppressed in the $DO^{-/-}$ mouse.

Depletion of Tregs in $DO^{-/-}$ mice

The overall effect of DO deficiency in influenza A appears to result in a blunted immune response, beginning with innate immunity and continuing into the adaptive immune response. With the exception of presentation of the NP311 epitope, multiple arms of cellular immunity are diminished in the $DO^{-/-}$ mouse, including

CD8 T cell responses, for which DO is unlikely to exert direct effects. We have previously observed increased Treg numbers in lymphoid tissue and thymus in the DO$^{-/-}$ mouse (unpublished results); when frequency and numbers of Tregs in the lung before and during influenza infection were examined, similar increases in lung tissue Tregs were observed in DO$^{-/-}$ compared to WT mice (Figure 4.6A-B). To test for a functional contribution of Tregs in the deficient immune response to influenza A in DO$^{-/-}$ mice, we used a model commonly used for Treg depletion[384,385], in which the diphtheria toxin (DT) receptor fused to GFP was inserted into exon 11 of the Foxp3 gene, allowing for depletion of Foxp3-expressing cells upon DT administration. We observed efficient ablation of Tregs in both DO$^{-/-}$ and WT mice

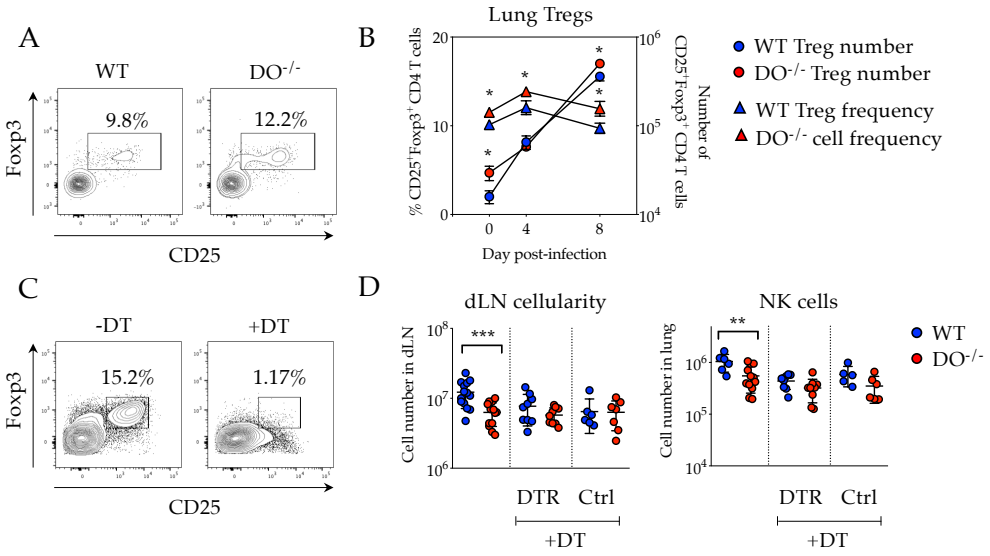

Figure 4.6. Tregs are increased in lungs of DO$^{-/-}$ mice. (A) Lung Tregs were identified as CD25^{+}Foxp3^{+} (following gating on CD4^{+}CD8^{-}). Representative dotplots are shown for lung samples of DO$^{-/-}$ and WT before infection. (B) Quantification of lung Tregs before and following A/PR8 infection (0.3 LD50) in DO$^{-/-}$ and WT mice is shown. Data are compiled from 3 independent experiments, with 3-5 mice/group/experiment. (C) dLN Treg frequencies, identified as in (A), are shown with and without administration of 2 consecutive doses of 40 mg/kg DT at days -1 and 0 before infection with 0.3 LD50 PR8. Representative dotplots shown. (D) dLN cellularity (left) and lung NK cell number (right) are shown for untreated DO$^{-/-}$ and WT mice, and for DTR-expressing or non-DTR-expressing DO$^{-/-}$ and WT mice treated with DT. Data represent 2-3 independent experiments, with 3-4 mice/group/experiment. Unpaired parametric t-tests were performed, mean ± SD shown, *p<0.05, **p<0.01, ***p<0.001.

using this model (Figure 4.6C), which resulted in reversal of DO-dependent defects in cellularity and NK cells (Figure 4.6D). However, we also observed that control $DO^{-/-}$ mice, which did not express the DT receptor but which were administered DT, did not recapitulate the phenotype that had been observed in the absence of DT (Figure 4.6D). DT has been shown previously to induce nonspecific inflammation[386,387], and so in this model we are unable to discern whether Tregs modulate the immune response to influenza A in the $DO^{-/-}$ mouse.

Discussion

The nonclassical MHC-II molecule DO serves to modulate the immunopeptidome and has been shown previously to play a role in the immune response to pathogens. The principal effect of DO or DM reported thus far in models of immunization or infection has been in mediating antibody production[259,288]. We show here that DO also functions early in infection, prior to induction of humoral immunity. Following inoculation with influenza A, DO is demonstrated to be required for efficient recovery, with $DO^{-/-}$ mice exhibiting a pronounced delay in their capacity to regain weight, as well as increased morbidity. The secondary lymphoid organs in which antigen presentation and T cell expansion occurs most efficiently in influenza infection were shown to be dramatically reduced in size and cellularity in $DO^{-/-}$ mice, and injection of BrdU demonstrated a deficiency in T cell proliferation when DO was absent. We observed a skewed pattern of epitope-specific responses and identified an influenza-derived epitope that is likely resistant to DM editing and therefore presented more efficiently by $DO^{-/-}$ APCs compared to WT. Out of the

panel of 7 CD4 epitopes for which we examined antigen presentation and T cell responses, we found the NP311 epitope to be presented better by $DO^{-/-}$ APCs compared to WT, while presentation of the remaining 6 epitopes were dampened in $DO^{-/-}$ mice. The overall pattern of epitope-specific T cell responses thus appears to be one that is suppressed in $DO^{-/-}$ mice compared to WT, with T cell responses to the NP311 epitope slightly increased. When NP311 Tg T cells were adoptively transferred at the time of infection into $DO^{-/-}$ and WT mice to assess their proliferative capacity independent of any possible differences in thymic selection of conventional CD4 T cells (which could affect NP311-specific responses in the $DO^{-/-}$ vs. WT mouse), their frequency was found to be greater in $DO^{-/-}$ mice, but their numbers were comparatively lower or unchanged. Based on these results, as well as based on our observations that CD8 T cell responses were diminished, lung APCs and innate immune cells were reduced in number, and cytokine levels were decreased, we reasoned that nonspecific suppression of the immune response by Tregs could account for the observed phenotype in influenza A-infected $DO^{-/-}$ mice. Tregs have been shown previously to suppress innate immunity and NK cell function[177,388,389]; in an experimental model of HSV infection, Tregs have also been shown to be important in coordinating recruitment of immune cells to the site of infection[384]. We have observed increased frequencies and numbers of Tregs in thymus and lymphoid tissue of the $DO^{-/-}$ mouse (Chapter III), and here we further report increased lung tissue Tregs when DO is absent. We therefore hypothesized that enhanced Treg function was responsible for the global suppressive effect observed in the absence of DO during influenza A infection. To test this hypothesis,

we used a model of DT-induced depletion of Tregs, but experimental results proved difficult to interpret, likely due to inflammation induced by DT administration. Tregs have been shown to limit the efficacy of immunity in models of infection[390-392], demonstrated by the effects of Treg depletion. In our model, however, we postulate that increased activity of Tregs in the $DO^{-/-}$ mouse results in insufficient immunity compared to WT. Administration of DT appears to increase inflammation to such a degree that effects on the immune response are no longer observed in the $DO^{-/-}$ mouse. At present, we are therefore unable to conclude whether the multiple defects in the immune response to influenza A in the absence of DO is due to Tregs. DT administration could conceivably affect multiple arms of immunity, and so it is also possible that an alternate mechanism may account for the phenotype observed in $DO^{-/-}$ mice following infection.

In summary, we show that DO is required for efficient recovery from influenza A infection, and that mice deficient in DO display defective innate and adaptive immune responses following A/PR8 infection. We identify an influenza-derived epitope uniquely affected by DO, and show that the predominant effect of DO ablation is to compromise effective immunity to influenza A. These data suggest that modulation of DO expression plays a critical role in the efficacy of the immune response to pathogens.

Table 4.1. Influenza-derived epitopes

Epitope	Protein	Sequence
HA16	Hemagglutinin	RSWSYIVETPNSENGIC
NA25	Neuraminidase	GDVFVIREPFISCSH
NA41	Neuraminidase	SVAWSASASHDGMGW
NA110	Neuraminidase	TVDWSWPDGAELPFT
NP45	Nucleoprotein	LILRGSVAHKSCLPACV
NP311	Nucleoprotein	QVYSLIRPNENPAHK
NP366	Nucleoprotein	ASNENMETM
NS1-19	Nonstructural protein 1	KQKVAGPLSIRMDQAIM
PA224	Polymerase	SSLENFRAYV

Materials and Methods

Mice

H2-O-deficient mice were provided by Dr. Xinjian Chen (University of Utah School of Medicine) after backcrossing to C57BL/6 mice for 10 generations, and these mice were further backcrossed at the University of Massachusetts Medical School to C57BL/6 mice obtained from Jackson Laboratory (Bar Harbor, ME). Heterozygous matings were performed to obtain $DO^{-/-}$ and WT littermate controls for experiments. The $DO^{-/-}$ mouse was also bred with B6.129(Cg)-*Foxp3*$^{tm3(DTR/GFP)Ayr}$/J ($Foxp3^{DTR}$) mice and B6.SJL-*Ptprc*^{a}*Pepc*^{b}/BoyJ (Ly5.1) mice for select experiments. Mice carrying a transgenic TCR specific for I-A^b and the immunodominant NP311 peptide were generated by Dr. Eric Huseby (University of Massachusetts Medical School) and will be described in detail elsewhere. 8-10-week-old mice were inoculated with influenza as described below. All mice were cared for and used in accordance with institutional guidelines.

Viral stocks and infection

Viral stocks (A/PR/8/1934[H1N1] and A/Philippines/2/82/x-79[H3N2]) were kindly provided by the laboratory of Dr. Susan Swain, and mice were inoculated via intranasal instillation as previously described[393,394]. Briefly, mice were anesthesized with isoflurane (Patterson Veterinary Supply, Devens, MA) via inhalation using a vaporizer chamber (VetEquip, Livermore, CA), and mice were then inoculated intranasally with 0.5 LD50 A/PR8 (unless otherwise indicated) or 300 LD50 A/Philippines in 50 μl PBS.

Viral titer quantitation

Viral titers were assessed by quantifying copy number of the A/PR8 polymerase (PA) gene as previously described[393,394]. RNA was isolated from whole lung homogenates using TRIzol (Thermo Fisher Scientific), together with the E.Z.N.A. RNA isolation kit (Omega Bio-Tek, Norcross, GA) and the TURBO DNA-free kit (Thermo Fisher Scientific) according to the manufacturer's instructions. Reverse transcription was performed using 2.5 μg RNA with random hexamer primers and Superscript II Reverse Transcriptase (Thermo Fisher Scientific). The PA gene was quantified by PCR using the Bio-Rad CFX96 Realtime PCR system (Bio-Rad, Hercules, CA) with 50 ng of cDNA per reaction and the following primers and probe: forward primer, 5′-CGGTCCAAATTCCTGCTGA-3′; reverse primer, 5′CATTGGGTTCCTTCCATCCA-3′; probe, 5′-6-FAM-CCAAGTCATGAAGGAGAGGGAATACCGCT-3′, provided by the Trudeau Institute Molecular Biology Core Facility (Saranac Lake, NY). The copy number of the PA gene per 50 ng of cDNA was calculated using a PA-containing plasmid of known concentration as a standard, which was then used to calculate PA copy number per lung.

Influenza-specific antibody isotype titer quantitation

Quantitation of A/PR8-specific antibody titers was performed as previously described[395]. Briefly, microtiter plates were coated overnight with 10^7 A/PR8 virus and then were washed and blocked with PBS containing 0.05% Tween 20 and 1%

BSA (blocking buffer). Washing was performed at each step. Serum samples isolated at day 21 post-infection were serially diluted in blocking buffer, added to pre-coated plates, and incubated for 2 h at room temperature (RT). HRP-conjugated anti-mouse antibodies specific for total IgM, IgG, IgG1, IgG2a, or IgG2b (Southern Biotech, Birmingham, AL) were added to plates at 0.5 μg/ml in blocking buffer for 1 h at RT. Substrate (*o*-phenylenediamine dihydrochloride, Sigma-Aldrich, St. Louis, MO) was then added, and the reaction was terminated by addition of sulfuric acid. The colorimetric reaction was read at 492 nM using a Victor X5 Plate Reader (Perkin Elmer, Waltham, MA). Endpoint serum titers were determined by comparison to unimmunized mice (negative controls).

I-A^b tetramer generation

Protein expression of I-A^b monomers was performed by infection of Hi5 insect cells (Thermo Fisher Scientific) with recombinant baculovirus generated by co-transfecting linearized baculovirus DNA together with a construct into which influenza A-derived peptides were cloned. Supernatant was collected, and protein purification was performed by affinity purification using rat anti-mouse MHC-II antibody (M5/114). Biotinylation was performed using BirA ligase (Avidity, Aurora, CO), followed by purification by gel filtration. Tetramerization was performed by addition of fluorescently-labeled streptavidin (Prozyme, Hayward, CA) at 10-minute intervals.

Flow cytometry

Single-cell suspensions of lungs (following perfusion through the right ventricle with 10 ml PBS), draining lymph nodes (dLNs), or spleens were blocked with 50 μg/ml anti-CD16/CD32 (BioXCell, West Lebanon, NH) prior to antibody staining. Staining was performed with the following antibodies purchased from BioLegend (San Diego, CA): TCRβ (H57-597), CD3 (145-2C11), CD8α (53-6.7), CD11c (N418), CD44 (IM7), CD45.1 (A20), and B220 (RA3-6B2), and NK1.1 (PK136). Antibodies purchased from BD Biosciences (Franklin Lakes, NJ) were CD4 (RM4-5), CD25 (PC61), and I-A^b (AF6-120.1). Antibodies purchased from Thermo Fisher Scientific (Waltham, MA) were Foxp3 (FJK-16s) and Live/Dead fixable stain. For MHC-II tetramer staining, cells were surface-stained, washed, then incubated with 6 μM monomer for 1 h at 37° C. MHC-I tetramers were provided by the NIH Tetramer Core Facility (Atlanta, GA); cell were surface-stained, washed, and incubated with 1:200 tetramer at 4° C for 1 h. The Foxp3/Transcription Factor Staining Buffer Set (Thermo Fisher Scientific) was used for fixation and permeabilization prior to staining for Foxp3. Mice were injected 24 h prior to sacrifice with 1 mg of 5-bromo-2'-deoxyuridine (BrdU, BD Biosciences), and proliferating cells were detected using the BrdU Flow Kit according to the manufacturer's instructions (BD Biosciences). Analysis of flow cytometric data was performed using FlowJo (version 10.3.5, Treestar, Ashland, OR).

Antigen presentation assays

Lung and draining LNs (dLNs) were isolated on day 4 post-infection, and single-cell suspensions were irradiated with 2500 rads. 10^5 lung or dLN cells were incubated with 10^5 per well of T cell hybrids specific for the influenza epitopes NA25, NA41, NP45, and HA16, kindly provided by the laboratory of Dr. Laurence Eisenlohr (University of Pennsylvania)[293]. Following overnight incubation at 37° C, 5% CO_2, substrate (methyl-umbelliferyl-β-D-galactoside [MUG], Sigma Aldrich) was added for 1 h at 37° C, 5% CO_2, and fluorescence (365/445) was read using a Victor X5 Plate Reader (Perkin Elmer, Waltham, MA). MUG units for each hybrid were determined by subtracting background fluorescence (from 10^5 T cell hybrids alone). Similar assays were performed with CD4 T cells isolated by negative selection from spleens of the NP311 mouse using the $CD4^+$ T cell Isolation Kit (Miltenyi Biotec, Auburn, CA) according to the manufacturer's instructions. CD4 T cells were labeled with Cell Trace Violet (Thermo Fisher Scientific) according to the manufacturer's instructions, and 10^5 CD4 T cells/well were co-cultured with 10^5 lung and dLN cells for 3 days. Proliferation was assessed by dilution of Cell Trace Violet following co-staining with anti-mouse CD4 and CD8 antibodies, as well as Live/Dead fixable stain (Thermo Fisher Scientific), by flow cytometric analysis.

ELISA

Cytokine ELISA kits to assess serum levels of IL-2, IL-6, and IFN-γ were purchased from BD Biosciences and/or BioLegend, and cytokine levels were

determined according to the manufacturer's instructions. Levels of G-CSF were quantified using a kit purchased from R&D Systems (Minneapolis, MN) according to the manufacturer's instructions.

CD4 T cell transfer

CD4 T cells were isolated from spleens of NP311 Tg mice as indicated above, and $5x10^4$ CD4 NP311 Tg T cells were injected i.v. at the time of A/PR8 infection into congenically-marked (Ly5.1) $DO^{-/-}$ and WT mice. Frequencies and numbers of NP311 Tg T cells were examined in lung, dLN, and spleen at day 7 post-infection.

Treg depletion

$DO^{-/-}$ and WT littermate $Foxp3^{DTR}$ were injected i.p. on days -1 and 0 with 40 mg/kg diphtheria toxin (DT) (Sigma Aldrich) before infection, followed by intranasal instillation of 0.3 LD50 A/PR8 as described above.

Statistical analysis

Unpaired parametric student t-tests, two-way ANOVA, and the Gehan-Breslow-Wilcoxon test for survival were used to calculate statistical significance. Prism (version 8.01, GraphPad, San Diego, CA) was used for statistical analysis and to generate graphical plots.

CHAPTER V

Conclusions and future directions

Summary of dissertation studies

The results presented in this work provide insight into the biological effects of the non-classical MHC-II molecule DO in several facets of MHC-II antigen presentation. We first demonstrate the global effect of DO on the MHC-II peptidome, and in doing so reconcile previous studies in which inconsistent results were reported. We have definitively determined, as shown in Chapter II, that DO functions to broaden the immunopeptidome. In the absence of DO, many fewer peptide species are presented, resulting in greater density of more abundant epitopes. The results of this study informed our examination of DO function in T cell selection, presented in Chapter III. Based on thymic expression of DO, which had been reported but for which effects had not been explored, we reasoned that DO could impact selection of both conventional CD4 T cells and Tregs. We show that the predominant effect of thymic expression of DO is on the Treg population, and that perturbation of DO alters Treg function, phenotype, and differentiation into Tfr. We further show that lack of DO augments autoantibody production associated with development of autoimmunity. These data also provide a potential explanation for expression of DO in both the thymus and periphery, such that modulation of the self-peptidome by DO may have evolved to improve self-tolerance specifically with respect to Treg selection and function. In Chapter IV, studies examining the

role of DO in influenza A are presented. $DO^{-/-}$ mice failed to recover efficiently from infection, and we demonstrate multiple deficiencies in innate and adaptive immunity in the absence of DO. DO is shown for the first time to play a role in effective T cell responses during infection, and to alter in vivo presentation of epitopes derived from a pathogen. Taken together, these data describe novel implications of DO expression important in the biology of autoimmunity and in the immune response to infection.

Challenges and limitations in the study of DO biology

Several aspects of the work presented here have proven challenging in furthering our understanding of the biological function of DO. First, DO is expressed by multiple cell types. Although DO is more restricted in its expression than MHC-II or DM, its expression in both the thymus and periphery may impact central tolerance mechanisms and peripheral MHC-II antigen presentation. In models of infection, for example, the precise effects of DO are difficult to tease apart, given that antigen specificities of conventional T cells may be altered, Tregs are affected both in number and likely in their specificity, and hierarchical epitope patterns may be changed during an immune response in the $DO^{-/-}$ mouse. Generation of a conditional DO knockout mouse, using Cre-lox or CRISPR/Cas9 technology to target DO in particular cell lineages, would help to overcome the challenge associated with DO expression in multiple cell types. Another difficulty in this project arises from that fact the effect of DO on the peptide repertoire and on T cell

selection is small (although reproducible). As with any small effect, current experimental tools available may be insufficient to precisely measure all DO-dependent differences. Lastly, DO exerts its function by inhibiting DM, which both removes CLIP from MHC-II dimers and acts as a peptide exchange factor. DO is thus implicitly linked to a second molecule, which for MHC alleles with high affinity for CLIP, also performs two functions. The factors that affect study of DO thus become multiplicative, and include differential DM sensitivity of various epitopes, CLIP affinity for MHC-II, pH susceptibility of the DO/DM complex, and regulation of DO and DM expression. The sum of these factors makes discerning the function of DO, particularly for in vivo studies, quite complex.

DO broadens the MHC-II immunopeptidome: future studies

We have shown that at the cellular level, DO functions to increase the breadth and diversity of the MHC-II immunopeptidome. Peptides were eluted from human B cell lines as well as from murine B cells, and we importantly demonstrate through immunization experiments that differential presentation of peptides due to DO expression has consequences for T cell activation. Results of our study could be extended by examination of the effects of DO overexpression, perhaps by transduction of a tetracycline-inducible construct to allow for modulation and control of DO levels. We would expect that the peptidome would become increasingly diverse as DO expression increases, although the DO/DM ratio would require careful calibration so that DM activity is sufficient for CLIP removal. We

also examined the effect of DO on the overall peptide repertoire only in B cells, where DO has been shown to be most highly expressed. Peptide elution using other DO-expressing cell types, including DCs and mTECs, could provide further insight into DO function in tolerance and immunity, as would elution studies in models of infection. In addition, examination of the effect of pH susceptibility of the DO/DM interaction as it relates to the peptides presented, perhaps by manipulation of endosomal pH, would further our understanding of the effects of DM inhibition by DO and may reconcile differences between the two models currently proposed for DO function (i.e. focusing antigen presentation on late endo/lysosomes vs. broadening the immunopeptidome).

DO modulates the Treg repertoire: future studies

We have demonstrated that DO affects selection of CD4 T cells into the Treg lineage, and that Tregs selected in the absence of DO display phenotypic and functional changes indicative of greater activation. We also show that mice deficient in DO exhibit elevated levels of anti-dsDNA antibodies, in agreement with an earlier report[288], as well as display alterations in GC subsets indicative of an aberrant GC reaction. In an experimental model of Sjogren's disease, these effects persist, suggesting that DO expression is necessary to subvert autoimmunity through modulation of Treg function.

While we have shown that $DO^{-/-}$ Tregs do not proliferate more or convert from conventional CD4 T cells at a greater rate than do WT Tregs, the evidence we

provide to show that increased Tregs is the $DO^{-/-}$ mouse is due to their increased selection in the thymus is not definitive. Due to peripheral expression of DO, increased Treg frequencies could result from clonotypic expansion in the periphery, and increased frequencies observed in the thymus could be due to thymic recirculation. Examination of the effect of DO in the Rag2pGFP transgenic mouse model[345], which can distinguish between newly selected and recirculating Tregs based on Rag2 expression, may clarify whether $DO^{-/-}$ Tregs are thymically-derived. Similarly, generation of a conditional DO knockout model, as proposed above, would be useful in resolving this issue. Using a conditional knockout model, the effect of DO expression in the mTEC compartment could be examined, for example, by crossing $DO^{fl/fl}$ and K14-Cre mice, which would selectively ablate DO in K14 promoter-expressing thymic epithelial cells[396]. Still, results of our BM chimera experiments in particular lend support to the idea of increased Treg selection being initiated in the thymus of $DO^{-/-}$ mice, as WT→DO BM chimeras showed similar increases in peripheral Tregs, where the effect of DO modulation on peripheral antigen presentation by hematopoietic-derived APCs does not play a role.

Results of TCR sequencing experiments suggest that DO serves to shift Treg selection and diversifies the clonotypic repertoire of Tregs. Our data do not demonstrate how this occurs, as Treg selection may be altered in $DO^{-/-}$ mice due to increased deletion of clonotypes selected in WT mice or may simply narrow the window of Treg specificity (Figure 5.1). Sequencing of TCR transgenic mice with different Vβ reactivities, as well as single-cell TCR sequencing, may lend further

insight into the manner in which Treg selection is shifted by DO expression. Additional experiments that may help determine the mechanism behind DO's effects on thymic selection include in vitro co-culture of pre-selection thymocytes with DO-sufficient or -deficient APCs, in which clonal deletion can be measured[337]. Fetal thymic organ cultures or the more recently developed technique of reaggregate thymus organ culture may also be useful in determining the mechanism of altered T cell selection in $DO^{-/-}$ mice[397]. Use of retrogenic TCR technology could allow for examination of the effect of DO on differentiation of certain clonotypes

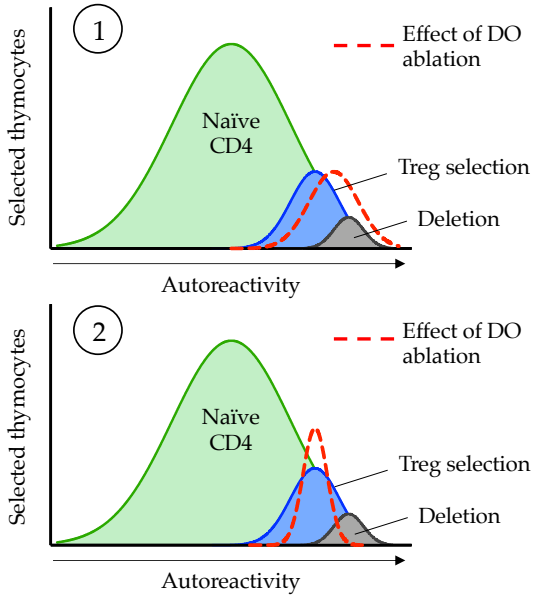

Figure 5.1. Possible models for altered Treg selection due to DO. (1) Lack of DO may shift the degree of self-reactivity due to increased avidity, resulting in greater deletion and lesser diversity of the Treg population. (2) Alternatively, DO may narrow the window of specificity for Tregs due to presentation of fewer peptides.

into the conventional T cell vs. Treg lineage upon transfer to $DO^{-/-}$ or WT mice. Another line of experimentation to help clarify DO action in thymic selection is identification of peptide ligands for TCRs that are differentially selected, which can

be accomplished by screening of cells engineered to express these TCRs against an array of potential ligands, and then further examined by characterization of TCR-MHC-peptide interactions using crystallographic or binding studies. Results could also lend insight into the mechanism of Treg selection, which is thought to integrate peptide affinity and avidity but which is not clearly understood[171]. I.v. injection of WT mice using different doses of the peptides identified[398], followed by examination of the effect on Treg frequency, might provide further support to the mechanism of action of DO in modulating peptide density and thereby in affecting T cell selection.

We have observed that despite the increased frequency of Tregs in $DO^{-/-}$ mice, fewer Tfr reside in the germinal center. We attribute the increased anti-dsDNA antibodies observed in older mice and in a model of autoimmunity to a deficiency in Tfr differentiation, but we do not causally demonstrate this effect. Experiments to prove this link may include depletion of Tregs in both $DO^{-/-}$ and WT mice using the $Foxp3^{DTR}$ model, followed by reconstitution with $DO^{-/-}$ or WT Tregs isolated from non-DTR-expressing mice and induction of experimental Sjogren's syndrome. The caveat with using DT to deplete Tregs is that it must be administered every 7 days to sustain Treg ablation, which may interfere with or exacerbate the normal progression of autoimmune disease in this model and render interpretation of results difficult. An alternative would be simply to inject isolated $DO^{-/-}$ or WT Tregs into $DO^{-/-}$ or WT mice, perhaps using a weekly or biweekly regimen, during induction of ESS. If Tfr differentiation is impaired and is responsible for increased autoantibody levels, provision of $DO^{-/-}$ Tregs to either

$DO^{-/-}$ or WT mice may have less of an effect on levels of anti-dsDNA antibodies than would provision of WT Tregs. A potential challenge using such a strategy may arise due to the fact that the Treg niche is already established, and therefore infused Tregs may not adequately proliferate when transferred. As discussed in Chapter III, we also noted increased GC B cells in these mice, and previous work suggests that expression of DO in thymic epithelium is sufficient to induce ANAs[288]. Results of those experiments suggest that thymically-derived Tregs are not responsible for the phenotype observed, while according to our hypothesis lack of thymic DO expression would be necessary for increased Treg frequencies and aberrant Tfr function. While many reports have demonstrated a role for Tfr in regulation of the expansion of GC cell subtypes[351-353], ablation of Bcl6 in Tregs has also been shown to have no effect on Tfh or GC B cells but rather to alter the antibody response[399]. Further studies are therefore required to determine the basis for increased levels of autoantibodies in these mice.

DO impacts the immune response to influenza A: future studies

We have demonstrated that $DO^{-/-}$ mice display a marked delay in recovery from influenza A infection compared to WT mice. We examined many aspects of the immune response and observed multiple deficiencies in immunity to influenza A in the $DO^{-/-}$ mouse. Presentation of several epitopes by lung and dLN APCs was reduced, as were the T cell responses associated with presentation of those epitopes. A sole epitope derived from the influenza virus nucleoprotein was shown to be

presented to a greater degree by DO$^{-/-}$ APCs, presumably due to its resistance to DM. T cell responses to this epitope, while increased in frequency, were reduced in number. We reasoned, based on these data as well as due to the fact that innate immunity also appeared suppressed, that increased Treg numbers and possibly increased suppressive capacity of Tregs in the DO$^{-/-}$ mouse accounted for the phenotype observed (Figure 5.2). While we show that lung tissue Tregs are increased during infection in DO$^{-/-}$ mice compared to WT, our efforts to deplete Tregs in order to test their function were complicated by nonspecific effects of DT,

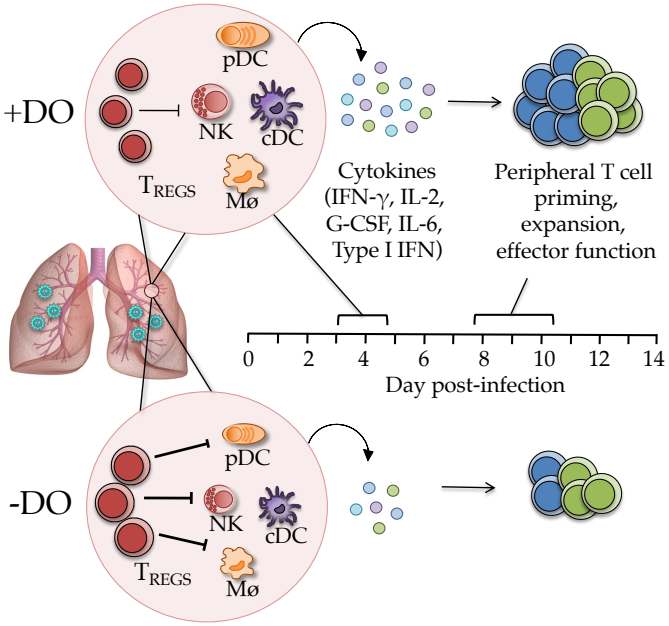

Figure 5.2. Working model for effect of DO in influenza A infection. In the absence of DO, increased suppression by Tregs reduces APC and innate immune cell function, leading to dampened cytokine and T cell responses.

and so we are unable to conclude that DO$^{-/-}$ Tregs are responsible for the observed phenotype.

In order to determine whether Tregs are indeed overactive in the $DO^{-/-}$ mouse during influenza infection, a system in which different cellular components affected by DO expression could be modulated may be useful in determining the mechanism underlying the deficient response to influenza A in the $DO^{-/-}$ mouse. Reconstitution of Rag-deficient or TCR-deficient mice with different combinations of $DO^{-/-}$ or WT cell types, for example, may allow for assessment of the differential contributions of Tregs, conventional CD4 T cells, and APCs in the observed phenotype. Here again, generation of a conditional DO knockout mouse may also prove useful in understanding these effects. The role of Tregs in this model could become apparent with Treg transfer prior to infection, to determine whether increased Treg frequencies show a similar suppressive effect. If increased suppression is also modulated by increased suppressive capacity of $DO^{-/-}$ Tregs, transfer of $DO^{-/-}$ vs. WT Tregs may show a detectable difference in suppression of the immune response, although again it is unclear whether sufficient proliferation of transferred Tregs would occur when the Treg niche is already established.

We also observed alterations in influenza epitope presentation in the $DO^{-/-}$ mouse, which may be at least in part due to Treg function. The possibility also exists that the epitope skewing observed is wholly responsible for the defective immune response in $DO^{-/-}$ mice. We transferred NP311 Tg T cells to test their capacity to proliferate in $DO^{-/-}$ and WT mice; if additional mouse models expressing influenza-specific TCRs on a C57BL/6 background were available, transfer of T cells from such mice would be useful to clarify whether the effect observed for NP311 Tg T cells is distinct. In our hands, transfer of polyclonal T cells does not

allow for the sensitivity required to assess the effect of DO, as the frequency of transferred cells is quite low, but here again a transfer system using TCR-deficient mice may be useful. Yet another possibility that could account for the effect observed on epitope skewing, which could also be the basis for the overall deficient response to influenza A in the $DO^{-/-}$ mouse, is differential expression of DO in lung epithelium, which to our knowledge has not been assessed in naïve or infected mice. MHC-II has been demonstrated in other contexts to be expressed during inflammation by endothelial and epithelial cells[400,401], and so DO and DM could be similarly upregulated. Use of lung epithelial cells isolated at different time points during infection in antigen presentation assays may therefore help determine whether differential presentation by non-professional APCs contributes to the altered immune response to influenza A in $DO^{-/-}$ mice.

Mice lacking DO were recently shown to produce higher titers of neutralizing antibodies during retroviral infection[259], indicating DO impacts the process of pathogen-specific antibody affinity maturation. While we did not observe effects on influenza-specific antibody isotypes, we did not examine functional aspects of antibodies produced in $DO^{-/-}$ vs. WT mice during influenza infection. Further experimentation may show that the affinity or neutralizing capacity of antibodies generated during influenza A infection is affected by DO expression, and that such alterations affect the response to influenza A in $DO^{-/-}$ mice.

Perspective and implications of DO function in the biology of disease

The results presented in this thesis provide further insight into the role of DO in antigen presentation at the cellular level, in tolerance to self, and in immunity to pathogens. Many questions remain, and many additional consequences of DO expression are possible. We have predominantly studied Tregs isolated from secondary lymphoid tissues, but what role might DO play in the function of tissue-specific Tregs, such as in the gut or the skin? Does DO function in the context of tumor immunity where the diversity of the MHC-II peptidome as well as Treg specificity and suppressive capacity are likely important? DO expression has been shown to prevent type 1 diabetes in the NOD mouse model[253], but does it exert any function in additional models of autoimmune disease in human or mouse? In this work, DO's effects in the context of the MHC-II molecules HLA-DR and I-A^b, both of which are sensitive to the effects of DM catalysis[24,402], were examined. Certain disease-associated MHC-II alleles, such as DQ2 and DQ8, have been shown to be more resistant to DM action, with reduced effects of DM posited to impact susceptibility to autoimmunity[30,271,403]. Does DO play an appreciable role in selection of epitopes specific for alleles that are less dependent on DM? In the context of immunity to pathogens, we show here that DO plays a role early in the immune response to influenza A, and DO has been implicated previously in generation of neutralizing antibodies during retroviral infection[259]. In other models of viral or bacterial infection, particularly in those in which CD4 T cell responses or Treg function have been shown to be important for pathogen clearance, does DO

exert a similar effect? Studies to examine these questions may provide the basis for development of novel therapeutics or vaccine design to more effectively treat autoimmune or infectious disease.

APPENDIX I

MHC-I peptide binding activity assessed by exchange after cleavage of peptide covalently linked to β2-microglobulin

Author contributions:

I performed all of the experimental work described in this appendix.

Abstract

A common approach to measuring binding constants involves combining receptor and ligand and measuring the distribution of bound and free states after equilibration. For class I major histocompatibility (MHC-I) proteins, which bind short peptides for presentation to T cells, this approach is precluded by instability of peptide-free protein. Here we develop a method wherein a weakly-binding peptide covalently attached to the N-terminus of the MHC-I β2m subunit is released from the peptide binding site after proteolytic cleavage of the linker. The resultant protein is able to bind added peptide. A direct binding assay and method for estimation of peptide binding constant (K_d) are described, in which fluorescence polarization is used to follow peptide binding. A competition binding assay and method for estimation of inhibitor binding constant (K_i) using the same principle also are also described. The method uses a cubic equation to relate observed binding to probe concentration, probe K_d, inhibitor concentration, and inhibitor K_i under general reaction conditions without assumptions relating to relative binding affinities or concentrations. We also delineate advantages of this approach compared to the Cheng-Prusoff and Munson-Rodbard approaches for estimation of K_i using competition binding data.

Introduction

Presentation of antigenic peptides to T cells is both requisite for initiation of an adaptive immune response and necessary for tolerance to self. The affinity and stability of antigenic peptides binding to MHC molecules are intrinsic aspects of T cell activation and have been used as predictors of immunogenicity and immunodominance[404,405]. Defining the molecular interactions between MHC molecules and peptide ligands thus has implications in effective vaccine design, in diagnostic capability, and in understanding basic immunological processes. In the last several decades, considerable progress has been made in characterizing these interactions, and peptide affinity for MHC has been shown to be a critical determinant of the T cell response in infection, autoimmunity, and tumor models[406-410]. Despite development of many assays to quantify or characterize MHC-peptide affinities, these methodologies are often encumbered by laborious and time-consuming experimental steps, such that substantial effort has been made to establish more efficient and high-throughput epitope screening methods.

Assays to evaluate the affinities of putative and known MHC-I epitopes have been developed over the last 30 years using both cell-based and cell-free platforms. Perhaps the earliest work on quantifying peptide affinity employed cell-free biochemical methods to measure binding of iodinated peptides to MHC-I[411-413]. Using this technique, MHC-I molecules are purified from cell lysates and solubilized in detergent, and affinity is measured by quantifying binding of radiolabeled peptides by gel filtration of MHC-I complexes vs. free peptide. Later

methods employed fluorescence labeling rather than iodination, thereby eliminating the radioactive waste and hazard, but this assay still necessitated purification of each peptide-MHC-I complex by chromatographic or electrophoretic separation and was therefore labor-intensive and low-throughput[414,415]. A high-throughput scintillation proximity assay based on radioactive peptide exchange using purified native MHC protein has been reported[416]. Cell-based methods have been used to evaluate MHC-I-peptide interactions, including a cell-surface stabilization assay, in which surface MHC-I of TAP-deficient T2 cells is stabilized by the addition of iodinated or fluorescently-labeled peptides[417,418], as well as cell-surface binding assays, in which endogenous peptides are exchanged in situ[419,420] or partially removed by acid treatment of surface MHC-I-bound peptides followed by addition of fluorescent peptides[421,422]. Surface plasmon resonance has also been used to measure peptide binding in indirect assays monitoring β2-microglobulin dissociation[423], and in direct assays following MHC-I binding to covalently-coupled peptides[424]. The peptide dependence of in vitro MHC-I folding reactions can serve as the basis for MHC-I-peptide binding assays, with detection using conformation-specific antibodies or pairs of antibodies specific for MHC-I heavy-chain and β2-microglobulin[425,426].

Due to the inherent instability of peptide-free "empty" MHC-I molecules, assays that measure peptide-binding affinity generally include some type of peptide exchange as a necessary step in the reaction. Full-length MHC-I proteins purified in detergent from mammalian cells are largely occupied with endogenous peptides, and while peptide exchange can be measured for these preparations, the efficiency

is low. Peptides can be removed from MHC-I preparations by partial denaturation, and assays based on this approach have been reported[427]. As an alternate approach, MHC-I subunits can be folded from heavy chain and β2-microglobulin subunits expressed in *E. coli* inclusion bodies[428,429]. Folding in vitro is highly peptide-dependent, and this provides a means to prepare MHC-I complexes with defined peptides. MHC-I proteins preloaded with weakly-binding, easily exchangeable peptides potentially could be used as starting material for peptide-exchange assays. This requires identification of peptides with MHC-I–peptide-binding affinity sufficiently high to allow for in vitro folding and purification but sufficiently low to allow for efficient exchange with test peptides. Dipeptides have been identified for some MHC-I proteins that could serve this purpose[430], but a "conditional ligand" strategy has proven more useful, wherein MHC-I complexes are folded with full-length peptides carrying photocleavable[431] or chemically-labile[432] amino acid residues that upon cleavage produce easily-exchangeable peptide fragments. Similar assays have been developed for evaluating affinities of MHC-II epitopes[329,414,433-436], facilitated in many cases by the increased stability of peptide-free MHC-II relative to MHC-I[326], and by the availability of recombinant MHC-II proteins expressed in *E. coli* or insect cells with empty peptide-binding sites or carrying only weakly-associating peptides[326,437-439].

Here, we describe a novel technique to measure peptide affinities, which incorporates a different mode of peptide exchange based on a covalent peptide approach. In that approach, a tight-binding peptide is tethered to the N-terminus of the β2-microglobulin subunit[440], where it is positioned near the peptide-binding

site, similar to covalent peptide approaches conventionally used for MHC-II molecules[441]. This allows for production of essentially homogenous MHC-I peptide complexes in mammalian cells[442]. Here, epitope-linked β2-microglobulin (ELBM) is expressed in mammalian cells with a weakly binding peptide tethered to the β2m subunit via a linker that contains a thrombin cleavage site, so that upon addition of protease, the peptide is released. This design circumvents issues that may be encountered with MHC molecules that are difficult to fold in vitro and avoids complications with handling MHC-I proteins folded with suboptimal peptides. Following recent studies[443,444], we monitored MHC-I-peptide binding using fluorescence polarization, a technique wherein plane-polarized light is employed to distinguish between bound and free ligands without the need for physical separation[329,443]. The degree of polarization is measured by excitation of a fluorophore label and calculated by measurement of fluorescence intensities both parallel and perpendicular to the plane of polarized light. In an MHC-peptide binding assay, the labeled peptide will exhibit high fluorescence polarization when bound to MHC-I due to decreased molecular mobility but will tumble freely in solution and display low polarization when unbound. Titration of unlabeled competitor peptides allows for computation of binding affinities, and this assay is also highly amenable to high-throughput screening. Using this approach, we developed direct binding and competition assays to evaluate binding affinities for peptides binding to the common human MHC-I allele HLA-A*02:01 (HLA-A2). The direct binding assay can be used to estimate binding affinities for labeled peptides binding to MHC-I. The competition binding assay, using unlabeled test

peptides and a single labeled probe peptide, is suitable for high-throughput analyses and can be used to give half-maximal inhibition (IC_{50}) values that report relative binding affinity of test peptides and estimates of inhibitor peptide-binding constant (K_i).

Traditionally, inhibition binding assays are interpreted in terms of the IC_{50} value, i.e. the concentration of unlabeled test peptide that causes 50% inhibition of binding of a probe peptide. Because IC_{50} values vary with experimental conditions, measurements of K_i, the equilibrium binding constant of the inhibitor peptide, are more useful in quantification of inhibitor peptide-binding affinity. Under some experimental conditions, IC_{50} and K_i values are similar. Requirements for this are that the probe peptide concentration is low relative to that of the test peptide, the probe peptide has a low K_d relative to the concentration used, and MHC concentration is low relative to peptide concentration. For experimental conditions in which these parameters deviate from concentration or binding constant limits, corrections have been proposed to calculate K_i from IC_{50} values. The most commonly used of these is the Cheng-Prusoff correction, which corrects for probe peptide concentration and binding affinity effects. However, the MHC concentration must remain low relative to the binding constants for this correction to be accurate. Munson and Rodbard proposed an exact correction for the Cheng-Prusoff approach when y_0, the ratio of bound to free probe peptide in the absence of inhibitor, is available. However, in practice this approach can lead to large errors if the relevant parameters are not precisely known. To circumvent these issues, we developed an analysis relating K_i to IC_{50} without assumptions about concentrations

or binding affinities, using a cubic equation. The cubic equation describes the amount of probe peptide bound in terms of concentrations and binding constants for both probe peptide and inhibitor peptide, and this approach is suitable for curve fitting inhibition binding data.

Results

Class I MHC produced as epitope-linked β2-microglobulin constructs

Epitope-linked β2m (ELBM) was prepared by co-expressing in mammalian cells a soluble HLA-A2 heavy chain construct and a β2-microglobulin construct carrying an N-terminal "stuffer" epitope peptide, a thrombin cleavage site, complementary leucine zippers, and purification tags (Figure A1.1). Both constructs have signal

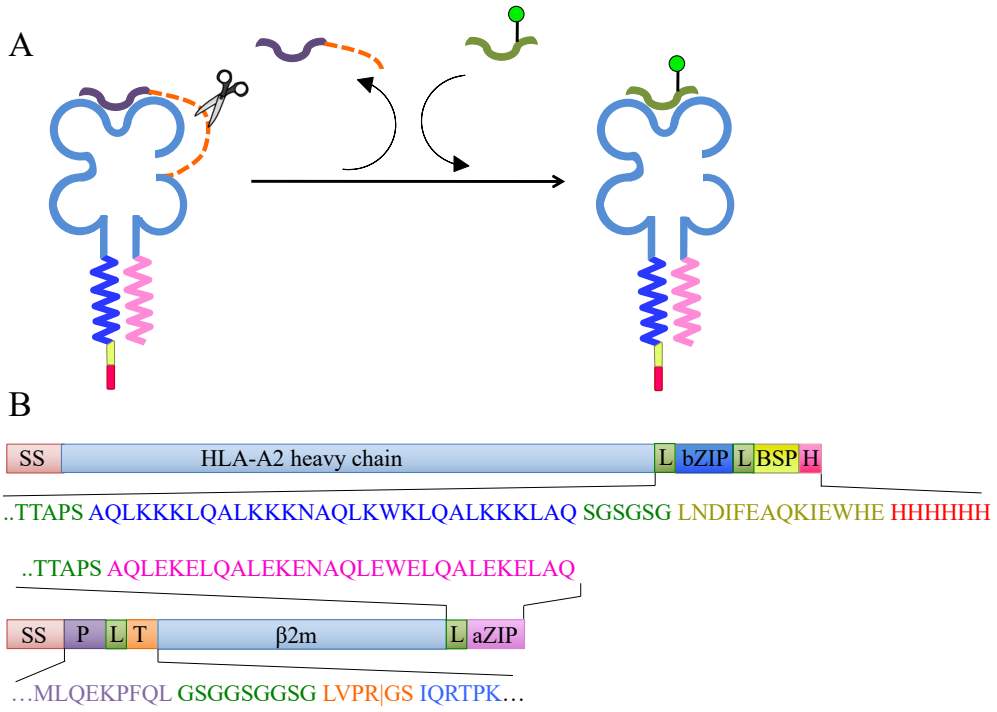

Figure A1.1. Peptide epitope-linked β2-microglobulin HLA-A2 constructs. (A) Schematic of peptide exchange using epitope-linked β2-microglobulin. (B) Schematic of constructs used to express ELBM (SS: secretion signal sequence; bZIP: basic leucine zipper; BSP: BSP85 peptide; H: His_6 tag; P: peptide: T: thrombin cleavage site; aZIP: acidic leucine zipper). Linker sequences shown in green. Vertical line in thrombin sequence shows expected cleavage site. The peptide epitope sequence shown is from the ML9 peptide, while in some experiments other sequences were used (see below). Not drawn to scale.

sequences, and so the resultant heterodimeric protein is secreted to the culture medium where it can be collected by affinity chromatography. The protein is designed such that with addition of thrombin, the linker peptide can be proteolytically cleaved, and a peptide of interest can be added to bind to the MHC-I complex (Figure A1.1). The ELBM protein was then used to develop a fluorescence polarization assay to measure direct binding and optimize a competitive inhibition strategy for affinity measurements for a panel of peptides.

Fluorescence polarization discriminates MHC-bound and free forms of an Alexa488-labeled peptide

To evaluate the dynamic range of this assay and to determine parameters needed to convert polarization values to fractional binding, we first measured mP values for free and fully MHC-bound peptide. FP values for free labeled peptide (25 nM Alexa488-RT[cys]) were 21±4.5 mP (mean±standard deviation, n=8), while recombinant HLA-A2 refolded with Alexa488-RT(cys) displayed FP values of 134±4.2 mP, independent of concentration in the range ~30 nM to 2 uM (Figure A1.2A). We evaluated practical limits on labeled peptide concentrations resulting from non-specific binding of peptide to the assay plate at low concentrations as well

as the sensitivity of the instrument used to measure FP. Based on titrations of peptide in glycerol to simulate peptide binding (Figure A1.3), ~25 nM peptide

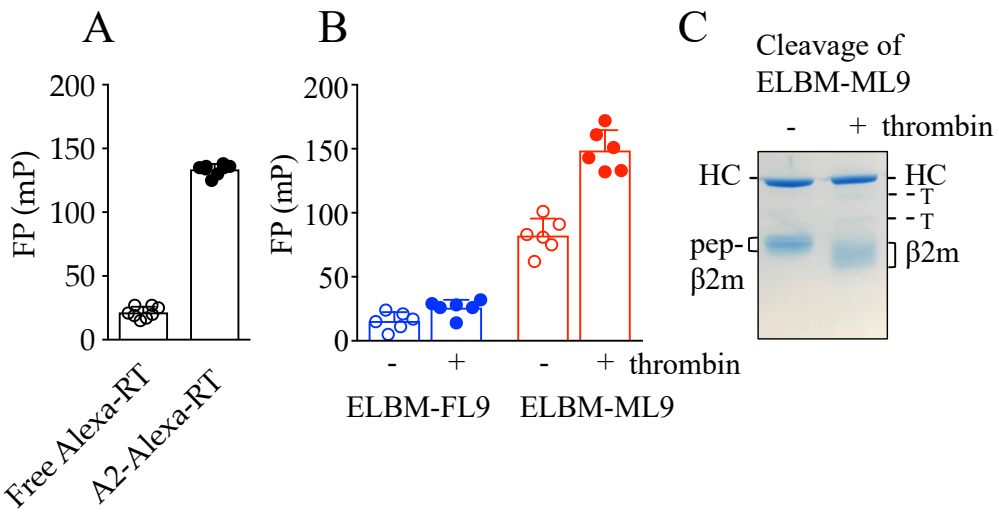

Figure A1.2. Optimization of peptide and assay conditions. (A) Fluorescence polarization of free peptide (25 nM Alexa488-RT[cys]) and bound peptide (HLA-A2 refolded with Alexa488-RT[cys]) were measured at 21±4.5 mP (free) and 134±4.2 mP (bound). Bound mP values were independent of MHC concentration. (B) Addition of 0.01 unit/µl thrombin to 300 nM ELBM-ML9 and 25 nM Alexa488-RT(cys) demonstrated an increase in FP, suggesting cleavage of the linker, release of the ML9 peptide, and binding of the Alexa488-RT(cys) peptide, while ELBM-FL9 displayed little polarization under the same conditions, with or without thrombin. (C) SDS-PAGE analysis of ELBM-ML9 before and after thrombin cleavage using a 12% Tris-Tricine gel demonstrates cleavage of the linker with the addition of thrombin. HC: heavy chain; pep-β2m: peptide-β2m; T: thrombin.

appears to be the lower limit for this assay, as FP values increased at lower peptide concentrations. Although mP values are reliably consistent when up to 400 nM peptide is used (Figure A1.3), higher peptide concentrations are not ideal for quantitative work. 25 nM probe peptide was therefore chosen as the concentration to be used for direct binding and competition assays.

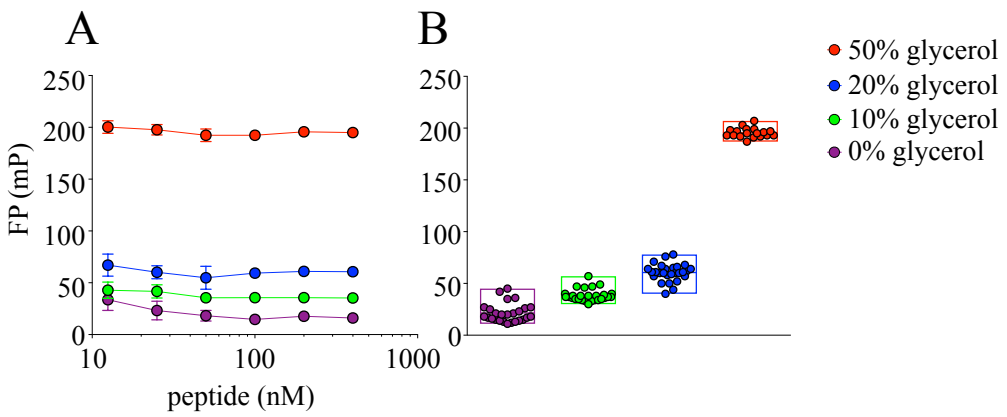

Figure A1.3. Concentration and viscosity effects on Alexa488-RT(cys) fluorescence polarization. (A) Higher glycerol (v/v) concentration increases FP of Alexa488-RT(cys) peptide, independently of peptide concentration. (B) All data points shown in (A) for a given glycerol concentration display similar FP values irrespective of peptide concentration.

We initially tested MHC-ELBM constructed with two different epitopes (FL9 or ML9 [Table A1.1], Figure A1.1), using different concentrations of MHC to determine the amount of MHC-ELBM necessary to bind 25 nM labeled Alexa488-RT(cys) peptide. Results indicated that ML9 was cleaved upon addition of thrombin, with increased binding of Alexa488-RT(cys) (Figure A1.2B, shown at 300 nM MHC). ELBM constructed with the FL9 peptide, however, demonstrated little to no fluorescence polarization even with addition of thrombin, indicating that the FL9 peptide either had not been cleaved or was inefficiently exchanged for the probe peptide (Figure A1.2B). All subsequent experiments were therefore performed with ELBM-ML9. SDS-PAGE of ELBM-ML9 further confirmed that the thrombin concentration used was effective in cleaving the ML9 peptide (Figure A1.2C). Additional parameters tested and optimized included buffer composition, concentration of thrombin, and reaction volume. To examine the kinetics of probe

peptide binding to ELBM-ML9 as well as to determine the optimal duration of the experiment, we performed an analysis using different concentrations of MHC with 25 nM Alexa488-RT(cys) and measured FP values over time (Figure A1.4A). Results indicated that, for all concentrations of MHC tested, MHC binding to probe peptide increased rapidly for ~200 min with slower changes continuing for up to 1000 min. In subsequent work reactions were analyzed after 16hr incubation. The rate of binding was shown to saturate with increasing MHC concentration (Figure A1.4B-C), indicating that the limiting step of this reaction - most likely cleavage or release of the cleaved fragment - occurs prior to peptide binding.

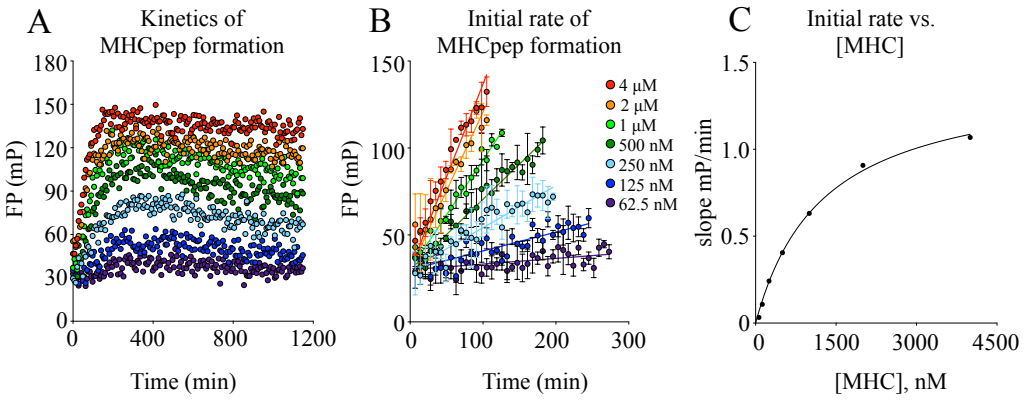

Figure A1.4. Kinetics of MHC-peptide formation. (A) Kinetics of fluorescence polarization using different concentrations of MHC show increased rates of probe peptide binding with greater MHC concentration. (B) Binding rate, as shown by initial rate of MHCpep formation, increases as MHC concentration increases. (C) Transformation of initial rate of MHCpep formation demonstrates saturation of rate of binding with increasing MHC concentration.

MHC and peptide titration

To estimate a value for the K_d of the probe peptide, we assessed equilibrium binding by measuring FP with varying concentrations of either MHC-I or probe peptide. The amount of MHCpeptide complex formed was calculated using the equation:

$$[MHCpep] = \frac{\mathrm{mP}-\mathrm{mP}_{\mathrm{free}}}{\mathrm{mP}_{\mathrm{bound}}-\mathrm{mP}_{\mathrm{free}}} \times Pep_{tot} \quad \text{Eq. 1}$$

where *mP* is the experimental FP value, mP_{free} and mP_{bound} are values for free and MHC-bound probe peptide, determined as described above, and Pep_{tot} is the total concentration of probe peptide, i.e. the amount added at the start of the reaction (This equation assumes additivity of fluorescence polarization, which strictly speaking is limited to fluorescence anisotropy, but for mP_{free} and mP_{bound} values observed here the simplification leads to fractional binding errors of <1%). With [peptide] fixed at 25 nM and [MHC] increased as in Figure A1.4A above, a sigmoidal binding curve with apparent saturation at [MHCpep] ~25 nM was observed (Figure A1.5A). Non-linear least-squares fitting to either a simple two-component binding equation:

$$[MHCpep] = \frac{Pep_{tot} * MHC_{tot}}{K_d + MHC_{tot}} \quad \text{Eq. 2}$$

where MHC_{tot} is the variable [MHC] and K_d is the equilibrium binding constant, or to a quadratic equation that accounted for ligand-depletion effects (see Addendum A):

$$[MHCpep] = \frac{(MHC_{tot}+Pep_{tot}+K_d)\pm\sqrt{(MHC_{tot}+Pep_{tot}+K_d)^2-4MHC_{tot}Pep_{tot}}}{2} \quad \text{Eq. 3}$$

revealed an apparent inhibition constant $K_{d,app}$ = 282±31 nM (Figure A1.5A). In a separate experiment with [MHC] fixed at 1000 nM and [peptide] increased, a sigmoidal binding curve again was observed (Figure A1.5B). The curve appeared to reach maximum [MHCpep] in the vicinity of 100 nM, although there was substantial experimental uncertainty at high [peptide] due to low bound fraction for the probe peptide and small denominator in Eq. 1. Fitting this curve to simple or quadratic competition binding equations (Eq. 2 and 3) revealed $K_{d,app}$ = 37±38 nM. The 5- to 10-fold discrepancy between half-maximal concentrations of peptide and MHC in the two titrations, and between corresponding saturation levels, is unexpected for a simple binding reaction, but could occur if only a fraction of the MHC participates in the reaction. This could be due to incomplete thrombin cleavage of the ELBM construct, incomplete peptide release, or conversion to an inactive form as previously observed for MHC-II[445].

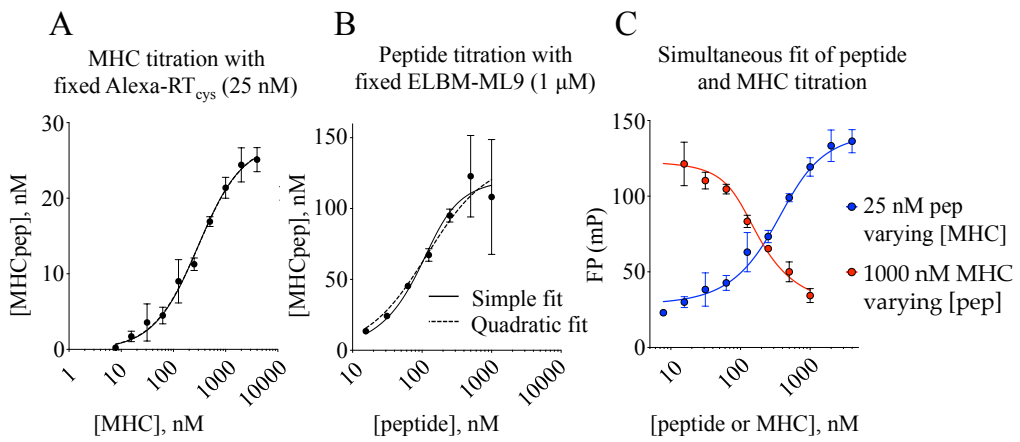

Figure A1.5. Direct binding assay for estimation of K_d. (A) With varying [MHC] and constant [Alexa488-RT(cys)], a curve is fit using a quadratic equation, or using an equation for one-site specific binding (simple fit). The $K_{d,app}$ is calculated to be 283±31 nM. (B) With varying [Alexa488-RT(cys)] and constant [MHC], curve fits are generated as above. The $K_{d,app}$ is calculated to be 37±18 nM. (C) Simultaneous fitting of MHC and peptide titrations using a quadratic equation gave a K_d value of 16±4 nM for the Alexa488-RT(cys) probe peptide and an active MHC fraction of 8.2±0.8%. Curves in (A) and (B) were fit using Eq. 2 and 3; curves in (C) were fit using Eq. 4.

Estimation of K_d and MHC active fraction

To analytically evaluate the fraction of MHC protein that participates in the binding reaction, we simultaneously fit the MHC and peptide titrations, using a quadratic binding equation that includes a term fr_{act} that describes the active MHC fraction (Figure A1.5C). To avoid transformations of the experimental data that result in non-linear amplification of experimental uncertainty, we recast the quadratic binding equation in terms of the experimentally observable fluorescence polarization mP_{obs}, as well as mP_{free}, mP_{bound} and the total reactant concentrations MHC_{tot} and Pep_{tot} (Addendum A):

$$mP_{obs} = \frac{(mP_{bound}-mP_{free})(fr_{act}MHC_{tot}+Pep_{tot}+K_d)\pm\sqrt{(-fr_{act}MHC_{tot}-Pep_{tot}-K_d)^2-4fr_{act}MHC_{tot}Pep_{tot}}}{2} + mP_{free} \quad \text{Eq. 4}$$

At fixed [peptide], mP_{obs} increases as MHC_{tot} is increased, reaching a saturating value at $mP_{bound.}$ (Figure A1.5C, blue symbols). At fixed [MHC], mP_{obs} decreases as Pep_{tot} is increased, given that the fractional amount of peptide decreases (Figure A1.5C, red symbols). Simultaneous fitting of both datasets revealed a K_d of ~16 nM with an active fraction of ~8%.

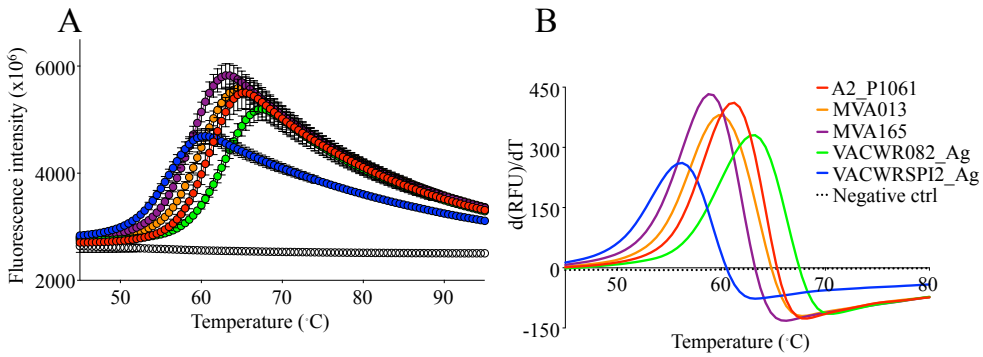

Figure A1.6. Differential scanning fluorimetry of MVA peptide-MHC complexes. (A) Fluorescence intensity of SYPRO Orange bound to HLA-A2-peptide complexes is shown over a range of temperatures as the complexes unfold. (B) Transformation of the fluorescence intensity data shown in (A) using the first derivative illustrates the T_m of each MHC-I-peptide complex at the apex of the curve.

Competition binding assay for determination of IC_{50}

Competition binding assays, in which binding of a fixed concentration of a probe binder is assessed as the concentration of an unlabeled competitor is varied, are useful in routine binding analysis given that they allow for testing of many unlabeled test peptides using a single preparation of labeled probe peptide. This is particularly true for FP-based MHC-peptide binding analysis, as introduction of a fluorescent probe is likely to alter MHC-peptide binding affinity due to extensive

and somewhat unpredictable MHC interactions all along the length of a bound peptide. To evaluate the utility of the ELBM FP assay in competitive binding assays, we selected a set of competitor peptides derived from vaccinia virus for which IC_{50} values and/or half-life measurements had been previously reported[446-449] (Table A1.2). As the full set of peptides had not been previously compared in the same assay, we evaluated the thermal stability of HLA-A2 complexes of the set of test peptides (Figure A1.6, Table A1.2) using a differential scanning fluorimetry assay [450]. The assay was performed with competitor peptides titrated in 2-fold dilutions starting from 2 μM (Figure A1.7). IC_{50} values were determined by fitting using nonlinear regression analysis with the equation:

$$mP_{obs} = \frac{(mP_{max} - mP_{min})}{1+\left(\frac{Comp_{tot}}{IC_{50}}\right)} + mP_{min} \qquad \text{Eq. 5}$$

where mP_{min} is measured in the absence of MHC (i.e. mP_{free}), mP_{max} is measured in a control binding reaction with MHC and probe peptide but in the absence of competitor peptide, $Comp_{tot}$ is the variable concentration of the (unlabeled) competitor peptide, and IC_{50} is $Comp_{tot}$ at half-maximal competition. As expected, increasing concentration of each of the vaccinia test peptides decreased the binding of labeled probe peptide (Figure A1.7). Best-fit IC_{50} values for these peptides ranged from ~230 nM to ~1250 nM.

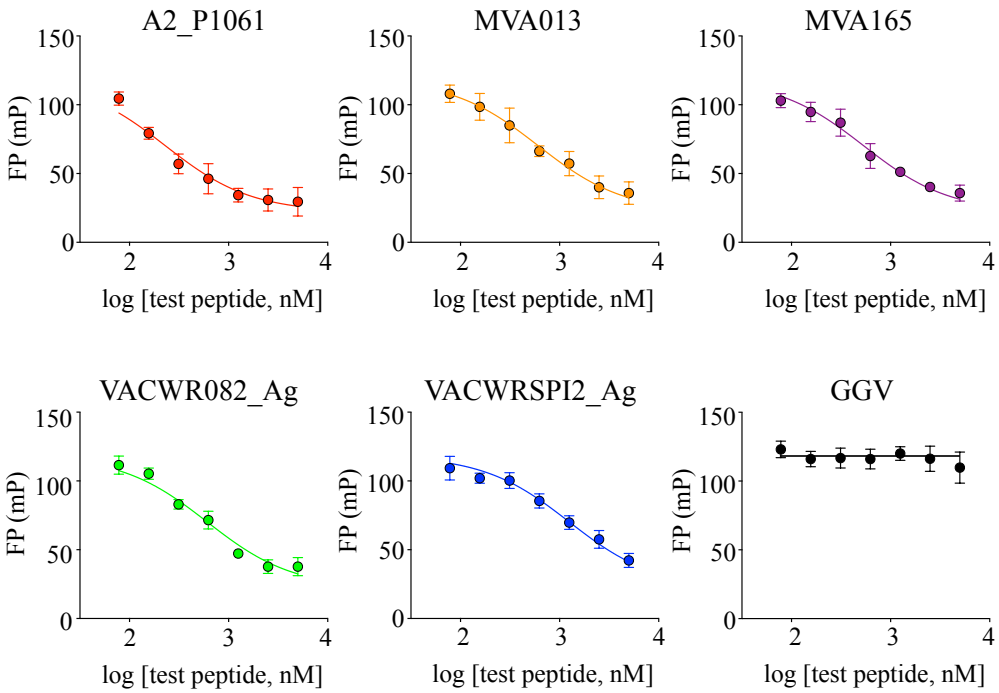

Figure A1.7. Measurement of IC_{50} for a set of vaccinia peptides. An inhibition assay was performed for determination of IC_{50} using 500 nM MHC and 25 nM Alexa488-RT(cys), with 2-fold dilutions (beginning at 2 μM) of the vaccinia competitor peptides A2_P1061, MVA013, MVA165, VACWR082_Ag, and VACWRSPI2_Ag. The GGV peptide was similarly diluted and used as a negative control. Curves were fit using Eq. 5.

Concentration dependence of IC_{50}

IC_{50} measurements are suitable for relative assessments of binding affinity, but often the absolute binding affinity of the inhibitor peptide, K_i, is desired. Under certain conditions, the IC_{50} value obtained in a competition binding assay approximates the K_i, in particular when the concentration of peptide is below its K_d and the concentration of MHC is low relative to the concentration of test and probe peptides. For FP assays with MHC proteins, these conditions are difficult to achieve

in practice. In our assay, the concentration of labeled peptide was necessarily >10 nM to obtain reliable FP measurements, but this is near the K_d, and the MHC concentration needed to be several fold greater in order to bring the bound fraction into a region where competition could be observed. We evaluated the concentration dependence of IC_{50} for three of the test peptides that spanned the range of observed IC_{50} values. Experiments at different MHC concentrations yielded different IC_{50} values, although the test peptide rank order and relative IC_{50} values were similar under the different conditions (Figure A1.8A-D, Table A1.2).

Estimation of K_i using Cheng-Prusoff and Munson-Robard approaches

Several approaches have been suggested in the literature to correct for these concentration effects and convert IC_{50} values to Ki[451-456]. In the Cheng-Prusoff approach, IC_{50} values can be converted to K_i using the known concentration of the labeled test peptide and its binding constant:

$$K_{i,corr} = \frac{IC_{50}}{1+\frac{Pep_{tot}}{K_d}} \qquad \text{Eq. 6}$$

Under our experimental conditions, the probe peptide concentration was similar to its binding affinity, with Pep_{tot}/K_d ~1.5, so the correction factor was substantial (Table A1.3). However, this equation does not consider the effect of high MHC concentration on depleting peptide, so that the free and total peptide concentrations are substantially different. Thus, even after application of the Cheng-Prusoff correction, we observed $K_{i,corr}$ to vary with [MHC] (Table A1.3).

In the Munson-Rodbard approach, ligand depletion is considered explicitly using a term (y_0) corresponding to the ratio of bound and free test peptide in the absence of inhibitor:

$$K_{i,corr} = \frac{IC_{50}}{\frac{1+Pep_{tot}*(y_0+2)}{(2K_d[y_0+1])+y_0}} + \frac{y_0*K_d}{[y_0+2]} \qquad \text{Eq. 7}$$

Although in principle this correction is exact, in practice y_0 can have substantial experimental uncertainty, leading to large deviations of the observed $K_{i,corr}$ from expected values. Under our assay conditions, at low [MHC] the y_0 factor was 1.9, with a reasonable 95% confidence interval of 1.4-2.8 based on the experimental uncertainly in mP_{min} and mP_{bound}, but at high [MHC], the y_0 factor was 8.8, with a very large 95% confidence interval of 4.7-36. Thus, even after Munson-Rodbard correction, we observed substantial $K_{i,corr}$ divergence (Table A1.3).

Estimation of K_i using a cubic equation

In order to determine more directly how MHC concentration (MHC_{tot}), probe peptide concentration (Pep_{tot}), and probe peptide binding affinity (K_d) would affect IC_{50} curves obtained, we modeled IC_{50} curves as a function of concentration of competitor peptide. Because of the effects of ligand depletion on both probe and test peptides, this requires a cubic equation[457,458]. We derived an exact equation for the free MHC concentration in terms of the other experimental parameters (see Addendum B):

$$[MHC] = \sqrt[3]{(1 - MHC_{tot} + K_d + K_i + Pep_{tot} + Comp_{tot} - MHC_{tot}K_d - MHC_{tot}K_i + K_dK_i + K_iPep_{tot} + K_dComp_{tot} - MHC_{tot}K_dK_i)}$$

Eq. 8

and used this to simulate competition binding curves under different conditions, using the test conservation equations [*MHCpep*]=MHC_{tot}-[*MHC*] and

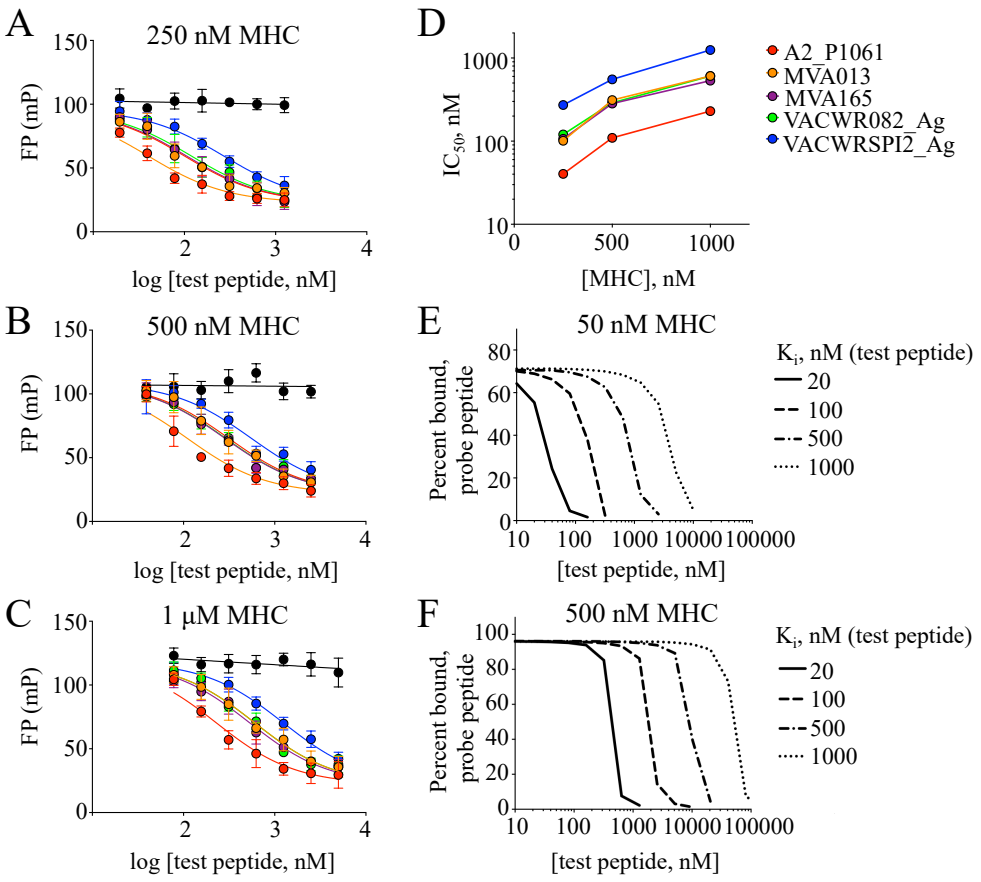

Figure A1.8. Dependence of IC_{50} on MHC concentration. (A-D) An inhibition assay to determine IC_{50} values was performed with different MHC concentrations and 25 nM Alexa488-RT(cys), with 2-fold dilutions of competitor peptides beginning at 5 µM (1 µM MHC), 2.5 µM (500 nM MHC), and 1.25 µM (250 nM MHC). As MHC concentration doubles from (A) 250 nM to (B) 500 nM to (C) 1 µM, IC_{50} values approximately double (D) for the vaccinia peptides tested (shown in Table A1.2.) Curves were fit using Eq. 5. (E-F) Simulated binding competition curves, calculated using Eq. 8, for 25 nM test peptide with K_d=20 nM and other parameters as shown.

Pep_{tot}=[Pep_{free}]+[MHC_{pep}] to relate the free MHC concentration to the percentage of test peptide bound observed experimentally. Calculated completion curves shift as each the experimental variables (MHC_{tot}, K_i, K_d) are changed (Figure A1.8E-F), but as we observed experimentally, differences between the IC_{50} curves are distinguishable regardless of the changes in these parameters.

We next simultaneously fit a family of experimental IC_{50} curves for a single test peptide obtained under different [MHC], with the idea that this might provide a reliable consensus K_i value, similarly to how simultaneous fits of MHC and peptide titrations provided a robust K_d determination as described above. We encountered difficulty implementing a non-linear least squares curve-fitting approach using the equation shown as Eq. 8, but we were able to simultaneously fit a single K_i value to sets of experimental binding inhibition curves obtained at different MHC concentrations (Figure A1.9). For this analysis we used an implicit equation version of the cubic equation (Addendum C). This fit included values for mP_{free}, mP_{bound}, [MHC], active fraction, K_d and Pep_{tot} in addition to K_i. Known or estimated values for these parameters could be included in the fit procedure, or values could be determined simultaneously with K_i. In practice, we found that the fit had a relatively narrow radius of convergence, so that initial values had to be chosen thoughtfully, and that K_i values were somewhat coupled to the probe peptide K_d and MHC active fraction, although they were relatively independent of mP_{free} and mP_{bound}. Best fit values for K_i for the test peptides, along with ranges consistent with experimental uncertainties in K_d and MHC active fraction, are shown in Table A1.3.

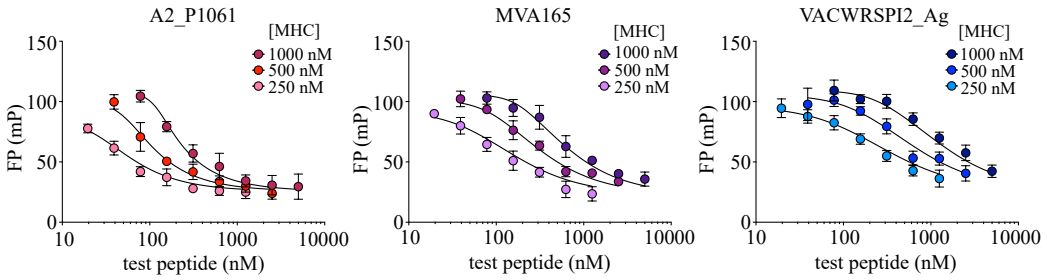

Figure A1.9. Fitting competitive binding inhibition curves using a cubic equation. To determine K_i values for the A2_P1061, MVA165, and VACWRSPI2_Ag peptides, three curves obtained at different [MHC] were simultaneously fit using an implicit cubic equation (Addendum C). Best fit K_i values obtained with K_d = 16 nM and fr_{act} = 0.2 shown in Table A1.3, along with a range of Ki values obtained with reasonable parameter values (mP_{free} = 22 to 28, mP_{bound} = 115 to 150, K_d = 10 to 20 nM, and fr_{act} = 0.08 to 0.2).

Discussion

In this work, we describe a method whereby MHC-I peptide affinities can be measured by direct binding or competition assays. While fluorescence polarization has been employed previously to measure the rate of peptide exchange and affinity in MHC-I and MHC-II binding assays[329,443,444], here we have used a novel recombinant HLA-A2 protein with a proteolytically cleavable linker tethered to the β2m subunit, which allows for efficient peptide release and measurement of probe peptide K_d. We show that relative binding affinities of competitor peptides can be measured by determination of IC_{50} values using this assay. Lastly, to estimate absolute K_i from IC_{50} values, we propose use of a cubic equation and demonstrate its application to determination of the K_i of competitor peptides.

A potential limitation of the ELBM method is the difficulty that may be encountered in designing a linker peptide with the appropriate features. For

efficient exchange to occur, this peptide must exhibit sufficient affinity for binding but also must be weak enough to be released after enzymatic cleavage. A different linker peptide for each MHC allele of interest must also be designed due to distinct allele-specific binding requirements. Suitable peptides similarly have been difficult to design for dipeptide and photocleavable peptide exchange assays, given that following cleavage, peptide fragments may inefficiently dissociate from the MHC protein[430,459]. The primary advantage of the ELBM approach over other available methods for producing MHC-I for peptide interaction measurements[414,428,430,431,444] is that covalent linkage of a replaceable peptide ligand allows for expression in mammalian cells, while at the same time allowing for high efficiency of peptide exchange in vitro. We used the ELBM constructs to characterize binding behavior of a known HLA-A2 ligand derived from HIV reverse-transcriptase.

To help understand how observed competition binding curves depend on experimental conditions and relate to intrinsic binding affinities for probe and test peptides, we developed a cubic equation that relates observable fluorescence polarization changes to intrinsic assay parameters. Conventional approaches for analyzing competition binding data and extracting intrinsic binding parameters[451,452] were developed for cases where the receptor concentration is very low and the sensitivity of detection high, such as for radiolabeled ligand binding to receptors on the surface of intact cells. These approaches were not applicable to our FP-based assay of peptides binding to recombinant soluble MHC-I proteins, and the derived $K_{i,app}$ values were highly dependent on experimental conditions. Fluorescence polarization assays in general measure the fraction of probe that is

bound to receptor, and thus require sufficient receptor concentration to achieve substantial fractional occupancy. Moreover, sensitivity of conventional microplate fluorescence readers in polarization mode is limited to probe concentrations of ~25 nM or greater, which is in the vicinity of many MHC-I-peptide binding constants. Thus, key assumptions used in conventional competition binding analysis to relate observed IC_{50} values to intrinsic K_i do not hold for our experimental conditions. Despite these caveats, relative IC_{50} values reliably reported relative binding affinity. In order to explore estimation of absolute K_i values from our competition binding data, we derived from first principles a cubic equation relating concentrations of all bound and free species present in the reactions and their binding constants. We also derived an intrinsic equation relating observed fluorescence polarization changes to these parameters, which proved more useful for routine curve fitting. Similar development of cubic equations for fitting other types of competition binding assays have been presented previously[457,458]. Using this approach, we were able to estimate intrinsic binding constants for a set of vaccinia-derived HLA-A2-binding peptides, although robust curve fitting required experiments at a range of MHC concentrations as well as a previously-determined value for the K_d of the probe peptide.

The ELBM approach may also represent a useful tool in additional applications such as generation of MHC-I tetramers with different peptide ligands to characterize antigen-specific T cell responses. ELBM potentially additionally could be employed to produce MHC-I-peptide complexes for biophysical studies. In sum, this work describes a novel method for producing specific MHC-I- peptide

complexes by peptide exchange, with particular application to assaying peptide binding affinity. This method may have applications in epitope discovery and assessment of peptide-MHC interactions and may prove useful in vaccine and immunotherapy development.

Materials and Methods

Peptide synthesis and labeling

All test peptides and probe peptide (shown in Table A1.1) were synthesized by 21st Century Biochemicals (Marlborough, MA). HIV-RT (ILKEPVCGV) was labeled with Alexa Fluor 488 C_5-maleimide (Thermo Fisher Scientific, Waltham, MA) via the thiol of C_7. Labeling was performed for 2h at RT, and separation of labeled peptide from free fluorophore was performed using Jupiter C18 reverse-phase chromatography (Phenomenex, Torrance, CA).

*HLA-A*0201 expression and purification*

The heavy chain of epitope-linked β2m (ELBM) consisted of the HLA-A2*0201 extracellular domain, a linker, the basic half of a heterodimeric leucine zipper[460], the biotinylation signal peptide 85[461], and a His6 tag[462], while the light chain encoded an N-terminal stuffer peptide (ML9 [MLQEKPFQL] or FL9 [FIALWIPDL]), a 20-amino-acid linker containing a thrombin cleavage site, β2m, an additional 15-amino-acid linker, and the acidic half of the leucine zipper. A signal sequence (SS) derived from human ceruloplasmin was also used, with a 2-amino-acid modification to incorporate an SbfI restriction site, (shown in bold: MKILILGIFLFLCSTP**AW**A → MKILILGIFLFLCSTP**LQ**A). Constructs are depicted in Figure 1. For generation of ELBM-ML9 recombinant protein, lentivirus

was produced via the calcium phosphate method by co-transfection of HEK293T/17 cells (293, ATCC #CRL-11268) using a second-generation lentiviral vector based on pWPI (Addgene #12254), which encoded the marker Thy1.1 and for which expression was driven by a CMV promoter, together with the packaging plasmids pMD2.G (Addgene #12259) and psPAX2 (Addgene #12260). 293 cells were cultured in complete DMEM media supplemented with 10% FCS, 1% antibiotic-antimycotic (Thermo Fisher) and 50 μM d-biotin (complete d-biotin medium, CDM), and transfections were performed with 45 μg each of the heavy and light chain expression constructs, 60 μg of psPAX2, and 30 μg of pMD2.G. Medium was replaced within 4-6 hours following transfection and was harvested at 2.5 days. Supernatants were centrifuged at 3000 g for 30 minutes, filtered through a 0.2 μm filter, and lentivirus was pelleted by ultracentrifugation (18000 rpm for 3 h). Concentrated lentivirus was used to transduce GnTI- HEK293S cells[463] previously transduced with BirA and EGFP and seeded at $2x10^4$ cells/well the day before in a 96-well plate in CDM. Fresh CDM was added after 24 h, and cells were expanded for a further 4-5 days with media changes. High expression of EGFP and Thy1.1 was confirmed post-transduction, and cells were expanded for protein production in CELLine 1000 flasks (DWK Life Sciences, Millville, NJ). Supernatant was collected once per week for 5-15 weeks, and the bimolecular complex was affinity-purified from culture supernatants with the anti-zipper mAb 2H11 (gift of Ellis Reinherz) using AKTAprime systems (GE, Chicago, IL), followed by concentration and buffer exchange using Amicon centrifugation filters (Millipore Sigma, Burlington MA). ELBM-FL9 was produced similarly, with the

following modifications; ELBM vectors expressed both Thy1.1 and DsRed, HEK293T cells were transduced for protein expression, and cells were sorted for marker expression following transduction. Protein yield was determined to be ~10 mg/L. For generation of pre-loaded MHC-peptide complexes for use as controls and in ThermoFluor experiments, we refolded *E. coli*-produced HLA-A2 heavy chain and β2m with Alexa488-RT(cys) or indicated peptides as described[428].

Fluorescence polarization (FP) assay and IC_{50} measurements

An FP assay using 500 nM ELBM-ML9, 25 nM Alexa488-RT(cys), and 0.01 unit/μl thrombin (MP Biomedicals, Santa Ana, CA) was performed in PBS containing 0.1% octylglucoside (Sigma Aldrich, St. Louis, MO) in 96-well black polypropylene microtiter plates (Greiner Bio-One, Monroe, NC) in a total volume of 120 μl. After 16h incubation at room temperature (RT), FP was measured as millipolarization (mP) units in a VICTOR X5 plate reader (Perkin Elmer, Waltham, MA) at 495 excitation and 520 emission. SDS-PAGE using a 12% Tris-Tricine gel was used to confirm cleavage of ELBM-ML9. To measure competition binding, test peptides were added at 2-fold dilutions ranging from 5 μM to ~40 nM. For equilibrium experiments, MHC concentration was varied from 4 μM to 7.8125 nM (2-fold dilutions) with a fixed probe peptide concentration of 25 nM, or probe peptide concentration was varied from 4 μM to 62.5 nM (2-fold dilutions) with a fixed MHC concentration of 1 μM. mP measurements in the absence of MHC (mP_{free}) as well as mP measurements of A2 refolded with Alexa488-RT(cys)

(mP_{bound}) were also determined to calculate concentration of MHC bound to probe peptide. For kinetic analyses, FP values were measured every 7 minutes for ~20h at RT with MHC concentrations ranging from 4 μM to 62.5 nM (2-fold dilutions).

Differential scanning fluorimetry (ThermoFluor assay)

The ThermoFluor assay was performed using 2.5 μM A2 complexes refolded with test peptides and a 500-fold dilution of SYPRO orange (Thermo Fisher Scientific) in PBS pH 7.4 in a total solution volume of 20 μl in optically clear 96-well plates. Temperatures were increased from 20°C to 95°C at 1°C/min in a Bio-Rad C1000 Thermal Cycler RT-PCR instrument (Bio-Rad, Hercules, CA). To determine the T_m or thermal stability of each complex, the temperature derivative of the melting curve was computed.

Curve fitting

Prism (version 7.0c, GraphPad Software, San Diego, CA) was used for curve fitting with ordinary unweighted nonlinear least-squares regression.

Table A1.1. Peptide sequences

Peptide	*Sequence*
ML9	MLQEKPFQ
FL9	FIALWIPDL
HIV-RT	ILKEPVCGV[1]
A2_P1061	GLFDFVNFV
MVA013	RLYDYFTRV
MVA165	KVDDTFYYV
VACWR082_Ag	ILDDNLYKV
VACWRSPI2_Ag	HVDGKILFV
GGV	GAGGGVGGV

[1]Cysteine residue introduced for addition of fluorescent label underlined

Table A1.2. Binding and stability parameters for test peptides

Peptide	*T_m (℃)*	*Reported IC_{50} (nM)*	*Reported $t_{1/2}$ (h)*
A2_P1061	61.2	1 [447,449]	N/A
MVA013	59.8	11 [447,449]	20.03 [446]
MVA165	58.7	4.2 [448]	12.2 [446]
VACWR082_Ag	63.3	2.2 [448]	26.21 [446]
VACWRSPI2_Ag	56.2	39 [447], 124 [449]	4.2 [446]

Table A1.3. IC_{50} as a function of MHC and estimated K_i using Cheng-Prusoff or Munson-Rodbard approaches

Peptide	[MHC] (nM)	IC_{50} (nM)	K_i Cheng-Prusoff	K_i Munson-Rodbard	Ki cubic fit[1]
A2_P1061	250	40	24	30	
	50	110	65	47	5 (3-9)
	1000	230	137	59	
MVA165	250	106	64	51	
	500	284	169	85	23 (17-42)
	1000	534	319	100	
VACWRSPI2_Ag	250	272	162	103	
	500	553	323	145	60 (49-138)
	1000	1249	745	196	

[1]Single value representing global fit to inhibition curves obtained at three MHC concentrations. Values in parentheses show range of K_i values obtained from fits allowing for observed experimental uncertainty in mP_{free}, mP_{bound}, K_d, and MHC active fraction parameters.

Addendum A. Derivation of a quadratic equation that describes single-site binding of a peptide to MHC protein

For a simple reaction between a peptide-binding protein (MHC) and a peptide (pep)
MHC + pep ⇒ MHCpep + MHC + pep

The following equilibrium binding equation applies:

$K_d = \frac{[MHC][pep]}{[MHCpep]}$ Eq. A.1

where [*MHC*] and [*pep*] refer to free (unbound) species and K_d is the equilibrium dissociation constant.

Typically, only the total concentrations are known:

$MHC_{tot} = [MHC] + [MHCpep]$ Eq. A.2
$Pep_{tot} = [pep] + [MHCpep].$ Eq. A.3

Substituting these into the equilibrium binding equation:

$K_d = \frac{(MHC_{tot} - [MHCpep])\,(Pep_{tot} - [MHCpep])}{[MHCpep]}$ Eq. A.4

and solving for [*MHCpep*] by applying the quadratic formula:

$K_d[MHCpep] = (MHC_{tot} - [MHCpep])\,(Pep_{tot} - [MHCpep])$ Eq. A.5

$K_d[MHCpep] = MHC_{tot}Pep_{tot} - MHC_{tot}[MHCpep] - Pep_{tot}[MHCpep] + [MHCpep]^2$ Eq. A.6

$0 = [MHCpep]^2 - (MHC_{tot} + Pep_{tot} + K_d)[MHCpep] + MHC_{tot}$ Eq. A.7

gives the desired equation relating the amount of bound complex MHCpep to the total MHC and peptide concentrations:

$[MHCpep] = \frac{(MHC_{tot} + Pep_{tot} + K_d) \pm \sqrt{(MHC_{tot} + Pep_{tot} + K_d)^2 - 4MHC_{tot}Pep_{tot}}}{2}$ Eq. A.8

In all cases, only the second (negative) root gives a physically reasonable solution with [*MHCpep*] greater than zero and less than MHC_{tot} and Pep_{tot}.

If [*MHCpep*] values have been determined from the experimental data, these can be fit using this equation.

Alternatively, for fluorescence polarization experiments the experimental mP values can be fit directly, assuming additivity of polarization values, by substituting Eq. A.8 into Eq. 1 and solving for mP_{obs}:

$$mP_{obs} = \frac{(mP_{bound} - mP_{free})(MHC_{tot} + Pep_{tot} + K_d) \pm \sqrt{(-MHC_{tot} - Pep_{tot} - K_d)^2 - 4MHC_{tot}Pep_{tot}}}{2} + mP_{free} \quad \text{Eq. A.9}$$

To account for the effect of incomplete cleavage and/or peptide release, MHC_{tot} is replaced with fr_{act}*MHC_{tot}, where fr_{act} represents the active fraction, and fr_{act}*MHC_{tot} the effective concentration of MHC molecules participating in the binding reaction:

$$mP_{obs} = \frac{(mP_{bound} - mP_{free})(fr_{act}MHC_{tot} + Pep_{tot} + K_d) \pm \sqrt{(-fr_{act}MHC_{tot} - Pep_{tot} - K_d)^2 - 4fr_{act}MHC_{tot}Pep_{tot}}}{2} + mP_{free} \quad \text{Eq. A.10}$$

This equation was used to fit data in Figure A1.5, using the following constraints and initial values for the non-linear least squares minimization: mP_{bound} and mP_{free}, constrained to experimentally determined values or fit from initial values corresponding to minimum and maximum observed values in entire experiment; fr_{act}, fit from initial value = 1.0; MHC_{tot} and Pep_{tot}, constrained to known values or used as independent variables; K_d, fit from initial value corresponding to concentration at which mP_{obs} was half-maximal.

Addendum B. Derivation of a cubic equation that describes single-site competitive binding of two peptides to an MHC protein

For a reaction between a peptide-binding protein (MHC) and two peptides (pep1 and pep2) competing for binding to the same site:

MHC + pep1 + pep2 ⇒ MHCpep1 + MHCpep2 + MHC + pep1 + pep2

Two binding equilibria apply simultaneously:

$K_{d,pep1} = \frac{[MHC][pep1]}{[MHCpep1]}$ Eq. B.1

and

$K_{d,pep2} = \frac{[MHC][pep2]}{[MHCpep1]}$ Eq. B.2

where $K_{d,pep1}$ and $K_{d,pep2}$ refer to the equilibrium dissociation constants for binding of pep1 and pep2 to MHC. In a typical experiment, one peptide would be labeled (referred to as the "probe" peptide) and used at a constant concentration with the concentration of the other peptide (referred to as the "test" peptide) varied over a wide range. The analysis that follows is general for arbitrary concentrations of MHC and peptides.

In this case the conservation equations are:

$MHC_{tot} = [MHC] + [MHCpep1] + [MHCpep2]$ Eq. B.3

$Pep1_{tot} = [pep1] + [MHCpep1]$ Eq. B.4

$Pep2_{tot} = [pep2] + [MHCpep2]$ Eq. B.5

Using the equation for conservation of pep1 and solving for the bound form we obtain:

$K_{d,pep1} = \frac{[MHC](Pep1_{tot} - [MHCpep1])}{[MHCpep1]}$ Eq. B.6

$K_{d,pep1}[MHCpep1] = [MHC](Pep1_{tot} - [MHCpep1])$ Eq. B.7

$K_{d,pep1}[MHCpep1] = [MHC]Pep1_{tot} - [MHC][MHCpep1]$ Eq. B.8

$[MHCpep1] = \frac{[MHC]Pep1_{tot}}{K_{d,pep1} + [MHC]}$ Eq. B.9

Similarly, for pep2:

$[MHCpep2] = \frac{[MHC]Pep2_{tot}}{K_{d,pep2} + [MHC]}$ Eq. B.10

Combining these with the conservation equation for MHC:

$MHC_{tot} = [MHC] + \frac{[MHC]Pep1_{tot}}{K_{d,pep1} + [MHC]} + \frac{[MHC]Pep2_{tot}}{K_{d,pep2} + [MHC]}$ Eq. B.11

and solving for the free MHC concentration:

$$MHC_{tot} - [MHC] = \frac{[MHC]Pep1_{tot}}{K_{d,pep1}+[MHC]} + \frac{[MHC]Pep2_{tot}}{K_{d,pep2}+[MHC]} \quad \text{Eq. B.12}$$

$$(MHC_{tot} - [MHC])\big(K_{d,pep1} + [MHC]\big)\big(K_{d,pep2} + [MHC]\big) = \big(K_{d,pep2} + [MHC]\big)([MHC]Pep1_{tot}) + \big(K_{d,pep1} + [MHC]\big)([MHC]Pep2_{tot}) \quad \text{Eq. B.13}$$

provides a cubic equation relating the concentration of free MHC to the known total concentrations of MHC, pep1, and pep2:

$$0 = [MHC]^3 + \big(-MHC_{tot} + K_{d,pep1} + K_{d,pep2} + Pep1_{tot} + Pep2_{tot}\big)[MHC]^2 + \big(-MHC_{tot}K_{d,pep1} - MHC_{tot}K_{d,pep2} + K_{d,pep1}K_{d,pep2} + K_{d,pep1}Pep2_{tot} + K_{d,pep2}Pep1_{tot}\big)[MHC] - \big(MHC_{tot}K_{d,pep1}K_{d,pep2}\big)$$

Eq. B.14

Although there is not a simple closed-form solution to this cubic equation, analytical solutions are available that differ depending on the value of the discriminant □,

$$\Delta = 18abcd - 4b^3d + b^2c^2 - 4ac^3 - 27a^2d^2 \quad \text{Eq. B.15}$$

where a,b,c,d are the polynomial coefficients

$$ax^3 + bx^3 + cx + d = 0 \quad \text{Eq. B.16}$$

There is one real solution for $\Delta < 0$ and multiple solutions for $\Delta >= 0$. In the case of multiple solutions, these have to be evaluated for physical reasonableness, $[MHC] >= MHC_{tot}$.

We used this equation to simulate competition binding data under different conditions (Figure A1.8).

We attempted to use this equation to fit experimental competition binding data, but implementation in Prism was difficult and the refinements did not converge well, so instead we used an implicit equation as described in Addendum C.

Addendum C. Derivation of a function that describes single-site competitive binding of two peptides to an MHC protein as an implicit equation

The scientific graphing and analysis program Prism (GraphPad Software, San Diego, CA) accepts implicit equations for fitting by numerical approximation, and we used this approach to fit experimentally observed values of mP_{obs} as a function of the total concentrations of probe and test peptides [$Pep1_{tot}$] and [$Pep2_{tot}$], the equilibrium dissociation constants for these peptides $Kd_{,pep1}$ and $Kd_{,pep2}$, the total MHC concentration M_{tot} and its active fraction fr_{act}, and the polarization values for free probe peptide and probe peptide fully bound to MHC, mP_{free} and mP_{bound}.

The concentration of the bound form of the probe peptide [MHCpep1] can be expressed as an implicit equation, making use of equilibrium binding and conservation equations similarly to the derivation in Appendices A and B:

$$K_{d,pep1} = \frac{[MHC][pep1]}{[MHCpep1]} \quad \text{Eq. C.1}$$

$$[MHCpep1] = \frac{[MHC][pep1]}{K_{d,pep1}} \quad \text{Eq. C.2}$$

$$[MHCpep1] = \frac{(MHC_{tot} - [MHCpep1] - [MHCpep2])(Pep1_{tot} - [MHCpep1])}{K_{d,pep1}} \quad \text{Eq. C.3}$$

The value for the concentration of bound inhibitor peptide [*MHCpep2*] can be replaced using the quadratic equation relating [*MHCpep2*] to the total concentrations MHC_{tot} and $Pep2_{tot}$, the inhibitor binding constant $K_{d,pep2}$, and the concentration of bound probe peptide [*MHCpep1*], exactly as in Addendum A, but taking into account the reduction in MHC_{tot} due to pep1 binding:

$$K_{d,pep2} = \frac{[MHC][pep2]}{[MHCpep2]} \quad \text{Eq. C.4}$$

$$K_{d,pep2}[MHCpep2] = (MHC_{tot} - [MHCpep1] - [MHCpep2])(Pep2_{tot} - [MHCpep2]) \quad \text{Eq. C.5}$$

$$K_{d,pep2}[MHCpep2] = MHC_{tot}Pep2_{tot} - MHC_{tot}[MHCpep2] - Pep2_{tot}[MHCpep1] + [MHCpep1][MHCpep2] - Pep2_{tot}[MHCpep2] + [MHCpep2]^2 \quad \text{Eq. C.6}$$

$$0 = [MHCpep2]^2 - \big(MHC_{tot} + Pep2_{tot} + K_{d,pep2} - [MHCpep1]\big)[MHCpep2] + MHC_{tot}Pep2_{tot} - [MHCpep1]Pep2_{tot} \quad \text{Eq. C.7}$$

$$[MHCpep2] = \frac{-b \pm \sqrt{b^2 - 4ac}}{2a} \quad \text{Eq. C.8}$$

where

$$a = 1 \quad \text{Eq. C.9}$$

$$b = -\left(MHC_{tot} + Pep2_{tot} + K_{d,pep2} - [MHCpep1]\right) \quad \text{Eq. C.10}$$
$$c = MHC_{tot}Pep2_{tot} - [MHCpep1]Pep2_{tot} \quad \text{Eq. C.11}$$

using the formula for [MHCpep2] (Eq C.8) and substituting into the equation for [MHCpep1] above (Eq. C.3), we obtain the desired relationship between the observable quantity [MHCpep1] and total concentrations and binding constants, which are fixed in the experiment.

$$[MHCpep1] = \frac{\left(MHC_{tot} - [MHCpep1] - \left(\frac{-b \pm \sqrt{b^2 - 4ac}}{2a}\right)\right)(Pep1_{tot} - [MHCpep1])}{K_{d,pep1}} \quad \text{Eq. C.12}$$

with a,b,c as defined above. This implicit equation can be used directly for curve fitting in Prism if [*MHCpep1]* has been calculated as described in the main text using Eq. C.13:

$$[MHCpep1] = \frac{(mP_{obs} - mP_{free})}{(mP_{bound} - mP_{free})} Pep1_{tot} \quad \text{Eq. C.13}$$

Alternatively, Eq. C.12 can be recast in terms of mP_{obs} instead of [*MHCpep1*] using Eq. C.13, to allow fitting and estimation of uncertainty values for mP_{bound} and mP_{free}:

$$mP_{obs} = \frac{\left(MHC_{tot} - \frac{(mP_{obs} - mP_{free})}{(mP_{bound} - mP_{free})} Pep1_{tot} - \left(\frac{-b \pm \sqrt{b^2 - 4ac}}{2a}\right)\right)\left(Pep1_{tot} - \frac{(mP_{obs} - mP_{free})}{(mP_{bound} - mP_{free})} Pep1_{tot}\right)(mP_{bound} - mP_{free})}{K_{d,pep1} Pep1_{tot}} + mP_{free}$$

Eq. C.14

Finally, we account for the active fraction of the MHC preparation as in Eq. A.10:

$$mP_{obs} = \frac{\left(fr_{act}MHC_{tot} - \frac{(mP_{obs} - mP_{free})}{(mP_{bound} - mP_{free})} Pep1_{tot} - \left(\frac{-b \pm \sqrt{b^2 - 4ac}}{2a}\right)\right)\left(Pep1_{tot} - \frac{(mP_{obs} - mP_{free})}{(mP_{bound} - mP_{free})} Pep1_{tot}\right)(mP_{bound} - mP_{free})}{K_{d,pep1} Pep1_{tot}} + mP_{free}$$

Eq. C.15

where

$$a = 1 \quad \text{Eq. C.16}$$
$$b = -\left(fr_{act}MHC_{tot} + Pep2_{tot} + K_{d,pep2} - [MHCpep1]\right) \quad \text{Eq. C.17}$$
$$c = fr_{act}MHC_{tot}Pep2_{tot} - [MHCpep1]Pep2_{tot} \quad \text{Eq. C.18}$$

This implicit equation relating mP_{obs} to $Pep2_{tot}$, where pep1 is the probe peptide and pep2 is the test peptide, was used to fit the competition binding data in Figure A1.9. Initial values and constraints for non-linear least squares fitting were the same as described in Addendum A, except $K_{d,pep1}$ was constrained to its experimental value as determined by simultaneous fitting of MHC and peptide titrations in Figure A1.5.

APPENDIX II

Identification of HLA-A2-restricted CTL epitopes derived from human herpesvirus 6B

Author contributions:

I performed experimental work in this chapter, with assistance in generating DCs and CD8 T cell lines provided by Dr. Mauricio Calvo-Calle and John Cruz, and MHC-I monomers refolded and purified by gel filtration by Guoqi Li. Dr. Calvo-Calle also performed analysis of restimulation assay data for this work.

Abstract

Human herpesvirus 6 (HHV-6) is a double-stranded DNA virus for which nearly all humans are seropositive by the age of three years. Two HHV-6 species have been identified, HHV-6A and HHV-6B, each of which is distinct in its antigenic properties, tissue tropism, and epidemiology. Initial encounter with HHV-6B results in a febrile illness associated with roseola infantum in children, whereas HHV-6A infection most often occurs later in life and has been shown to be more neurotropic in its pathogenesis. As primary infection is usually self-limiting, the principal clinical burden lies with viral reactivation, which has been associated with myriad conditions, including transplant dysfunction and rejection, multiple sclerosis, and encephalitis. Currently, the immune response to HHV-6 is poorly understood, and limited studies have been performed with regard to epitope discovery, perhaps due to the low frequency of HHV-6-specific T cells. In this work, we performed binding studies using putative HLA-A2-restricted HHV-6B epitopes, and then examined a subset of these peptides as epitopes using restimulation assays with PBMCs from healthy subjects. Finally, we generated tetramers using 3 of the peptides reproducibly identified as an epitope in multiple donors. These results thus report novel HHV-6B-derived MHC-I epitopes and provide information potentially important in treatment of reactivated HHV-6.

Introduction

Human herpesvirus 6 (HHV-6) is the sixth identified member of the double-stranded DNA human herpesviridae family. Discovered in 1986, HHV-6 has since been classified as two variants or subspecies, HHV-6A and HHV-6B, each of which is distinct in its epidemiology, tissue tropism, and effect on the host immune system[464]. Primary infection with HHV-6B most often occurs within the first three years of life and results in a self-limiting febrile illness commonly known as roseola or sixth disease[465]. Infection with HHV-6A is less prevalent, occurs later in life, and is more neurotropic and neurovirulent in its pathogenesis[466]. Following primary infection, HHV-6 establishes a latent infection thus far detected in the brain, salivary glands, and periphery[467]. Reactivation of either virus represents the primary clinical burden of HHV-6 infection and occurs most often in immunocompromised individuals such as transplant or AIDS patients, but associations with a multitude of diseases including multiple sclerosis, chronic fatigue syndrome, and cancer exist[467,468]. Moreover, HHV-6 is the only known human herpesvirus capable of integration into chromosome telomeres and transmission through the germline[469]. Despite the prevalence of HHV-6 in the human population and the complications associated with its reactivation, comparatively little data exists with regard to presentation of HHV-6 antigens or modulation of the host immune response by HHV-6.

Much like its betaherpesviridae family members HHV-5 (CMV) and HHV-7[470,471], HHV-6 may have evolved to specifically inhibit antigen presentation in

order to subvert the immune response. Viral evasion strategies in the context of MHC-I antigen presentation have been shown to include inhibition of the proteasome, TAP, or tapasin, retention of MHC complexes in the ER, induction of ER-associated degradation (ERAD), and diversion of MHC complexes to the lysosome[472]. Study of the MHC-I-specific responses associated with HHV-6 infection are thus important in design of potential treatment strategies and in understanding of the disease. Nastke *et al.*[473] identified 11 MHC-II epitopes using a systematic approach in which they used a DR-binding assay, ELISPOT to assess the peptide-specific response, and tetramers to stain T cells specific for the epitopes identified[474]. Here, a similar approach will be undertaken to identify CTL HHV-6-derived epitopes.

Results

Evaluation of binding affinity for putative HLA-A2-restricted HHV-6B epitopes

The IEDB (www.iedb.org), BIMAS (www-bimas.cit.nih.gov), and SYFPETHI (www.syfpeithi.de) prediction algorithms were used to design a set of 147 predicted HLA-A2-binding peptides derived from the HHV-6B genome. The binding affinities of these peptides were assessed using a fluorescence polarization assay previously optimized to measure IC_{50} values (Appendix I), with the goal of selecting a smaller set of HLA-A2-binding peptides to evaluate as HHV-6B epitopes using human CD8 T cells. We performed a screen in which competitor

peptides were serially diluted to compute IC_{50} values, which revealed surprising results. Only 6 out of 147 peptides were found to be nonbinders; the remaining 141

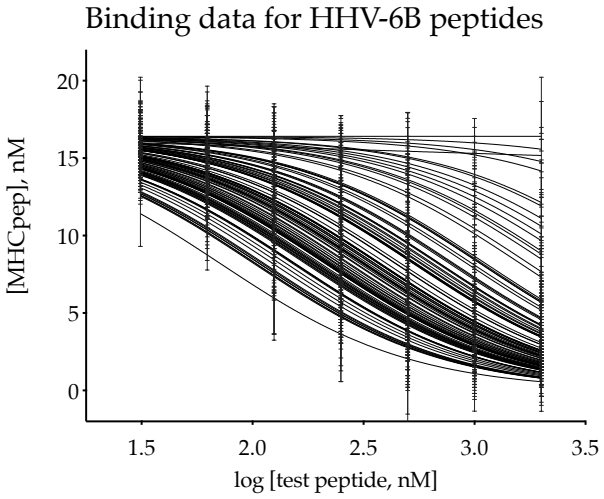

Figure A2.1. Results of binding assay to determine IC_{50} values for HHV-6B-derived peptides.

peptides ranged in IC_{50} values from 71 nM to 7.64 μM (Figure A2.1, Table A2.1, data summarized in Table A2.2).

Identification of HLA-A2-restricted HHV-6B epitopes

In order to determine whether the peptides that were determined to bind to HLA-A2 serve as actual epitopes for $CD8^+$ T cells, we next raised CD8 T cell lines against peptide pools. We chose 57 peptides based on their parent proteins; proteins that were relatively ubiquitous as well as easily accessed by the MHC-I host machinery (e.g. capsid, tegument, and glycoprotein) were selected as putative epitopes. Peptides were grouped into pools of 4-9 peptides with similar IC_{50} values (Tables A2.3 and A2.4). PBMCs were isolated from healthy HLA-A2-positive donors, and DCs generated from $CD14^+$ monocytes were pulsed with peptides and co-cultured

with autologous $CD8^+$ T cells. Following additional restimulation, reactivity to peptide pools was assessed by IFN-γ ELISPOT, and pools were then deconvoluted. Of the 60 peptides tested, responses were observed in 83% of the peptides (50/60), and 29 peptides were considered to elicit "strong responses" (please see Materials and Methods). Results of these assays are further described in Table A2.3, with responses to peptides derived from proteins involved in the early vs. late phases of

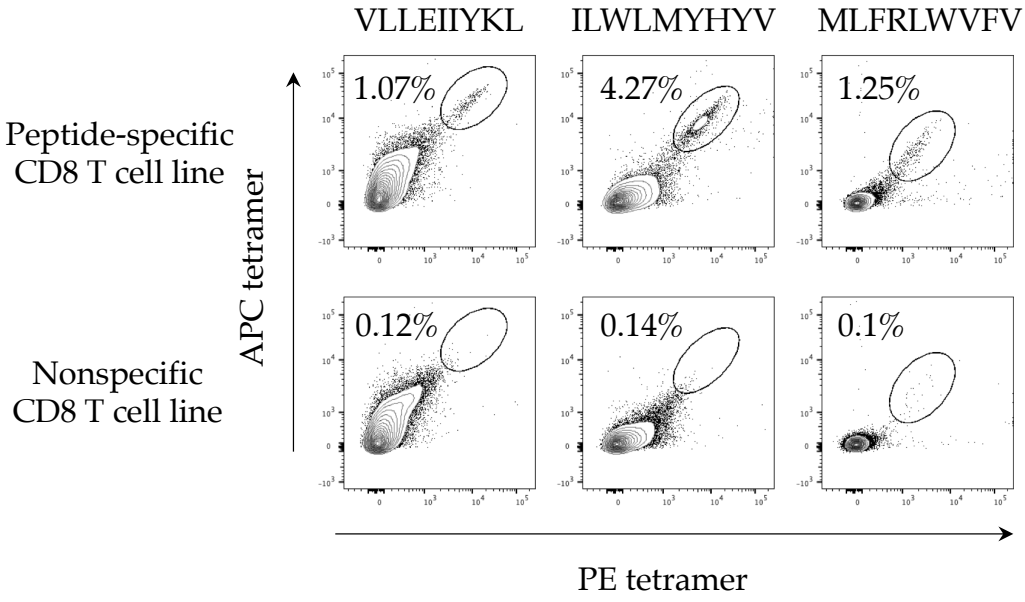

Figure A2.2. Tetramer staining for T cells specific for selected epitopes. CD8 T cell lines were raised against peptide pools and stained with tetramers specific for peptides contained within the pools against which the lines were raised (following gating on Live/$Dead^-CD8^+CD4^-$ cells). Staining was also performed using a CD8 T cell line raised against a different peptide pool (nonspecific CD8 T cell line) as a negative control. Monomers were tetramerized with both streptavidin-PE and streptavidin-APC to allow for more sensitive detection of epitope-specific responses.

HHV-6 infection shown in Table A2.4. In addition, we performed tetramer studies by refolding peptides with MHC-I subunits and found these reagents to be suitable for identification of HHV-6B T cell responses (Figure A2.2).

Table A2.1. HHV-6B-derived peptides and IC_{50} values

Core epitope	Parent protein	Gene name	IC_{50} (nM)*
ILISEIAFL	>gi|19263428|ref|NP_597817.1|G-protein_coupled_receptor_fragment	B3	314.9
FLYAFYGKV	>gi|9633148|ref|NP_050258.1|hypothetical_protein_HhV6Bgp083	B7	224.1
FLLKWVRTL	>gi|9633158|ref|NP_050268.1|hypothetical_protein_HhV6Bgp093	B8	617.4
LLPLGLITL	>gi|9633070|ref|NP_050176.1|putative_DNA-directed_RNA_polymerase_II	DR1	148.9
YLLSHSVSL	>gi|9633070|ref|NP_050176.1|putative_DNA-directed_RNA_polymerase_II	DR1	107.2
VLDGGAWRV	>gi|9633074|ref|NP_050177.1|hypothetical_protein_HhV6Bgp002	DR3	217
RLASQILSL	>gi|9633161|ref|NP_050271.1|spliced_envelope_glycoprotein	U100	1010
YLVTSINKL	>gi|9633084|ref|NP_050192.1|antigenic_virion_protein	U11	785.9
SLMSGVEPL	>gi|9633084|ref|NP_050192.1|antigenic_virion_protein	U11	341.8
ILWLMYHYV	>gi|9633084|ref|NP_050192.1|antigenic_virion_protein	U11	320.6
VLLEIIYKL	>gi|9633170|ref|NP_050196.1|hypothetical_protein_HhV6Bgp021	U12	354.4
SMLAIIATI	>gi|9633171|ref|NP_050193.1|G-protein_coupled_receptor	U12	181.7
NLWKFATIV	>gi|9633092|ref|NP_050197.1|transcription_regulator	U12	314.9
CLTKTLVFV	>gi|9633092|ref|NP_050197.1|transcription_regulator	U12	1120
LLYPKTMFV	>gi|9633092|ref|NP_050197.1|transcription_regulator	U12	4193
FLLSSTGQV	>gi|9633088|ref|NP_050199.1|immediate-early_protein_4	U12	196.8
KLFEICIFA	>gi|9633086|ref|NP_050195.1|hypothetical_protein_HhV6Bgp020	U12	371.3
FLAMGVRKL	>gi|9633172|ref|NP_050184.1|transactivator	U2	472.9
VLMDQVGRV	>gi|9633172|ref|NP_050184.1|transactivator	U2	257.6
HLWTMQLPV	>gi|9633172|ref|NP_050184.1|transactivator	U2	132.4
TLAEGIGKL	>gi|9633089|ref|NP_050200.1|glycoprotein	U20	204.3
FLARNTTYV	>gi|9633089|ref|NP_050200.1|glycoprotein	U20	541.9
RLHAGLQYV	>gi|9633089|ref|NP_050200.1|glycoprotein	U20	632.6
FLVFRCFQV	>gi|9633090|ref|NP_050201.1|putative_membrane_glycoprotein	U21	5668
VLAGLLWIL	>gi|9633090|ref|NP_050201.1|putative_membrane_glycoprotein	U21	143.5
DLILKIASL	>gi|9633090|ref|NP_050201.1|putative_membrane_glycoprotein	U21	NB
FLPRYERFV	>gi|9633093|ref|NP_050202.1|glycoprotein	U22	1084
FLSSLVIWI	>gi|9633169|ref|NP_050203.1|glycoprotein	U23	330.8
SLLDVVFIV	>gi|9633096|ref|NP_050206.1|hypothetical_protein_HhV6Bgp025	U25	267.9
KLPSFLSAV	>gi|9633097|ref|NP_050207.1|hypothetical_protein_HhV6Bgp033	U26	217.1
FLSDTEHFL	>gi|9633098|ref|NP_050208.1|Polymerase_processivity_factor	U27	176
MMCEHIYYT	>gi|9633099|ref|NP_050209.1|large_ribonuclease_reductase	U28	172.8
LLYKTGFKV	>gi|9633099|ref|NP_050209.1|large_ribonuclease_reductase	U28	790.2
ELTEEIDFV	>gi|9633099|ref|NP_050209.1|large_ribonuclease_reductase	U28	2433
LLAPELENL	>gi|9633100|ref|NP_050210.1|capsid_assembly_and_DNA_maturation	U29	201.3
FLCSNAFNV	>gi|9633100|ref|NP_050210.1|capsid_assembly_and_DNA_maturation	U29	235.8
DLSEKKVFV	>gi|9633100|ref|NP_050210.1|capsid_assembly_and_DNA_maturation	U29	1755

KLQYGIYVV	>gi|9633100|ref|NP_050210.1|capsid_assembly_and_DNA_maturation	U29	239.2
FLKGDIVVL	>gi|9633078|ref|NP_050185.1|transactivator	U3	209.9
QLVSSLQFV	>gi|9633078|ref|NP_050185.1|transactivator	U3	535.4
ALQKFIDTV	>gi|9633101|ref|NP_050211.1|capsid_assembly_protein	U30	717.8
WLYAFSINV	>gi|9633101|ref|NP_050211.1|capsid_assembly_protein	U30	184.5
FLFFTASTV	>gi|9633101|ref|NP_050211.1|capsid_assembly_protein	U30	342.9
NLFEKWGDV	>gi|9633101|ref|NP_050211.1|capsid_assembly_protein	U30	528.6
KLYSWFLHI	>gi|9633101|ref|NP_050211.1|capsid_assembly_protein	U30	213.6
STIEFVYMV	>gi|9633101|ref|NP_050211.1|capsid_assembly_protein	U30	110.4
LLNAYTDYL	>gi|9633101|ref|NP_050211.1|capsid_assembly_protein	U30	123.2
MLLNIITSV	>gi|9633101|ref|NP_050211.1|capsid_assembly_protein	U30	NB
YLVNLYFNI	>gi|9633102|ref|NP_050212.1|large_tegument_protein	U31	757.2
ALFESVLTL	>gi|9633102|ref|NP_050212.1|large_tegument_protein	U31	136.8
FLWNRVFHL	>gi|9633102|ref|NP_050212.1|large_tegument_protein	U31	311.5
KLYDNTQFL	>gi|9633102|ref|NP_050212.1|large_tegument_protein	U31	370.9
SQFNWTIYL	>gi|9633102|ref|NP_050212.1|large_tegument_protein	U31	3653
FLFEQQLLL	>gi|9633104|ref|NP_050214.1|capsid_protein	U33	216.5
LLRQLLAPL	>gi|9633104|ref|NP_050214.1|capsid_protein	U33	1135
GLFVLLAYL	>gi|9633104|ref|NP_050214.1|capsid_protein	U33	NB
GLATSVISL	>gi|9633104|ref|NP_050214.1|capsid_protein	U33	210.8
VLLAYLYFV	>gi|9633104|ref|NP_050214.1|capsid_protein	U33	5293
YLLSLWEHV	>gi|9633105|ref|NP_050215.1|putative_virion_protein	U34	272.7
LLALYFCYV	>gi|9633105|ref|NP_050215.1|putative_virion_protein	U34	647.8
KMYDELLSA	>gi|9633105|ref|NP_050215.1|putative_virion_protein	U34	188.8
KMIDRVQFV	>gi|9633107|ref|NP_050217.1|virion_protein	U36	569.3
MLCSTVDYV	>gi|9633109|ref|NP_050219.1|DNA_polymerase	U38	288.8
FLSFGWYNV	>gi|9633109|ref|NP_050219.1|DNA_polymerase	U38	181.7
VLYLDMYPV	>gi|9633109|ref|NP_050219.1|DNA_polymerase	U38	107.2
ELAEDPNYV	>gi|9633109|ref|NP_050219.1|DNA_polymerase	U38	1607
YLDETFSAI	>gi|9633109|ref|NP_050219.1|DNA_polymerase	U38	223.8
KQINYHYEV	>gi|9633109|ref|NP_050219.1|DNA_polymerase	U38	345
KMSEGFFII	>gi|9633110|ref|NP_050220.1|Glycoprotein_B	U39	159.8
RLLELLDSL	>gi|9633079|ref|NP_050186.1|hypothetical_protein_HhV6Bgp009	U4	257.8
VLEGFLNTL	>gi|9633079|ref|NP_050186.1|hypothetical_protein_HhV6Bgp009	U4	307.4
SLINKVVSV	>gi|9633111|ref|NP_050221.1|transport/capsid_assembly	U40	4628
QLISKINSV	>gi|9633111|ref|NP_050221.1|transport/capsid_assembly	U40	982.7
RLIDLVTGL	>gi|9633111|ref|NP_050221.1|transport/capsid_assembly	U40	460.9
RLYVGSIYV	>gi|9633111|ref|NP_050221.1|transport/capsid_assembly	U40	539
SLHGLTSKL	>gi|9633112|ref|NP_050222.1|major_DNA_binding_protein	U41	650.8

SLMERNSPV	>gi|9633112|ref|NP_050222.1|major_DNA_binding_protein	U41	532.1
FLTFAYYKV	>gi|9633112|ref|NP_050222.1|major_DNA_binding_protein	U41	248.2
SIQEYLVYV	>gi|9633112|ref|NP_050222.1|major_DNA_binding_protein	U41	184.5
DLYKSGKYV	>gi|9633112|ref|NP_050222.1|major_DNA_binding_protein	U41	NB
FLMLVDSVV	>gi|9633112|ref|NP_050222.1|major_DNA_binding_protein	U41	151.3
LLSYVVWNL	>gi|9633112|ref|NP_050222.1|major_DNA_binding_protein	U41	770.9
CLAFTVATV	>gi|9633113|ref|NP_050223.1|transactivator	U42	342.9
LMGDRIFSL	>gi|9633113|ref|NP_050223.1|transactivator	U42	154.2
SLWLFYILV	>gi|9633117|ref|NP_050227.1|putative_membrane_/secreted_protein	U46	212.6
YVSLWLFYI	>gi|9633117|ref|NP_050227.1|putative_membrane_/secreted_protein	U46	3201
MLFRLWVFV	>gi|9633119|ref|NP_050229.1|glycoprotein_H	U48	103.1
NLLSIDSFV	>gi|9633119|ref|NP_050229.1|glycoprotein_H	U48	369.1
SLNELIFPV	>gi|9633119|ref|NP_050229.1|glycoprotein_H	U48	112.6
YLRSGLVAI	>gi|9633121|ref|NP_050231.1|viron_protein	U50	1290
LLLGTIAHL	>gi|9633122|ref|NP_050232.1|G-protein_coupled_receptor	U51	168
FMALPVLKV	>gi|9633122|ref|NP_050232.1|G-protein_coupled_receptor	U51	237.4
WLMLVYSVV	>gi|9633122|ref|NP_050232.1|G-protein_coupled_receptor	U51	376.3
ALAKVCFPI	>gi|9633122|ref|NP_050232.1|G-protein_coupled_receptor	U51	439.8
FMDEFGLSL	>gi|9633123|ref|NP_050233.1|hypothetical_protein_HhV6Bgp058	U52	155.3
LLCGNLLIL	>gi|9633125|ref|NP_050235.1|virion_transactivator	U54	1165
YLFNADIWI	>gi|9633125|ref|NP_050235.1|virion_transactivator	U54	202.1
KLYPFLWFA	>gi|9633126|ref|NP_050236.1|hypothetical_protein_HhV6Bgp062	U55	229.2
FLTIFLRNV	>gi|9633126|ref|NP_050236.1|hypothetical_protein_HhV6Bgp062	U55	441.2
FLWFAQEPL	>gi|9633126|ref|NP_050236.1|hypothetical_protein_HhV6Bgp062	U55	101.1
LLCIGLIAV	>gi|9633127|ref|NP_050237.1|capsid_protein	U56	384.1
KLGDWELTV	>gi|9633127|ref|NP_050237.1|capsid_protein	U56	192.1
VLLGPIGSI	>gi|9633128|ref|NP_050238.1|major_capsid_protein	U57	348.8
CLISPITTL	>gi|9633128|ref|NP_050238.1|major_capsid_protein	U57	559.9
NLYESRQEV	>gi|9633128|ref|NP_050238.1|major_capsid_protein	U57	682.7
LQLTFFFPL	>gi|9633128|ref|NP_050238.1|major_capsid_protein	U57	374.9
YLEYYPYFL	>gi|9633129|ref|NP_050239.1|hypothetical_protein_HhV6Bgp064	U58	178
LLLYYDYSL	>gi|9633129|ref|NP_050239.1|hypothetical_protein_HhV6Bgp064	U58	138.9
VLLQELNNV	>gi|9633129|ref|NP_050239.1|hypothetical_protein_HhV6Bgp064	U58	1061
KLLEYLAET	>gi|9633129|ref|NP_050239.1|hypothetical_protein_HhV6Bgp064	U58	248.2
YLAETSTAI	>gi|9633129|ref|NP_050239.1|hypothetical_protein_HhV6Bgp064	U58	695.7
FVYGKTLYV	>gi|9633129|ref|NP_050239.1|hypothetical_protein_HhV6Bgp064	U58	370.1
TLPDTLLSV	>gi|9633130|ref|NP_050240.1|hypothetical_protein_HhV6Bgp065	U59	212.6
YLRDIGSRV	>gi|9633133|ref|NP_050244.1|tegument_protein	U64	2871
FLLKNIEGI	>gi|9633135|ref|NP_050241.1|Putative_terminase	U66	140.9

DLECLLWLV	>gi|9633136|ref|NP_050246.1|hypothetical_protein_HhV6Bgp071	U67	NB
VLAEHVVLL	>gi|9633138|ref|NP_050248.1|Phosphotransferase	U69	342.3
FLTNIVFIV	>gi|9633091|ref|NP_050187.1|hypothetical_protein_HhV6Bgp013	U7	805.3
MLNGELPVL	>gi|9633091|ref|NP_050187.1|hypothetical_protein_HhV6Bgp013	U7	138
FITKFLTPV	>gi|9633091|ref|NP_050187.1|hypothetical_protein_HhV6Bgp013	U7	141.6
FLLDKLYAI	>gi|9633139|ref|NP_050249.1|Alkaline_exonuclease	U70	103.1
LLLDPSSGV	>gi|9633139|ref|NP_050249.1|Alkaline_exonuclease	U70	401
KLSVFQKAV	>gi|9633139|ref|NP_050249.1|Alkaline_exonuclease	U70	2312
ILLTTEFTV	>gi|9633140|ref|NP_050250.1|Myristylated_virion_protein	U71	465.5
LVMACIYSI	>gi|9633141|ref|NP_050251.1|glycoprotein_M	U72	603.7
LIMAILFLL	>gi|9633141|ref|NP_050251.1|glycoprotein_M	U72	NB
IMDTFQLFV	>gi|9633141|ref|NP_050251.1|glycoprotein_M	U72	153.7
MLIDLAFLA	>gi|9633142|ref|NP_050252.1|origin_binding_protein	U73	2139
FLCDEYFVL	>gi|9633142|ref|NP_050252.1|origin_binding_protein	U73	97.92
FLSFLQILV	>gi|9633142|ref|NP_050252.1|origin_binding_protein	U73	922.1
FLHEKIFAV	>gi|9633143|ref|NP_050253.1|helicase/primase_complex	U74	192.5
MLYEHIHLL	>gi|9633143|ref|NP_050253.1|helicase/primase_complex	U74	1061
WLLVRDLHV	>gi|9633143|ref|NP_050253.1|helicase/primase_complex	U74	579.8
VLFPVLSPV	>gi|9633144|ref|NP_050254.1|hypothetical_protein_HhV6Bgp080	U75	320.6
SLIKFLLNL	>gi|9633145|ref|NP_050255.1|putative_viron_protein	U76	4481
FIQEITPSI	>gi|9633145|ref|NP_050255.1|putative_viron_protein	U76	220
LIVDKVASL	>gi|9633146|ref|NP_050256.1|Helicase/primase_complex	U77	798.8
ILRHILHTV	>gi|9633146|ref|NP_050256.1|Helicase/primase_complex	U77	601.6
KLKERLDYV	>gi|9633149|ref|NP_050259.1|DNA_replication	U79	354.4
VLYFRYFIV	>gi|9633081|ref|NP_050189.1|hypothetical_protein_HhV6Bgp012	U8	292.6
SLDDVERFV	>gi|9633081|ref|NP_050189.1|hypothetical_protein_HhV6Bgp012	U8	545.5
LLLNSIFTV	>gi|9633150|ref|NP_050260.1|Uracyl-DNA_glycosylase	U81	303.7
YLPERITYV	>gi|9633151|ref|NP_050261.1|Glycoprotein_L	U82	71.4
KLDDCIAAV	>gi|9633151|ref|NP_050261.1|Glycoprotein_L	U82	693.6
SLELGLSKL	>gi|9633152|ref|NP_050262.1|Intercrine_cytokine	U83	6383
ILACLIVLI	>gi|9633157|ref|NP_050267.1|probable_membrane_glycoprotein	U91	7637
VLLCENKWV	>gi|9633160|ref|NP_050270.1|immediate-early_protein_IE2	U95	973.2

*NB denotes nonbinding peptide

Table A2.2 Summary of HLA-A2 binding data

Binding scale (nM)	Relative binding	Number of peptides	Mean IC_{50} (nM)
<=50	High	0	
>50 <=1000	Medium	45	336
>1000 <=7500	Low	10	2778
>7500	Borderline	1	7637

Table A2.3. Summary of responses and IC_{50} values

Parameter	Mean IC_{50} (nM)
Positive response	979
Negative response	265
Observed in >50% of donors	434
Observed in >75% of donors	302
Observed in >85% of donors	110

Table A2.4. Summary of early and late gene-derived epitope responses

	E*	L*
Number of peptides tested	12	35
Positive response	10	31
Negative response	2	4
Observed in >50% of donors	5	11
Observed in >75% of donors	1	5
Observed in >85% of donors	0	1

*E and L denote whether peptides were derived from early or late genes.

Discussion

An understanding of the precise mechanism(s) by which HHV-6 evades detection by the immune system will aid in development of targeted therapies to treat HHV-6 infection. Here, we have evaluated putative HLA-A2-restricted epitopes derived from the HHV-6B genome. We have assessed epitope binding capacity, performed in vitro epitope mapping studies, and generated tetramers for epitopes that reproducibly elicited substantial responses. Results from these studies may aid in design of therapies to treat HHV-6 reactivation.

Materials and Methods

HLA-A2 binding assay

Binding was assessed using epitope-linked β2m (ELBM) as previously described (Appendix I). Briefly, 0.25 μM ELBM was incubated with 0.01 unit/μl thrombin (MP Biomedicals, Santa Ana, CA) and 25 nM Alexa488-RT(cys), and competitor peptides (synthesized by 21st Century Biochemicals, Marlborough, MA) were diluted two-fold, from 2 μM to 31.25 nM, and added to determine IC_{50} values. Following 16 h incubation at room temperature (RT), fluorescence polarization (FP) was measured as millipolarization (mP) units in a VICTOR X5 plate reader (Perkin Elmer, Waltham, MA) at 495 excitation and 520 emission.

In vitro generation of DCs

The CD14 Microbead Kit (Miltenyi Biotec, Auburn, CA) was used to isolate $CD14^+$ monocytes from PBMCs of healthy donors according to the manufacturer's instructions. $2x10^6$ monocytes/well in 12-well plates were cultured at 37° C 5% CO_2 in RPMI 1640 (Thermo Fisher Scientific, Waltham, MA) containing Glutamax and 1% penicillin-streptomycin (Thermo Fisher Scientific) and 10% FBS, as well as 1000 U/ml recombinant human GM-CSF and 40 ng/ml recombinant human IL-4 (both from Peprotech, Rocky Hill, NJ). On day 3, additional medium was added, and on day 5, nonadherent cells were collected, centrifuged, and stimulated for 24h in medium containing 100 ng/ml LPS (Sigma Aldrich, St. Louis, MO).

Generation of CD8 T cell lines

$CD8^+$ T cells were isolated from PBMCs of HLA-A2-positive donors using the $CD8^+$ T cell Isolation Kit (Miltenyi Biotec, Auburn, CA). DCs generated as above were pulsed with peptide pools (5 μg/ml each peptide), and 10^6 CD8 T cells and $2.5x10^5$ peptide-pulsed DCs were co-cultured at 37° C 5% CO_2 in 24-well plates in AIM-V medium (Thermo Fisher Scientific) containing 1% Glutamax, 1% penicillin-streptomycin, 50 uM 2-ME (Sigma-Adrich), 10% FBS, and 50 U/ml recombinant human IL-2 and 10 ng/ml recombinant human IL-7 (both from Peprotech). After 7 days, $2x10^5$ peptide-pulsed and irradiated T2-A2 cells (ATCC, Manassas, VA) were added to cultures, and this was repeated on days 14 and 21. ELISPOT assays for human IFN-γ were performed using $5x10^4$ peptide-pulsed T2-A2 cells with 10^5 CD8 T cells per well according to the manufacturer's instructions (BD Biosciences, San Jose, CA).

Statistical analysis of T cell responses

The DFR server (http://www.scharp.org/zoe/runDFR/) was used to perform statistical analysis of data obtained in ELISPOT assays, using the distribution-free resampling method[475]. The algorithm reports statistical significances at "1X" (onefold difference between background and experimental wells) and "2X" (twofold difference between background and experimental means). In addition, we also assessed responses that fit the "2X" criteria with delta responses demonstrating >25 specific spots. Responses to these peptides are denoted "strong positives".

Tetramer staining

HLA-A2 monomers were generated as previously described[476]. Tetramerization was performed using fluorescently-labeled streptavidin (Prozyme, Hayward, CA) at 10-minute intervals. CD8 T cell lines raised against peptide pools as above were blocked with 10 μg/ml human IgG (Sigma Aldrich), followed by staining with anti-human CD8 and anti-human CD4 (both from BD Biosciences), as well as with Live/Dead Violet (Thermo Fisher Scientific). Cells were then incubated with tetramers (200 nM of monomer) at 4° C for 1 h. Cell acquisition was performed on an LSR II flow cytometer (Becton Dickinson, Franklin Lakes, NJ), and data were analyzed using FlowJo version 10.5.3 software (Tree Star, Ashland, OR).

References

1 Yin, L. & Stern, L. J. A novel method to measure HLA-DM-susceptibility of peptides bound to MHC class II molecules based on peptide binding competition assay and differential IC(50) determination. *J Immunol Methods* **406**, 21-33, doi:10.1016/j.jim.2014.02.008 (2014).

2 Clement, C. C. *et al.* The Dendritic Cell Major Histocompatibility Complex II (MHC II) Peptidome Derives from a Variety of Processing Pathways and Includes Peptides with a Broad Spectrum of HLA-DM Sensitivity. *J Biol Chem* **291**, 5576-5595, doi:10.1074/jbc.M115.655738 (2016).

3 Denzin, L. K., Robbins, N. F., Carboy-Newcomb, C. & Cresswell, P. Assembly and intracellular transport of HLA-DM and correction of the class II antigen-processing defect in T2 cells. *Immunity* **1**, 595-606 (1994).

4 Yin, L. *et al.* Susceptibility to HLA-DM protein is determined by a dynamic conformation of major histocompatibility complex class II molecule bound with peptide. *J Biol Chem* **289**, 23449-23464, doi:10.1074/jbc.M114.585539 (2014).

5 Mellins, E. D. & Stern, L. J. HLA-DM and HLA-DO, key regulators of MHC-II processing and presentation. *Curr Opin Immunol* **26**, 115-122, doi:10.1016/j.coi.2013.11.005 (2014).

6 Reith, W., LeibundGut-Landmann, S. & Waldburger, J. M. Regulation of MHC class II gene expression by the class II transactivator. *Nat Rev Immunol* **5**, 793-806, doi:10.1038/nri1708 (2005).

7 Masternak, K. *et al.* CIITA is a transcriptional coactivator that is recruited to MHC class II promoters by multiple synergistic interactions with an enhanceosome complex. *Genes Dev* **14**, 1156-1166 (2000).

8 Elliott, E. A. *et al.* The invariant chain is required for intracellular transport and function of major histocompatibility complex class II molecules. *J Exp Med* **179**, 681-694 (1994).

9 Roche, P. A. & Cresswell, P. Invariant chain association with HLA-DR molecules inhibits immunogenic peptide binding. *Nature* **345**, 615-618, doi:10.1038/345615a0 (1990).

10 Cresswell, P. Invariant chain structure and MHC class II function. *Cell* **84**, 505-507 (1996).

11 Pieters, J., Bakke, O. & Dobberstein, B. The MHC class II-associated invariant chain contains two endosomal targeting signals within its cytoplasmic tail. *J Cell Sci* **106 (Pt 3)**, 831-846 (1993).

12 Lotteau, V. *et al.* Intracellular transport of class II MHC molecules directed by invariant chain. *Nature* **348**, 600-605, doi:10.1038/348600a0 (1990).

13 Riese, R. J. *et al.* Essential role for cathepsin S in MHC class II-associated invariant chain processing and peptide loading. *Immunity* **4**, 357-366 (1996).

14 Riese, R. J. *et al.* Cathepsin S activity regulates antigen presentation and immunity. *J Clin Invest* **101**, 2351-2363, doi:10.1172/JCI1158 (1998).

15 Blum, J. S., Wearsch, P. A. & Cresswell, P. Pathways of antigen processing. *Annu Rev Immunol* **31**, 443-473, doi:10.1146/annurev-immunol-032712-095910 (2013).
16 Villadangos, J. A. *et al.* Proteases involved in MHC class II antigen presentation. *Immunol Rev* **172**, 109-120 (1999).
17 van Kasteren, S. I. & Overkleeft, H. S. Endo-lysosomal proteases in antigen presentation. *Curr Opin Chem Biol* **23**, 8-15, doi:10.1016/j.cbpa.2014.08.011 (2014).
18 Villadangos, J. A. & Ploegh, H. L. Proteolysis in MHC class II antigen presentation: who's in charge? *Immunity* **12**, 233-239 (2000).
19 Hsieh, C. S., deRoos, P., Honey, K., Beers, C. & Rudensky, A. Y. A role for cathepsin L and cathepsin S in peptide generation for MHC class II presentation. *J Immunol* **168**, 2618-2625 (2002).
20 Pos, W. *et al.* Crystal structure of the HLA-DM-HLA-DR1 complex defines mechanisms for rapid peptide selection. *Cell* **151**, 1557-1568, doi:10.1016/j.cell.2012.11.025 (2012).
21 Vogt, A. B., Kropshofer, H., Moldenhauer, G. & Hammerling, G. J. Kinetic analysis of peptide loading onto HLA-DR molecules mediated by HLA-DM. *Proc Natl Acad Sci U S A* **93**, 9724-9729 (1996).
22 Sloan, V. S. *et al.* Mediation by HLA-DM of dissociation of peptides from HLA-DR. *Nature* **375**, 802-806, doi:10.1038/375802a0 (1995).
23 Weber, D. A., Evavold, B. D. & Jensen, P. E. Enhanced dissociation of HLA-DR-bound peptides in the presence of HLA-DM. *Science* **274**, 618-620 (1996).
24 Kropshofer, H. *et al.* Editing of the HLA-DR-peptide repertoire by HLA-DM. *EMBO J* **15**, 6144-6154 (1996).
25 Painter, C. A. *et al.* Conformational lability in the class II MHC 310 helix and adjacent extended strand dictate HLA-DM susceptibility and peptide exchange. *Proc Natl Acad Sci U S A* **108**, 19329-19334, doi:10.1073/pnas.1108074108 (2011).
26 Anders, A. K. *et al.* HLA-DM captures partially empty HLA-DR molecules for catalyzed removal of peptide. *Nat Immunol* **12**, 54-61, doi:10.1038/ni.1967 (2011).
27 Narayan, K., Su, K. W., Chou, C. L., Khoruzhenko, S. & Sadegh-Nasseri, S. HLA-DM mediates peptide exchange by interacting transiently and repeatedly with HLA-DR1. *Molecular immunology* **46**, 3157-3162, doi:10.1016/j.molimm.2009.07.001 (2009).
28 Zarutskie, J. A. *et al.* The kinetic basis of peptide exchange catalysis by HLA-DM. *Proc Natl Acad Sci U S A* **98**, 12450-12455, doi:10.1073/pnas.211439398 (2001).
29 Alvaro-Benito, M., Morrison, E., Abualrous, E. T., Kuropka, B. & Freund, C. Quantification of HLA-DM-Dependent Major Histocompatibility Complex of Class II Immunopeptidomes by the Peptide Landscape Antigenic Epitope Alignment Utility. *Front Immunol* **9**, 872, doi:10.3389/fimmu.2018.00872 (2018).

30 Zhou, Z. *et al.* Peptidomic analysis of type 1 diabetes associated HLA-DQ molecules and the impact of HLA-DM on peptide repertoire editing. *Eur J Immunol* **47**, 314-326, doi:10.1002/eji.201646656 (2017).
31 Busch, R. *et al.* On the perils of poor editing: regulation of peptide loading by HLA-DQ and H2-A molecules associated with celiac disease and type 1 diabetes. *Expert reviews in molecular medicine* **14**, e15, doi:10.1017/erm.2012.9 (2012).
32 Guce, A. I. *et al.* HLA-DO acts as a substrate mimic to inhibit HLA-DM by a competitive mechanism. *Nat Struct Mol Biol* **20**, 90-98, doi:10.1038/nsmb.2460 (2013).
33 Yoon, T. *et al.* Mapping the HLA-DO/HLA-DM complex by FRET and mutagenesis. *Proc Natl Acad Sci U S A* **109**, 11276-11281, doi:10.1073/pnas.1113966109 (2012).
34 Xiu, F. *et al.* Cutting edge: HLA-DO impairs the incorporation of HLA-DM into exosomes. *J Immunol* **187**, 1547-1551, doi:10.4049/jimmunol.1100199 (2011).
35 Deshaies, F. *et al.* A point mutation in the groove of HLA-DO allows egress from the endoplasmic reticulum independent of HLA-DM. *Proc Natl Acad Sci U S A* **102**, 6443-6448, doi:10.1073/pnas.0500853102 (2005).
36 Kropshofer, H. *et al.* A role for HLA-DO as a co-chaperone of HLA-DM in peptide loading of MHC class II molecules. *EMBO J* **17**, 2971-2981, doi:10.1093/emboj/17.11.2971 (1998).
37 Denzin, L. K., Sant'Angelo, D. B., Hammond, C., Surman, M. J. & Cresswell, P. Negative regulation by HLA-DO of MHC class II-restricted antigen processing. *Science* **278**, 106-109 (1997).
38 Mommen, G. P. *et al.* Sampling From the Proteome to the Human Leukocyte Antigen-DR (HLA-DR) Ligandome Proceeds Via High Specificity. *Mol Cell Proteomics* **15**, 1412-1423, doi:10.1074/mcp.M115.055780 (2016).
39 Bergseng, E. *et al.* Different binding motifs of the celiac disease-associated HLA molecules DQ2.5, DQ2.2, and DQ7.5 revealed by relative quantitative proteomics of endogenous peptide repertoires. *Immunogenetics* **67**, 73-84, doi:10.1007/s00251-014-0819-9 (2015).
40 Sofron, A., Ritz, D., Neri, D. & Fugmann, T. High-resolution analysis of the murine MHC class II immunopeptidome. *Eur J Immunol* **46**, 319-328, doi:10.1002/eji.201545930 (2016).
41 Strug, I. *et al.* Vaccinia peptides eluted from HLA-DR1 isolated from virus-infected cells are recognized by CD4+ T cells from a vaccinated donor. *J Proteome Res* **7**, 2703-2711, doi:10.1021/pr700780x (2008).
42 Draheim, M. *et al.* Profiling MHC II immunopeptidome of blood-stage malaria reveals that cDC1 control the functionality of parasite-specific CD4 T cells. *EMBO Mol Med* **9**, 1605-1621, doi:10.15252/emmm.201708123 (2017).
43 Fugmann, T., Sofron, A., Ritz, D., Bootz, F. & Neri, D. The MHC Class II Immunopeptidome of Lymph Nodes in Health and in Chemically Induced

Colitis. *J Immunol* **198**, 1357-1364, doi:10.4049/jimmunol.1601157 (2017).
44 Schellens, I. M. *et al.* Comprehensive Analysis of the Naturally Processed Peptide Repertoire: Differences between HLA-A and B in the Immunopeptidome. *PLoS One* **10**, e0136417, doi:10.1371/journal.pone.0136417 (2015).
45 West, M. A., Prescott, A. R., Eskelinen, E. L., Ridley, A. J. & Watts, C. Rac is required for constitutive macropinocytosis by dendritic cells but does not control its downregulation. *Curr Biol* **10**, 839-848 (2000).
46 Sallusto, F., Cella, M., Danieli, C. & Lanzavecchia, A. Dendritic cells use macropinocytosis and the mannose receptor to concentrate macromolecules in the major histocompatibility complex class II compartment: downregulation by cytokines and bacterial products. *J Exp Med* **182**, 389-400 (1995).
47 Steinman, R. M., Brodie, S. E. & Cohn, Z. A. Membrane flow during pinocytosis. A stereologic analysis. *J Cell Biol* **68**, 665-687 (1976).
48 Savina, A. & Amigorena, S. Phagocytosis and antigen presentation in dendritic cells. *Immunol Rev* **219**, 143-156, doi:10.1111/j.1600-065X.2007.00552.x (2007).
49 Allavena, P., Chieppa, M., Monti, P. & Piemonti, L. From pattern recognition receptor to regulator of homeostasis: the double-faced macrophage mannose receptor. *Crit Rev Immunol* **24**, 179-192 (2004).
50 Linehan, S. A., Martinez-Pomares, L., Stahl, P. D. & Gordon, S. Mannose receptor and its putative ligands in normal murine lymphoid and nonlymphoid organs: In situ expression of mannose receptor by selected macrophages, endothelial cells, perivascular microglia, and mesangial cells, but not dendritic cells. *J Exp Med* **189**, 1961-1972 (1999).
51 Jiang, W. *et al.* The receptor DEC-205 expressed by dendritic cells and thymic epithelial cells is involved in antigen processing. *Nature* **375**, 151-155, doi:10.1038/375151a0 (1995).
52 Guilliams, M., Bruhns, P., Saeys, Y., Hammad, H. & Lambrecht, B. N. The function of Fcgamma receptors in dendritic cells and macrophages. *Nat Rev Immunol* **14**, 94-108, doi:10.1038/nri3582 (2014).
53 Underhill, D. M. & Goodridge, H. S. Information processing during phagocytosis. *Nat Rev Immunol* **12**, 492-502, doi:10.1038/nri3244 (2012).
54 Flannagan, R. S., Jaumouille, V. & Grinstein, S. The cell biology of phagocytosis. *Annu Rev Pathol* **7**, 61-98, doi:10.1146/annurev-pathol-011811-132445 (2012).
55 Savina, A. *et al.* The small GTPase Rac2 controls phagosomal alkalinization and antigen crosspresentation selectively in CD8(+) dendritic cells. *Immunity* **30**, 544-555, doi:10.1016/j.immuni.2009.01.013 (2009).
56 Rock, K. L., Benacerraf, B. & Abbas, A. K. Antigen presentation by hapten-specific B lymphocytes. I. Role of surface immunoglobulin receptors. *J Exp Med* **160**, 1102-1113 (1984).
57 Lanzavecchia, A. Antigen-specific interaction between T and B cells. *Nature* **314**, 537-539 (1985).

58 Adler, L. N. *et al.* The Other Function: Class II-Restricted Antigen Presentation by B Cells. *Front Immunol* **8**, 319, doi:10.3389/fimmu.2017.00319 (2017).
59 Roche, P. A. & Furuta, K. The ins and outs of MHC class II-mediated antigen processing and presentation. *Nat Rev Immunol* **15**, 203-216, doi:10.1038/nri3818 (2015).
60 Malhotra, S., Kovats, S., Zhang, W. & Coggeshall, K. M. B cell antigen receptor endocytosis and antigen presentation to T cells require Vav and dynamin. *J Biol Chem* **284**, 24088-24097, doi:10.1074/jbc.M109.014209 (2009).
61 Klionsky, D. J. Autophagy: from phenomenology to molecular understanding in less than a decade. *Nat Rev Mol Cell Biol* **8**, 931-937, doi:10.1038/nrm2245 (2007).
62 Takeshige, K., Baba, M., Tsuboi, S., Noda, T. & Ohsumi, Y. Autophagy in yeast demonstrated with proteinase-deficient mutants and conditions for its induction. *J Cell Biol* **119**, 301-311 (1992).
63 Levine, B. & Klionsky, D. J. Development by self-digestion: molecular mechanisms and biological functions of autophagy. *Dev Cell* **6**, 463-477 (2004).
64 Brazil, M. I., Weiss, S. & Stockinger, B. Excessive degradation of intracellular protein in macrophages prevents presentation in the context of major histocompatibility complex class II molecules. *Eur J Immunol* **27**, 1506-1514, doi:10.1002/eji.1830270629 (1997).
65 Dengjel, J. *et al.* Autophagy promotes MHC class II presentation of peptides from intracellular source proteins. *Proc Natl Acad Sci U S A* **102**, 7922-7927, doi:10.1073/pnas.0501190102 (2005).
66 Crotzer, V. L. & Blum, J. S. Autophagy and its role in MHC-mediated antigen presentation. *J Immunol* **182**, 3335-3341, doi:10.4049/jimmunol.0803458 (2009).
67 Veerappan Ganesan, A. P. & Eisenlohr, L. C. The elucidation of non-classical MHC class II antigen processing through the study of viral antigens. *Curr Opin Virol* **22**, 71-76, doi:10.1016/j.coviro.2016.11.009 (2017).
68 Kaushik, S. & Cuervo, A. M. The coming of age of chaperone-mediated autophagy. *Nat Rev Mol Cell Biol* **19**, 365-381, doi:10.1038/s41580-018-0001-6 (2018).
69 Schmid, D., Pypaert, M. & Munz, C. Antigen-loading compartments for major histocompatibility complex class II molecules continuously receive input from autophagosomes. *Immunity* **26**, 79-92, doi:10.1016/j.immuni.2006.10.018 (2007).
70 Zhou, D. *et al.* Lamp-2a facilitates MHC class II presentation of cytoplasmic antigens. *Immunity* **22**, 571-581, doi:10.1016/j.immuni.2005.03.009 (2005).
71 Ireland, J. M. & Unanue, E. R. Autophagy in antigen-presenting cells results in presentation of citrullinated peptides to CD4 T cells. *J Exp Med* **208**, 2625-2632, doi:10.1084/jem.20110640 (2011).

72 Wu, C., Aichinger, M., Nedjic, J. & Klein, L. Thymic epithelial cells use macroautophagy to turn their inside out for CD4 T cell tolerance. *Autophagy* **9**, 931-932, doi:10.4161/auto.24374 (2013).
73 Nedjic, J., Aichinger, M., Emmerich, J., Mizushima, N. & Klein, L. Autophagy in thymic epithelium shapes the T-cell repertoire and is essential for tolerance. *Nature* **455**, 396-400, doi:10.1038/nature07208 (2008).
74 Liang, Z. *et al.* MTOR signaling is essential for the development of thymic epithelial cells and the induction of central immune tolerance. *Autophagy* **14**, 505-517, doi:10.1080/15548627.2017.1376161 (2018).
75 Aichinger, M., Wu, C., Nedjic, J. & Klein, L. Macroautophagy substrates are loaded onto MHC class II of medullary thymic epithelial cells for central tolerance. *J Exp Med* **210**, 287-300, doi:10.1084/jem.20122149 (2013).
76 Cone, R. E., Sprent, J. & Marchalonis, J. J. Antigen-binding specificity of isolated cell-surface immunoglobulin from thymus cells activated to histocompatibility antigens. *Proc Natl Acad Sci U S A* **69**, 2556-2560 (1972).
77 Joly, E. & Hudrisier, D. What is trogocytosis and what is its purpose? *Nat Immunol* **4**, 815, doi:10.1038/ni0903-815 (2003).
78 Nakayama, M. Antigen Presentation by MHC-Dressed Cells. *Front Immunol* **5**, 672, doi:10.3389/fimmu.2014.00672 (2014).
79 Klein, L., Hinterberger, M., Wirnsberger, G. & Kyewski, B. Antigen presentation in the thymus for positive selection and central tolerance induction. *Nat Rev Immunol* **9**, 833-844, doi:10.1038/nri2669 (2009).
80 Millet, V., Naquet, P. & Guinamard, R. R. Intercellular MHC transfer between thymic epithelial and dendritic cells. *Eur J Immunol* **38**, 1257-1263, doi:10.1002/eji.200737982 (2008).
81 Kroger, C. J., Spidale, N. A., Wang, B. & Tisch, R. Thymic Dendritic Cell Subsets Display Distinct Efficiencies and Mechanisms of Intercellular MHC Transfer. *J Immunol* **198**, 249-256, doi:10.4049/jimmunol.1601516 (2017).
82 Hwang, I. *et al.* T cells can use either T cell receptor or CD28 receptors to absorb and internalize cell surface molecules derived from antigen-presenting cells. *J Exp Med* **191**, 1137-1148 (2000).
83 Villadangos, J. A., Driessen, C., Shi, G. P., Chapman, H. A. & Ploegh, H. L. Early endosomal maturation of MHC class II molecules independently of cysteine proteases and H-2DM. *EMBO J* **19**, 882-891, doi:10.1093/emboj/19.5.882 (2000).
84 Reid, P. A. & Watts, C. Cycling of cell-surface MHC glycoproteins through primaquine-sensitive intracellular compartments. *Nature* **346**, 655-657, doi:10.1038/346655a0 (1990).
85 Li, P. *et al.* Disruption of MHC class II-restricted antigen presentation by vaccinia virus. *J Immunol* **175**, 6481-6488 (2005).
86 Pathak, S. S. & Blum, J. S. Endocytic recycling is required for the presentation of an exogenous peptide via MHC class II molecules. *Traffic* **1**, 561-569 (2000).

87 Griffin, J. P., Chu, R. & Harding, C. V. Early endosomes and a late endocytic compartment generate different peptide-class II MHC complexes via distinct processing mechanisms. *J Immunol* **158**, 1523-1532 (1997).
88 Lindner, R. & Unanue, E. R. Distinct antigen MHC class II complexes generated by separate processing pathways. *EMBO J* **15**, 6910-6920 (1996).
89 Pathak, S. S., Lich, J. D. & Blum, J. S. Cutting edge: editing of recycling class II:peptide complexes by HLA-DM. *J Immunol* **167**, 632-635 (2001).
90 Spencer, C. T. *et al.* Sculpting MHC class II-restricted self and non-self peptidome by the class I Ag-processing machinery and its impact on Th-cell responses. *Eur J Immunol* **43**, 1162-1172, doi:10.1002/eji.201243087 (2013).
91 Tewari, M. K., Sinnathamby, G., Rajagopal, D. & Eisenlohr, L. C. A cytosolic pathway for MHC class II-restricted antigen processing that is proteasome and TAP dependent. *Nat Immunol* **6**, 287-294, doi:10.1038/ni1171 (2005).
92 Olsson, N. *et al.* T-Cell Immunopeptidomes Reveal Cell Subtype Surface Markers Derived From Intracellular Proteins. *Proteomics* **18**, e1700410, doi:10.1002/pmic.201700410 (2018).
93 Huseby, E. S. *et al.* How the T cell repertoire becomes peptide and MHC specific. *Cell* **122**, 247-260, doi:10.1016/j.cell.2005.05.013 (2005).
94 Nakagawa, T. *et al.* Cathepsin L: critical role in Ii degradation and CD4 T cell selection in the thymus. *Science* **280**, 450-453 (1998).
95 Gommeaux, J. *et al.* Thymus-specific serine protease regulates positive selection of a subset of CD4+ thymocytes. *Eur J Immunol* **39**, 956-964, doi:10.1002/eji.200839175 (2009).
96 Sallusto, F. & Lanzavecchia, A. Efficient presentation of soluble antigen by cultured human dendritic cells is maintained by granulocyte/macrophage colony-stimulating factor plus interleukin 4 and downregulated by tumor necrosis factor alpha. *J Exp Med* **179**, 1109-1118 (1994).
97 Nijman, H. W. *et al.* Antigen capture and major histocompatibility class II compartments of freshly isolated and cultured human blood dendritic cells. *J Exp Med* **182**, 163-174 (1995).
98 Cella, M., Engering, A., Pinet, V., Pieters, J. & Lanzavecchia, A. Inflammatory stimuli induce accumulation of MHC class II complexes on dendritic cells. *Nature* **388**, 782-787, doi:10.1038/42030 (1997).
99 Stoeckle, C. *et al.* Cathepsin G is differentially expressed in primary human antigen-presenting cells. *Cell Immunol* **255**, 41-45, doi:10.1016/j.cellimm.2008.10.001 (2009).
100 Burster, T. *et al.* Differential processing of autoantigens in lysosomes from human monocyte-derived and peripheral blood dendritic cells. *J Immunol* **175**, 5940-5949 (2005).
101 Hornell, T. M. *et al.* Human dendritic cell expression of HLA-DO is subset specific and regulated by maturation. *J Immunol* **176**, 3536-3547 (2006).
102 Pierre, P. *et al.* Developmental regulation of MHC class II transport in mouse dendritic cells. *Nature* **388**, 787-792, doi:10.1038/42039 (1997).

103 Villadangos, J. A. *et al.* MHC class II expression is regulated in dendritic cells independently of invariant chain degradation. *Immunity* **14**, 739-749 (2001).
104 Nakagawa, T. Y. *et al.* Impaired invariant chain degradation and antigen presentation and diminished collagen-induced arthritis in cathepsin S null mice. *Immunity* **10**, 207-217 (1999).
105 Bergmann, H. *et al.* B cell survival, surface BCR and BAFFR expression, CD74 metabolism, and CD8- dendritic cells require the intramembrane endopeptidase SPPL2A. *J Exp Med* **210**, 31-40, doi:10.1084/jem.20121076 (2013).
106 Chain, B. M. *et al.* The expression and function of cathepsin E in dendritic cells. *J Immunol* **174**, 1791-1800 (2005).
107 Driessen, C. *et al.* Cathepsin S controls the trafficking and maturation of MHC class II molecules in dendritic cells. *J Cell Biol* **147**, 775-790 (1999).
108 Moss, C. X., Villadangos, J. A. & Watts, C. Destructive potential of the aspartyl protease cathepsin D in MHC class II-restricted antigen processing. *Eur J Immunol* **35**, 3442-3451, doi:10.1002/eji.200535320 (2005).
109 Trombetta, E. S., Ebersold, M., Garrett, W., Pypaert, M. & Mellman, I. Activation of lysosomal function during dendritic cell maturation. *Science* **299**, 1400-1403, doi:10.1126/science.1080106 (2003).
110 West, L. C., Grotzke, J. E. & Cresswell, P. MHC class II-restricted presentation of the major house dust mite allergen Der p 1 Is GILT-dependent: implications for allergic asthma. *PLoS One* **8**, e51343, doi:10.1371/journal.pone.0051343 (2013).
111 Fallas, J. L. *et al.* Ectopic expression of HLA-DO in mouse dendritic cells diminishes MHC class II antigen presentation. *J Immunol* **173**, 1549-1560 (2004).
112 Chen, X., Reed-Loisel, L. M., Karlsson, L. & Jensen, P. E. H2-O expression in primary dendritic cells. *J Immunol* **176**, 3548-3556 (2006).
113 Fiebiger, E. *et al.* Cytokines regulate proteolysis in major histocompatibility complex class II-dependent antigen presentation by dendritic cells. *J Exp Med* **193**, 881-892 (2001).
114 Pierre, P. & Mellman, I. Developmental regulation of invariant chain proteolysis controls MHC class II trafficking in mouse dendritic cells. *Cell* **93**, 1135-1145 (1998).
115 Pires, D. *et al.* Role of Cathepsins in Mycobacterium tuberculosis Survival in Human Macrophages. *Sci Rep* **6**, 32247, doi:10.1038/srep32247 (2016).
116 Ranella, A. *et al.* Constitutive intracellular expression of human leukocyte antigen (HLA)-DO and HLA-DR but not HLA-DM in trophoblast cells. *Hum Immunol* **66**, 43-55, doi:10.1016/j.humimm.2004.10.002 (2005).
117 Santin, A. D. *et al.* Expression of surface antigens during the differentiation of human dendritic cells vs macrophages from blood monocytes in vitro. *Immunobiology* **200**, 187-204 (1999).
118 Reilly, J. J., Jr., Chen, P., Sailor, L. Z., Mason, R. W. & Chapman, H. A., Jr. Uptake of extracellular enzyme by a novel pathway is a major

determinant of cathepsin L levels in human macrophages. *J Clin Invest* **86**, 176-183, doi:10.1172/JCI114682 (1990).

119 Barascuk, N. *et al.* Human macrophage foam cells degrade atherosclerotic plaques through cathepsin K mediated processes. *BMC Cardiovasc Disord* **10**, 19, doi:10.1186/1471-2261-10-19 (2010).

120 Baumgart, M., Moos, V., Schuhbauer, D. & Muller, B. Differential expression of major histocompatibility complex class II genes on murine macrophages associated with T cell cytokine profile and protective/suppressive effects. *Proc Natl Acad Sci U S A* **95**, 6936-6940 (1998).

121 Shi, G. P. *et al.* Role for cathepsin F in invariant chain processing and major histocompatibility complex class II peptide loading by macrophages. *J Exp Med* **191**, 1177-1186 (2000).

122 Beers, C., Honey, K., Fink, S., Forbush, K. & Rudensky, A. Differential regulation of cathepsin S and cathepsin L in interferon gamma-treated macrophages. *J Exp Med* **197**, 169-179 (2003).

123 Driessen, C., Lennon-Dumenil, A. M. & Ploegh, H. L. Individual cathepsins degrade immune complexes internalized by antigen-presenting cells via Fcgamma receptors. *Eur J Immunol* **31**, 1592-1601, doi:10.1002/1521-4141(200105)31:5<1592::AID-IMMU1592>3.0.CO;2-K (2001).

124 Manoury, B. *et al.* Destructive processing by asparagine endopeptidase limits presentation of a dominant T cell epitope in MBP. *Nat Immunol* **3**, 169-174, doi:10.1038/ni754 (2002).

125 Kakehashi, H. *et al.* Differential regulation of the nature and functions of dendritic cells and macrophages by cathepsin E. *J Immunol* **179**, 5728-5737 (2007).

126 Walter, W., Loos, M. & Maeurer, M. J. Differential expression of alternative H2-M isoforms in B cells, dendritic cells and macrophages by proinflammatory cytokines. *Molecular immunology* **36**, 733-743 (1999).

127 Lee, J. *et al.* The MHC class II antigen presentation pathway in human monocytes differs by subset and is regulated by cytokines. *PLoS One* **12**, e0183594, doi:10.1371/journal.pone.0183594 (2017).

128 Zawada, A. M. *et al.* SuperSAGE evidence for CD14++CD16+ monocytes as a third monocyte subset. *Blood* **118**, e50-61, doi:10.1182/blood-2011-01-326827 (2011).

129 Senior, R. M. & Campbell, E. J. Cathepsin G in human mononuclear phagocytes: comparisons between monocytes and U937 monocyte-like cells. *J Immunol* **132**, 2547-2551 (1984).

130 Gren, S. T. *et al.* A Single-Cell Gene-Expression Profile Reveals Inter-Cellular Heterogeneity within Human Monocyte Subsets. *PLoS One* **10**, e0144351, doi:10.1371/journal.pone.0144351 (2015).

131 Glazier, K. S. *et al.* Germinal center B cells regulate their capability to present antigen by modulation of HLA-DO. *J Exp Med* **195**, 1063-1069 (2002).

132 Burster, T. *et al.* Cathepsin G, and not the asparagine-specific endoprotease, controls the processing of myelin basic protein in lysosomes from human B lymphocytes. *J Immunol* **172**, 5495-5503 (2004).
133 Burster, T. *et al.* Cathepsin E regulates the presentation of tetanus toxin C-fragment in PMA activated primary human B cells. *Biochem Biophys Res Commun* **377**, 1299-1303, doi:10.1016/j.bbrc.2008.10.162 (2008).
134 Arunachalam, B., Phan, U. T., Geuze, H. J. & Cresswell, P. Enzymatic reduction of disulfide bonds in lysosomes: characterization of a gamma-interferon-inducible lysosomal thiol reductase (GILT). *Proc Natl Acad Sci U S A* **97**, 745-750 (2000).
135 Chalouni, C., Banchereau, J., Vogt, A. B., Pascual, V. & Davoust, J. Human germinal center B cells differ from naive and memory B cells by their aggregated MHC class II-rich compartments lacking HLA-DO. *Int Immunol* **15**, 457-466 (2003).
136 Manoury, B. *et al.* An asparaginyl endopeptidase processes a microbial antigen for class II MHC presentation. *Nature* **396**, 695-699, doi:10.1038/25379 (1998).
137 Fallas, J. L., Yi, W., Draghi, N. A., O'Rourke, H. M. & Denzin, L. K. Expression patterns of H2-O in mouse B cells and dendritic cells correlate with cell function. *J Immunol* **178**, 1488-1497 (2007).
138 Honey, K. *et al.* Cathepsin S regulates the expression of cathepsin L and the turnover of gamma-interferon-inducible lysosomal thiol reductase in B lymphocytes. *J Biol Chem* **276**, 22573-22578, doi:10.1074/jbc.M101851200 (2001).
139 Pluger, E. B. *et al.* Specific role for cathepsin S in the generation of antigenic peptides in vivo. *Eur J Immunol* **32**, 467-476, doi:10.1002/1521-4141(200202)32:2<467::AID-IMMU467>3.0.CO;2-Y (2002).
140 Rausch, M. P. *et al.* GILT accelerates autoimmunity to the melanoma antigen tyrosinase-related protein 1. *J Immunol* **185**, 2828-2835, doi:10.4049/jimmunol.1000945 (2010).
141 Chen, X. *et al.* Regulated expression of human histocompatibility leukocyte antigen (HLA)-DO during antigen-dependent and antigen-independent phases of B cell development. *J Exp Med* **195**, 1053-1062 (2002).
142 Shi, G. P. *et al.* Cathepsin S required for normal MHC class II peptide loading and germinal center development. *Immunity* **10**, 197-206 (1999).
143 Rouse, R. V., Parham, P., Grumet, F. C. & Weissman, I. L. Expression of HLA antigens by human thymic epithelial cells. *Hum Immunol* **5**, 21-34 (1982).
144 Tolosa, E. *et al.* Cathepsin V is involved in the degradation of invariant chain in human thymus and is overexpressed in myasthenia gravis. *J Clin Invest* **112**, 517-526, doi:10.1172/JCI18028 (2003).
145 Douek, D. C. & Altmann, D. M. T-cell apoptosis and differential human leucocyte antigen class II expression in human thymus. *Immunology* **99**, 249-256 (2000).

146 Yang, S. J. *et al.* The quantitative assessment of MHC II on thymic epithelium: implications in cortical thymocyte development. *Int Immunol* **18**, 729-739, doi:10.1093/intimm/dxl010 (2006).
147 Kasai, M., Kominami, E. & Mizuochi, T. The antigen presentation pathway in medullary thymic epithelial cells, but not that in cortical thymic epithelial cells, conforms to the endocytic pathway. *Eur J Immunol* **28**, 1867-1876, doi:10.1002/(SICI)1521-4141(199806)28:06<1867::AID-IMMU1867>3.0.CO;2-K (1998).
148 Karlsson, L., Surh, C. D., Sprent, J. & Peterson, P. A. A novel class II MHC molecule with unusual tissue distribution. *Nature* **351**, 485-488, doi:10.1038/351485a0 (1991).
149 Douek, D. C. & Altmann, D. M. HLA-DO is an intracellular class II molecule with distinctive thymic expression. *Int Immunol* **9**, 355-364 (1997).
150 Surh, C. D. *et al.* Two subsets of epithelial cells in the thymic medulla. *J Exp Med* **176**, 495-505 (1992).
151 Vandenabeele, S., Hochrein, H., Mavaddat, N., Winkel, K. & Shortman, K. Human thymus contains 2 distinct dendritic cell populations. *Blood* **97**, 1733-1741 (2001).
152 Stoeckle, C. *et al.* Cathepsin S dominates autoantigen processing in human thymic dendritic cells. *J Autoimmun* **38**, 332-343, doi:10.1016/j.jaut.2012.02.003 (2012).
153 Scott, H., Solheim, B. G., Brandtzaeg, P. & Thorsby, E. HLA-DR-like antigens in the epithelium of the human small intestine. *Scand J Immunol* **12**, 77-82 (1980).
154 Lin, X. P., Almqvist, N. & Telemo, E. Human small intestinal epithelial cells constitutively express the key elements for antigen processing and the production of exosomes. *Blood Cells Mol Dis* **35**, 122-128, doi:10.1016/j.bcmd.2005.05.011 (2005).
155 Hershberg, R. M. *et al.* Intestinal epithelial cells use two distinct pathways for HLA class II antigen processing. *J Clin Invest* **100**, 204-215, doi:10.1172/JCI119514 (1997).
156 Pober, J. S. *et al.* Lymphocytes recognize human vascular endothelial and dermal fibroblast Ia antigens induced by recombinant immune interferon. *Nature* **305**, 726-729 (1983).
157 Wiman, K. *et al.* Occurrence of Ia antigens on tissues on non-lymphoid origin. *Nature* **276**, 711-713 (1978).
158 Daar, A. S., Fuggle, S. V., Fabre, J. W., Ting, A. & Morris, P. J. The detailed distribution of MHC Class II antigens in normal human organs. *Transplantation* **38**, 293-298 (1984).
159 Bania, J. *et al.* Human cathepsin S, but not cathepsin L, degrades efficiently MHC class II-associated invariant chain in nonprofessional APCs. *Proc Natl Acad Sci U S A* **100**, 6664-6669, doi:10.1073/pnas.1131604100 (2003).
160 Barrera, C. *et al.* Expression of cathepsins B, L, S, and D by gastric epithelial cells implicates them as antigen presenting cells in local immune responses. *Hum Immunol* **62**, 1081-1091 (2001).

161 Kreisel, D. *et al.* Cutting edge: MHC class II expression by pulmonary nonhematopoietic cells plays a critical role in controlling local inflammatory responses. *J Immunol* **185**, 3809-3813, doi:10.4049/jimmunol.1000971 (2010).
162 Muzaki, A. R. *et al.* Intestinal CD103(+)CD11b(-) dendritic cells restrain colitis via IFN-gamma-induced anti-inflammatory response in epithelial cells. *Mucosal Immunol* **9**, 336-351, doi:10.1038/mi.2015.64 (2016).
163 Beers, C. *et al.* Cathepsin S controls MHC class II-mediated antigen presentation by epithelial cells in vivo. *J Immunol* **174**, 1205-1212 (2005).
164 Honey, K., Nakagawa, T., Peters, C. & Rudensky, A. Cathepsin L regulates CD4+ T cell selection independently of its effect on invariant chain: a role in the generation of positively selecting peptide ligands. *J Exp Med* **195**, 1349-1358 (2002).
165 Miyazaki, T. *et al.* Mice lacking H2-M complexes, enigmatic elements of the MHC class II peptide-loading pathway. *Cell* **84**, 531-541 (1996).
166 Martin, W. D. *et al.* H2-M mutant mice are defective in the peptide loading of class II molecules, antigen presentation, and T cell repertoire selection. *Cell* **84**, 543-550 (1996).
167 Klein, L., Kyewski, B., Allen, P. M. & Hogquist, K. A. Positive and negative selection of the T cell repertoire: what thymocytes see (and don't see). *Nat Rev Immunol* **14**, 377-391, doi:10.1038/nri3667 (2014).
168 Mathis, D. & Benoist, C. Aire. *Annu Rev Immunol* **27**, 287-312, doi:10.1146/annurev.immunol.25.022106.141532 (2009).
169 Adamopoulou, E. *et al.* Exploring the MHC-peptide matrix of central tolerance in the human thymus. *Nat Commun* **4**, 2039, doi:10.1038/ncomms3039 (2013).
170 Collado, J. A. *et al.* Composition of the HLA-DR-associated human thymus peptidome. *Eur J Immunol* **43**, 2273-2282, doi:10.1002/eji.201243280 (2013).
171 Hsieh, C. S., Lee, H. M. & Lio, C. W. Selection of regulatory T cells in the thymus. *Nat Rev Immunol* **12**, 157-167, doi:10.1038/nri3155 (2012).
172 Klein, L. & Jovanovic, K. Regulatory T cell lineage commitment in the thymus. *Semin Immunol* **23**, 401-409, doi:10.1016/j.smim.2011.06.003 (2011).
173 Benoist, C. & Mathis, D. Treg cells, life history, and diversity. *Cold Spring Harb Perspect Biol* **4**, a007021, doi:10.1101/cshperspect.a007021 (2012).
174 Aschenbrenner, K. *et al.* Selection of Foxp3+ regulatory T cells specific for self antigen expressed and presented by Aire+ medullary thymic epithelial cells. *Nat Immunol* **8**, 351-358, doi:10.1038/ni1444 (2007).
175 Moran, A. E. *et al.* T cell receptor signal strength in Treg and iNKT cell development demonstrated by a novel fluorescent reporter mouse. *J Exp Med* **208**, 1279-1289, doi:10.1084/jem.20110308 (2011).
176 Gubser, C., Schmaler, M., Rossi, S. W. & Palmer, E. Monoclonal regulatory T cells provide insights into T cell suppression. *Sci Rep* **6**, 25758, doi:10.1038/srep25758 (2016).

177 Onishi, Y., Fehervari, Z., Yamaguchi, T. & Sakaguchi, S. Foxp3+ natural regulatory T cells preferentially form aggregates on dendritic cells in vitro and actively inhibit their maturation. *Proc Natl Acad Sci U S A* **105**, 10113-10118, doi:10.1073/pnas.0711106105 (2008).
178 Lee, H. M., Bautista, J. L., Scott-Browne, J., Mohan, J. F. & Hsieh, C. S. A broad range of self-reactivity drives thymic regulatory T cell selection to limit responses to self. *Immunity* **37**, 475-486, doi:10.1016/j.immuni.2012.07.009 (2012).
179 Xing, Y. & Hogquist, K. A. T-cell tolerance: central and peripheral. *Cold Spring Harb Perspect Biol* **4**, doi:10.1101/cshperspect.a006957 (2012).
180 Mueller, D. L. Mechanisms maintaining peripheral tolerance. *Nat Immunol* **11**, 21-27, doi:10.1038/ni.1817 (2010).
181 Fife, B. T. *et al.* Interactions between PD-1 and PD-L1 promote tolerance by blocking the TCR-induced stop signal. *Nat Immunol* **10**, 1185-1192, doi:10.1038/ni.1790 (2009).
182 Nishimura, H., Nose, M., Hiai, H., Minato, N. & Honjo, T. Development of lupus-like autoimmune diseases by disruption of the PD-1 gene encoding an ITIM motif-carrying immunoreceptor. *Immunity* **11**, 141-151 (1999).
183 Steinman, R. M. *et al.* Dendritic cell function in vivo during the steady state: a role in peripheral tolerance. *Ann N Y Acad Sci* **987**, 15-25 (2003).
184 Fletcher, A. L., Malhotra, D. & Turley, S. J. Lymph node stroma broaden the peripheral tolerance paradigm. *Trends Immunol* **32**, 12-18, doi:10.1016/j.it.2010.11.002 (2011).
185 Kanamori, M., Nakatsukasa, H., Okada, M., Lu, Q. & Yoshimura, A. Induced Regulatory T Cells: Their Development, Stability, and Applications. *Trends Immunol* **37**, 803-811, doi:10.1016/j.it.2016.08.012 (2016).
186 Yadav, M., Stephan, S. & Bluestone, J. A. Peripherally induced tregs - role in immune homeostasis and autoimmunity. *Front Immunol* **4**, 232, doi:10.3389/fimmu.2013.00232 (2013).
187 Vignali, D. A. Mechanisms of T(reg) Suppression: Still a Long Way to Go. *Front Immunol* **3**, 191, doi:10.3389/fimmu.2012.00191 (2012).
188 Shevach, E. M. From vanilla to 28 flavors: multiple varieties of T regulatory cells. *Immunity* **25**, 195-201, doi:10.1016/j.immuni.2006.08.003 (2006).
189 Sakaguchi, S., Sakaguchi, N., Asano, M., Itoh, M. & Toda, M. Immunologic self-tolerance maintained by activated T cells expressing IL-2 receptor alpha-chains (CD25). Breakdown of a single mechanism of self-tolerance causes various autoimmune diseases. *J Immunol* **155**, 1151-1164 (1995).
190 Ramsdell, F. & Ziegler, S. F. FOXP3 and scurfy: how it all began. *Nat Rev Immunol* **14**, 343-349, doi:10.1038/nri3650 (2014).
191 Gambineri, E., Torgerson, T. R. & Ochs, H. D. Immune dysregulation, polyendocrinopathy, enteropathy, and X-linked inheritance (IPEX), a syndrome of systemic autoimmunity caused by mutations of FOXP3, a critical regulator of T-cell homeostasis. *Curr Opin Rheumatol* **15**, 430-435 (2003).

192 Belkaid, Y. Regulatory T cells and infection: a dangerous necessity. *Nat Rev Immunol* **7**, 875-888, doi:10.1038/nri2189 (2007).
193 Fortier, M. H. *et al.* The MHC class I peptide repertoire is molded by the transcriptome. *J Exp Med* **205**, 595-610, doi:10.1084/jem.20071985 (2008).
194 Muixi, L. *et al.* Unraveling features of the natural MHC class II peptidome of skin-migrated dendritic cells. *Int Immunol* **24**, 59-69, doi:10.1093/intimm/dxr096 (2012).
195 Calderon, B., Carrero, J. A. & Unanue, E. R. The central role of antigen presentation in islets of Langerhans in autoimmune diabetes. *Curr Opin Immunol* **26**, 32-40, doi:10.1016/j.coi.2013.10.011 (2014).
196 Villasenor, J., Besse, W., Benoist, C. & Mathis, D. Ectopic expression of peripheral-tissue antigens in the thymic epithelium: probabilistic, monoallelic, misinitiated. *Proc Natl Acad Sci U S A* **105**, 15854-15859, doi:10.1073/pnas.0808069105 (2008).
197 Derbinski, J. & Kyewski, B. How thymic antigen presenting cells sample the body's self-antigens. *Curr Opin Immunol* **22**, 592-600, doi:10.1016/j.coi.2010.08.003 (2010).
198 Sipila, K. H. *et al.* Joint inflammation related citrullination of functional arginines in extracellular proteins. *Sci Rep* **7**, 8246, doi:10.1038/s41598-017-08597-4 (2017).
199 Nguyen, H. & James, E. A. Immune recognition of citrullinated epitopes. *Immunology* **149**, 131-138, doi:10.1111/imm.12640 (2016).
200 Babon, J. A. *et al.* Analysis of self-antigen specificity of islet-infiltrating T cells from human donors with type 1 diabetes. *Nat Med* **22**, 1482-1487, doi:10.1038/nm.4203 (2016).
201 Delong, T. *et al.* Pathogenic CD4 T cells in type 1 diabetes recognize epitopes formed by peptide fusion. *Science* **351**, 711-714, doi:10.1126/science.aad2791 (2016).
202 Jin, N. *et al.* N-terminal additions to the WE14 peptide of chromogranin A create strong autoantigen agonists in type 1 diabetes. *Proc Natl Acad Sci U S A* **112**, 13318-13323, doi:10.1073/pnas.1517862112 (2015).
203 Mohan, J. F., Petzold, S. J. & Unanue, E. R. Register shifting of an insulin peptide-MHC complex allows diabetogenic T cells to escape thymic deletion. *J Exp Med* **208**, 2375-2383, doi:10.1084/jem.20111502 (2011).
204 Mohan, J. F. & Unanue, E. R. Unconventional recognition of peptides by T cells and the implications for autoimmunity. *Nat Rev Immunol* **12**, 721-728, doi:10.1038/nri3294 (2012).
205 Nguyen, T. B. *et al.* Unraveling the structural basis for the unusually rich association of human leukocyte antigen DQ2.5 with class-II-associated invariant chain peptides. *J Biol Chem* **292**, 9218-9228, doi:10.1074/jbc.M117.785139 (2017).
206 Lazarski, C. A. *et al.* The kinetic stability of MHC class II:peptide complexes is a key parameter that dictates immunodominance. *Immunity* **23**, 29-40, doi:10.1016/j.immuni.2005.05.009 (2005).
207 Yin, L., Calvo-Calle, J. M., Dominguez-Amorocho, O. & Stern, L. J. HLA-DM constrains epitope selection in the human CD4 T cell response to

vaccinia virus by favoring the presentation of peptides with longer HLA-DM-mediated half-lives. *J Immunol* **189**, 3983-3994, doi:10.4049/jimmunol.1200626 (2012).
208 Ferrante, A., Templeton, M., Hoffman, M. & Castellini, M. J. The Thermodynamic Mechanism of Peptide-MHC Class II Complex Formation Is a Determinant of Susceptibility to HLA-DM. *J Immunol* **195**, 1251-1261, doi:10.4049/jimmunol.1402367 (2015).
209 McDouall, R. M., Yacoub, M. & Rose, M. L. Isolation, culture, and characterisation of MHC class II-positive microvascular endothelial cells from the human heart. *Microvasc Res* **51**, 137-152, doi:10.1006/mvre.1996.0016 (1996).
210 Garrett, W. S. *et al.* Developmental control of endocytosis in dendritic cells by Cdc42. *Cell* **102**, 325-334 (2000).
211 Drutman, S. B. & Trombetta, E. S. Dendritic cells continue to capture and present antigens after maturation in vivo. *J Immunol* **185**, 2140-2146, doi:10.4049/jimmunol.1000642 (2010).
212 Bosedasgupta, S. & Pieters, J. Inflammatory stimuli reprogram macrophage phagocytosis to macropinocytosis for the rapid elimination of pathogens. *PLoS Pathog* **10**, e1003879, doi:10.1371/journal.ppat.1003879 (2014).
213 Platt, C. D. *et al.* Mature dendritic cells use endocytic receptors to capture and present antigens. *Proc Natl Acad Sci U S A* **107**, 4287-4292, doi:10.1073/pnas.0910609107 (2010).
214 Cho, K. J., Walseng, E., Ishido, S. & Roche, P. A. Ubiquitination by March-I prevents MHC class II recycling and promotes MHC class II turnover in antigen-presenting cells. *Proc Natl Acad Sci U S A* **112**, 10449-10454, doi:10.1073/pnas.1507981112 (2015).
215 Lee, H. K. *et al.* In vivo requirement for Atg5 in antigen presentation by dendritic cells. *Immunity* **32**, 227-239, doi:10.1016/j.immuni.2009.12.006 (2010).
216 Jagannath, C. *et al.* Autophagy enhances the efficacy of BCG vaccine by increasing peptide presentation in mouse dendritic cells. *Nat Med* **15**, 267-276, doi:10.1038/nm.1928 (2009).
217 Paludan, C. *et al.* Endogenous MHC class II processing of a viral nuclear antigen after autophagy. *Science* **307**, 593-596, doi:10.1126/science.1104904 (2005).
218 Chang, C. H., Fontes, J. D., Peterlin, M. & Flavell, R. A. Class II transactivator (CIITA) is sufficient for the inducible expression of major histocompatibility complex class II genes. *J Exp Med* **180**, 1367-1374 (1994).
219 Thelemann, C. *et al.* Interferon-gamma induces expression of MHC class II on intestinal epithelial cells and protects mice from colitis. *PLoS One* **9**, e86844, doi:10.1371/journal.pone.0086844 (2014).
220 Abrahimi, P. *et al.* Blocking MHC class II on human endothelium mitigates acute rejection. *JCI Insight* **1**, doi:10.1172/jci.insight.85293 (2016).

221 Chow, A., Toomre, D., Garrett, W. & Mellman, I. Dendritic cell maturation triggers retrograde MHC class II transport from lysosomes to the plasma membrane. *Nature* **418**, 988-994, doi:10.1038/nature01006 (2002).
222 Lautwein, A. *et al.* Inflammatory stimuli recruit cathepsin activity to late endosomal compartments in human dendritic cells. *Eur J Immunol* **32**, 3348-3357, doi:10.1002/1521-4141(200212)32:12<3348::AID-IMMU3348>3.0.CO;2-S (2002).
223 Blander, J. M. & Medzhitov, R. Toll-dependent selection of microbial antigens for presentation by dendritic cells. *Nature* **440**, 808-812, doi:10.1038/nature04596 (2006).
224 Sealy, L. *et al.* Regulation of cathepsin E expression during human B cell differentiation in vitro. *Eur J Immunol* **26**, 1838-1843, doi:10.1002/eji.1830260826 (1996).
225 Raddrizzani, L. *et al.* Identification of destabilizing residues in HLA class II-selected bacteriophage display libraries edited by HLA-DM. *Eur J Immunol* **29**, 660-668, doi:10.1002/(SICI)1521-4141(199902)29:02<660::AID-IMMU660>3.0.CO;2-I (1999).
226 Chou, C. L. & Sadegh-Nasseri, S. HLA-DM recognizes the flexible conformation of major histocompatibility complex class II. *J Exp Med* **192**, 1697-1706 (2000).
227 Ferrante, A. & Gorski, J. A Peptide/MHCII conformer generated in the presence of exchange peptide is substrate for HLA-DM editing. *Sci Rep* **2**, 386, doi:10.1038/srep00386 (2012).
228 Ferrante, A. & Gorski, J. Cutting edge: HLA-DM-mediated peptide exchange functions normally on MHC class II-peptide complexes that have been weakened by elimination of a conserved hydrogen bond. *J Immunol* **184**, 1153-1158, doi:10.4049/jimmunol.0902878 (2010).
229 Zhou, Z., Callaway, K. A., Weber, D. A. & Jensen, P. E. Cutting edge: HLA-DM functions through a mechanism that does not require specific conserved hydrogen bonds in class II MHC-peptide complexes. *J Immunol* **183**, 4187-4191, doi:10.4049/jimmunol.0901663 (2009).
230 Pos, W., Sethi, D. K. & Wucherpfennig, K. W. Mechanisms of peptide repertoire selection by HLA-DM. *Trends Immunol* **34**, 495-501, doi:10.1016/j.it.2013.06.002 (2013).
231 Fujinami, R. S. Viruses and autoimmune disease--two sides of the same coin? *Trends Microbiol* **9**, 377-381 (2001).
232 Christen, U. & von Herrath, M. G. Infections and autoimmunity--good or bad? *J Immunol* **174**, 7481-7486 (2005).
233 Fujinami, R. S., von Herrath, M. G., Christen, U. & Whitton, J. L. Molecular mimicry, bystander activation, or viral persistence: infections and autoimmune disease. *Clin Microbiol Rev* **19**, 80-94, doi:10.1128/CMR.19.1.80-94.2006 (2006).
234 Cusick, M. F., Libbey, J. E. & Fujinami, R. S. Molecular mimicry as a mechanism of autoimmune disease. *Clin Rev Allergy Immunol* **42**, 102-111, doi:10.1007/s12016-011-8293-8
10.1007/s12016-011-8294-7 (2012).

235 Wucherpfennig, K. W. & Strominger, J. L. Molecular mimicry in T cell-mediated autoimmunity: viral peptides activate human T cell clones specific for myelin basic protein. *Cell* **80**, 695-705 (1995).
236 Hemmer, B. *et al.* Identification of high potency microbial and self ligands for a human autoreactive class II-restricted T cell clone. *J Exp Med* **185**, 1651-1659 (1997).
237 Fujinami, R. S. & Oldstone, M. B. Amino acid homology between the encephalitogenic site of myelin basic protein and virus: mechanism for autoimmunity. *Science* **230**, 1043-1045 (1985).
238 Colf, L. A. *et al.* How a single T cell receptor recognizes both self and foreign MHC. *Cell* **129**, 135-146, doi:10.1016/j.cell.2007.01.048 (2007).
239 Harkiolaki, M. *et al.* T cell-mediated autoimmune disease due to low-affinity crossreactivity to common microbial peptides. *Immunity* **30**, 348-357, doi:10.1016/j.immuni.2009.01.009 (2009).
240 Trowsdale, J. & Kelly, A. The human HLA class II alpha chain gene DZ alpha is distinct from genes in the DP, DQ and DR subregions. *EMBO J* **4**, 2231-2237 (1985).
241 Inoko, H., Ando, A., Kimura, M. & Tsuji, K. Isolation and characterization of the cDNA clone and genomic clones of a new HLA class II antigen heavy chain, DO alpha. *J Immunol* **135**, 2156-2159 (1985).
242 Tonnelle, C., DeMars, R. & Long, E. O. DO beta: a new beta chain gene in HLA-D with a distinct regulation of expression. *EMBO J* **4**, 2839-2847 (1985).
243 Servenius, B., Rask, L. & Peterson, P. A. Class II genes of the human major histocompatibility complex. The DO beta gene is a divergent member of the class II beta gene family. *J Biol Chem* **262**, 8759-8766 (1987).
244 Larhammar, D., Hammerling, U., Rask, L. & Peterson, P. A. Sequence of gene and cDNA encoding murine major histocompatibility complex class II gene A beta 2. *J Biol Chem* **260**, 14111-14119 (1985).
245 Braunstein, N. S. & Germain, R. N. The mouse E beta 2 gene: a class II MHC beta gene with limited intraspecies polymorphism and an unusual pattern of transcription. *EMBO J* **5**, 2469-2476 (1986).
246 Cho, S. G., Attaya, M. & Monaco, J. J. New class II-like genes in the murine MHC. *Nature* **353**, 573-576, doi:10.1038/353573a0 (1991).
247 Hermel, E., Yuan, J. & Monaco, J. J. Characterization of polymorphism within the H2-M MHC class II loci. *Immunogenetics* **42**, 136-142 (1995).
248 Peleraux, A., Karlsson, L., Chambers, J. & Peterson, P. A. Genomic organization of a mouse MHC class II region including the H2-M and Lmp2 loci. *Immunogenetics* **43**, 204-214 (1996).
249 Jonsson, A. K. & Rask, L. Human class II DNA and DOB genes display low sequence variability. *Immunogenetics* **29**, 411-413 (1989).
250 Alvaro-Benito, M., Wieczorek, M., Sticht, J., Kipar, C. & Freund, C. HLA-DMA polymorphisms differentially affect MHC class II peptide loading. *J Immunol* **194**, 803-816, doi:10.4049/jimmunol.1401389 (2015).

251 Amria, S. *et al.* HLA-DM negatively regulates HLA-DR4-restricted collagen pathogenic peptide presentation and T cell recognition. *Eur J Immunol* **38**, 1961-1970, doi:10.1002/eji.200738100 (2008).
252 Louis-Plence, P. *et al.* The down-regulation of HLA-DM gene expression in rheumatoid arthritis is not related to their promoter polymorphism. *J Immunol* **165**, 4861-4869 (2000).
253 Yi, W. *et al.* Targeted regulation of self-peptide presentation prevents type I diabetes in mice without disrupting general immunocompetence. *J Clin Invest* **120**, 1324-1336, doi:10.1172/JCI40220 (2010).
254 Morgan, M. A. *et al.* The nonconventional MHC class II molecule DM governs diabetes susceptibility in NOD mice. *PLoS One* **8**, e56738, doi:10.1371/journal.pone.0056738 (2013).
255 Mohan, J. F. *et al.* Unique autoreactive T cells recognize insulin peptides generated within the islets of Langerhans in autoimmune diabetes. *Nat Immunol* **11**, 350-354, doi:10.1038/ni.1850 (2010).
256 Stadinski, B. D. *et al.* Diabetogenic T cells recognize insulin bound to IAg7 in an unexpected, weakly binding register. *Proc Natl Acad Sci U S A* **107**, 10978-10983, doi:10.1073/pnas.1006545107 (2010).
257 Pu, X. *et al.* Inflammation-related genetic variations and survival in patients with advanced non-small cell lung cancer receiving first-line chemotherapy. *Clin Pharmacol Ther* **96**, 360-369, doi:10.1038/clpt.2014.89 (2014).
258 Sindhi, R. *et al.* Genetic variants in major histocompatibility complex-linked genes associate with pediatric liver transplant rejection. *Gastroenterology* **135**, 830-839, 839 e831-810, doi:10.1053/j.gastro.2008.05.080 (2008).
259 Denzin, L. K. *et al.* Neutralizing Antibody Responses to Viral Infections Are Linked to the Non-classical MHC Class II Gene H2-Ob. *Immunity* **47**, 310-322 e317, doi:10.1016/j.immuni.2017.07.013 (2017).
260 Yao, Y. *et al.* Association between human leucocyte antigen-DO polymorphisms and interferon/ribavirin treatment response in hepatitis C virus type 1 infection in Chinese population: a prospective study. *BMJ Open* **8**, e019406, doi:10.1136/bmjopen-2017-019406 (2018).
261 Chen, X. & Jensen, P. E. The expression of HLA-DO (H2-O) in B lymphocytes. *Immunol Res* **29**, 19-28, doi:10.1385/IR:29:1-3:019 (2004).
262 Alfonso, C. *et al.* Analysis of H2-O influence on antigen presentation by B cells. *J Immunol* **171**, 2331-2337 (2003).
263 Hake, S. B., Tobin, H. M., Steimle, V. & Denzin, L. K. Comparison of the transcriptional regulation of classical and non-classical MHC class II genes. *Eur J Immunol* **33**, 2361-2371, doi:10.1002/eji.200323795 (2003).
264 Liljedahl, M. *et al.* HLA-DO is a lysosomal resident which requires association with HLA-DM for efficient intracellular transport. *EMBO J* **15**, 4817-4824 (1996).
265 Kropshofer, H., Arndt, S. O., Moldenhauer, G., Hammerling, G. J. & Vogt, A. B. HLA-DM acts as a molecular chaperone and rescues empty HLA-DR molecules at lysosomal pH. *Immunity* **6**, 293-302 (1997).

266 Ullrich, H. J. *et al.* Interaction between HLA-DM and HLA-DR involves regions that undergo conformational changes at lysosomal pH. *Proc Natl Acad Sci U S A* **94**, 13163-13168 (1997).
267 Jiang, W. *et al.* pH-susceptibility of HLA-DO tunes DO/DM ratios to regulate HLA-DM catalytic activity. *Sci Rep* **5**, 17333, doi:10.1038/srep17333 (2015).
268 Mosyak, L., Zaller, D. M. & Wiley, D. C. The structure of HLA-DM, the peptide exchange catalyst that loads antigen onto class II MHC molecules during antigen presentation. *Immunity* **9**, 377-383 (1998).
269 Schulze, M. S., Anders, A. K., Sethi, D. K. & Call, M. J. Disruption of hydrogen bonds between major histocompatibility complex class II and the peptide N-terminus is not sufficient to form a human leukocyte antigen-DM receptive state of major histocompatibility complex class II. *PLoS One* **8**, e69228, doi:10.1371/journal.pone.0069228 (2013).
270 Belmares, M. P., Busch, R., Wucherpfennig, K. W., McConnell, H. M. & Mellins, E. D. Structural factors contributing to DM susceptibility of MHC class II/peptide complexes. *J Immunol* **169**, 5109-5117 (2002).
271 Hou, T. *et al.* An insertion mutant in DQA1*0501 restores susceptibility to HLA-DM: implications for disease associations. *J Immunol* **187**, 2442-2452, doi:10.4049/jimmunol.1100255 (2011).
272 Lovitch, S. B., Petzold, S. J. & Unanue, E. R. Cutting edge: H-2DM is responsible for the large differences in presentation among peptides selected by I-Ak during antigen processing. *J Immunol* **171**, 2183-2186 (2003).
273 Blum, J. S., Ma, C. & Kovats, S. Antigen-presenting cells and the selection of immunodominant epitopes. *Crit Rev Immunol* **17**, 411-417 (1997).
274 Patil, N. S. *et al.* Autoantigenic HCgp39 epitopes are presented by the HLA-DM-dependent presentation pathway in human B cells. *J Immunol* **166**, 33-41 (2001).
275 Lich, J. D., Jayne, J. A., Zhou, D., Elliott, J. F. & Blum, J. S. Editing of an immunodominant epitope of glutamate decarboxylase by HLA-DM. *J Immunol* **171**, 853-859 (2003).
276 Perraudeau, M. *et al.* Altered major histocompatibility complex class II peptide loading in H2-O-deficient mice. *Eur J Immunol* **30**, 2871-2880, doi:10.1002/1521-4141(200010)30:10<2871::AID-IMMU2871>3.0.CO;2-B (2000).
277 Kremer, A. N. *et al.* Endogenous HLA class II epitopes that are immunogenic in vivo show distinct behavior toward HLA-DM and its natural inhibitor HLA-DO. *Blood* **120**, 3246-3255, doi:10.1182/blood-2011-12-399311 (2012).
278 Poluektov, Y. O., Kim, A., Hartman, I. Z. & Sadegh-Nasseri, S. HLA-DO as the optimizer of epitope selection for MHC class II antigen presentation. *PLoS One* **8**, e71228, doi:10.1371/journal.pone.0071228 (2013).
279 Liljedahl, M. *et al.* Altered antigen presentation in mice lacking H2-O. *Immunity* **8**, 233-243 (1998).

280 van Ham, M. *et al.* Modulation of the major histocompatibility complex class II-associated peptide repertoire by human histocompatibility leukocyte antigen (HLA)-DO. *J Exp Med* **191**, 1127-1136 (2000).
281 Sant, A. J., Chaves, F. A., Leddon, S. A. & Tung, J. The control of the specificity of CD4 T cell responses: thresholds, breakpoints, and ceilings. *Front Immunol* **4**, 340, doi:10.3389/fimmu.2013.00340 (2013).
282 Kim, A. *et al.* Divergent paths for the selection of immunodominant epitopes from distinct antigenic sources. *Nat Commun* **5**, 5369, doi:10.1038/ncomms6369 (2014).
283 Sant, A. J. *et al.* The relationship between immunodominance, DM editing, and the kinetic stability of MHC class II:peptide complexes. *Immunol Rev* **207**, 261-278, doi:10.1111/j.0105-2896.2005.00307.x (2005).
284 Gondre-Lewis, T. A., Moquin, A. E. & Drake, J. R. Prolonged antigen persistence within nonterminal late endocytic compartments of antigen-specific B lymphocytes. *J Immunol* **166**, 6657-6664 (2001).
285 Denzin, L. K., Fallas, J. L., Prendes, M. & Yi, W. Right place, right time, right peptide: DO keeps DM focused. *Immunol Rev* **207**, 279-292, doi:10.1111/j.0105-2896.2005.00302.x (2005).
286 Fung-Leung, W. P. *et al.* Antigen presentation and T cell development in H2-M-deficient mice. *Science* **271**, 1278-1281 (1996).
287 Surh, C. D., Lee, D. S., Fung-Leung, W. P., Karlsson, L. & Sprent, J. Thymic selection by a single MHC/peptide ligand produces a semidiverse repertoire of CD4+ T cells. *Immunity* **7**, 209-219 (1997).
288 Gu, Y., Jensen, P. E. & Chen, X. Immunodeficiency and autoimmunity in H2-O-deficient mice. *J Immunol* **190**, 126-137, doi:10.4049/jimmunol.1200993 (2013).
289 Nanda, N. K. & Bikoff, E. K. DM peptide-editing function leads to immunodominance in CD4 T cell responses in vivo. *J Immunol* **175**, 6473-6480 (2005).
290 Alfonso, C., Han, J. O., Williams, G. S. & Karlsson, L. The impact of H2-DM on humoral immune responses. *J Immunol* **167**, 6348-6355 (2001).
291 Tourne, S. *et al.* Selection of a broad repertoire of CD4+ T cells in H-2Ma0/0 mice. *Immunity* **7**, 187-195 (1997).
292 Draghi, N. A. & Denzin, L. K. H2-O, a MHC class II-like protein, sets a threshold for B-cell entry into germinal centers. *Proc Natl Acad Sci U S A* **107**, 16607-16612, doi:10.1073/pnas.1004664107 (2010).
293 Miller, M. A., Ganesan, A. P., Luckashenak, N., Mendonca, M. & Eisenlohr, L. C. Endogenous antigen processing drives the primary CD4+ T cell response to influenza. *Nat Med* **21**, 1216-1222, doi:10.1038/nm.3958 (2015).
294 Bellemare-Pelletier, A. *et al.* HLA-DO transduced in human monocyte-derived dendritic cells modulates MHC class II antigen processing. *J Leukoc Biol* **78**, 95-105, doi:10.1189/jlb.0105020 (2005).
295 Ritz, D., Kinzi, J., Neri, D. & Fugmann, T. Data-Independent Acquisition of HLA Class I Peptidomes on the Q Exactive Mass Spectrometer Platform. *Proteomics* **17**, doi:10.1002/pmic.201700177 (2017).

296 Stern, L. J. & Santambrogio, L. The melting pot of the MHC II peptidome. *Curr Opin Immunol* **40**, 70-77, doi:10.1016/j.coi.2016.03.004 (2016).
297 Andreatta, M. *et al.* Accurate pan-specific prediction of peptide-MHC class II binding affinity with improved binding core identification. *Immunogenetics* **67**, 641-650, doi:10.1007/s00251-015-0873-y (2015).
298 Jost, L. Entropy and diversity. *Oikos* **113**, 363-375, doi:10.1111/j.2006.0030-1299.14714.x (2006).
299 Colwell, N. J. G. a. R. K. in *Biological Diversity: Frontiers In Measurement And Assessment* (ed Magurran and McGill) 39-54 (Oxford University Press, 2010).
300 Lai, X., Wang, L. & Witzmann, F. A. Issues and applications in label-free quantitative mass spectrometry. *International journal of proteomics* **2013**, 756039, doi:10.1155/2013/756039 (2013).
301 Jahnke, M., Trowsdale, J. & Kelly, A. P. Ubiquitination of HLA-DO by MARCH family E3 ligases. *Eur J Immunol* **43**, 1153-1161, doi:10.1002/eji.201243043 (2013).
302 Ashburner, M. *et al.* Gene ontology: tool for the unification of biology. The Gene Ontology Consortium. *Nat Genet* **25**, 25-29, doi:10.1038/75556 (2000).
303 The Gene Ontology, C. Expansion of the Gene Ontology knowledgebase and resources. *Nucleic acids research* **45**, D331-D338, doi:10.1093/nar/gkw1108 (2017).
304 Ferrante, A., Anderson, M. W., Klug, C. S. & Gorski, J. HLA-DM mediates epitope selection by a "compare-exchange" mechanism when a potential peptide pool is available. *PLoS One* **3**, e3722, doi:10.1371/journal.pone.0003722 (2008).
305 Alfonso, C., Williams, G. S. & Karlsson, L. H2-O influence on antigen presentation in H2-E-expressing mice. *Eur J Immunol* **33**, 2014-2021, doi:10.1002/eji.200323853 (2003).
306 Brocke, P., Armandola, E., Garbi, N. & Hammerling, G. J. Downmodulation of antigen presentation by H2-O in B cell lines and primary B lymphocytes. *Eur J Immunol* **33**, 411-421, doi:10.1002/immu.200310015 (2003).
307 Rost, H. L. *et al.* OpenSWATH enables automated, targeted analysis of data-independent acquisition MS data. *Nat Biotechnol* **32**, 219-223, doi:10.1038/nbt.2841 (2014).
308 Rock, K. L., Reits, E. & Neefjes, J. Present Yourself! By MHC Class I and MHC Class II Molecules. *Trends Immunol* **37**, 724-737, doi:10.1016/j.it.2016.08.010 (2016).
309 Ran, F. A. *et al.* Genome engineering using the CRISPR-Cas9 system. *Nature protocols* **8**, 2281-2308, doi:10.1038/nprot.2013.143 (2013).
310 Cong, L. *et al.* Multiplex genome engineering using CRISPR/Cas systems. *Science* **339**, 819-823, doi:10.1126/science.1231143 (2013).
311 Chicz, R. M. *et al.* Predominant naturally processed peptides bound to HLA-DR1 are derived from MHC-related molecules and are heterogeneous in size. *Nature* **358**, 764-768, doi:10.1038/358764a0 (1992).

312 Gorga, J. C., Horejsi, V., Johnson, D. R., Raghupathy, R. & Strominger, J. L. Purification and characterization of class II histocompatibility antigens from a homozygous human B cell line. *J Biol Chem* **262**, 16087-16094 (1987).
313 Wolpl, A. *et al.* Human monoclonal antibody with T-cell-like specificity recognizes MHC class I self-peptide presented by HLA-DR1 on activated cells. *Tissue Antigens* **51**, 258-269 (1998).
314 Li, B. & Dewey, C. N. RSEM: accurate transcript quantification from RNA-Seq data with or without a reference genome. *BMC bioinformatics* **12**, 323, doi:10.1186/1471-2105-12-323 (2011).
315 Langmead, B. & Salzberg, S. L. Fast gapped-read alignment with Bowtie 2. *Nat Methods* **9**, 357-359, doi:10.1038/nmeth.1923 (2012).
316 Karolchik, D. *et al.* The UCSC Table Browser data retrieval tool. *Nucleic Acids Res* **32**, D493-496, doi:10.1093/nar/gkh103 (2004).
317 Kent, W. J. *et al.* The human genome browser at UCSC. *Genome research* **12**, 996-1006, doi:10.1101/gr.229102 (2002).
318 Huang da, W., Sherman, B. T. & Lempicki, R. A. Systematic and integrative analysis of large gene lists using DAVID bioinformatics resources. *Nature protocols* **4**, 44-57, doi:10.1038/nprot.2008.211 (2009).
319 Huang da, W., Sherman, B. T. & Lempicki, R. A. Bioinformatics enrichment tools: paths toward the comprehensive functional analysis of large gene lists. *Nucleic Acids Res* **37**, 1-13, doi:10.1093/nar/gkn923 (2009).
320 Jensen, K. K. *et al.* Improved methods for predicting peptide binding affinity to MHC class II molecules. *Immunology*, doi:10.1111/imm.12889 (2018).
321 Calvo-Calle, J. M., Strug, I., Nastke, M. D., Baker, S. P. & Stern, L. J. Human CD4+ T cell epitopes from vaccinia virus induced by vaccination or infection. *PLoS Pathog* **3**, 1511-1529, doi:10.1371/journal.ppat.0030144 (2007).
322 Neilson, K. A. *et al.* Less label, more free: approaches in label-free quantitative mass spectrometry. *Proteomics* **11**, 535-553, doi:10.1002/pmic.201000553 (2011).
323 Gamez-Pozo, A. *et al.* PTRF/cavin-1 and MIF proteins are identified as non-small cell lung cancer biomarkers by label-free proteomics. *PLoS One* **7**, e33752, doi:10.1371/journal.pone.0033752 (2012).
324 Mueller, L. N., Brusniak, M. Y., Mani, D. R. & Aebersold, R. An assessment of software solutions for the analysis of mass spectrometry based quantitative proteomics data. *J Proteome Res* **7**, 51-61, doi:10.1021/pr700758r (2008).
325 Lemeer, S., Hahne, H., Pachl, F. & Kuster, B. Software tools for MS-based quantitative proteomics: a brief overview. *Methods Mol Biol* **893**, 489-499, doi:10.1007/978-1-61779-885-6_29 (2012).
326 Stern, L. J. & Wiley, D. C. The human class II MHC protein HLA-DR1 assembles as empty alpha beta heterodimers in the absence of antigenic peptide. *Cell* **68**, 465-477 (1992).

327 Denzin, L. K. & Cresswell, P. HLA-DM induces CLIP dissociation from MHC class II alpha beta dimers and facilitates peptide loading. *Cell* **82**, 155-165 (1995).
328 Rudensky, A., Rath, S., Preston-Hurlburt, P., Murphy, D. B. & Janeway, C. A., Jr. On the complexity of self. *Nature* **353**, 660-662, doi:10.1038/353660a0 (1991).
329 Yin, L. & Stern, L. J. Measurement of Peptide Binding to MHC Class II Molecules by Fluorescence Polarization. *Curr Protoc Immunol* **106**, 5 10 11-12, doi:10.1002/0471142735.im0510s106 (2014).
330 Nanaware, P. P., Jurewicz, M. M., Leszyk, J. D., Shaffer, S. A. & Stern, L. J. HLA-DO Modulates the Diversity of the MHC-II Self-peptidome. *Mol Cell Proteomics* **18**, 490-503, doi:10.1074/mcp.RA118.000956 (2019).
331 Jameson, S. C., Hogquist, K. A. & Bevan, M. J. Positive selection of thymocytes. *Annu Rev Immunol* **13**, 93-126, doi:10.1146/annurev.iy.13.040195.000521 (1995).
332 Wirnsberger, G., Hinterberger, M. & Klein, L. Regulatory T-cell differentiation versus clonal deletion of autoreactive thymocytes. *Immunol Cell Biol* **89**, 45-53, doi:10.1038/icb.2010.123 (2011).
333 Stadinski, B. D. *et al.* A role for differential variable gene pairing in creating T cell receptors specific for unique major histocompatibility ligands. *Immunity* **35**, 694-704, doi:10.1016/j.immuni.2011.10.012 (2011).
334 Vanguri, V., Govern, C. C., Smith, R. & Huseby, E. S. Viral antigen density and confinement time regulate the reactivity pattern of CD4 T-cell responses to vaccinia virus infection. *Proc Natl Acad Sci U S A* **110**, 288-293, doi:10.1073/pnas.1208328110 (2013).
335 Izraelson, M. *et al.* Comparative analysis of murine T-cell receptor repertoires. *Immunology* **153**, 133-144, doi:10.1111/imm.12857 (2018).
336 Feng, Y. *et al.* A mechanism for expansion of regulatory T-cell repertoire and its role in self-tolerance. *Nature* **528**, 132-136, doi:10.1038/nature16141 (2015).
337 Stadinski, B. D. *et al.* Hydrophobic CDR3 residues promote the development of self-reactive T cells. *Nat Immunol* **17**, 946-955, doi:10.1038/ni.3491 (2016).
338 Liu, Y. *et al.* A critical function for TGF-beta signaling in the development of natural CD4+CD25+Foxp3+ regulatory T cells. *Nat Immunol* **9**, 632-640, doi:10.1038/ni.1607 (2008).
339 Yang, S., Fujikado, N., Kolodin, D., Benoist, C. & Mathis, D. Immune tolerance. Regulatory T cells generated early in life play a distinct role in maintaining self-tolerance. *Science* **348**, 589-594, doi:10.1126/science.aaa7017 (2015).
340 Sun, C. M. *et al.* Small intestine lamina propria dendritic cells promote de novo generation of Foxp3 T reg cells via retinoic acid. *J Exp Med* **204**, 1775-1785, doi:10.1084/jem.20070602 (2007).
341 Yamazaki, S. *et al.* Dendritic cells are specialized accessory cells along with TGF- for the differentiation of Foxp3+ CD4+ regulatory T cells from

peripheral Foxp3 precursors. *Blood* **110**, 4293-4302, doi:10.1182/blood-2007-05-088831 (2007).
342 Thompson, L. J., Valladao, A. C. & Ziegler, S. F. Cutting edge: De novo induction of functional Foxp3+ regulatory CD4 T cells in response to tissue-restricted self antigen. *J Immunol* **186**, 4551-4555, doi:10.4049/jimmunol.1003573 (2011).
343 Lathrop, S. K., Santacruz, N. A., Pham, D., Luo, J. & Hsieh, C. S. Antigen-specific peripheral shaping of the natural regulatory T cell population. *J Exp Med* **205**, 3105-3117, doi:10.1084/jem.20081359 (2008).
344 Paiva, R. S. *et al.* Recent thymic emigrants are the preferential precursors of regulatory T cells differentiated in the periphery. *Proc Natl Acad Sci U S A* **110**, 6494-6499, doi:10.1073/pnas.1221955110 (2013).
345 Wyss, L. *et al.* Affinity for self antigen selects Treg cells with distinct functional properties. *Nat Immunol* **17**, 1093-1101, doi:10.1038/ni.3522 (2016).
346 Huehn, J. *et al.* Developmental stage, phenotype, and migration distinguish naive- and effector/memory-like CD4+ regulatory T cells. *J Exp Med* **199**, 303-313, doi:10.1084/jem.20031562 (2004).
347 Cretney, E., Kallies, A. & Nutt, S. L. Differentiation and function of Foxp3(+) effector regulatory T cells. *Trends Immunol* **34**, 74-80, doi:10.1016/j.it.2012.11.002 (2013).
348 Fontenot, J. D., Gavin, M. A. & Rudensky, A. Y. Foxp3 programs the development and function of CD4+CD25+ regulatory T cells. *Nat Immunol* **4**, 330-336, doi:10.1038/ni904 (2003).
349 Shimizu, J., Yamazaki, S., Takahashi, T., Ishida, Y. & Sakaguchi, S. Stimulation of CD25(+)CD4(+) regulatory T cells through GITR breaks immunological self-tolerance. *Nat Immunol* **3**, 135-142, doi:10.1038/ni759 (2002).
350 Chen, X. *et al.* Cutting edge: expression of TNFR2 defines a maximally suppressive subset of mouse CD4+CD25+FoxP3+ T regulatory cells: applicability to tumor-infiltrating T regulatory cells. *J Immunol* **180**, 6467-6471 (2008).
351 Sage, P. T. & Sharpe, A. H. T follicular regulatory cells. *Immunol Rev* **271**, 246-259, doi:10.1111/imr.12411 (2016).
352 Vaeth, M. *et al.* Follicular regulatory T cells control humoral autoimmunity via NFAT2-regulated CXCR5 expression. *J Exp Med* **211**, 545-561, doi:10.1084/jem.20130604 (2014).
353 Fu, W. *et al.* Deficiency in T follicular regulatory cells promotes autoimmunity. *J Exp Med* **215**, 815-825, doi:10.1084/jem.20170901 (2018).
354 Sebastian, M. *et al.* Helios Controls a Limited Subset of Regulatory T Cell Functions. *J Immunol* **196**, 144-155, doi:10.4049/jimmunol.1501704 (2016).
355 Sage, P. T., Francisco, L. M., Carman, C. V. & Sharpe, A. H. The receptor PD-1 controls follicular regulatory T cells in the lymph nodes and blood. *Nat Immunol* **14**, 152-161, doi:10.1038/ni.2496 (2013).

356 Flament, T. *et al.* Pulmonary manifestations of Sjogren's syndrome. *Eur Respir Rev* **25**, 110-123, doi:10.1183/16000617.0011-2016 (2016).
357 Vivino, F. B. Sjogren's syndrome: Clinical aspects. *Clin Immunol* **182**, 48-54, doi:10.1016/j.clim.2017.04.005 (2017).
358 Miles, B. *et al.* Follicular regulatory T cells impair follicular T helper cells in HIV and SIV infection. *Nat Commun* **6**, 8608, doi:10.1038/ncomms9608 (2015).
359 Walker, S. E. & Lorsch, J. RNA purification--precipitation methods. *Methods Enzymol* **530**, 337-343, doi:10.1016/B978-0-12-420037-1.00019-1 (2013).
360 Shugay, M. *et al.* Towards error-free profiling of immune repertoires. *Nat Methods* **11**, 653-655, doi:10.1038/nmeth.2960 (2014).
361 Bolotin, D. A. *et al.* MiXCR: software for comprehensive adaptive immunity profiling. *Nat Methods* **12**, 380-381, doi:10.1038/nmeth.3364 (2015).
362 Shugay, M. *et al.* VDJtools: Unifying Post-analysis of T Cell Receptor Repertoires. *PLoS Comput Biol* **11**, e1004503, doi:10.1371/journal.pcbi.1004503 (2015).
363 Huter, E. N. *et al.* TGF-beta-induced Foxp3+ regulatory T cells rescue scurfy mice. *Eur J Immunol* **38**, 1814-1821, doi:10.1002/eji.200838346 (2008).
364 Robinson, J. H. & Delvig, A. A. Diversity in MHC class II antigen presentation. *Immunology* **105**, 252-262 (2002).
365 Wan, Y. Y. & Flavell, R. A. How diverse--CD4 effector T cells and their functions. *J Mol Cell Biol* **1**, 20-36, doi:10.1093/jmcb/mjp001 (2009).
366 Sant, A. J., Richards, K. A. & Nayak, J. Distinct and complementary roles of CD4 T cells in protective immunity to influenza virus. *Curr Opin Immunol* **53**, 13-21, doi:10.1016/j.coi.2018.03.019 (2018).
367 Denzin, L. K. Inhibition of HLA-DM Mediated MHC Class II Peptide Loading by HLA-DO Promotes Self Tolerance. *Front Immunol* **4**, 465, doi:10.3389/fimmu.2013.00465 (2013).
368 Karlsson, L. DM and DO shape the repertoire of peptide-MHC-class-II complexes. *Curr Opin Immunol* **17**, 65-70, doi:10.1016/j.coi.2004.11.003 (2005).
369 Nanaware, P. P., Jurewicz, M. M., Leszyk, J., Shaffer, S. A. & Stern, L. J. HLA-DO modulates the diversity of the MHC-II self-peptidome. *Mol Cell Proteomics*, doi:10.1074/mcp.RA118.000956 (2018).
370 Hamada, H. *et al.* Multiple redundant effector mechanisms of CD8+ T cells protect against influenza infection. *J Immunol* **190**, 296-306, doi:10.4049/jimmunol.1200571 (2013).
371 Bender, B. S., Croghan, T., Zhang, L. & Small, P. A., Jr. Transgenic mice lacking class I major histocompatibility complex-restricted T cells have delayed viral clearance and increased mortality after influenza virus challenge. *J Exp Med* **175**, 1143-1145 (1992).
372 Mozdzanowska, K., Furchner, M., Maiese, K. & Gerhard, W. CD4+ T cells are ineffective in clearing a pulmonary infection with influenza type A virus

in the absence of B cells. *Virology* **239**, 217-225, doi:10.1006/viro.1997.8882 (1997).
373 Topham, D. J. & Doherty, P. C. Clearance of an influenza A virus by CD4+ T cells is inefficient in the absence of B cells. *J Virol* **72**, 882-885 (1998).
374 Sun, J., Dodd, H., Moser, E. K., Sharma, R. & Braciale, T. J. CD4+ T cell help and innate-derived IL-27 induce Blimp-1-dependent IL-10 production by antiviral CTLs. *Nat Immunol* **12**, 327-334, doi:10.1038/ni.1996 (2011).
375 Abdul-Careem, M. F. *et al.* Critical role of natural killer cells in lung immunopathology during influenza infection in mice. *J Infect Dis* **206**, 167-177, doi:10.1093/infdis/jis340 (2012).
376 Schultz-Cherry, S. Role of NK cells in influenza infection. *Curr Top Microbiol Immunol* **386**, 109-120, doi:10.1007/82_2014_403 (2015).
377 Zarnegar, B. *et al.* Influenza Infection in Mice Induces Accumulation of Lung Mast Cells through the Recruitment and Maturation of Mast Cell Progenitors. *Front Immunol* **8**, 310, doi:10.3389/fimmu.2017.00310 (2017).
378 Paget, C. *et al.* Potential role of invariant NKT cells in the control of pulmonary inflammation and CD8+ T cell response during acute influenza A virus H3N2 pneumonia. *J Immunol* **186**, 5590-5602, doi:10.4049/jimmunol.1002348 (2011).
379 Marshall, N. B. *et al.* NKG2C/E Marks the Unique Cytotoxic CD4 T Cell Subset, ThCTL, Generated by Influenza Infection. *J Immunol* **198**, 1142-1155, doi:10.4049/jimmunol.1601297 (2017).
380 Aljurayyan, A. *et al.* Activation and Induction of Antigen-Specific T Follicular Helper Cells Play a Critical Role in Live-Attenuated Influenza Vaccine-Induced Human Mucosal Anti-influenza Antibody Response. *J Virol* **92**, doi:10.1128/JVI.00114-18 (2018).
381 Brown, D. M., Lee, S., Garcia-Hernandez Mde, L. & Swain, S. L. Multifunctional CD4 cells expressing gamma interferon and perforin mediate protection against lethal influenza virus infection. *J Virol* **86**, 6792-6803, doi:10.1128/JVI.07172-11 (2012).
382 Song, Y. *et al.* Repeated Low-Dose Influenza Virus Infection Causes Severe Disease in Mice: a Model for Vaccine Evaluation. *J Virol* **89**, 7841-7851, doi:10.1128/JVI.00976-15 (2015).
383 Leon, B., Ballesteros-Tato, A., Randall, T. D. & Lund, F. E. Prolonged antigen presentation by immune complex-binding dendritic cells programs the proliferative capacity of memory CD8 T cells. *J Exp Med* **211**, 1637-1655, doi:10.1084/jem.20131692 (2014).
384 Lund, J. M., Hsing, L., Pham, T. T. & Rudensky, A. Y. Coordination of early protective immunity to viral infection by regulatory T cells. *Science* **320**, 1220-1224, doi:10.1126/science.1155209 (2008).
385 Moltedo, B., Hemmers, S. & Rudensky, A. Y. Regulatory T cell ablation causes acute T cell lymphopenia. *PLoS One* **9**, e86762, doi:10.1371/journal.pone.0086762 (2014).
386 Roberts, L. M. *et al.* Depletion of alveolar macrophages in CD11c diphtheria toxin receptor mice produces an inflammatory response. *Immun Inflamm Dis* **3**, 71-81, doi:10.1002/iid3.51 (2015).

387 Chapman, T. J. & Georas, S. N. Adjuvant effect of diphtheria toxin after mucosal administration in both wild type and diphtheria toxin receptor engineered mouse strains. *J Immunol Methods* **400-401**, 122-126, doi:10.1016/j.jim.2013.10.010 (2013).
388 Littwitz-Salomon, E. *et al.* Activated regulatory T cells suppress effector NK cell responses by an IL-2-mediated mechanism during an acute retroviral infection. *Retrovirology* **12**, 66, doi:10.1186/s12977-015-0191-3 (2015).
389 Littwitz-Salomon, E., Malyshkina, A., Schimmer, S. & Dittmer, U. The Cytotoxic Activity of Natural Killer Cells Is Suppressed by IL-10(+) Regulatory T Cells During Acute Retroviral Infection. *Front Immunol* **9**, 1947, doi:10.3389/fimmu.2018.01947 (2018).
390 Suvas, S., Kumaraguru, U., Pack, C. D., Lee, S. & Rouse, B. T. CD4+CD25+ T cells regulate virus-specific primary and memory CD8+ T cell responses. *J Exp Med* **198**, 889-901, doi:10.1084/jem.20030171 (2003).
391 Dittmer, U. *et al.* Functional impairment of CD8(+) T cells by regulatory T cells during persistent retroviral infection. *Immunity* **20**, 293-303 (2004).
392 Suvas, S., Azkur, A. K., Kim, B. S., Kumaraguru, U. & Rouse, B. T. CD4+CD25+ regulatory T cells control the severity of viral immunoinflammatory lesions. *J Immunol* **172**, 4123-4132 (2004).
393 Strutt, T. M. *et al.* Direct IL-6 Signals Maximize Protective Secondary CD4 T Cell Responses against Influenza. *J Immunol* **197**, 3260-3270, doi:10.4049/jimmunol.1600033 (2016).
394 Bautista, B. L. *et al.* Short-Lived Antigen Recognition but Not Viral Infection at a Defined Checkpoint Programs Effector CD4 T Cells To Become Protective Memory. *J Immunol* **197**, 3936-3949, doi:10.4049/jimmunol.1600838 (2016).
395 Brahmakshatriya, V. *et al.* IL-6 Production by TLR-Activated APC Broadly Enhances Aged Cognate CD4 Helper and B Cell Antibody Responses In Vivo. *J Immunol* **198**, 2819-2833, doi:10.4049/jimmunol.1601119 (2017).
396 Sukseree, S. *et al.* Autophagy in the thymic epithelium is dispensable for the development of self-tolerance in a novel mouse model. *PLoS One* **7**, e38933, doi:10.1371/journal.pone.0038933 (2012).
397 Anderson, G. & Jenkinson, E. J. Review article: thymus organ cultures and T-cell receptor repertoire development. *Immunology* **100**, 405-410 (2000).
398 Atibalentja, D. F., Byersdorfer, C. A. & Unanue, E. R. Thymus-blood protein interactions are highly effective in negative selection and regulatory T cell induction. *J Immunol* **183**, 7909-7918, doi:10.4049/jimmunol.0902632 (2009).
399 Wu, H. *et al.* Follicular regulatory T cells repress cytokine production by follicular helper T cells and optimize IgG responses in mice. *Eur J Immunol* **46**, 1152-1161, doi:10.1002/eji.201546094 (2016).
400 Pober, J. S., Merola, J., Liu, R. & Manes, T. D. Antigen Presentation by Vascular Cells. *Front Immunol* **8**, 1907, doi:10.3389/fimmu.2017.01907 (2017).

401 Wosen, J. E., Mukhopadhyay, D., Macaubas, C. & Mellins, E. D. Epithelial MHC Class II Expression and Its Role in Antigen Presentation in the Gastrointestinal and Respiratory Tracts. *Front Immunol* **9**, 2144, doi:10.3389/fimmu.2018.02144 (2018).
402 Honey, K., Forbush, K., Jensen, P. E. & Rudensky, A. Y. Effect of decreasing the affinity of the class II-associated invariant chain peptide on the MHC class II peptide repertoire in the presence or absence of H-2M. *J Immunol* **172**, 4142-4150 (2004).
403 Kim, C. Y., Quarsten, H., Bergseng, E., Khosla, C. & Sollid, L. M. Structural basis for HLA-DQ2-mediated presentation of gluten epitopes in celiac disease. *Proc Natl Acad Sci U S A* **101**, 4175-4179, doi:10.1073/pnas.0306885101 (2004).
404 Irvine, K. & Bennink, J. Factors influencing immunodominance hierarchies in TCD8+ -mediated antiviral responses. *Expert Rev Clin Immunol* **2**, 135-147, doi:10.1586/1744666X.2.1.135 (2006).
405 van der Burg, S. H., Visseren, M. J., Brandt, R. M., Kast, W. M. & Melief, C. J. Immunogenicity of peptides bound to MHC class I molecules depends on the MHC-peptide complex stability. *J Immunol* **156**, 3308-3314 (1996).
406 Engels, B. *et al.* Relapse or eradication of cancer is predicted by peptide-major histocompatibility complex affinity. *Cancer Cell* **23**, 516-526, doi:10.1016/j.ccr.2013.03.018 (2013).
407 Regner, M., Mullbacher, A., Blanden, R. V. & Lobigs, M. Immunogenicity of two peptide determinants in the cytolytic T-cell response to flavivirus infection: inverse correlation between peptide affinity for MHC class I and T-cell precursor frequency. *Viral Immunol* **14**, 135-149, doi:10.1089/088282401750234510 (2001).
408 Busch, D. H. & Pamer, E. G. T cell affinity maturation by selective expansion during infection. *J Exp Med* **189**, 701-710 (1999).
409 Dockree, T. *et al.* CD8(+) T-cell specificity is compromised at a defined MHCI/CD8 affinity threshold. *Immunol Cell Biol* **95**, 68-76, doi:10.1038/icb.2016.85 (2017).
410 Fairchild, P. J. & Wraith, D. C. Peptide-MHC interaction in autoimmunity. *Curr Opin Immunol* **4**, 748-753 (1992).
411 Sette, A. *et al.* Peptide binding to the most frequent HLA-A class I alleles measured by quantitative molecular binding assays. *Molecular immunology* **31**, 813-822 (1994).
412 Chen, B. P. & Parham, P. Direct binding of influenza peptides to class I HLA molecules. *Nature* **337**, 743-745, doi:10.1038/337743a0 (1989).
413 Olsen, A. C. *et al.* A quantitative assay to measure the interaction between immunogenic peptides and purified class I major histocompatibility complex molecules. *Eur J Immunol* **24**, 385-392, doi:10.1002/eji.1830240218 (1994).
414 Sidney, J. *et al.* Measurement of MHC/peptide interactions by gel filtration or monoclonal antibody capture. *Curr Protoc Immunol* **Chapter 18**, Unit 18 13, doi:10.1002/0471142735.im1803s100 (2013).

415 Parker, K. C., Bednarek, M. A. & Coligan, J. E. Scheme for ranking potential HLA-A2 binding peptides based on independent binding of individual peptide side-chains. *J Immunol* **152**, 163-175 (1994).
416 Harndahl, M., Rasmussen, M., Roder, G. & Buus, S. Real-time, high-throughput measurements of peptide-MHC-I dissociation using a scintillation proximity assay. *J Immunol Methods* **374**, 5-12, doi:10.1016/j.jim.2010.10.012 (2011).
417 Schumacher, T. N. *et al.* Direct binding of peptide to empty MHC class I molecules on intact cells and in vitro. *Cell* **62**, 563-567 (1990).
418 Hosken, N. A. & Bevan, M. J. Defective presentation of endogenous antigen by a cell line expressing class I molecules. *Science* **248**, 367-370 (1990).
419 Kessler, J. H. *et al.* Competition-based cellular peptide binding assay for HLA class I. *Curr Protoc Immunol* **Chapter 18**, Unit 18 12, doi:10.1002/0471142735.im1812s61 (2004).
420 Kessler, J. H. *et al.* Competition-based cellular peptide binding assays for 13 prevalent HLA class I alleles using fluorescein-labeled synthetic peptides. *Hum Immunol* **64**, 245-255 (2003).
421 Storkus, W. J., Zeh, H. J., 3rd, Salter, R. D. & Lotze, M. T. Identification of T-cell epitopes: rapid isolation of class I-presented peptides from viable cells by mild acid elution. *J Immunother Emphasis Tumor Immunol* **14**, 94-103 (1993).
422 Townsend, A. *et al.* Association of class I major histocompatibility heavy and light chains induced by viral peptides. *Nature* **340**, 443-448, doi:10.1038/340443a0 (1989).
423 Miles, K. M., Miles, J. J., Madura, F., Sewell, A. K. & Cole, D. K. Real time detection of peptide-MHC dissociation reveals that improvement of primary MHC-binding residues can have a minimal, or no, effect on stability. *Molecular immunology* **48**, 728-732, doi:10.1016/j.molimm.2010.11.004 (2011).
424 Khilko, S. N. *et al.* Measuring interactions of MHC class I molecules using surface plasmon resonance. *J Immunol Methods* **183**, 77-94 (1995).
425 Sylvester-Hvid, C. *et al.* Establishment of a quantitative ELISA capable of determining peptide - MHC class I interaction. *Tissue Antigens* **59**, 251-258 (2002).
426 Wulf, M., Hoehn, P. & Trinder, P. Identification of human MHC class I binding peptides using the iTOPIA- epitope discovery system. *Methods Mol Biol* **524**, 361-367, doi:10.1007/978-1-59745-450-6_26 (2009).
427 Silver, M. L., Parker, K. C. & Wiley, D. C. Reconstitution by MHC-restricted peptides of HLA-A2 heavy chain with beta 2-microglobulin, in vitro. *Nature* **350**, 619-622, doi:10.1038/350619a0 (1991).
428 Garboczi, D. N., Hung, D. T. & Wiley, D. C. HLA-A2-peptide complexes: refolding and crystallization of molecules expressed in Escherichia coli and complexed with single antigenic peptides. *Proc Natl Acad Sci U S A* **89**, 3429-3433 (1992).
429 Ferre, H. *et al.* Purification of correctly oxidized MHC class I heavy-chain molecules under denaturing conditions: a novel strategy exploiting disulfide

assisted protein folding. *Protein Sci* **12**, 551-559, doi:10.1110/ps.0233003 (2003).
430 Saini, S. K. *et al.* Dipeptides promote folding and peptide binding of MHC class I molecules. *Proc Natl Acad Sci U S A* **110**, 15383-15388, doi:10.1073/pnas.1308672110 (2013).
431 Toebes, M. *et al.* Design and use of conditional MHC class I ligands. *Nat Med* **12**, 246-251, doi:10.1038/nm1360 (2006).
432 Rodenko, B. *et al.* Class I major histocompatibility complexes loaded by a periodate trigger. *J Am Chem Soc* **131**, 12305-12313, doi:10.1021/ja9037565 (2009).
433 Buus, S., Sette, A., Colon, S. M., Jenis, D. M. & Grey, H. M. Isolation and characterization of antigen-Ia complexes involved in T cell recognition. *Cell* **47**, 1071-1077 (1986).
434 Kim, A. *et al.* Studying MHC class II peptide loading and editing in vitro. *Methods Mol Biol* **960**, 447-459, doi:10.1007/978-1-62703-218-6_33 (2013).
435 Roche, P. A. & Cresswell, P. High-affinity binding of an influenza hemagglutinin-derived peptide to purified HLA-DR. *J Immunol* **144**, 1849-1856 (1990).
436 Tompkins, S. M., Rota, P. A., Moore, J. C. & Jensen, P. E. A europium fluoroimmunoassay for measuring binding of antigen to class II MHC glycoproteins. *J Immunol Methods* **163**, 209-216 (1993).
437 Frayser, M., Sato, A. K., Xu, L. & Stern, L. J. Empty and peptide-loaded class II major histocompatibility complex proteins produced by expression in Escherichia coli and folding in vitro. *Protein Expr Purif* **15**, 105-114, doi:10.1006/prep.1998.0987 (1999).
438 Hansen, B. E. *et al.* Functional characterization of HLA-DRA1*0101/DRB1*0401 molecules expressed in Drosophila melanogaster cells. *Tissue Antigens* **51**, 119-128 (1998).
439 Moro, M. *et al.* Generation of functional HLA-DR*1101 tetramers receptive for loading with pathogen- or tumour-derived synthetic peptides. *BMC Immunol* **6**, 24, doi:10.1186/1471-2172-6-24 (2005).
440 Hansen, T., Yu, Y. Y. & Fremont, D. H. Preparation of stable single-chain trimers engineered with peptide, beta2 microglobulin, and MHC heavy chain. *Curr Protoc Immunol* **Chapter 17**, Unit17 15, doi:10.1002/0471142735.im1705s87 (2009).
441 Kozono, H., White, J., Clements, J., Marrack, P. & Kappler, J. Production of soluble MHC class II proteins with covalently bound single peptides. *Nature* **369**, 151-154, doi:10.1038/369151a0 (1994).
442 Wooster, A. L., Anderson, T. S. & Lowe, D. B. Expression and characterization of soluble epitope-defined major histocompatibility complex (MHC) from stable eukaryotic cell lines. *J Immunol Methods* **464**, 22-30, doi:10.1016/j.jim.2018.10.006 (2019).
443 Dedier, S., Reinelt, S., Rion, S., Folkers, G. & Rognan, D. Use of fluorescence polarization to monitor MHC-peptide interactions in solution. *J Immunol Methods* **255**, 57-66 (2001).

444 Buchli, R. *et al.* Development and validation of a fluorescence polarization-based competitive peptide-binding assay for HLA-A*0201--a new tool for epitope discovery. *Biochemistry* **44**, 12491-12507, doi:10.1021/bi050255v (2005).
445 Joshi, R. V., Zarutskie, J. A. & Stern, L. J. A three-step kinetic mechanism for peptide binding to MHC class II proteins. *Biochemistry* **39**, 3751-3762 (2000).
446 Gilchuk, P. *et al.* Discovering naturally processed antigenic determinants that confer protective T cell immunity. *J Clin Invest* **123**, 1976-1987, doi:10.1172/JCI67388 (2013).
447 Assarsson, E. *et al.* A quantitative analysis of the variables affecting the repertoire of T cell specificities recognized after vaccinia virus infection. *J Immunol* **178**, 7890-7901 (2007).
448 Oseroff, C. *et al.* HLA class I-restricted responses to vaccinia recognize a broad array of proteins mainly involved in virulence and viral gene regulation. *Proc Natl Acad Sci U S A* **102**, 13980-13985, doi:10.1073/pnas.0506768102 (2005).
449 Pasquetto, V. *et al.* HLA-A*0201, HLA-A*1101, and HLA-B*0702 transgenic mice recognize numerous poxvirus determinants from a wide variety of viral gene products. *J Immunol* **175**, 5504-5515 (2005).
450 Hellman, L. M. *et al.* Differential scanning fluorimetry based assessments of the thermal and kinetic stability of peptide-MHC complexes. *J Immunol Methods* **432**, 95-101, doi:10.1016/j.jim.2016.02.016 (2016).
451 Cheng, Y. & Prusoff, W. H. Relationship between the inhibition constant (K1) and the concentration of inhibitor which causes 50 per cent inhibition (I50) of an enzymatic reaction. *Biochem Pharmacol* **22**, 3099-3108 (1973).
452 Munson, P. J. & Rodbard, D. An exact correction to the "Cheng-Prusoff" correction. *J Recept Res* **8**, 533-546 (1988).
453 Cer, R. Z., Mudunuri, U., Stephens, R. & Lebeda, F. J. IC50-to-Ki: a web-based tool for converting IC50 to Ki values for inhibitors of enzyme activity and ligand binding. *Nucleic Acids Res* **37**, W441-445, doi:10.1093/nar/gkp253 (2009).
454 Wyllie, D. J. & Chen, P. E. Taking the time to study competitive antagonism. *Br J Pharmacol* **150**, 541-551, doi:10.1038/sj.bjp.0706997 (2007).
455 Nikolovska-Coleska, Z. *et al.* Development and optimization of a binding assay for the XIAP BIR3 domain using fluorescence polarization. *Anal Biochem* **332**, 261-273, doi:10.1016/j.ab.2004.05.055 (2004).
456 Zhen, J., Antonio, T., Dutta, A. K. & Reith, M. E. Concentration of receptor and ligand revisited in a modified receptor binding protocol for high-affinity radioligands: [3H]Spiperone binding to D2 and D3 dopamine receptors. *J Neurosci Methods* **188**, 32-38, doi:10.1016/j.jneumeth.2010.01.031 (2010).
457 Wang, Z. X. An exact mathematical expression for describing competitive binding of two different ligands to a protein molecule. *FEBS Lett* **360**, 111-114 (1995).

458 Douglass, E. F., Jr., Miller, C. J., Sparer, G., Shapiro, H. & Spiegel, D. A. A comprehensive mathematical model for three-body binding equilibria. *J Am Chem Soc* **135**, 6092-6099, doi:10.1021/ja311795d (2013).
459 Negroni, M. P. & Stern, L. J. The N-terminal region of photocleavable peptides that bind HLA-DR1 determines the kinetics of fragment release. *PLoS One* **13**, e0199704, doi:10.1371/journal.pone.0199704 (2018).
460 Chang, H. C. *et al.* A general method for facilitating heterodimeric pairing between two proteins: application to expression of alpha and beta T-cell receptor extracellular segments. *Proc Natl Acad Sci U S A* **91**, 11408-11412, doi:10.1073/pnas.91.24.11408 (1994).
461 Beckett, D., Kovaleva, E. & Schatz, P. J. A minimal peptide substrate in biotin holoenzyme synthetase-catalyzed biotinylation. *Protein Sci* **8**, 921-929, doi:10.1110/ps.8.4.921 (1999).
462 Khan, F., He, M. & Taussig, M. J. Double-hexahistidine tag with high-affinity binding for protein immobilization, purification, and detection on ni-nitrilotriacetic acid surfaces. *Anal Chem* **78**, 3072-3079, doi:10.1021/ac060184l (2006).
463 Reeves, P. J., Callewaert, N., Contreras, R. & Khorana, H. G. Structure and function in rhodopsin: high-level expression of rhodopsin with restricted and homogeneous N-glycosylation by a tetracycline-inducible N-acetylglucosaminyltransferase I-negative HEK293S stable mammalian cell line. *Proc Natl Acad Sci U S A* **99**, 13419-13424, doi:10.1073/pnas.212519299 (2002).
464 Caserta, M. T., Mock, D. J. & Dewhurst, S. Human herpesvirus 6. *Clin Infect Dis* **33**, 829-833, doi:CID010117 [pii], 10.1086/322691 (2001).
465 Asano, Y. *et al.* Clinical features of infants with primary human herpesvirus 6 infection (exanthem subitum, roseola infantum). *Pediatrics* **93**, 104-108 (1994).
466 De Bolle, L., Naesens, L. & De Clercq, E. Update on human herpesvirus 6 biology, clinical features, and therapy. *Clin Microbiol Rev* **18**, 217-245, doi:18/1/217 [pii], 10.1128/CMR.18.1.217-245.2005 (2005).
467 Mori, Y. & Yamanishi, K. HHV-6A, 6B, and 7: pathogenesis, host response, and clinical disease. doi:NBK47394 [bookaccession] (2007).
468 Le, J. & Gantt, S. Human herpesvirus 6, 7 and 8 in solid organ transplantation. *Am J Transplant* **13 Suppl 4**, 128-137, doi:10.1111/ajt.12106.
469 Arbuckle, J. H. & Medveczky, P. G. The molecular biology of human herpesvirus-6 latency and telomere integration. *Microbes Infect* **13**, 731-741, doi:S1286-4579(11)00089-X [pii], 10.1016/j.micinf.2011.03.006.
470 Schneider, C. L. & Hudson, A. W. The human herpesvirus-7 (HHV-7) U21 immunoevasin subverts NK-mediated cytoxicity through modulation of MICA and MICB. *PLoS Pathog* **7**, e1002362, doi:10.1371/journal.ppat.1002362, PPATHOGENS-D-11-00266 [pii]
471 Jackson, S. E., Mason, G. M. & Wills, M. R. Human cytomegalovirus immunity and immune evasion. *Virus Res* **157**, 151-160, doi:S0168-1702(10)00390-4 [pii], 10.1016/j.virusres.2010.10.031.

472 Hansen, T. H. & Bouvier, M. MHC class I antigen presentation: learning from viral evasion strategies. *Nat Rev Immunol* **9**, 503-513, doi:nri2575 [pii] 10.1038/nri2575 (2009).
473 Nastke, M. D. *et al.* Human CD4+ T cell response to human herpesvirus 6. *J Virol* **86**, 4776-4792, doi:10.1128/JVI.06573-11 (2012).
474 Nastke, M. D. *et al.* Human CD4+ T cell response to human herpesvirus 6. *J Virol* **86**, 4776-4792, doi:JVI.06573-11 [pii], 10.1128/JVI.06573-11.
475 Moodie, Z. *et al.* Response definition criteria for ELISPOT assays revisited. *Cancer Immunol Immunother* **59**, 1489-1501, doi:10.1007/s00262-010-0875-4 (2010).
476 Shen, Z. T. *et al.* Bi-specific MHC heterodimers for characterization of cross-reactive T cells. *J Biol Chem* **285**, 33144-33153, doi:10.1074/jbc.M110.141051 (2010).